THE UNIVERSITY of ADELAIDE

Ginsenoside Rg3 as a Potential Treatment for Metastatic Triple-Negative Breast Cancer

A thesis submitted for the degree of Doctor of Philosophy

Maryam Nakhjavani

Adelaide Medical School, Discipline of Medicine

The University of Adelaide

May 2021

Table of Contents

List of publications

1. **Nakhjavani, M.**, Hardingham, J. E., Palethorpe, H. M., Tomita, Y., Smith, E., Price, T. J., and Townsend, A. R. (2019). Ginsenoside Rg3: Potential molecular targets and therapeutic indication in metastatic breast cancer. *Medicines*, 6(1), 17.
2. **Nakhjavani, M.**, Smith, E., Townsend, A. R., Price, T. J., and Hardingham, J. E. (2020). Anti-Angiogenic Properties of Ginsenoside Rg3. *Molecules*, 25(21), 4905.
3. **Nakhjavani, M.**, Hardingham, J. E., Palethorpe, H. M., Price, T. J., and Townsend, A. R. (2019). Druggable molecular targets for the treatment of triple negative breast cancer. *Journal of Breast Cancer*, 22(3), 341.
4. **Nakhjavani, M.**, Palethorpe, H. M., Tomita, Y., Smith, E., Price, T. J., Yool, A. J., Pei, J. V., Townsend, A. R., and Hardingham, J. E. (2019). Stereoselective anti-cancer activities of ginsenoside Rg3 on triple negative breast cancer cell models. *Pharmaceuticals*, 12(3), 117.
5. **Nakhjavani, M.**, Smith, E., Yeo, K., Palethorpe, H. M., Tomita, Y., Price, T. J., Townsend, A. R., and Hardingham, J. E. (2021) Anti-angiogenic properties of ginsenoside Rg3 epimers: in vitro assessment of single and combination treatments. *Cancers,* 13(9), 2223.
6. **Nakhjavani, M.**, Smith, E., Palethorpe, H. M., Tomita, Y., Yeo, K., Price, T. J., Townsend, A. R., and Hardingham, J. E. Anti-cancer effects of an optimised combination of ginsenoside Rg3 epimers on triple negative breast cancer models. Submitted to *Pharmaceuticals* (under revision).
7. **Nakhjavani, M.**, Smith, E., Yeo, K., Tomita, Y., Price, T. J., Yool, A. J., Townsend, A. R., and Hardingham, J. E. (2021) Differential anticancer activities of the active metabolites of ginsenoside Rg3. Accepted for publication in *Journal of Ginseng Research*.

Abstract

Triple-negative breast cancer (TNBC) is a subtype of breast cancer for which no approved targeted therapy is available, and chemotherapy is the mainstay of the treatment for these patients. Administration of various chemotherapies can be limited by toxicities and the development of tumour resistance and the median overall survival of these patients is low. This research aimed at studying the efficacy of epimers of ginsenoside Rg3 (Rg3), 20(S)-Rg3 (SRg3) and 20(R)-Rg3 (RRg3), in inhibition of cancer growth and angiogenesis for the potential treatment of this disease. The preliminary molecular docking studies predicted that Rg3 interacted well with aquaporin 1 (AQP1), which plays important roles in cancer progression.

First, stereoselectivity of Rg3 epimers was shown in inhibition of proliferation, migration and invasion of TNBC cell lines and blocking AQP1 water channel. Due to this stereoselectivity, the combination of both epimers was optimised for inhibition of loop formation in endothelial cells, using response surface methodology (RSM). It was shown that this optimised combination, referred to as C3, significantly inhibited the proliferation and migration of human and murine endothelial cells. Rg3 epimers worked as allosteric modulators of vascular endothelial growth factor receptor 2 (VEGFR2). C3 decreased the expression of VEGF and significantly decreased the expression of AQP1 and the phosphorylation of proteins downstream of AKT signalling in hypoxic and normoxic conditions.

In TNBC monolayer cultures, C3 significantly decreased cell migration but did not inhibit cell proliferation. In TNBC mammospheres, C3 decreased mammosphere formation efficiency, with no significant reduction in cell viability. C3 decreased the expression of CD44 and the ratio of CD44/24. C3 also decreased the function of cells via affecting the proteins downstream of activation of the mammalian target of rapamycin (mTOR). In molecular docking, Rg3 epimers showed good binding scores with VEGFR2 and insulin growth factor-1 receptor amongst the tested tyrosine kinase receptors. Rg3 epimers also showed a good binding score with rapamycin-binding site of mTOR and activator of mTOR, Rheb. In a mouse model of metastatic TNBC, when an extrapolated dose of C3 (23 mg/kg SRg3 + 11 mg/kg RRg3) or an escalated dose (46 mg/kg SRg3 + 23 mg/kg RRg3) was injected into mice, a significant reduction in the primary tumour volume and decreased load of metastasis in the lungs was noticed. Furthermore, the number of affected axillary lymph nodes was significantly reduced.

Since Rg3 is prone to extensive metabolism *in vivo*, the efficacy of deglycosylated metabolites of Rg3 epimers was also studied. It was shown that these metabolites were inhibitors of cell proliferation in TNBC and endothelial cells. The mechanism for this action was induction of necroptosis/necrosis in TNBC cell lines and apoptosis in endothelial cells. Among the tested metabolites, 20(S)-ginsenoside Rh2 (S-Rh2) showed the best inhibition of loop formation, and allosteric modulatory action on

VEGFR2. It was also predicted to be a good blocker of the AQP1 water channel. Altogether, the findings of this project show the possibilities of Rg3, as a potential inhibitor of mTOR signalling for the treatment of TNBC patients.

Thesis Declaration

I certify that this work contains no material which has been accepted for the award of any other degree or diploma in my name, in any university or other tertiary institution and, to the best of my knowledge and belief, contains no material previously published or written by another person, except where due reference has been made in the text. In addition, I certify that no part of this work will, in the future, be used in a submission in my name, for any other degree or diploma in any university or other tertiary institution without the prior approval of the University of Adelaide and where applicable, any partner institution responsible for the joint-award of this degree.

I acknowledge that copyright of published works contained within this thesis resides with the copyright holder(s) of those works.

I also give permission for the digital version of my thesis to be made available on the web, via the University's digital research repository, the Library Search and also through web search engines, unless permission has been granted by the University to restrict access for a period of time.

I acknowledge the support I have received for my research through the provision of an Australian Government Research Training Program Scholarship.

Maryam Nakhjavani

21/1/21

Acknowledgements

I would like to express my appreciation for my best supervising panel for their great guidance, insightful inputs, encouragement, endless support, and friendship. My deepest appreciation and sincere gratitude to my principal supervisor, Dr Jennifer Hardingham. Without her guidance, feedback, enthusiasm, and patience this thesis would not have been possible. I would also like to acknowledge the contribution, feedback and support of my co-supervisor, Dr Amanda Townsend.

Special thanks and appreciation with deep love to my amazing husband, Mohsen, who has always been a unique supportive friend, a heart-warming company and a constant source of support and encouragement. Special thanks to two angels of my life, my mother and father, for their unconditional love and support, for encouraging me to never stop and to reach for the stars. I am very grateful to my beautiful supporting and caring sisters, Mina and Shima, who made my world wonderful, and my exceptional grandmother for always being there for me. I am very grateful to my amazing loving mother-in-law (may her soul rest in peace) and father-in-law and my beautiful and caring sister-in-law, Marzieh. I am so blessed to have such a beautiful family. This thesis is dedicated to them.

I wish to thank all the people whose assistance was a milestone in the completion of this project. I would like to express my sincere thanks to all the following people who were of great support: Dr Eric Smith, Dr Helen Palethorpe, Dr Kevin Fenix, Dr Irene Zinonos, and Dr Irene Stafford. I would like to appreciate my friends' support and encouragement; Dr Leila Rahnama, Gohar Shaghayegh, Dr Shari Javadian, Dr Mahnaz Ramezanpour, Bimala Dhakal, and Dr Yoko Tomita. Their unconditional support helped me get through the ups and downs of this journey.

In addition, “Margaret Elcombe Hospital Research Foundation Research Grant" is acknowledged for its financial support during my PhD program. The last but not the least is to acknowledge “Adelaide Scholarship International (ASI)” and the “Doctor Chun Chung Wong and Madam So Sau Lam Memorial Postgraduate Cancer Research Top-Up” scholarships, which were grand financial supports to accomplish the thesis.

Chapter 1 Introduction and Literature Review

Triple-negative breast cancer (TNBC) is an aggressive subtype of breast cancer, with higher prevalence in women < 50 years old, a higher probability of relapse and poorer overall survival. Due to the lack of targeted therapy for this subtype of breast cancer, patients have fewer treatment options available. The treatment is limited to chemotherapy, the application of which is usually limited by toxicities and development of drug resistance. This thesis aimed at studying a new treatment option for these patients, ginsenoside Rg3 (Rg3). Rg3 is extracted from a traditional herbal medicine, *Panax ginseng*, which has been used by humans safely for thousands of years. Rg3 is one of the most pharmacologically important molecules extracted from this plant. Several studies focused on the anticancer effects of Rg3. Rg3 has two structurally related epimers; 20(S)-Rg3 (SRg3) and 20(R)-Rg3 (RRg3).

This thesis reports studies on the potential of Rg3 epimers as a treatment for TNBC. The thesis includes 6 chapters. Chapter 1 presents an in-depth review of the literature on the anti-cancer and anti-angiogenic properties of Rg3 epimers and the druggable targets in TNBC. Chapter one of this thesis includes 3 review papers. The first review paper comprehensively studied and categorised the efficacy of each of the epimers as anticancer agents, focusing on mechanisms of action of these molecules, their application in combination with chemotherapy treatments, the pharmacokinetics of these molecules and outcomes of clinical trials on Rg3. The review also discusses the potential of Rg3 as a blocker of the water transport function of AQP1, which plays important roles in cancer progression and discusses the potential of Rg3 as a treatment for TNBC.

The next review paper focused on the anti-angiogenic properties of Rg3 epimers and for the first time discussed the controversies in the literature regarding the anti- or pro-angiogenic effects of Rg3. The paper also described pharmacodynamics of action of Rg3 as an anti-angiogenic drug and summarised the evidence on the anti-angiogenic actions of Rg3, *in vitro* and *in vivo*.

The third review paper discussed druggable targets in TNBC patients, to bring insight into the current status of the disease and ongoing clinical trials on these patients. The paper also summarised the promising molecular targets at preclinical and phase I clinical trial stages.

Chapter 2 focuses on the specific functions of each epimer in TNBC and shows the stereoselectivity of Rg3. Based on these results, in chapter 3, the concentrations of SRg3 and RRg3 were optimised in combination for anti-angiogenic action and some mechanisms of the action of this combination were studied. In chapter 4, it was shown that this combination was optimised for its anti-cancer action in TNBC *in vitro* models and mechanisms of anti-cancer actions of this combination were suggested. Furthermore, the combination was tested *in vivo* in a metastatic breast cancer mouse

model. Rg3 is prone to deglycosylation and producing active metabolites. In chapter 5, differential anti-cancer potential of these metabolites is investigated. Chapter 6 summarises the significance of the findings and proposed future studies.

1.1 Publications arising from this thesis

The research conducted in this thesis led to several publications in well-known peer-reviewed journals. Some of them are still under review for possible publication in high impact journals. The following is the list of papers published and those still under review for publication:

Nakhjavani, M., Hardingham, J. E., Palethorpe, H. M., Tomita, Y., Smith, E., Price, T. J., and Townsend, A. R. (2019). Ginsenoside Rg3: Potential molecular targets and therapeutic indication in metastatic breast cancer. *Medicines*, 6(1), 17.

Nakhjavani, M., Smith, E., Townsend, A. R., Price, T. J., and Hardingham, J. E. (2020). Anti-Angiogenic Properties of Ginsenoside Rg3. *Molecules*, 25(21), 4905.

Nakhjavani, M., Hardingham, J. E., Palethorpe, H. M., Price, T. J., and Townsend, A. R. (2019). Druggable molecular targets for the treatment of triple negative breast cancer. *Journal of Breast Cancer*, 22(3), 341.

Nakhjavani, M., Palethorpe, H. M., Tomita, Y., Smith, E., Price, T. J., Yool, A. J., Pei, J. V., Townsend, A. R., and Hardingham, J. E. (2019). Stereoselective anti-cancer activities of ginsenoside Rg3 on triple negative breast cancer cell models. *Pharmaceuticals*, 12(3), 117.

Nakhjavani, M., Smith, E., Yeo, K., Palethorpe, H. M., Tomita, Y., Price, T. J., Townsend, A. R., and Hardingham, J. E. (2021) Anti-angiogenic properties of ginsenoside Rg3 epimers: in vitro assessment of single and combination treatments. *Cancers*, 13(9), 2223.

Nakhjavani, M., Smith, E., Palethorpe, H. M., Tomita, Y., Yeo, K., Price, T. J., Townsend, A. R., and Hardingham, J. E. Anti-cancer effects of an optimised combination of ginsenoside Rg3 epimers on triple negative breast cancer models. Submitted to *Pharmaceuticals* (under revision).

Nakhjavani, M., Smith, E., Yeo, K., Tomita, Y., Price, T. J., Yool, A. J., Townsend, A. R., and Hardingham, J. E. (2021) Differential anticancer activities of the active metabolites of ginsenoside Rg3. Accepted for publication in *Journal of Ginseng Research*.

1.2 Conference presentations arising from this thesis

This research was presented at well-known and peer-reviewed conferences and was awarded in some of them, as listed below:

Nakhjavani, M., Smith, E., Price, T. J., Townsend, A. R., and Hardingham, J. E. Ginsenoside Rg3 enantiomers in a defined ratio as a novel treatment for metastatic triple negative breast cancer. Poster presentation at *San Antonio Breast Cancer Symposium*, 2020 (virtual).

Nakhjavani, M., Smith, E., Price, T. J., Townsend, A. R., Hardingham, J. E. Ginsenoside Rg3 enantiomers in a defined ratio as a novel treatment for triple negative breast cancer. Oral presentation in *TQEH Research Day* 2020, SA, Australia. 2020.

Nakhjavani, M., Smith, E., Price, T. J., Townsend, A. R., Hardingham, J. E. Ginsenoside Rg3, a potential novel treatment for metastatic breast cancer. Poster presentation in *Florey's Postgraduate Research Conference*, SA, Australia. 2020. **Awarded for Innovation and Commercial Partners Prize**

Nakhjavani, M. Palethorpe, H. M., Tomita, Y., Smith, E., Price, T. J., Townsend, A. R., Hardingham, J. E. Novel candidates for the treatment of metastatic breast cancer. Oral presentation in *Adelaide Pharmacology Group (APG) Meeting*. 2019. SA, Australia.

Nakhjavani, M. Palethorpe, H. M., Tomita, Y., Smith, E., Pei, J. V., Price, T. J., Yool, A. J., Townsend, A. R., Hardingham, J. E. Anti-cancer properties of ginsenoside Rg3 epimers. Mini-oral presentation in *TQEH Research Day* 2019, SA, Australia. 2019. **Awarded for best mini-oral presentation.**

Nakhjavani, M., Palethorpe, H. M., Tomita, Y., Smith, E., Yool, A. J., Townsend, A. R., Hardingham, J. E. Comparison of the molecular modelling of bacopaside I and bacopaside II, candidate anti-angiogenic agents, with sorafenib. Oral presentation in *ASMR SA Scientific Meeting*. 2018. SA, Australia.

Nakhjavani, M., Palethorpe, H. M., Tomita, Y., Smith, E., Price, T. J., Yool, A. J., Townsend, A. R., Hardingham, J. E. Ginsenoside Rg3; an anti-invasion candidate for triple negative breast cancer. Poster presentation in *Florey's Postgraduate Research Conference*. SA, Australia. 2018.

Nakhjavani, M., Palethorpe, H. M., Tomita, Y., Smith, E., Price, T. J., Yool, A. J., Townsend, A. R., Hardingham, J. E. 20(S)-ginsenoside Rg3; an anti-invasive candidate for triple negative breast cancer. Oral presentation in *TQEH Research Expo*. 2018. SA, Australia.

1.3 Awards and prizes

This research received the following awards and prizes:

Innovation and Commercial Partners Prize, Florey's Postgraduate Research Conference 2020

The Doctor Chun Chung Wong and Madam So Sau Lam Memorial Postgraduate Cancer Research Top-Up Scholarship, 7000 AUD (2019)

Nominated as one of the 50 women of impact and influence, University of Adelaide (2019)

Best mini-oral presentation, TQEH Research Expo, Adelaide (2019)

1.4 Thesis Format

This thesis is based on the collection of the manuscripts produced during the course of the research and has been submitted according to the format approved by the University of Adelaide. The thesis is provided and available in both hard and soft copy which are identical. The soft copy is available online at the University of Adelaide Library and can be viewed using Adobe Reader.

1.5 Statement of authorship

Statement of Authorship

Title of Paper	Ginsenoside Rg3: Potential molecular targets and therapeutic indication in metastatic breast cancer
Publication Status	☑ Published ☐ Accepted for Publication ☐ Submitted for Publication ☐ Unpublished and Unsubmitted work written in manuscript style
Publication Details	Nakhjavani, M., Hardingham, J. E., Palethorpe, H. M., Tomita, Y., Smith, E., Price, T. J., & Townsend, A. R. (2019). Ginsenoside Rg3: Potential molecular targets and therapeutic indication in metastatic breast cancer. Medicines, 6(1), 17.

Principal Author

Name of Principal Author (Candidate)	Maryam Nakhjavani		
Contribution to the Paper	Conceptualised, designed and prepared the Tables and Figures and substantially wrote the manuscript.		
Overall percentage (%)	70		
Certification:	This paper reports on original research I conducted during the period of my Higher Degree by Research candidature and is not subject to any obligations or contractual agreements with a third party that would constrain its inclusion in this thesis. I am the primary author of this paper.		
Signature		Date	10th Feb 2021

Co-Author Contributions

By signing the Statement of Authorship, each author certifies that:

i. the candidate's stated contribution to the publication is accurate (as detailed above);
ii. permission is granted for the candidate in include the publication in the thesis; and
iii. the sum of all co-author contributions is equal to 100% less the candidate's stated contribution.

Name of Co-Author	Jennifer E Hardingham		
Contribution to the Paper	Conceptualised and contributed to designing the paper, Figures and Tables, and drafting and reviewing the paper.		
Signature		Date	10th Feb 2021

Name of Co-Author	Helen M Palethorpe		
Contribution to the Paper	Contributed to drafting and reviewing the paper.		
Signature		Date	8th February 2021

Name of Co-Author	Yoko Tomita		
Contribution to the Paper	Contributed to drafting and reviewing the paper.		
Signature		Date	12th Feb 2021

Name of Co-Author	Eric Smith		
Contribution to the Paper	Contributed to drafting and reviewing the paper.		
Signature		Date	10th Feb 2021

Name of Co-Author	Tim J Price		
Contribution to the Paper	Contributed to drafting and reviewing the paper.		
Signature		Date	11th Feb 2021

Name of Co-Author	Amanda R Townsend		
Contribution to the Paper	Contributed to drafting and reviewing the paper.		
Signature		Date	11th Feb 2021

medicines

MDPI

Review

Ginsenoside Rg3: Potential Molecular Targets and Therapeutic Indication in Metastatic Breast Cancer

Maryam Nakhjavani [1,2], Jennifer E Hardingham [1,2,*], Helen M Palethorpe [1,2], Yoko Tomita [1,2,3], Eric Smith [1,2], Tim J Price [2,3] and Amanda R Townsend [2,3]

1 Molecular Oncology, Basil Hetzel Institute, The Queen Elizabeth Hospital, Woodville South, SA 5011, Australia; maryam.nakhjavani@adelaide.edu.au (M.N.); helen.palethorpe@adelaide.edu.au (H.M.P.); yoko.tomita@adelaide.edu.au (Y.T.); eric.smith@adelaide.edu.au (E.S.)
2 Adelaide Medical School, University of Adelaide, Adelaide, SA 5005, Australia; timothy.price@sa.gov.au (T.J.P.); amanda.townsend@sa.gov.au (A.R.T.)
3 Oncology Unit, The Queen Elizabeth Hospital, Woodville South, SA 5011, Australia
* Correspondence: jenny.hardingham@sa.gov.au; Tel.: +61-8-8222-6142

Received: 20 December 2018; Accepted: 23 January 2019; Published: 23 January 2019

Abstract: Breast cancer is still one of the most prevalent cancers and a leading cause of cancer death worldwide. The key challenge with cancer treatment is the choice of the best therapeutic agents with the least possible toxicities on the patient. Recently, attention has been drawn to herbal compounds, in particular ginsenosides, extracted from the root of the Ginseng plant. In various studies, significant anti-cancer properties of ginsenosides have been reported in different cancers. The mode of action of ginsenoside Rg3 (Rg3) in in vitro and in vivo breast cancer models and its value as an anti-cancer treatment for breast cancer will be reviewed.

Keywords: Ginsenoside Rg3; breast cancer; AQP-1; epimer; angiogenesis

1. Metastatic Breast Cancer

Metastatic breast cancer (MBC) is classified as stage IV where the tumor has metastasized to distant organs such as bones, lungs, liver, or brain [1]. Breast tumors are subdivided into different categories based on the receptors expressed in the cells: estrogen receptor (ER)- or progesterone receptor (PR)-positive, human epidermal growth factor receptor 2 (HER2) positive, and triple negative breast tumors ($ER^-/PR^-/HER2^-$) (Figure 1). Hormone receptor expressing tumors including luminal A or luminal B subtypes constitute the largest portion of patients and have the best prognosis, as these tumors are inherently less aggressive compared to other subtypes of breast cancer and that the majority of these tumors are responsive to hormone therapy options such as tamoxifen or letrozole [2]. HER2-expressing tumors constitute 15–20% of the patients [3]. The prognosis of this group of patients has improved following the introduction of targeted anti-HER2 medications, such as trastuzumab [4]. Some 15% of patients have triple negative (basal-like) breast cancer (TNBC) [5] and for these patients, chemotherapy remains the main treatment option [6]. TNBC is associated with younger age (<50 years) at diagnosis and BRCA1 mutation, and by the time of diagnosis have larger tumor size, higher grade tumor and the worst prognosis [7]. Recently, inhibitors of poly ADP ribose polymerase (PARP) have been found to be effective in the treatment of TNBC patients with BRCA-1 or -2 mutations. Likewise, platinum-based cytotoxic drugs are being tested in such patients [2]. However, still there is no ultimate cure for MBC and these patients suffer from the side effects of chemotherapy, until the tumor develops acquired resistance [8] and the patients succumb to the disease. Hence, many cancer researchers are actively looking for better treatment options to improve the quality of life of the MBC patients, reduce the toxicities of the chemotherapy regimens, restrict tumor metastasis, and improve survival. In this

review, the medicinal herb ginseng and the important group of chemicals in its extract are suggested as one such therapy with the potential for reduced toxicity.

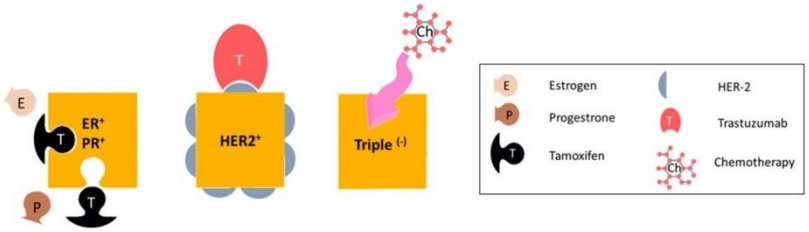

Figure 1. Subtypes of metastatic breast cancer, based on receptor expression. Hormone-receptor expressing tumors are treated with anti-hormone therapy (such as tamoxifen), HER2-expressing tumors are given targeted anti-HER2 monoclonal antibody therapy such as trastuzimab. The main treatment option for triple negative breast tumors is chemotherapy.

2. Ginseng—History and Medicinal Use

Ginseng, with a long history of human use as a traditional medicine, has various pharmacological effects [9–11], and is widely used for its nutritional value as a food, energizing the body [10], improving body performance in sports, relieving menopausal symptoms, and alleviating sexual dysfunction [12]. *Panax ginseng*, also known as Chinese or Korean ginseng is a species of ginseng, the extract of which has the highest medicinal value among other species. Ginsenosides are the group of chemicals in this extract having the highest medicinal value [13]. So far, 38 ginsenosides have been identified [14]. Ginsenosides are saponins having a steroid-like hydrophobic backbone connected to sugar moieties. Based on their chemical structure, they are categorized into panaxadiol, panaxatriol, and oleanolic groups [13], with protopanaxadiols being the most abundant group. Protopanaxadiols include Rb1, Rb2, Rg3, Rh2, Rc, Rd, Ra, and F2 [12] and have various medicinal properties, including anti-diabetic effects, protection against cardiovascular diseases and anticancer properties [10,12].

Not all of these protopanaxadiols are available in ginseng extract. Commercial ginseng is produced either by air-drying or steaming (120°C, 4 h) the plant. These processes produce white or red ginseng, respectively [15–17]. Due to the conversions and chemical changes following heating, the heat processed or red ginseng has higher medicinal properties than white ginseng. Within this heating process, polar ginsenosides such as Rb1 or Rb3 convert to less polar ginsenosides such as Rg2 and Rg3 [15,18].

Ginsenoside Rg3 is one of the well-studied members of protopanaxadiols, and arises following loss of the sugar moiety on C_{20} in the heating process. Like other ginsenosides, Rg3 has a stereocenter on C_{20}, giving it two epimers; 20(R)- and 20(S)-ginsenoside Rg3 (Figure 2). This is due to the selective attachment of the hydroxyl group to the C_{20} after losing the sugar structure. In the 20(R)-Rg3 epimer, the hydroxyl on C_{20} is far from the hydroxyl on C_{12}, whilst in 20(S)-Rg3, these two hydroxyls are close to each other. Also, the alkene chain connected to C_{20} in 20(R)-Rg3 is more flexible compared to its fixed orientation in 20(S)-Rg3. This makes the alkene in 20(S)-Rg3 less accessible to water and more prone to hydrophobic interactions while leaving the hydroxyl groups to interact with the receptors. This may play a part in the increased water solubility of 20(S)-Rg3 compared with 20(R)-Rg3 [19,20].

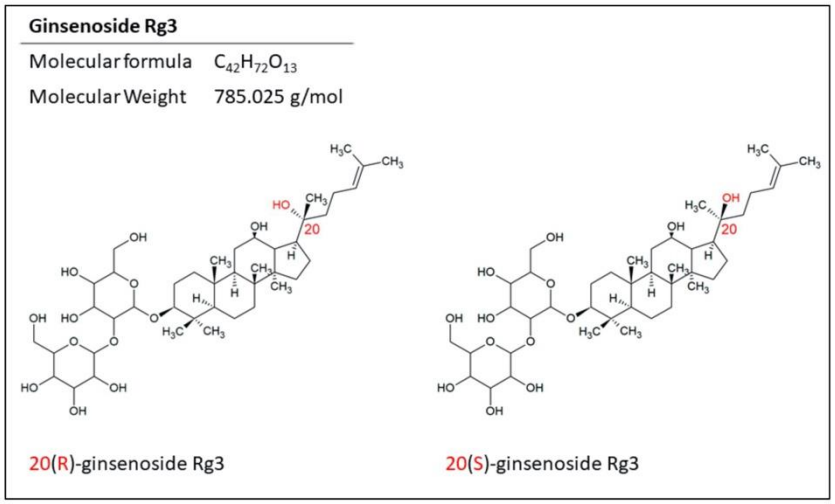

Figure 2. The structure of the epimers of ginsenoside Rg3. The position of the hydrogen on C_{20} makes two epimers for this molecule.

3. Epimers of Ginsenoside Rg3 in the Treatment of Cancer

Depending on the biological system being tested, the two epimers of ginsenoside Rg3, 20(S)- and 20(R)-Rg3, have distinct effects. For example, while both epimers inhibited the 5-HT_{3A} and α3β4 nACh receptors, only 20(S)-Rg3 inhibited the voltage-dependent Ca^{2+}, K^+, and Na^+ channel currents [21,22]. The 20(S)-Rg3 was also a better scavenger of hydroxyl radicals [23] and in the human gastric cancer cell line AGS, was responsible for inducing apoptosis (through activation of caspase-3, -8, and -9) [24]. In human hepatocellular carcinoma cell line HepG2, 20(S)-Rg3 was the more effective epimer in inhibiting cell growth, downregulating the expression of DNA methyltransferases, reducing global DNA methylation, and in particular, modifying the methylation of the promoter region of some relevant genes in cancer such as VEGF, TP53, and BCL-2 [25].

In contrast, 20(R)-Rg3 was a better antioxidant against the oxidative stress induced by cyclophosphamide in mice [26] and can promote the immune response in mice better than 20(S)-Rg3 [27,28]. It was also a better inhibitor of tumor growth in mice bearing H22-transplanted hepatocellular tumors [28]. Epimers of Rg3 have also been tested in epithelial–mesenchymal transition (EMT) in lung adenocarcinoma in vitro models. For instance, 20(R)-Rg3 epimer inhibited EMT via increasing the expression of E-cadherin and inhibiting the expression of vimentin and upregulation of Snail [29].

4. Mechanisms of Action of Ginsenoside Rg3 in Breast Cancer

Regardless of the stereotype, Rg3 has been studied in several cancer models and various mechanisms are suggested for its actions. These mechanisms include induction of apoptosis [24,30–52], induction of autophagy through upregulation of autophagy-associated molecules [53], inhibition of proliferation [24,25,38,41,42,44–46,50,51,54–63], inhibition of metastasis [29,50,62,64–71] and angiogenesis [55,56,66], cell cycle arrest [47], immunomodulatory effects [72], sensitization to radiation [73], reducing multidrug resistance [74], and inducing genotoxicity to the cancer cells [75]. A few studies have focused on the effects of Rg3 in breast cancer models; these mechanisms are discussed as follows.

4.1. Induction of Apoptosis and Inhibition of Proliferation

Induction of apoptosis is one of the most studied mechanisms of action of Rg3 in different cancers. Apoptosis is a complex process, regulated by extrinsic (via the death receptor) and intrinsic (via mitochondrial) pathways. The intrinsic pathway is activated by DNA damage and oxidative stress whilst the extrinsic pathway can be triggered by the activation of the members of the TNF receptor superfamily. Both pathways ultimately activate caspase enzymes.

Caspases can interact with an apoptosis inhibitor such as inhibitors of apoptosis proteins (IAP) and the Bcl-2 family. Caspases can also go through auto-activation and cleave other substrates, one of which is PARP, an important DNA repair enzyme. In a TNBC cell line, MDA-MB-231, Rg3 activated caspase-3, and degraded PARP through the generation of reactive oxygen species (ROS) [30]. In addition, Rg3 caused an increased ratio of pro-apoptotic Bax and the anti-apoptotic Bcl-2 [30]. Also, it inhibited the binding of NF-κB to DNA. NF-κB is a transcription factor that is constitutively active in breast cancer cells and drives further cell cycle progression, proliferation and inhibition of apoptosis. Proteins Akt and ERK are two kinases involved in the activation of NF-κB and it is observed that in MDA-MB-231 cell line, Rg3 inhibited the phosphorylation of Akt and ERK and hence prevented the activation of NF-Kb [31]. P53, a tumor suppressor protein, has a negative regulatory effect on Bcl-2 while mutant P53 can prolong the activation of NF-κB and affect the apoptosis of cancer cells. In MDA-MB-231 cells, Rg3 destabilized mutant P53, suppressed the expression of Bcl-2, and induced apoptosis [31]. Figure 3 summarizes these mechanisms.

Inhibition of proliferation is another important function proposed for Rg3. For example, in in vivo settings, Rg3 has shown inhibition of tumor growth in the cancer models of colon [54], lung [38,72], liver [39], pancreas [76], and gallbladder [32]. As a specific epimer, 20(S)-Rg3 has caused similar responses in tumors of the gallbladder [47] and ovary [51,68] and 20(R)-Rg3 in melanoma [61,63], lung [62], and liver [28] cancer models. In vitro, in MCF-7 breast cancer cell lines, 20(S)-Rg3 (100–300 μM), caused a cell cycle arrest in G_1-phase and hence inhibited cell proliferation [57]. Table 1 shows other suggested mechanisms of Rg3 in induction of apoptosis and inhibition of proliferation in other cancer models.

4.2. Inhibition of Migration, Invasion, Angiogenesis, and Metastasis

Ginsenoside Rg3 has been shown to reduce the migration, invasion, and angiogenesis of human umbilical vein endothelial cells (HUVECs) both in vitro and in vivo. Treatment of HUVECs with 20(R)-Rg3 reduced cell viability with an IC_{50} of 10 nM. There was a dose-dependent reduction in the tube forming capacity of these cells (1-1000 nM) and inhibition of VEGF-induced chemo-invasion in vitro. In vivo Rg3 inhibited angiogenesis (150 and 600 nM) in a matrigel plug assay. The mechanisms suggested were inhibition of matrix metalloproteinase (MMP)-2 and -9 [77].

Rg3 has been shown to degrade serum levels of IGF-1 and hence inhibits angiogenesis and tumor growth in breast cancer [78]. In a study by Chen et al. [69], in the MDA-MB-231 cell line, 20(S)-Rg3 decreased the expression of CXCR4, an important chemokine receptor expressed by breast cancer cells which is involved in migration and invasion (Figure 3) [69]. Other suggested mechanisms for this action in other cancer models include decreased expression of MMP-2 [29,77], -9 [66], and -13 [67], reducing the expression of HIF-1α [55,68], AQP1 [71], and HDAC3 [63], suppressing NF-κB and its products (c-Myc, COX-2, MMP-9) [55,64], inhibiting TGF-β1, inactivating proteins involved in EMT (p38 MAPK and Smad2) [29,55], downregulating FUT4 and EGFR mediated migration through MAPK and NF-κB [55,62], and decreasing the expression of VEGF [55] and VEGF dependent p38/ERK signaling [56] (Table 2). Rg3 has also resulted in an increased survival in mice bearing melanoma [50] and liver tumors [39].

4.3. Multidrug Resistance (MDR) and Combination Therapy

Rg3 can decrease MDR via inducing membrane fluidity and blocking drug efflux in leukemia cell lines [74]. In the Caco-2 cell line, 20(S)-Rg3 (80 μM) was shown to inhibit P-glycoprotein (Pgp) [79]. It has also been shown to increase the accumulation of drugs such as vincristine in MDR cells, but not in sensitive cells [80]. Likewise, mice bearing MDR tumors showed an increased survival time and less tumor weight when treated with a combination of doxorubicin and Rg3, rather than doxorubicin alone [80].

Few studies have shown the effects of co-administration of Rg3 and a chemotherapy agent in breast tumor models. What is known so far is that mice bearing breast tumors that received a combination of continuous low-dose capecitabine, a prodrug of fluorouracil (5-FU), and Rg3 showed less toxicity induced by capecitabine, longer survival, and reduced susceptibility to drug resistance [81]. This is in part due to the antiangiogenic effect of Rg3 as evidenced by the decreased VEGF expression and reduced microvasculature density. The outcomes of this study are promising for the oral administration of capecitabine and improvement in tolerance of the patients.

In addition, Rg3 when co-administered orally with paclitaxel, significantly increased the relative bioavailability of paclitaxel and decreased the relative breast tumor growth rate in mice bearing MCF-7 xenograft [79]. Rg3 has been tested in other cancer models in combination with cyclophosphamide [82,83], gemcitabine [84], temozolomide [85], cisplatin [86–88], docetaxel [89,90], doxorubicin [91,92], and As_2O_3 [93] (Table 3).

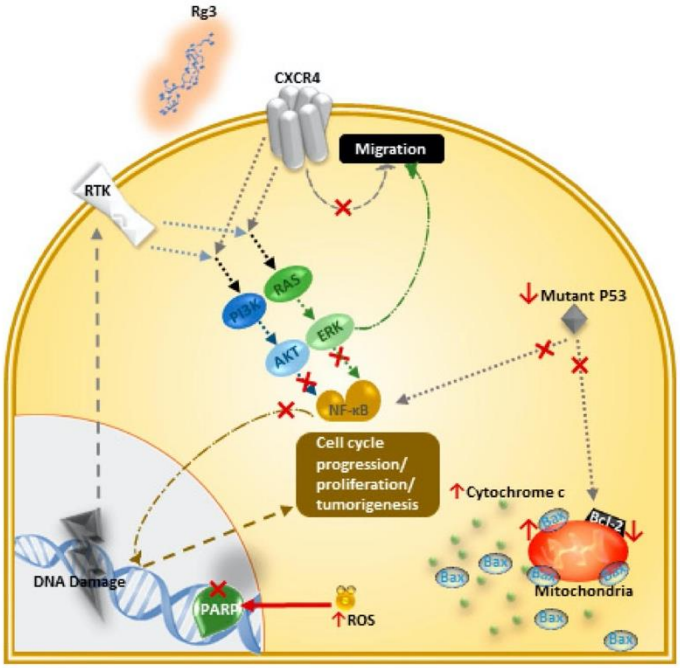

Figure 3. Rg3 inhibits cell proliferation and induces apoptosis via different effector molecules and pathways, in MDA-MB-231 cell line [30,31]. Changes in specific molecules involved in signalling pathways upon exposure of the cells to Rg3 is shown in this figure. The ↑ and ↓ arrows are indicating increased and decreased levels of certain molecules, respectively, and the × signs show the inhibition of a signalling pathway or function of a certain protein in the MDA-MB-231 cell line.

Table 1. Suggested mechanisms for induction of apoptosis (IA) and inhibition of proliferation (IP) by Rg3 in various cancers are summarized in Table 1. The function of different epimers are indicated by symbols; * and ◊ represent 20(S)- and 20(R)-Rg3, respectively.

Cancer		Mechanism of Action	Reference
Ovary	IA	Downregulation of PI3K/Akt and the proteins of the IAP family *	[52]
		Activation of caspases -3 and -9 *	
		Inhibition of Warburg effect by inactivation of Stat3 *	[51]
	IP	Suppression of the Warburg effect and modulating the Stat3/HK2 pathway	[51]
Colon	IA	Activation of AMPK *	[45,46]
		Increased DNA fragmentation, cleavage of PARP *	
		Downregulation of Bcl-2 *	
		Upregulation of p53, Bax, release of cytochrome c and caspase-3 and -9 *	
		Inhibiting the function of β-catenin and the ß-catenin/Tcf signalling	[54]
	IP	Inhibits cell proliferation	
		Reduced mitosis-related proteins *	[46]
		Reduced DNA-repair proteins *	
		Changes in the Eph/ephrin signalling axis *	[58]
Lung	IA	Activation of the intrinsic and extrinsic pathways	[38,40,41]
		Regulation of apoptosis-associated proteins such as BCL2, BAX, PARP-1	
		Cleaving caspase-3	
	IP	Inhibition of EGFR, Stat3, Akt and PI3/Akt signalling	
		Decreasing the expression of FUT4 and biosynthesis of LeY ◊	[38,62]
		Decreasing the activation of EGFR and its downstream signaling ◊	
		Suppression of some of the cell cycle proteins such as cyclin D1 and E, CDK-2 and -4	[41]
		Suppression of some of the MAPK-associated growth proteins such as JNK, ERK and P38	
Liver	IA	Activation of the intrinsic and extrinsic pathways through increasing Bax, caspase-3, release of cytochrome c, decreasing Bcl-2, Bcl-xL	[39,44,49]
		Sensitizing liver cancer cells to TRAIL-induced cell death	[43]
		Promoting TRAIL-induced caspase-dependent apoptosis (via DR5 upregulation and induction of CHOP)	
Multiple myeloma	IA	Increasing the activity of caspase-3 and expression of Bax	[35]
	IP	Inhibiting the secretion of IGF-1	[42]
		Affecting the Akt/mTOR signalling and their proliferation	
Leukaemia	IA	Activating caspases -3 and -9	[48]
		Downregulating PI3K/Akt family proteins	
Gallbladder	IA	Increasing caspase-12 (an endoplasmic reticulum stress-mediated apoptosis)	[32]
		Activating p53 pathway and intrinsic apoptosis pathway *	[47]
		Inducing cell senescence *	
Gastric	IA	Blocking TRMP7	[24,34]
		Upregulation of caspase-3, -8, -9, Bax and downregulation of Bcl2	
		Inhibiting the expression of FUT4 (via regulation of SP1 and HSD1)	[24,33]
		Activation of caspase-3, -8 and -9	
Melanoma	IA	Preventing the binding of NF-κB to the FUT4 promoter	[36]
		Activating intrinsic and extrinsic apoptosis pathways	
		Increasing the expression of caspase and Bcl-2 *	[50]
		Decreasing the levels of active Akt *	[50]
	IP	Dysregulating the PI3K/Akt pathway, hence affecting the cell cycle *	
		Inducing a G0/G1 cell cycle arrest ◊	[63]
		Decreasing the HDAC3 ◊	
		Increasing the acetylation and stability of p53 ◊	
		Reducing FUT4 and LeY ◊	[61]
		Inhibiting the EGFR/MAPK signalling pathway ◊	
Glioblastoma multiforme	IA	Suppressing the MEK/MAPK signalling pathway and activating ROS by the antioxidant enzyme system, leading to apoptosis	[37]
Prostate	IP	Inhibition of DNA synthesis *	[60]
		Affecting the MAPK activity through ERKs, p38 and JNK *	
Glioma	IP	Activating Akt and p53/p21 dependent signalling pathways causing cell senescence *	[59]

Table 2. Suggested mechanisms of inhibition of migration and invasion in different cancer models. The function of different epimers are indicated by symbols; * and ◊ represent 20(S)- and 20(R)-Rg3, respectively.

Cancer	Mechanism	Reference
Ovary	Inhibition of angiogenesis and cell invasion Decreased expression of MMP-9	[66]
	Blocking the EMT * Reducing HIF-1α expression *	[68]
Colon	Suppressing NF-κB and its products (c-Myc, COX-2, MMP-9)	[64]
Prostate	Decreasing the expression of AQP1 *	[71]
Melanoma	Inhibiting the expression of MMP-13 Reducing cell adhesion, invasion and angiogenesis *	[50,67,70]
	Decreasing the expression of HDAC3 ◊	[63]
Lung	Inhibiting TGF-β1 Inactivating proteins involved in EMT (MMP-2, p38 MAPK and Smad2) ◊	[29]
	Downregulating FUT4 and EGFR mediated migration (through MAPK and NF-κB) ◊	[62]
Endothelial progenitor cells	Decreasing the activation of the VEGF dependent p38/ERK signalling	[56]
Esophageal and renal	Decreasing the expression of VEGF Inhibiting other signalling pathways of HIF-1α, COX-2, NF-κB, STAT3 and MAPKs	[55]

4.4. Aquaporin (AQP) 1—a Putative Target of Rg3

One suggested mechanism of action of Rg3 is by targeting AQP1 [71]. This molecule has roles in tumor growth, angiogenesis [94–96], metastasis [97,98], acquired resistance in tumors [99], and is highly expressed in aggressive tumors [100]. AQP1 is a member of the family of AQP membrane channels which are primarily known for their role in water transport across the lipophilic cell membrane. AQP1 was the first of the 13 members of the AQP proteins to be discovered [95,101,102]. It is a unique AQP in that, as well as acting as a water channel, it has a second function of transporting single charged cations, regulated by cGMP gating. AQP1 also transports gases such as nitric oxide, carbon dioxide, and ammonia (Figure 4) [102–105]. Rg3 was found to inhibit expression of AQP1 at both the mRNA and protein levels. Further, in a prostate cancer cell line (PC-3M), Rg3 (up to 10 μM) did not affect cell proliferation but inhibited cell migration in a transwell assay. Overexpression of AQP1 in this cell line attenuated the effect of Rg3 in inhibiting migration while silencing AQP1 gene via shRNA resulted in reduced PC-3M cell migration, and a diminished response to Rg3. These results indicated a critical role for AQP1 mediating the anti-migratory role of Rg3 [71]. This suggests that Rg3 targeting AQP1 could also be relevant in breast tumors.

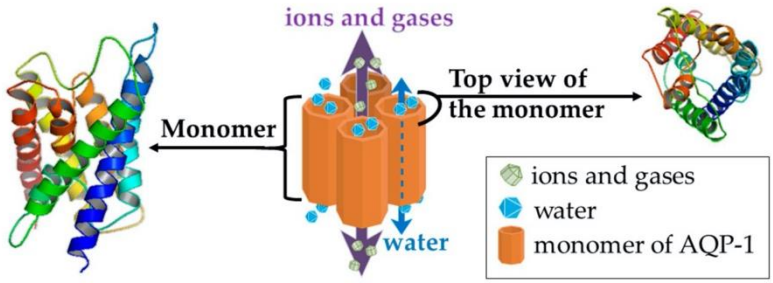

Figure 4. The structure of AQP1 channel, as a homotetramer, with the dashed arrow showing the water passage through the water channel of each monomer. The solid violet arrow represents the passage of ions and gases. The 3D structures were prepared in PyMol, version 1.7.4.5 (Schrödinger, Inc, Tokyo, Japan).

AQP1 and Breast Cancer

In vitro data suggest that stable overexpression of AQP1 in MCF-7 (ER^+ and PR^+) and MDA-MB-231 (TNBC) breast cancer cell lines significantly increases cell invasion and proliferation [106]. In HUVECs, expression of AQP1 is known to be upregulated by estrogen, because the promoter of the AQP1 gene has a functional estrogen response element (ERE) and the homodimerized complex of estrogen-ER can activate this ERE [107]. AQP1 is expressed in all microvasculature endothelial cells including HUVECs. In HUVECs, estrogen increased the proliferation, migration, invasion, and tube forming capacity, and these effects were inhibited by knockdown of AQP1 expression using siRNA [107]. Epidermal growth factor stimulation induced translocation of AQP1 from the cytoplasm to the cell membrane to enhance cell invasion [106]. AQP1 was also found to colocalize with ezrin, a cytoskeletal protein involved in the proliferation, cell adhesion, and NO production in the endothelial cells [107].

Animal studies show that AQP1 is highly expressed in mouse breast tumor [108], and AQP1-null mice show impaired angiogenesis [109]. In mouse models of breast carcinoma with lung metastasis, AQP1 deficiency decreased the expression of VEGFR2 leading to significantly reduced tumor mass and volume, microvasculature density, and the number of lung metastases [110].

In humans, AQP1 is abundantly expressed in the endothelium of many tissues [111] including the endothelium of tumor micro-vasculature, positive for CD31 [100,107]. In normal breast tissues, the expression of AQP1 is low and limited to the ducts, lymphatics and connective tissue microvessels [112]. Breast cancer is one of the tumors with increased microvessels and angiogenesis compared to its matched normal tissue and there is an increased AQP1 expression in the microvasculature of breast tumor [112,113]. Breast tumors of basal-like TNBC subtype and advanced breast tumors have higher levels of AQP1 expression compared to normal tissues [112–114]. Benign breast lesions and ductal carcinoma in situ samples express AQP1 on the membrane of myoepithelial cells of the ducts, but the majority of invasive ductal carcinoma samples predominantly express AQP1 in the cytoplasm [106,115]. So far, studies have shown that membrane AQP1 expression is associated with triple-negativity, expression of cytokeratin 14 and smooth muscle actin, higher tumor grade, medullary-like histology and poor clinical prognosis [113,114]. High AQP1 expression was found to be an independent prognostic factor in the high-grade subgroup, in the ER-negative subgroup and in the node-negative subgroup [114]. Cytoplasmic expression of APQ1 is correlated with lymph node metastasis and advanced features of invasive ductal carcinoma [106].

4.5. Other Suggested Mechanisms of Action

Rg3, when orally administered to mice bearing lung tumors, had immunomodulatory effects, causing increased splenocyte proliferation [72]. It also increased genotoxicity in osteosarcoma cell lines, through increased DNA damage and double-strand breaks [75]. This compound sensitized lung cancer tumors to radiation via suppressing the activation of NF-κB and the proteins regulated by this transcription factor (such as COX2, MMP-9, VEGF, c-Myc, and cyclin D1), which are either induced by radiation or are involved in radio-resistance [73].

Table 3. Suggested effects of Rg3 in combination with chemotherapy agents in in vitro and in vivo models.

Studied Model	Drug Combination	Effects	Reference
Lewis lung cancer mouse model	Rg3 + cyclophosphamide (continuous low-dose)	Less toxicity induced by capecitabine Longer animal survival Reduced susceptibility to drug resistance Increased anti-angiogenic activity	[82]
Mouse model	20(S)-Rg3 + cyclophosphamide	Inhibiting cyclophosphamide-induced DNA damages in the peripheral lymphocyte cells and bone marrow cells Reducing number of apoptotic cells of mice and improving the anti-oxidative markers in mice (such as SOD, MDA and GPX)	[83]
Mouse bearing hepatocellular carcinoma model	Rg3 + cyclophosphamide	Alteration of the expression of Bcl-2 family and induction of intrinsic pathway of apoptosis Prolonging mouse survival	[39]
Mouse bearing lung tumor model	Rg3 + gemcitabin	Enhancing the efficacy of gemcitabine on suppressing tumor growth Increasing the quality of life Prolonging mice survival Increasing tumor's necrosis rate Decreasing VEGF expression, microvessel density (assessed by the expression of CD31) and arterial blood flow in tumors such as peak systolic velocity	[84]
Glioma cell line	Rg3 + temozolomide	Inducing cell cycle arrest and apoptosis Attenuating the expression of VEGF-a and Bcl-2	[85]
Glioma allograft model of mouse	Rg3 + temozolomide	Antiangiogenic effect (reduced relative cerebral blood volume, VEGF levels and microvessel density) Improving the antiangiogenic effects of temozolomide No additive effect on tumor growth	[85]
Mouse bearing colon tumor	Rg3 + cisplatin	Improving anti-cancer effects of cisplatin Inhibiting tumor growth Reducing the toxicities of cisplatin (decreasing the intracellular levels of ROS)	[86]
Kidney, liver and colon resistant cancer cells	Rg3 + cisplatin	Decreasing the high levels of etoxifying enzymes such as heme-oxygenase (HO-1) and NAD(P)H quinone oxidoreductase (NQO-1)	[86]
Cisplatin-resistant bladder tumor cell lines	Rg3 + cisplatin	Synergistic effect in inhibiting the proliferation (possibly through activating the intrinsic apoptosis pathway (decreased Bcl-2 and increased cytochrome c and caspase-3) and cell cycle alterations in G2/M phase)	[87]
Mouse bearing oesophageal squamous cell carcinoma	Rg3 + cisplatin	Enhancing the inhibitory effects of cisplatin Reducing the proliferation of cancer cells Decreasing the microvascular density of the tumors	[88]
Colon cancer cell lines	Rg3 + docetaxel	Sensitizing the cells to the docetaxel Improving its apoptotic effect (via inhibiting NF-κB and the expression of anti-apoptotic proteins such as Bcl-2, XIAP, and ciap-1) Increasing the expression of pro-apoptotic proteins (such as Bax, caspase-3 and -9)	[89]
Prostate cancer cell lines	Rg3 + docetaxel	Inhibiting cell growth Inducing apoptosis and its associated protein Arresting the cells at G0/G1 Modulating cell cycle-associated proteins Inhibiting the activity of NF-κB	[90]

Table 3. *Cont.*

Studied Model	Drug Combination	Effects	Reference
Prostate cancer cell lines	Rg3 + docetaxel + cisplatin	More effective inhibition of the activity of NF-κB and cell growth	[90]
Mouse bearing hepatocellular tumor	20(S)-Rg3 + doxorubicin	Suppressing the autophagy via regulating autophagy-associated proteins Inhibiting autophagic flux	[91]
Rat model	Rg3 + doxorubicin	Synergistic effects in inhibiting tumor growth Reducing doxorubicin-induced cardiotoxicity (by improving the ejection fraction, fractional shortening and left ventricular outflow) Improving the oxidative damage and apoptosis induced by doxorubicin (via the activation of Akt and the Nrf2-ARE pathway)	[92]
NCI-H1299 lung cancer cells	Rg3 + As2O3	Inhibiting the proliferation of NCI-H1299 lung cancer cells	[93]
Mouse bearing lung tumors	Rg3 + As2O3	Promoting apoptosis in tumor cells Prolonging the survival of the mice	[93]

5. Metabolism and Pharmacokinetics of Rg3

Together with the clinical trials, it is pertinent to consider the pharmacokinetics of Rg3 following oral administration. So far, various studies have focused on the metabolism and pharmacokinetics of Rg3, as a general compound, and 20(R)-Rg3 in in vitro, animal models and healthy human volunteers. It is not yet clarified whether the metabolism of 20(S)- and 20(R)-Rg3 differ in any aspects. The general understanding is that following oral administration, ginsenosides undergo a partial or complete hydrolysis in the acidic conditions of the stomach and the intestinal microbial flora [116,117]. Rg3, like other protopanaxadiol ginsenosides, can lose a sugar moiety following metabolism by the anaerobic intestinal bacteria [118]. Compound K, the final metabolite of the metabolism of ginsenosides can be detected in human plasma after seven hours post-ingestion [118].

In vitro studies have shown that Rg3 has interactions with isoenzymes of cytochrome P450. Rg3 can weakly inhibit CYP3A4, moderately inhibit CYP2C19 and CYP1A2, and potently inhibit CYP2D4 [119] and so interactions between Rg3 and the drugs that are mainly metabolized with these isoenzymes should be considered. Also, incubation of Rg3 with human fecal microflora resulted in the formation of ginsenoside Rh2 [120], another member of the ginsenoside family with anticancer properties [121]. Studies in dogs however failed to detect any Rh2 in the plasma samples following oral or intravenous (IV) administration of 20(R)-Rg3 [122]. Although in vitro studies suggest that deglycosylation is one of the main pathways of the metabolism of Rg3, this study failed to show existence of such molecules in dog plasma samples [122]. This study also suggested a low degree of metabolism of 20(R)-Rg3, as evidenced by the maximum of 70% of 20(R)-Rg3 recovered from bile [122].

In rats, deglycosylation and oxygenation are reported as two major routes of metabolism for 20(R)-Rg3 [123]. The half-life of Rg3 in rats after an intravenous administration is reported to be 14 min [124] and 18.5 min [123]. The difference between these two reports might be due to the difference in the solubilisation of Rg3, however, both suggest a rapid rate of metabolic clearance for this molecule. Absolute bioavailablility of Rg3 in rats was about 2.63% [125].

Intra-species differences seem to play an important role in the metabolism and pharmacokinetics of Rg3, since in healthy human volunteers, Rg3 can be detected in the plasma for 8 [126,127] and up to 216 hours [126], following oral and intramuscular (IM) administration, respectively.

The epimers of Rg3 also differ in terms of tissue distribution. 20(S)-Rg3, following oral administration of 68 mg/kg to Sprague–Dawley rats was more concentrated in the gastrointestinal tissues compared to the plasma. It was also highly distributed in the liver, with the concentration being four and three times the plasma concentration at two and four hours, respectively. The concentration of Rg3 in other tissues such as muscle, spleen, lung, and fat was similar or lower than plasma concentration and trace amounts were detected in the brain, heart, and kidney. However, 20(R)-Rg3

was only localized in liver and the gastrointestinal tract, and not detected in the plasma [128]. Table 4 summarizes the results of the studies on the pharmacokinetics of Rg3 in animal models and human trials.

Table 4. A summary of the studies on the pharmacokinetics of Rg3 and the 20(R) epimer in in vivo models.

Ginsenoside	Model	Route	Dose	Sample	Detected Rg3	Outcomes	Reference
Rg3	Sprague–Dawley rats	IV	1 mg/kg	Plasma	Detected for 12 h	$t_{1/2\alpha}$: 0.12 ± 0.03 h $t_{1/2\beta}$: 2.09 ± 0.50 h	[125]
		Oral	10 mg/kg	Plasma	Detected for 12 h		
	Healthy humans	Oral	3.2 mg/kg	Plasma	Detected for 8 h	C_{max}: 15.67 ± 6.14 ng/mL t_{max}: 0.66 ± 0.01 h	[129]
	Healthy humans	IM	10, 30 and 60 mg	Plasma	Detected for 216 h		[126]
	Sprague–Dawley rats	IV	5 mg/kg	Plasma	Detected for 1.5 h	$t_{1/2}$: 14 min	[124]
				Urine	Not detected		
		Oral	50 mg/kg	Urine	Not detected in 1 h	rapid GI metabolism	
				Plasma	Not detected in 1 h		
20(R)-Rg3	Dogs	IV	0.3 mg/kg	Plasma	Detected for 12 h	$t_{1/2}$: 1.71 (± 0.11) h	[122]
		Oral	2 mg/kg	Plasma	Detected for 24 h	$t_{1/2}$: 5.99 (± 1.16) h	
	Sprague–Dawley rats	IV	5 mg/kg, within 1 min	Plasma	Detected for 1.5 h	$t_{1/2}$: 18.5 min	[123]
				Urine	Not detectable	N/A	
		Oral	100 mg/kg	Plasma	Not detectable		
				Urine	Not detectable	N/A	
				Feces	6 different deglycosylated and oxygenated metabolites		
	Healthy humans	Oral	3.2 mg/kg	Plasma	Detected for 8 h	t_{max}: 0.66 ± 0.10 h C_{max}: 1± 6 ng/mL $t_{1/2\alpha}$: 0.46 ± 0.12 h $t_{1/2\beta}$: 4.9 1.1 h $t_{1/2(Ka)}$: 0.28 ± 0.04 h	[127]

6. Clinical Trials

6.1. Application and Safety of Ginseng Extract on Healthy Human Volunteers

Studies on healthy human volunteers suggest that administration of the total extract of *Panax ginseng* C.A. Meyer is well tolerated and does not cause serious adverse reactions [130,131]. In a randomized, double-blind, placebo-controlled trial investigating the anti-oxidant properties of the total extract, 82 healthy volunteers received either placebo (n = 27), 1 or 2 g/day (n = 27 and n = 28, respectively) for a month [130]. Of the 82 volunteers, 80 completed the trial; only two, both female, randomized to receive 2 g/day of the total extract withdrew, one due to insomnia and palpitations after seven days, and the other due to non-health related reasons. Administration of the total extract improved the serum levels of anti-oxidant markers. In another randomized, double-blind, placebo-controlled trial investigating the anti-oxidant effects in postmenopausal women, 41 volunteers received placebo and 41 received 1 g of the extract thrice daily for 12 weeks [131]. Five volunteers receiving placebo and six receiving the extract failed to complete the trial. Administration of the total extract increased the enzyme activity of the serum antioxidant, superoxide dismutase, suggesting that the total extract may reduce oxidative stress in postmenopausal women. At this dose, reported side effects included dizziness, sleeplessness, nervousness, and uterine bleeding [131]. Adverse effects following administration of 1 or 2 g/day of total extract of ginseng to healthy subjects for a month were reported to be mild (constipation and dyspepsia, insomnia, and hot flash) and it was concluded that this extract does not cause serious adverse reactions and is safe and tolerable [132].

6.2. Clinial Trials and Application of Rg3 in Cancer Patients

Presently, there are only three published clinical trials utilizing Rg3 in the treatment of cancer; two on non-small cell lung carcinoma (NSCLC) [95] [96] and one on hepatocellular carcinoma

(HCC) [99]. In the first study, a total of 133 patients with stage II-III NSCLC received either Rg3 alone (43 cases), Rg3 + chemotherapy (46 cases), or chemotherapy alone (44 cases) [133]. Rg3 was administered twice a day (0.8 mg/kg, equivalent to 40–50 mg/day) for at least 6 months. This study showed that Rg3 + chemotherapy improved the 3-year survival rates compared to either Rg3 or chemotherapy alone (54.3% versus either 46.5% or 47.7%, respectively; $p > 0.05$). In patients expressing VEGF, chemotherapy treatment alone resulted in decreased 3-year survival rates compared to patients with negative VEGF expression ($p < 0.01$); however, there were no significant differences for the other two groups. In addition, patients that received Rg3 had a lower incidence of adverse effects and better immune system function, as evidenced by the increased activity of NK cells and $CD4^+$ T cells and the normal ratio of $CD4^+/CD8^+$ T cells [133]. This suggests that the option of combining Rg3 therapy with immunotherapy would be worth investigating.

In the second study, 124 patients with advanced (stage III-IV), unresectable NSCLC with EGFR mutations were divided into two groups receiving a tyrosine kinase inhibitor (TKI) + Rg3 (20 mg orally for at least 2 months) or TKI alone [134]. The results of this study demonstrated that Rg3 improved the median progression-free survival by 2.5 months ($p = 0.049$). Rg3 delayed the acquired resistance to TKI and had a low toxicity profile, with rash being the worst side effect in both groups and nausea, diarrhea, and anorexia being the most common side effects in both groups [134].

In the third study, 228 patients diagnosed with advanced (Barcelona clinic liver cancer-stage C) HCC were randomized in two groups, to receive trans-arterial chemoembolization (TACE) alone or in combination with Rg3 (20 mg, twice a day, orally) [135]. TACE is a successful method for delivering chemotherapy directly to the tumor within the liver which prolongs patient survival, but its application is limited by high recurrence rate, in part due to inflammatory factors promoting metastasis of the tumor. Inflammation and angiogenesis are associated phenomena in that pro-inflammatory cytokines such as IL-1ß or TNF-α released from activated neutrophils and macrophages cause vasculature modifications, enhancing proliferation of endothelial cells and hyper-neovascularization [136,137]. Hence, using an anti-angiogenic drug should limit this adverse effect. This study showed that the patients receiving TACE + Rg3 had longer median overall survival compared to those who received TACE alone (13.2 versus 10 months; $p = 0.002$), while there was no significant difference in progression free survival. Rg3 was well-tolerated, the reported adverse effects being grade 1 or 2 constipation, epistaxis, and hypertension, and importantly, Rg3 treatment tended to alleviate adverse effects related to TACE [135].

7. Conclusions

So far, many studies have shown the effects of Rg3 in different cancer models with fewer studies in human clinical trials. A limited number of studies have focused on the effects of Rg3 in breast cancer models and more specifically in advanced breast cancer. Out of the six studies on the effects of Rg3 in breast cancer, only one study has focused on the effects of an isomer, 20(S)-Rg3, and its in vivo effects in mice in increasing the efficacy of oral paclitaxel [79]. The rest of these studies used Rg3 as a whole compound [30,31,69,81,138]. In some cases, the source of the Rg3 used is self-produced, and of unknown purity [30,31]. Given the fact that Rg3 can have stereospecific activities [24,28,29], a mixture of two enantiomers, with unknown ratios of each enantiomer, cannot scientifically justify the resulting effects. With this view, stereospecific activity of Rg3 in human breast cancer models, including cell lines and patient tumor-derived cancer cells, in 2D and 3D in vitro models, and in vivo, is not known. Furthermore, considering the importance of AQP1 in angiogenesis and the invasiveness of tumors, together with evidence of survival benefit from clinical trials, the selectivity of Rg3 in targeting AQP1 in metastatic breast tumors should be studied.

Funding: This research received no external funding.

Conflicts of Interest: The authors declare no conflict of interest.

References

1. Giuliano, A.E.; Connolly, J.L.; Edge, S.B.; Mittendorf, E.A.; Rugo, H.S.; Solin, L.J.; Weaver, D.L.; Winchester, D.J.; Hortobagyi, G.N. Breast cancer—Major changes in the American Joint Committee on Cancer eighth edition cancer staging manual. *CA Cancer J. Clin.* **2017**, *67*, 290–303. [CrossRef] [PubMed]
2. Eckstein, N. Platinum resistance in breast and ovarian cancer cell lines. *J. Exp. Clin. Cancer Res.* **2011**, *30*, 1. [CrossRef] [PubMed]
3. Cronin, K.A.; Harlan, L.C.; Dodd, K.W.; Abrams, J.S.; Ballard-Barbash, R. Population-based estimate of the prevalence of HER-2 positive breast cancer tumors for early stage patients in the US. *Cancer Investig.* **2010**, *28*, 963–968. [CrossRef] [PubMed]
4. Fischer, O.M.; Streit, S.; Hart, S.; Ullrich, A. Beyond herceptin and gleevec. *Curr. Opin. Chem. Biol.* **2003**, *7*, 490–495. [CrossRef]
5. Elias, A.D. Triple-negative breast cancer: A short review. *Am. J. Clin. Oncol.* **2010**, *33*, 637–645. [CrossRef] [PubMed]
6. Eisenberg, S. Systemic Therapy. In *Breast Cancer*; Mahon, S.M., Ed.; Oncology Nursing Society: Pittsburgh, PA, USA, 2011.
7. Anders, C.K.; Carey, L.A. Biology, metastatic patterns, and treatment of patients with triple-negative breast cancer. *Clin. Breast Cancer* **2009**, *9*, S73–S81. [CrossRef] [PubMed]
8. Robert, N.; Leyland-Jones, B.; Asmar, L.; Belt, R.; Ilegbodu, D.; Loesch, D.; Raju, R.; Valentine, E.; Sayre, R.; Cobleigh, M. Randomized phase III study of trastuzumab, paclitaxel, and carboplatin compared with trastuzumab and paclitaxel in women with HER-2–overexpressing metastatic breast cancer. *J. Clin. Oncol.* **2006**, *24*, 2786–2792. [CrossRef] [PubMed]
9. Attele, A.S.; Wu, J.A.; Yuan, C.-S. Ginseng pharmacology: Multiple constituents and multiple actions. *Biochem. Pharmacol.* **1999**, *58*, 1685–1693. [CrossRef]
10. Park, J.D.; Rhee, D.K.; Lee, Y.H. Biological activities and chemistry of saponins from Panax ginseng CA Meyer. *Phytochem. Rev.* **2005**, *4*, 159–175. [CrossRef]
11. Park, H.J.; Kim, D.H.; Park, S.J.; Kim, J.M.; Ryu, J.H. Ginseng in traditional herbal prescriptions. *J. Ginseng Res.* **2012**, *36*, 225. [CrossRef] [PubMed]
12. Yang, M.S.; Wu, M.Y. Chinese ginseng. In *Nutraceuticals*; Elsevier: New York City, NY, USA, 2016; pp. 693–705.
13. Chang-Xiao, L.; Pei-Gen, X. Recent advances on ginseng research in China. *J. Ethnopharmacol.* **1992**, *36*, 27–38. [CrossRef]
14. Choi, K.-T. Botanical characteristics, pharmacological effects and medicinal components of Korean Panax ginseng CA Meyer. *Acta Pharmacol. Sin.* **2008**, *29*, 1109. [CrossRef] [PubMed]
15. Wang, C.-Z.; Aung, H.H.; Ni, M.; Wu, J.-A.; Tong, R.; Wicks, S.; He, T.-C.; Yuan, C.-S. Red American ginseng: Ginsenoside constituents and antiproliferative activities of heat-processed Panax quinquefolius roots. *Planta Med.* **2007**, *73*, 669. [CrossRef] [PubMed]
16. Sun, S.; Wang, C.-Z.; Tong, R.; Li, X.-L.; Fishbein, A.; Wang, Q.; He, T.-C.; Du, W.; Yuan, C.-S. Effects of steaming the root of Panax notoginseng on chemical composition and anticancer activities. *Food Chem.* **2010**, *118*, 307–314. [CrossRef]
17. Chang, Y.H.; Ng, P.K. Effects of Extrusion process variables on extractable ginsenosides in wheat-ginseng extrudates. *J. Agric. Food Chem.* **2009**, *57*, 2356–2362. [CrossRef] [PubMed]
18. Ren, G.; Chen, F. Degradation of ginsenosides in American ginseng (Panax quinquefolium) extracts during microwave and conventional heating. *J. Agric. Food Chem.* **1999**, *47*, 1501–1505. [CrossRef] [PubMed]
19. Kang, D.-I.; Lee, J.-Y.; Yang, J.-Y.; Jeong, S.M.; Lee, J.-H.; Nah, S.-Y.; Kim, Y. Evidence that the tertiary structure of 20 (S)-ginsenoside Rg 3 with tight hydrophobic packing near the chiral center is important for Na+ channel regulation. *Biochem. Biophys. Res. Commun.* **2005**, *333*, 1194–1201. [CrossRef] [PubMed]
20. Qi, L.-W.; Wang, C.-Z.; Yuan, C.-S. Ginsenosides from American ginseng: Chemical and pharmacological diversity. *Phytochemistry* **2011**, *72*, 689–699. [CrossRef] [PubMed]
21. Jeong, S.M.; Lee, J.-H.; Kim, J.-H.; Lee, B.-H.; Yoon, I.-S.; Lee, J.-H.; Kim, D.-H.; Rhim, H.; Kim, Y.; Nah, S.-Y. Stereospecificity of Ginsenoside Rg 3 Action on Ion Channels. *Mol Cells* **2004**, *18*, 383–389. [PubMed]
22. Kim, J.-H.; Lee, J.-H.; Jeong, S.M.; Lee, B.-H.; Yoon, I.-S.; Lee, J.-H.; Choi, S.-H.; Kim, D.-H.; Park, T.-K.; Kim, B.-K. Stereospecific effects of ginsenoside Rg3 epimers on swine coronary artery contractions. *Biol. Pharm. Bull.* **2006**, *29*, 365–370. [CrossRef]

23. Lee, Y.J.; Kim, H.Y.; Kang, K.S.; Lee, J.G.; Yokozawa, T.; Park, J.H. The chemical and hydroxyl radical scavenging activity changes of ginsenoside-Rb1 by heat processing. *Bioorg. Med. Chem. Lett.* **2008**, *18*, 4515–4520. [CrossRef] [PubMed]
24. Park, E.-H.; Kim, Y.-J.; Yamabe, N.; Park, S.-H.; Kim, H.-K.; Jang, H.-J.; Kim, J.H.; Cheon, G.J.; Ham, J.; Kang, K.S. Stereospecific anticancer effects of ginsenoside Rg3 epimers isolated from heat-processed American ginseng on human gastric cancer cell. *J. Ginseng Res.* **2014**, *38*, 22–27. [CrossRef] [PubMed]
25. Teng, S.; Wang, Y.; Li, P.; Liu, J.; Wei, A.; Wang, H.; Meng, X.; Pan, D.; Zhang, X. Effects of R type and S type ginsenoside Rg3 on DNA methylation in human hepatocarcinoma cells. *Mol. Med. Rep.* **2017**, *15*, 2029–2038. [CrossRef] [PubMed]
26. Wei, X.; Su, F.; Su, X.; Hu, T.; Hu, S. Stereospecific antioxidant effects of ginsenoside Rg3 on oxidative stress induced by cyclophosphamide in mice. *Fitoterapia* **2012**, *83*, 636–642. [CrossRef] [PubMed]
27. Wei, X.; Chen, J.; Su, F.; Su, X.; Hu, T.; Hu, S. Stereospecificity of ginsenoside Rg3 in promotion of the immune response to ovalbumin in mice. *Int. Immunol.* **2012**, *24*, 465–471. [CrossRef] [PubMed]
28. Wu, R.; Ru, Q.; Chen, L.; Ma, B.; Li, C. Stereospecificity of Ginsenoside Rg3 in the Promotion of Cellular Immunity in Hepatoma H22-Bearing Mice. *J. Food Sci.* **2014**, *79*, H1430–H1435. [CrossRef] [PubMed]
29. Kim, Y.-J.; Choi, W.-I.; Jeon, B.-N.; Choi, K.-C.; Kim, K.; Kim, T.-J.; Ham, J.; Jang, H.J.; Kang, K.S.; Ko, H. Stereospecific effects of ginsenoside 20-Rg3 inhibits TGF-β1-induced epithelial–mesenchymal transition and suppresses lung cancer migration, invasion and anoikis resistance. *Toxicology* **2014**, *322*, 23–33. [CrossRef] [PubMed]
30. Kim, B.-M.; Kim, D.-H.; Park, J.-H.; Na, H.-K.; Surh, Y.-J. Ginsenoside Rg3 induces apoptosis of human breast cancer (MDA-MB-231) cells. *J. Cancer Prev.* **2013**, *18*, 177. [CrossRef] [PubMed]
31. Kim, B.-M.; Kim, D.-H.; Park, J.-H.; Surh, Y.-J.; Na, H.-K. Ginsenoside Rg3 inhibits constitutive activation of NF-κB signaling in human breast cancer (MDA-MB-231) cells: ERK and Akt as potential upstream targets. *J. Cancer Prev.* **2014**, *19*, 23. [CrossRef]
32. Wu, K.; Li, N.; Sun, H.; Xu, T.; Jin, F.; Nie, J. Endoplasmic reticulum stress activation mediates Ginseng Rg3-induced anti-gallbladder cancer cell activity. *Biochem. Biophys. Res. Commun.* **2015**, *466*, 369–375. [CrossRef]
33. Aziz, F.; Wang, X.; Liu, J.; Yan, Q. Ginsenoside Rg3 induces FUT4-mediated apoptosis in H. pylori CagA-treated gastric cancer cells by regulating SP1 and HSF1 expressions. *Toxicol. In Vitro* **2016**, *31*, 158–166. [CrossRef] [PubMed]
34. Kim, B.J.; Nah, S.Y.; Jeon, J.H.; So, I.; Kim, S.J. Transient Receptor Potential Melastatin 7 Channels are Involved in Ginsenoside Rg3-Induced Apoptosis in Gastric Cancer Cells. *Basic Clin. Pharmacol. Toxicol.* **2011**, *109*, 233–239. [CrossRef] [PubMed]
35. Luo, Y.; Zhang, P.; Zeng, H.Q.; Lou, S.F.; Wang, D.X. Ginsenoside Rg3 induces apoptosis in human multiple myeloma cells via the activation of Bcl-2-associated X protein. *Mol. Med. Rep.* **2015**, *12*, 3557–3562. [CrossRef] [PubMed]
36. Shan, X.; Tian, L.L.; Zhang, Y.M.; Wang, X.Q.; Yan, Q.; Liu, J.W. Ginsenoside Rg3 suppresses FUT4 expression through inhibiting NF-κB/p65 signaling pathway to promote melanoma cell death. *Int. J. Oncol.* **2015**, *47*, 701–709. [CrossRef]
37. Choi, Y.J.; Lee, H.J.; Kang, D.W.; Han, I.H.; Choi, B.K.; Cho, W.H. Ginsenoside Rg3 induces apoptosis in the U87MG human glioblastoma cell line through the MEK signaling pathway and reactive oxygen species. *Oncol. Rep.* **2013**, *30*, 1362–1370. [CrossRef] [PubMed]
38. Joo, E.J.; Chun, J.; Ha, Y.W.; Ko, H.J.; Xu, M.-Y.; Kim, Y.S. Novel roles of ginsenoside Rg3 in apoptosis through downregulation of epidermal growth factor receptor. *Chem. Biol. Interact.* **2015**, *233*, 25–34. [CrossRef] [PubMed]
39. Jiang, J.-W.; Chen, X.-M.; Chen, X.-H.; Zheng, S.-S. Ginsenoside Rg3 inhibit hepatocellular carcinoma growth via intrinsic apoptotic pathway. *World J. Gastroenterol.* **2011**, *17*, 3605. [CrossRef]
40. Xie, Q.; Wen, H.; Zhang, Q.; Zhou, W.; Lin, X.; Xie, D.; Liu, Y. Inhibiting PI3K-AKt signaling pathway is involved in antitumor effects of ginsenoside Rg3 in lung cancer cell. *Biomed. Pharmacother.* **2017**, *85*, 16–21. [CrossRef]
41. Sun, H.Y.; Lee, J.H.; Han, Y.-S.; Yoon, Y.M.; Yun, C.W.; Kim, J.H.; Song, Y.S.; Lee, S.H. Pivotal roles of ginsenoside Rg3 in tumor apoptosis through regulation of reactive oxygen species. *Anticancer Res.* **2016**, *36*, 4647–4654. [CrossRef]

42. Li, Y.; Yang, T.; Li, J.; Hao, H.L.; Wang, S.Y.; Yang, J.; Luo, J.M. Inhibition of multiple myeloma cell proliferation by ginsenoside Rg3 via reduction in the secretion of IGF-1. *Mol. Med. Rep.* **2016**, *14*, 2222–2230. [CrossRef] [PubMed]
43. Lee, J.-Y.; Jung, K.H.; Morgan, M.J.; Kang, Y.-R.; Lee, H.-S.; Koo, G.-B.; Hong, S.-S.; Kwon, S.W.; Kim, Y.-S. Sensitization of TRAIL-induced cell death by 20 (S)-ginsenoside Rg3 via CHOP-mediated DR5 upregulation in human hepatocellular carcinoma cells. *Mol. Cancer Ther.* **2013**, *12*, 274–285. [CrossRef]
44. Zhang, C.; Liu, L.; Yu, Y.; Chen, B.; Tang, C.; Li, X. Antitumor effects of ginsenoside Rg3 on human hepatocellular carcinoma cells. *Mol. Med. Rep.* **2012**, *5*, 1295–1298. [PubMed]
45. Yuan, H.-D.; Quan, H.-Y.; ZHanG, Y.; KiM, S.H.; Chung, S.-H. 20 (S)-Ginsenoside Rg3-induced apoptosis in HT-29 colon cancer cells is associated with AMPK signaling pathway. *Mol. Med. Rep.* **2010**, *3*, 825–831. [PubMed]
46. Lee, S.Y.; Kim, G.T.; Roh, S.H.; Song, J.-S.; Kim, H.-J.; Hong, S.-S.; Kwon, S.W.; Park, J.H. Proteomic analysis of the anti-cancer effect of 20S-ginsenoside Rg3 in human colon cancer cell lines. *Biosci. Biotechnol. Biochem.* **2009**, *73*, 811–816. [CrossRef] [PubMed]
47. Zhang, F.; Li, M.; Wu, X.; Hu, Y.; Cao, Y.; Wang, X.A.; Xiang, S.; Li, H.; Jiang, L.; Tan, Z. 20 (S)-ginsenoside Rg3 promotes senescence and apoptosis in gallbladder cancer cells via the p53 pathway. *Drug Des. Devel. Ther.* **2015**, *9*, 3969. [PubMed]
48. Qiu, X.-M.; Bai, X.; Jiang, H.-F.; He, P.; Wang, J.-H. 20-(s)-ginsenoside Rg3 induces apoptotic cell death in human leukemic U937 and HL-60 cells through PI3K/Akt pathways. *Anticancer Drugs* **2014**, *25*, 1072–1080. [CrossRef]
49. Park, H.-M.; Kim, S.-J.; Kim, J.-S.; Kang, H.-S. Reactive oxygen species mediated ginsenoside Rg3-and Rh2-induced apoptosis in hepatoma cells through mitochondrial signaling pathways. *Food Chem. Toxicol.* **2012**, *50*, 2736–2741. [CrossRef] [PubMed]
50. Chen, J.; Peng, H.; Ou-Yang, X.; He, X. Research on the antitumor effect of ginsenoside Rg3 in B16 melanoma cells. *Melanoma Res.* **2008**, *18*, 322–329. [CrossRef]
51. Li, J.; Liu, T.; Zhao, L.; Chen, W.; Hou, H.; Ye, Z.; Li, X. Ginsenoside 20 (S)-Rg3 inhibits the Warburg effect through STAT3 pathways in ovarian cancer cells. *Int. J. Oncol.* **2015**, *46*, 775–781. [CrossRef]
52. Wang, J.-H.; Nao, J.-F.; Zhang, M.; He, P. 20 (s)-ginsenoside Rg3 promotes apoptosis in human ovarian cancer HO-8910 cells through PI3K/Akt and XIAP pathways. *Tumour Biol.* **2014**, *35*, 11985–11994. [CrossRef]
53. Zheng, X.; Chen, W.; Hou, H.; Li, J.; Li, H.; Sun, X.; Zhao, L.; Li, X. Ginsenoside 20 (S)-Rg3 induced autophagy to inhibit migration and invasion of ovarian cancer. *Biomed. Pharmacother.* **2017**, *85*, 620–626. [CrossRef] [PubMed]
54. He, B.-C.; Gao, J.-L.; Luo, X.; Luo, J.; Shen, J.; Wang, L.; Zhou, Q.; Wang, Y.-T.; Luu, H.H.; Haydon, R.C. Ginsenoside Rg3 inhibits colorectal tumor growth through the down-regulation of Wnt/ss-catenin signaling. *Int. J. Oncol.* **2011**, *38*, 437–445. [CrossRef] [PubMed]
55. Chen, Q.-J.; Zhang, M.-Z.; Wang, L.-X. Gensenoside Rg3 inhibits hypoxia-induced VEGF expression in human cancer cells. *Cell. Physiol. Biochem.* **2010**, *26*, 849–858. [CrossRef] [PubMed]
56. Kim, J.-W.; Jung, S.-Y.; Kwon, Y.-H.; Lee, J.-H.; Lee, Y.M.; Lee, B.-Y.; Kwon, S.-M. Ginsenoside Rg3 attenuates tumor angiogenesis via inhibiting bioactivities of endothelial progenitor cells. *Cancer Biol. Ther.* **2012**, *13*, 504–515. [CrossRef] [PubMed]
57. Wang, C.-Z.; Aung, H.H.; Zhang, B.; Sun, S.; Li, X.-L.; He, H.; Xie, J.-T.; He, T.-C.; Du, W.; Yuan, C.-S. Chemopreventive effects of heat-processed Panax quinquefolius root on human breast cancer cells. *Anticancer Res.* **2008**, *28*, 2545–2551. [PubMed]
58. Luo, X.; Wang, C.-Z.; Chen, J.; Song, W.-X.; Luo, J.; Tang, N.; He, B.-C.; Kang, Q.; Wang, Y.; Du, W. Characterization of gene expression regulated by American ginseng and ginsenoside Rg3 in human colorectal cancer cells. *Int. J. Oncol.* **2008**, *32*, 975–983. [CrossRef]
59. Sin, S.; Kim, S.Y.; Kim, S.S. Chronic treatment with ginsenoside Rg3 induces Akt-dependent senescence in human glioma cells. *Int. J. Oncol.* **2012**, *41*, 1669–1674. [CrossRef]
60. Kim, H.-S.; Lee, E.-H.; Ko, S.-R.; Choi, K.-J.; Park, J.-H.; Im, D.-S. Effects of ginsenosides Rg 3 and Rh 2 on the proliferation of prostate cancer cells. *Arch. Pharm. Res.* **2004**, *27*, 429. [CrossRef]
61. Shan, X.; Aziz, F.; Tian, L.L.; Wang, X.Q.; Yan, Q.; Liu, J.W. Ginsenoside Rg3-induced EGFR/MAPK pathway deactivation inhibits melanoma cell proliferation by decreasing FUT4/LeY expression. *Int. J. Oncol.* **2015**, *46*, 1667–1676. [CrossRef]

62. Tian, L.; Shen, D.; Li, X.; Shan, X.; Wang, X.; Yan, Q.; Liu, J. Ginsenoside Rg3 inhibits epithelial-mesenchymal transition (EMT) and invasion of lung cancer by down-regulating FUT4. *Oncotarget* **2016**, *7*, 1619. [CrossRef]
63. Shan, X.; Fu, Y.-S.; Aziz, F.; Wang, X.-Q.; Yan, Q.; Liu, J.-W. Ginsenoside Rg3 inhibits melanoma cell proliferation through down-regulation of histone deacetylase 3 (HDAC3) and increase of p53 acetylation. *PLoS ONE* **2014**, *9*, e115401. [CrossRef] [PubMed]
64. Junmin, S.; Hongxiang, L.; Zhen, L.; Chao, Y.; Chaojie, W. Ginsenoside Rg3 inhibits colon cancer cell migration by suppressing nuclear factor kappa B activity. *J. Tradit. Chin. Med.* **2015**, *35*, 440–444. [CrossRef]
65. Shinkai, K.; Akedo, H.; Mukai, M.; Imamura, F.; Isoai, A.; Kobayashi, M.; Kitagawa, I. Inhibition of in vitro tumor cell invasion by ginsenoside Rg3. *Cancer Sci.* **1996**, *87*, 357–362.
66. Tm, X.; Man-hua, C.; Xin, Y.; Lp, G. Inhibitory effect of ginsenoside Rg3 on ovarian cancer metastasis. *Chin. Med. J.* **2008**, *121*, 1394–1397.
67. Lee, S.G.; Kang, Y.J.; Nam, J.-O. Anti-metastasis effects of ginsenoside Rg3 in B16F10 cells. *J. Microbiol. Biotechnol.* **2015**, *25*, 1997–2006. [CrossRef]
68. Liu, T.; Zhao, L.; Zhang, Y.; Chen, W.; Liu, D.; Hou, H.; Ding, L.; Li, X. Ginsenoside 20 (S)-Rg3 targets HIF-1α to block hypoxia-induced epithelial-mesenchymal transition in ovarian cancer cells. *PLoS ONE* **2014**, *9*, e103887. [CrossRef]
69. Chen, X.-P.; Qian, L.-L.; Jiang, H.; Chen, J.-H. Ginsenoside Rg3 inhibits CXCR 4 expression and related migrations in a breast cancer cell line. *Int. J. Clin. Oncol.* **2011**, *16*, 519–523. [CrossRef] [PubMed]
70. Mochizuki, M.; Yoo, Y.; Matsuzawa, K.; Sato, K.; Saiki, I.; Tonooka, S.; Samukawa, K.; Azuma, I. Inhibitory effect of tumor metastasis in mice by saponins, ginsenoside-Rb2, 20 (R)-and 20 (S)-ginsenoside-Rg3, of red ginseng. *Biol. Pharm. Bull.* **1995**, *18*, 1197–1202. [CrossRef]
71. Pan, X.-Y.; Guo, H.; Han, J.; Hao, F.; An, Y.; Xu, Y.; Xiaokaiti, Y.; Pan, Y.; Li, X.-J. Ginsenoside Rg3 attenuates cell migration via inhibition of aquaporin 1 expression in PC-3M prostate cancer cells. *Eur. J. Pharmacol.* **2012**, *683*, 27–34. [CrossRef]
72. Park, D.; Bae, D.-K.; Jeon, J.H.; Lee, J.; Oh, N.; Yang, G.; Yang, Y.-H.; Kim, T.K.; Song, J.; Lee, S.H. Immunopotentiation and antitumor effects of a ginsenoside Rg3-fortified red ginseng preparation in mice bearing H460 lung cancer cells. *Environ. Toxicol. Pharmacol.* **2011**, *31*, 397–405. [CrossRef]
73. Wang, L.; Li, X.; Song, Y.M.; Wang, B.; Zhang, F.R.; Yang, R.; Wang, H.Q.; Zhang, G.J. Ginsenoside Rg3 sensitizes human non-small cell lung cancer cells to γ-radiation by targeting the nuclear factor-κB pathway. *Mol. Med. Rep.* **2015**, *12*, 609–614. [CrossRef] [PubMed]
74. Kwon, H.-Y.; Kim, E.-H.; Kim, S.-W.; Kim, S.-N.; Park, J.-D.; Rhee, D.-K. Selective toxicity of ginsenoside Rg 3 on multidrug resistant cells by membrane fluidity modulation. *Arch. Pharm. Res.* **2008**, *31*, 171–177. [CrossRef] [PubMed]
75. Zhang, Y.-H.; Li, H.-D.; Li, B.; Jiang, S.-D.; Jiang, L.-S. Ginsenoside Rg3 induces DNA damage in human osteosarcoma cells and reduces MNNG-induced DNA damage and apoptosis in normal human cells. *Oncol. Rep.* **2014**, *31*, 919–925. [CrossRef] [PubMed]
76. Guo, J.-Q.; Zheng, Q.-H.; Chen, H.; Chen, L.; Xu, J.-B.; Chen, M.-Y.; Lu, D.; Wang, Z.-H.; Tong, H.-F.; Lin, S. Ginsenoside Rg3 inhibition of vasculogenic mimicry in pancreatic cancer through downregulation of VE-cadherin/EphA2/MMP9/MMP2 expression. *Int. J. Oncol.* **2014**, *45*, 1065–1072. [CrossRef] [PubMed]
77. Yue, P.Y.; Wong, D.Y.; Wu, P.; Leung, P.; Mak, N.; Yeung, H.; Liu, L.; Cai, Z.; Jiang, Z.-H.; Fan, T. The angiosuppressive effects of 20 (R)-ginsenoside Rg3. *Biochem. Pharmacol.* **2006**, *72*, 437–445. [CrossRef] [PubMed]
78. Tang, H.; Ren, Y.; Zhang, J.; Ma, S.; Gao, F.; Wu, Y. Correlation of insulin-like growth factor-1 (IGF-1) to angiogenesis of breast cancer in IGF-1-deficient mice. *Ai Zheng* **2007**, *26*, 1215–1220. [PubMed]
79. Yang, L.Q.; Wang, B.; Gan, H.; Fu, S.T.; Zhu, X.X.; Wu, Z.N.; Zhan, D.W.; Gu, R.L.; Dou, G.F.; Meng, Z.Y. Enhanced oral bioavailability and anti-tumour effect of paclitaxel by 20 (s)-ginsenoside Rg3 in vivo. *Biopharm. Drug Dispos.* **2012**, *33*, 425–436. [CrossRef] [PubMed]
80. Kim, S.-W.; Kwon, H.-Y.; Chi, D.-W.; Shim, J.-H.; Park, J.-D.; Lee, Y.-H.; Pyo, S.; Rhee, D.-K. Reversal of P-glycoprotein-mediated multidrug resistance by ginsenoside Rg3. *Biochem. Pharmacol.* **2003**, *65*, 75–82. [CrossRef]
81. Zhang, Q.; Kang, X.; Yang, B.; Wang, J.; Yang, F. Antiangiogenic effect of capecitabine combined with ginsenoside Rg3 on breast cancer in mice. *Cancer Biother. Radiopharm.* **2008**, *23*, 647–654. [CrossRef]

82. Zhang, Q.; Kang, X.; Zhao, W. Antiangiogenic effect of low-dose cyclophosphamide combined with ginsenoside Rg3 on Lewis lung carcinoma. *Biochem. Biophys. Res. Commun.* **2006**, *342*, 824–828. [CrossRef]
83. Zhang, Q.H.; Wu, C.F.; Duan, L.; Yang, J.Y. Protective effects of ginsenoside Rg 3 against cyclophosphamide-induced DNA damage and cell apoptosis in mice. *Arch. Toxicol.* **2008**, *82*, 117–123. [CrossRef] [PubMed]
84. Liu, T.-G.; Huang, Y.; Cui, D.-D.; Huang, X.-B.; Mao, S.-H.; Ji, L.-L.; Song, H.-B.; Yi, C. Inhibitory effect of ginsenoside Rg3 combined with gemcitabine on angiogenesis and growth of lung cancer in mice. *BMC Cancer* **2009**, *9*, 250. [CrossRef] [PubMed]
85. Sun, C.; Yu, Y.; Wang, L.; Wu, B.; Xia, L.; Feng, F.; Ling, Z.; Wang, S. Additive antiangiogenesis effect of ginsenoside Rg3 with low-dose metronomic temozolomide on rat glioma cells both in vivo and in vitro. *J. Exp. Clin. Cancer Res.* **2016**, *35*, 32. [CrossRef] [PubMed]
86. Lee, C.K.; Park, K.-K.; Chung, A.-S.; Chung, W.-Y. Ginsenoside Rg3 enhances the chemosensitivity of tumors to cisplatin by reducing the basal level of nuclear factor erythroid 2-related factor 2-mediated heme oxygenase-1/NAD (P) H quinone oxidoreductase-1 and prevents normal tissue damage by scavenging cisplatin-induced intracellular reactive oxygen species. *Food Chem. Toxicol.* **2012**, *50*, 2565–2574. [PubMed]
87. Lee, Y.J.; Lee, S.; Ho, J.N.; Byun, S.-S.; Hong, S.K.; Lee, S.E.; Lee, E. Synergistic antitumor effect of ginsenoside Rg3 and cisplatin in cisplatin-resistant bladder tumor cell line. *Oncol. Rep.* **2014**, *32*, 1803–1808. [CrossRef] [PubMed]
88. Chang, L.; Huo, B.; Lv, Y.; Wang, Y.; Liu, W. Ginsenoside Rg3 enhances the inhibitory effects of chemotherapy on esophageal squamous cell carcinoma in mice. *Mol. Clin. Oncol.* **2014**, *2*, 1043–1046. [CrossRef] [PubMed]
89. Kim, S.M.; Lee, S.Y.; Yuk, D.Y.; Moon, D.C.; Choi, S.S.; Kim, Y.; Han, S.B.; Oh, K.-W.; Hong, J.T. Inhibition of NF-κB by ginsenoside Rg3 enhances the susceptibility of colon cancer cells to docetaxel. *Arch. Pharm. Res.* **2009**, *32*, 755–765. [CrossRef] [PubMed]
90. Kim, S.M.; Lee, S.Y.; Cho, J.S.; Son, S.M.; Choi, S.S.; Yun, Y.P.; Yoo, H.S.; Oh, K.-W.; Han, S.B.; Hong, J.T. Combination of ginsenoside Rg3 with docetaxel enhances the susceptibility of prostate cancer cells via inhibition of NF-κB. *Eur. J. Pharmacol.* **2010**, *631*, 1–9. [CrossRef] [PubMed]
91. Kim, D.-G.; Jung, K.H.; Lee, D.-G.; Yoon, J.-H.; Choi, K.S.; Kwon, S.W.; Shen, H.-M.; Morgan, M.J.; Hong, S.-S.; Kim, Y.-S. 20 (S)-Ginsenoside Rg3 is a novel inhibitor of autophagy and sensitizes hepatocellular carcinoma to doxorubicin. *Oncotarget* **2014**, *5*, 4438. [CrossRef] [PubMed]
92. Wang, X.; Chen, L.; Wang, T.; Jiang, X.; Zhang, H.; Li, P.; Lv, B.; Gao, X. Ginsenoside Rg3 antagonizes adriamycin-induced cardiotoxicity by improving endothelial dysfunction from oxidative stress via upregulating the Nrf2-ARE pathway through the activation of akt. *Phytomedicine* **2015**, *22*, 875–884. [CrossRef]
93. Che, J.-B.; Liu, Z.-H.; Ma, H.-B.; Li, Y.; Zhao, H.; Li, X.-H.; Liu, W.-C.; Shi, G.-N. Influence of As2O3 combined with ginsenosides Rg3 on inhibition of lung cancer NCI-H1299 cells and on subsistence of nude mice bearing hepatoma. *Asian Pac. J. Trop. Med.* **2014**, *7*, 772–775. [CrossRef]
94. Yool, A.J.; Brown, E.A.; Flynn, G.A. Roles for novel pharmacological blockers of aquaporins in the treatment of brain oedema and cancer. *Clin. Exp. Pharmacol. Physiol.* **2010**, *37*, 403–409. [CrossRef] [PubMed]
95. Yool, A.J. Functional domains of aquaporin-1: Keys to physiology, and targets for drug discovery. *Curr. Pharm. Des.* **2007**, *13*, 3212–3221. [CrossRef] [PubMed]
96. Dorward, H.S.; Du, A.; Bruhn, M.A.; Wrin, J.; Pei, J.V.; Evdokiou, A.; Price, T.J.; Yool, A.J.; Hardingham, J.E. Pharmacological blockade of aquaporin-1 water channel by AqB013 restricts migration and invasiveness of colon cancer cells and prevents endothelial tube formation in vitro. *J. Exp. Clin. Cancer Res.* **2016**, *35*, 36. [CrossRef] [PubMed]
97. Papadopoulos, M.; Saadoun, S.; Verkman, A. Aquaporins and cell migration. *Pflüg. Arch* **2008**, *456*, 693–700. [CrossRef] [PubMed]
98. Hu, J.; Verkman, A.; Hu, J.; Verkman, A. Increased migration and metastatic potential of tumor cells expressing aquaporin water channels. *FASEB J.* **2006**, *20*, 1892–1894. [CrossRef] [PubMed]
99. Wragg, J.W.; Heath, V.L.; Bicknell, R. Sunitinib treatment enhances metastasis of innately drug resistant breast tumors. *Cancer Res.* **2016**, *77*, 1008–1020. [CrossRef] [PubMed]
100. Verkman, A.; Hara-Chikuma, M.; Papadopoulos, M.C. Aquaporins—New players in cancer biology. *J. Mol. Med.* **2008**, *86*, 523–529. [CrossRef]

101. Agre, P.; Preston, G.M.; Smith, B.L.; Jung, J.S.; Raina, S.; Moon, C.; Guggino, W.B.; Nielsen, S. Aquaporin CHIP: The archetypal molecular water channel. *Am. J. Physiol. Ren. Physiol.* **1993**, *265*, F463–F476. [CrossRef]
102. Yool, A.J.; Campbell, E.M. Structure, function and translational relevance of aquaporin dual water and ion channels. *Mol. Asp. Med.* **2012**, *33*, 553–561. [CrossRef]
103. De Ieso, M.L.; Yool, A.J. Mechanisms of Aquaporin-Facilitated Cancer Invasion and Metastasis. *Front. Chem.* **2018**, *6*, 135. [CrossRef] [PubMed]
104. Campbell, E.M.; Birdsell, D.N.; Yool, A.J. The activity of human aquaporin 1 as a cGMP-gated cation channel is regulated by tyrosine phosphorylation in the carboxyl terminal domain. *Mol. Pharmacol.* **2011**, *81*, 97–105. [CrossRef] [PubMed]
105. Baetz, N.W.; Stamer, W.D.; Yool, A.J. Stimulation of aquaporin-mediated fluid transport by cyclic GMP in human retinal pigment epithelium in vitro. *Investig. Ophthalmol. Vis. Sci.* **2012**, *53*, 2127–2132. [CrossRef] [PubMed]
106. Qin, F.; Zhang, H.; Shao, Y.; Liu, X.; Yang, L.; Huang, Y.; Fu, L.; Gu, F.; Ma, Y. Expression of aquaporin1, a water channel protein, in cytoplasm is negatively correlated with prognosis of breast cancer patients. *Oncotarget* **2016**, *7*, 8143. [CrossRef] [PubMed]
107. Zou, L.-B.; Shi, S.; Zhang, R.-J.; Wang, T.-T.; Tan, Y.-J.; Zhang, D.; Fei, X.-Y.; Ding, G.-L.; Gao, Q.; Chen, C. Aquaporin-1 plays a crucial role in estrogen-induced tubulogenesis of vascular endothelial cells. *J. Clin. Endocrinol. Metab.* **2013**, *98*, E672–E682. [CrossRef] [PubMed]
108. Endo, M.; Jain, R.K.; Witwer, B.; Brown, D. Water channel (aquaporin 1) expression and distribution in mammary carcinomas and glioblastomas. *Microvasc. Res.* **1999**, *58*, 89–98. [CrossRef] [PubMed]
109. Saadoun, S.; Papadopoulos, M.C.; Hara-Chikuma, M.; Verkman, A. Impairment of angiogenesis and cell migration by targeted aquaporin-1 gene disruption. *Nature* **2005**, *434*, 786. [CrossRef]
110. Esteva-Font, C.; Jin, B.-J.; Verkman, A. Aquaporin-1 gene deletion reduces breast tumor growth and lung metastasis in tumor-producing MMTV-PyVT mice. *FASEB J.* **2014**, *28*, 1446–1453. [CrossRef]
111. Mobasheri, A.; Shakibaei, M.; Marples, D. Immunohistochemical localization of aquaporin 10 in the apical membranes of the human ileum: A potential pathway for luminal water and small solute absorption. *Histochem. Cell Biol.* **2004**, *121*, 463–471. [CrossRef]
112. Mobasheri, A.; Airley, R.; Hewitt, S.M.; Marples, D. Heterogeneous expression of the aquaporin 1 (AQP1) water channel in tumors of the prostate, breast, ovary, colon and lung: A study using high density multiple human tumor tissue microarrays. *Int. J. Oncol.* **2005**, *26*, 1149–1158. [CrossRef]
113. Shi, Z.; Zhang, T.; Luo, L.; Zhao, H.; Cheng, J.; Xiang, J.; Zhao, C. Aquaporins in human breast cancer: Identification and involvement in carcinogenesis of breast cancer. *J. Surg. Oncol.* **2012**, *106*, 267–272. [CrossRef] [PubMed]
114. Otterbach, F.; Callies, R.; Adamzik, M.; Kimmig, R.; Siffert, W.; Schmid, K.W.; Bankfalvi, A. Aquaporin 1 (AQP1) expression is a novel characteristic feature of a particularly aggressive subgroup of basal-like breast carcinomas. *Breast Cancer Res. Treat.* **2010**, *120*, 67–76. [CrossRef] [PubMed]
115. Zhang, B.; Liu, F.; Ma, Y.; Gu, F. Cytoplasmic expression of aquaporin-1 in breast cancer cells and its relationship with clinicopathological characteristics and prognosis. *Zhonghua Zhong Liu Za Zhi* **2013**, *35*, 904–909. [PubMed]
116. Kanaoka, M. Metabolism of ginseng saponins, ginsenosides, by human intestinal bacteria. *J. Trad. Med.* **1994**, *11*, 241–245.
117. Karikura, M.; Miyase, T.; Tanizawa, H.; Taniyama, T.; Takino, Y. Studies on absorption, distribution, excretion and metabolism of ginseng saponins. VII. Comparison of the decomposition modes of ginsenoside-Rb1 and-Rb2 in the digestive tract of rats. *Chem. Pharm. Bull.* **1991**, *39*, 2357–2361. [CrossRef] [PubMed]
118. Lee, J.; Lee, E.; Kim, D.; Lee, J.; Yoo, J.; Koh, B. Studies on absorption, distribution and metabolism of ginseng in humans after oral administration. *J. Ethnopharmacol.* **2009**, *122*, 143–148. [CrossRef] [PubMed]
119. Hao, M.; Zhao, Y.; Chen, P.; Huang, H.; Liu, H.; Jiang, H.; Zhang, R.; Wang, H. Structure-activity relationship and substrate-dependent phenomena in effects of ginsenosides on activities of drug-metabolizing P450 enzymes. *PLoS ONE* **2008**, *3*, e2697. [CrossRef]
120. Bae, E.-A.; Han, M.J.; Choo, M.-K.; Park, S.-Y.; Kim, D.-H. Metabolism of 20 (S)-and 20 (R)-ginsenoside Rg3 by human intestinal bacteria and its relation to in vitro biological activities. *Biol. Pharm. Bull.* **2002**, *25*, 58–63. [CrossRef]

121. Lu, J.-M.; Yao, Q.; Chen, C. Ginseng compounds: An update on their molecular mechanisms and medical applications. *Curr. Vasc. Pharmacol.* **2009**, *7*, 293–302. [CrossRef]
122. Li, K.; Chen, X.; Xu, J.; Li, X.; Zhong, D. Liquid chromatography/tandem mass spectrometry for pharmacokinetic studies of 20 (R)-ginsenoside Rg3 in dog. *Rapid Commun. Mass Spectrom.* **2005**, *19*, 813–817. [CrossRef]
123. Qian, T.; Cai, Z.; Wong, R.N.; Mak, N.K.; Jiang, Z.-H. In vivo rat metabolism and pharmacokinetic studies of ginsenoside Rg3. *J. Chromatogr. B* **2005**, *816*, 223–232. [CrossRef]
124. Cai, Z.; Qian, T.; Wong, R.N.; Jiang, Z.-H. Liquid chromatography–electrospray ionization mass spectrometry for metabolism and pharmacokinetic studies of ginsenoside Rg3. *Anal. Chim. Acta* **2003**, *492*, 283–293. [CrossRef]
125. Xie, H.-T.; Wang, G.-J.; Sun, J.-G.; Tucker, I.; Zhao, X.-C.; Xie, Y.-Y.; Li, H.; Jiang, X.-L.; Wang, R.; Xu, M.-J. High performance liquid chromatographic–mass spectrometric determination of ginsenoside Rg3 and its metabolites in rat plasma using solid-phase extraction for pharmacokinetic studies. *J. Chromatogr. B* **2005**, *818*, 167–173. [CrossRef] [PubMed]
126. Zhao, Q.; Zheng, X.; Jiang, J.; Zhou, H.; Hu, P. Determination of ginsenoside Rg3 in human plasma and urine by high performance liquid chromatography–tandem mass spectrometry. *J. Chromatogr. B* **2010**, *878*, 2266–2273. [CrossRef]
127. Huan, P.; Hailin, W.; Li, F.; Chengye, S. Pharmacokinetics of 20 (R)-Ginsenoside Rg3 in Human Volunteers. *JCPS* **2001**, *10*, 140–143.
128. Bae, S.H.; Park, J.B.; Zheng, Y.F.; Jang, M.J.; Kim, S.O.; Kim, J.Y.; Yoo, Y.H.; Yoon, K.D.; Oh, E.; Bae, S.K. Pharmacokinetics and tissue distribution of ginsenoside Rh2 and Rg3 epimers after oral administration of BST204, a purified ginseng dry extract, in rats. *Xenobiotica* **2014**, *44*, 1099–1107. [CrossRef] [PubMed]
129. Wang, H.; Zou, H.; Kong, L.; Zhang, Y.; Pang, H.; Su, C.; Liu, G.; Hui, M.; Fu, L. Determination of ginsenoside Rg3 in plasma by solid-phase extraction and high-performance liquid chromatography for pharmacokinetic study. *J. Chromatogr. B Biomed. Sci. Appl.* **1999**, *731*, 403–409. [CrossRef]
130. Kim, H.-G.; Yoo, S.-R.; Park, H.-J.; Lee, N.-H.; Shin, J.-W.; Sathyanath, R.; Cho, J.-H.; Son, C.-G. Antioxidant effects of Panax ginseng CA Meyer in healthy subjects: A randomized, placebo-controlled clinical trial. *Food Chem. Toxicol.* **2011**, *49*, 2229–2235. [CrossRef]
131. Seo, S.K.; Hong, Y.; Yun, B.H.; Chon, S.J.; Jung, Y.S.; Park, J.H.; Cho, S.; Choi, Y.S.; Lee, B.S. Antioxidative effects of Korean red ginseng in postmenopausal women: A double-blind randomized controlled trial. *J. Ethnopharmacol.* **2014**, *154*, 753–757. [CrossRef]
132. Lee, N.-H.; Yoo, S.-R.; Kim, H.-G.; Cho, J.-H.; Son, C.G. Safety and tolerability of Panax ginseng root extract: A randomized, placebo-controlled, clinical trial in healthy Korean volunteers. *J. Altern. Complement. Med.* **2012**, *18*, 1061–1069. [CrossRef]
133. Lu, P.; Su, W.; Miao, Z.-H.; Niu, H.-R.; Liu, J.; Hua, Q.-L. Effect and mechanism of ginsenoside Rg3 on postoperative life span of patients with non-small cell lung cancer. *Chin. J. Integr. Med.* **2008**, *14*, 33–36. [CrossRef] [PubMed]
134. Li, Y.; Wang, Y.; Niu, K.; Chen, X.; Xia, L.; Lu, D.; Kong, R.; Chen, Z.; Duan, Y.; Sun, J. Clinical benefit from EGFR-TKI plus ginsenoside Rg3 in patients with advanced non-small cell lung cancer harboring EGFR active mutation. *Oncotarget* **2016**, *7*, 70535. [CrossRef] [PubMed]
135. Zhou, B.; Yan, Z.; Liu, R.; Shi, P.; Qian, S.; Qu, X.; Zhu, L.; Zhang, W.; Wang, J. Prospective study of transcatheter arterial chemoembolization (TACE) with ginsenoside Rg3 versus TACE alone for the treatment of patients with advanced hepatocellular carcinoma. *Radiology* **2016**, *280*, 630–639. [CrossRef] [PubMed]
136. Szewczyk, G.; Rak, J.; Ruth, J.H. Inflammatory Mediators of Angiogenesis. *Med. Inflamm.* **2013**, *2013*, 610543. [CrossRef] [PubMed]

137. Naldini, A.; Carraro, F. Role of inflammatory mediators in angiogenesis. *Curr. Drug Targets Inflamm. Allergy* **2005**, *4*, 3–8. [CrossRef] [PubMed]
138. Yuan, Z.; Jiang, H.; Zhu, X.; Liu, X.; Li, J. Ginsenoside Rg3 promotes cytotoxicity of Paclitaxel through inhibiting NF-κB signaling and regulating Bax/Bcl-2 expression on triple-negative breast cancer. *Biomed. Pharmacother.* **2017**, *89*, 227–232. [CrossRef] [PubMed]

1.7 Statement of authorship

Statement of Authorship

Title of Paper	Anti-Angiogenic Properties of Ginsenoside Rg3
Publication Status	☑ Published ☐ Accepted for Publication ☐ Submitted for Publication ☐ Unpublished and Unsubmitted work written in manuscript style
Publication Details	Nakhjavani, M., Smith, E., Townsend, A. R., Price, T. J., & Hardingham, J. E. (2020). Anti-Angiogenic Properties of Ginsenoside Rg3. Molecules, 25(21), 4905.

Principal Author

Name of Principal Author (Candidate)	Maryam Nakhjavani		
Contribution to the Paper	Conceptualised, designed and prepared the Tables and Figures and substantially wrote the manuscript.		
Overall percentage (%)	70		
Certification:	This paper reports on original research I conducted during the period of my Higher Degree by Research candidature and is not subject to any obligations or contractual agreements with a third party that would constrain its inclusion in this thesis. I am the primary author of this paper.		
Signature		Date	10th Feb 2021

Co-Author Contributions

By signing the Statement of Authorship, each author certifies that:

i. the candidate's stated contribution to the publication is accurate (as detailed above);
ii. permission is granted for the candidate in include the publication in the thesis; and
iii. the sum of all co-author contributions is equal to 100% less the candidate's stated contribution.

Name of Co-Author	Eric Smith		
Contribution to the Paper	Contributed to drafting and reviewing the paper.		
Signature		Date	10th Feb 2021

Name of Co-Author	Amanda R Townsend		
Contribution to the Paper	Contributed to drafting and reviewing the paper.		
Signature		Date	11th Feb 2021

Name of Co-Author	Timothy J. Price		
Contribution to the Paper	Contributed to drafting and reviewing the paper.		
Signature		Date	11th Feb 2021

Name of Co-Author	Jennifer E. Hardingham		
Contribution to the Paper	Conceptualised and contributed to designing the paper, Figures and Tables, and drafting and reviewing.		
Signature		Date	10th Feb 2021

Please cut and paste additional co-author panels here as required.

molecules

MDPI

Review

Anti-Angiogenic Properties of Ginsenoside Rg3

Maryam Nakhjavani [1,2], Eric Smith [1,2], Amanda R. Townsend [2,3], Timothy J. Price [2,3] and Jennifer E. Hardingham [1,2,*]

1 Molecular Oncology, Basil Hetzel Institute for Translational Health Research, The Queen Elizabeth Hospital, Woodville South, SA 5011, Australia; maryam.nakhjavani@adelaide.edu.au (M.N.); eric.smith@adelaide.edu.au (E.S.)
2 Adelaide Medical School, University of Adelaide, Adelaide, SA 5005, Australia; amanda.townsend@sa.gov.au (A.R.T.); timothy.price@sa.gov.au (T.J.P.)
3 Medical Oncology Unit, The Queen Elizabeth Hospital, Woodville South, SA 5011, Australia
* Correspondence: jennifer.hardingham@adelaide.edu.au; Tel.: +61-8-8222-6142

Academic Editor: Deok-Chun Yang
Received: 24 June 2020; Accepted: 21 October 2020; Published: 23 October 2020

check for updates

Abstract: Ginsenoside Rg3 (Rg3) is a member of the ginsenoside family of chemicals extracted from *Panax ginseng*. Like other ginsenosides, Rg3 has two epimers: 20(S)-ginsenoside Rg3 (SRg3) and 20(R)-ginsenoside Rg3 (RRg3). Rg3 is an intriguing molecule due to its anti-cancer properties. One facet of the anti-cancer properties of Rg3 is the anti-angiogenic action. This review describes the controversies on the effects and effective dose range of Rg3, summarizes the evidence on the efficacy of Rg3 on angiogenesis, and raises the possibility that Rg3 is a prodrug.

Keywords: ginsenoside Rg3; 20(S)-ginsenoside Rg3; 20(R)-ginsenoside Rg3; angiogenesis; epimer

1. Introduction

The root of the plant *Panax ginseng* C.A. Meyer, commonly known as ginseng, has been used as a traditional medicine in Asian countries for thousands of years. It was primarily used as a food and source of energy and strength. Gradually several pharmacological effects of ginseng on immune function, cardiovascular system, neurological disorders and cancer treatment were discovered [1]. The major bioactive components of ginseng responsible for its pharmacological action are ginsenoside saponins. The general structure of ginsenosides is a four-ring steroid backbone with hydrophobic properties, which is connected to sugar molecules, responsible for the hydrophilicity of the molecule. Based on the positioning of hydrogen on carbon 20 (C20), ginsenosides have two stereoisomers; 20(S) and 20(R) epimers. Ginsenoside Rg3 (Rg3) is a member of the ginsenoside family of saponins, and like other members, Rg3 has two epimers, 20(S)-ginsenoside Rg3 (SRg3) and 20(R)-ginsenoside Rg3 (RRg3) (Figure 1).

Steam heating the white fresh ginseng for several hours prepares red ginseng which has improved pharmacological efficacy and is enriched for some ginsenosides including Rg3 [2,3]. This process produces mainly SRg3 as the major epimer. Furthermore, enzymatic hydrolysis [4,5] or alkali hydrolysis [6] are other methods of preparation of SRg3. However, production of RRg3 requires procedures that are more complex [7]. The quantity of Rg3 in red ginseng is very much dependent on the method of preparation and various methods have resulted in various contents, for example, 1.2 mg/mL Rg3 was recovered by *Phellinus linteus* fermentation method [8]. The steaming condition also results in different amounts of Rg3 as reported by different studies such as 25 μg/mL [9], 39 mg/g [2] or 0.28% *w/w* [10].

a

Epimer	A	B
20(S)-ginsenoside Rg3	CH_3	OH
20(R)-ginsenoside Rg3	OH	CH_3

b

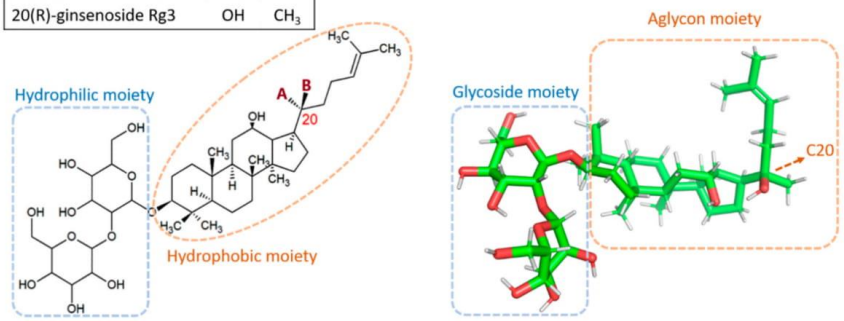

Figure 1. Structure of ginsenoside Rg3 as 2D (**a**) and 3D, generated in UCSF Chimera program (**b**), showing the chiral center at carbon 20, aglycone steroid-like backbone with hydrophobic properties and glycoside hydrophilic moiety, responsible for the water solubility of ginsenoside Rg3 (Rg3).

Rg3 is one of the most studied and pharmacologically active ginsenosides, with stereoselective activities by the epimers SRg3 and RRg3 [11,12]. The chemistry of Rg3 epimers could explain this stereoselective activity. For example, stereoselective activity of Rg3 epimers in interaction with Na^+ channels has been described [13]. Positioning of hydroxyl on C20 seems to play an important role in the pharmacological effects of Rg3. The alkene chain in the aglycone moiety of Rg3 (Figure 1) produces a tight hydrophobic packing near C20 which makes it inaccessible to water molecules, facilitates hydrophobic bonding between SRg3 and Na^+ ion channels and makes a more stabilized hydrogen binding between the two [13].

One of the important properties of Rg3 is its anti-cancer properties. The mechanisms of Rg3 in inhibition of proliferation, migration and invasion of cancer cells was reviewed previously [11]. Angiogenesis plays a major role in the growth and metastasis of a tumor and one of the important properties of Rg3 is its action on angiogenesis. This review paper aims to look at the different aspects of anti-angiogenic properties of Rg3, using PubMed as the search engine with Mesh terms ginsenoside Rg3 and angiogenesis for all published papers between 1995 and 2020. The first study demonstrating the anti-angiogenic properties of Rg3 was published by Mochizuki et al. in 1995 [14]. They showed in a mouse model of metastatic melanoma that 100 μg/mouse intravenous (i.v.) or 300 μg/mouse oral (p.o.) of either epimer inhibited the formation of vessels oriented towards the tumor mass. This animal study was, however, a short-term study (6 days), with only three mice per group. It was a remarkable study in the area since it not only demonstrated the anti-angiogenic potential of Rg3 in vivo, but also tested both epimers, separately [14]. This is especially important since most of the research published on Rg3 has not described which specific epimer was studied. Since then, several studies have been conducted in vitro and in vivo, which are reviewed here.

2. The Controversies on the Effects of Rg3 on Angiogenesis

Studying the proliferation and tube formation of human umbilical vein endothelial cells (HUVECs) on a layer of Matrigel is the mainstay of drug studies investigating anti-angiogenic properties. With Rg3, both of these aspects are a matter of controversy. A few studies have shown that the effective concentration of Rg3 for inhibition of loop formation was at nM ranges (Table 1) [15–19]. For example, RRg3 at 1–1000 nM inhibited tube-formation and chemotactic migration of HUVECs. At this concentration, RRg3 also decreased microvascular sprouting and hemoglobin content of tumors (in a Matrigel plug assay) [15]. Concentrations as low as 1.3 μM Rg3 (not as a specific epimer)

inhibited tube-forming capacity of HUVECs and hemoglobin content of Matrigel plugs [16]. At 60 and 300 ng/mL, Rg3 showed effectiveness in inhibition of differentiation of endothelial progenitor cells (EPCs) [18], though it did not inhibit the proliferation of these cells [17]. Although these studies showed the effectiveness of nM concentrations of Rg3, other studies tested higher doses at μM scale and in most cases showed anti-angiogenic properties. The exceptions are the studies that suggested Rg3 at μM concentrations was proangiogenic (Table 1) [20,21].

Table 1. Controversies on the proangiogenic or anti-angiogenic effects of Rg3 on endothelial cells.

	Epimer	Concentration	Tested Cell	Effect	Ref
Anti-angiogenic	RRg3	1–1000 nM	HUVEC	↓ tube-formation ↓ chemotactic migration ↓ microvascular sprouting ↓ hemoglobin content of tumors	[15]
	Rg3	1.3 μM	HUVEC	↓ tube-forming capacity ↓ hemoglobin content of Matrigel plugs	[16]
	Rg3	60–600 nm/mL	EPC	↓ expression of VEGF and VEGFR2 ↓ proliferation, migration and tube formation	[17]
	Rg3	60, 300 ng/mL	EPC	inhibition of differentiation	[18]
	RRg3	100 nM	HUVEC	↑ miR-520h ↓ EphB2 and EphB4 ↓ proliferation and loop formation	[19]
Pro-angiogenic	Rg3	1–10 μg/mL	ECV 304	↑ expression and phosphorylation of eNOS ↑ expression of PI3K, JNK, p38 MAPK ↑ gene transcription mediated by ER and GR ↑ CaMK-II and AMPK	[21]
	SRg3	15 μM	HUVEC	↑ proliferation (50%) ↑ DNA synthesis ↑ migration ↑ loop formation ↑ activation of ERK/Akt/eNOS ↑activation of PPARγ	[20]
	RRg3	15 μM	HUVEC	↑ proliferation (10%) ↑ loop formation	
Anti-angiogenic	RRg3	65 μM	HUVEC	↓ tube formation and migration ↓ protein and transcript expression of VEGF, b-FGF, MMP-2, MMP-9	[22]
	Rg3	180 μg/mL	HUVEC	↓ proliferation ↓ expression of VEGF and Bcl-2 S-phase cell cycle arrest	[23]

The study by Kwok et al. showed that 15 μM of SRg3 and RRg3 increased the rate of proliferation by 50 and 10%, respectively. Only SRg3 induced DNA synthesis (15 μM) and migration of HUVECs (15–30 μM). SRg3 and to a lower degree RRg3, increased loop formation in HUVECs. Exposing the cells with SRg3 and not RRg3 led to a prompt and continuous activation of extracellular signal-regulated kinase (ERK) followed by activation of Akt (phosphorylation at Ser473) and endothelial nitric oxide synthase (eNOS) (phosphorylation at Ser1177). It also showed that these two epimers, stereoselectively and with different potencies, interact with and activate peroxisome proliferator-activated receptor-gamma (PPARγ) [20]. PPARγ is one of the ligand-dependent transcriptional factors with polyunsaturated fatty acids as its endogenous ligands. One of the roles of

PPARγ is in regulating angiogenesis [20,24] and they showed that the activation of ERK/Akt/eNOS pathway by Rg3 is dependent on the activation of PPARγ. It is noteworthy that in this study, instead of vascular endothelial growth factor (VEGF) as a supplement for the growth of HUVECs, fetal bovine serum was used. This might explain the observed controversy in the literature (see Section 3).

Other studies showed anti-angiogenic effects of Rg3 at μM range. At 65 μM, Rg3 inhibited tube formation and migration. This inhibition was associated with decreased protein and transcript expression of vascular endothelial growth factor (VEGF), basic fibroblast growth factor (b-FGF) and matrix metalloproteinase-2 (MMP-2) and protein expression of MMP-9 [22]. The anti-angiogenic properties of Rg3 were also studied in combination with temozolomide. Temozolomide is one of the effective drugs to improve survival rate and progression-free survival of glioblastoma patients. In a study by Sun et al., the in vitro data suggested that the combination of the oral chemotherapeutic temozolomide (10 μg/mL) and Rg3 (10 μg/mL) had additive effects on inhibition of HUVEC proliferation [23]. At 180 μg/mL, temozolomide and 180 μg/mL Rg3 (144 h), inhibition of proliferation was observed in HUVECs. This combination also decreased the transcript expression of VEGF and Bcl-2, a regulator of apoptosis that inhibits the function of proapoptotic proteins, in HUVECs [23].

Other than the reported controversy about the pro- or anti-angiogenic effect of Rg3 at μM range, some studies have not shown an anti-proliferative effect of Rg3 on HUVECs. For example, 50 μg/mL Rg3 did not inhibit the proliferation of HUVECs within 72 h [22] and the anti-proliferative effect at 1–1000 nM, while significant, was very weak and not dose-dependent [15]. A time- and dose-dependent inhibition of proliferation of HUVECs was reported with Rg3 (0–180 μg/mL). At 180 μg/mL (144 h) about 28% inhibition of proliferation was observed. Rg3 at these concentrations induced S-phase cell cycle arrest (not time-dependent). Exposure of HUVECs for 72 h to Rg3 (80 μg/mL) decreased the expression of VEGF and Bcl-2 [23].

3. Pharmacodynamic Aspects of the Effect of Rg3 on Angiogenesis

To address the question about controversies on the effects of Rg3 on angiogenesis at various concertation ranges, the possible explanations might depend on the pharmacodynamics of the interaction of Rg3 with its receptors. VEGF is the main ligand to its receptor, VEGFR2, the interaction of which plays the key role in angiogenesis. Any full agonist binds to the same binding site of VEGF on VEGFR2 and mimics the action of VEGF, leading to a maximal effect (Emax).

One possible explanation could be that Rg3 might be a partial agonist at nM concentrations. A partial agonist, in the absence of an agonist activates the receptor, while in the presence of agonist acts like an antagonist. In vitro assays with endothelial cells usually use a constant concentration of VEGF in the media. This concentration is usually low and at the levels of ng/mL. At nM concentrations, Rg3, if considered as a partial agonist, and in the presence of a constant level of VEGF, might have a role of a competitive antagonist for VEGFR2. At higher concentrations it could act as an agonist of the receptor. Two examples of the anti- and pro-angiogenic effects of Rg3 on HUVECs were discussed above. At nM concentrations and in the presence of VEGF, RRg3 showed anti-angiogenic affects [15] and at low μM range (up to 30 μM) in the presence of fetal bovine serum, Rg3 had pro-angiogenic effects [20]. Therefore, at nM range and in the presence of VEGF, Rg3 acted as an antagonist and in the absence of VEGF acted as agonist.

The other explanation is the possibility of Rg3 having a biphasic U-shaped dose-response curve. In that case, Rg3 would be one of the many examples of molecules having such a biphasic dose-response curve. Examples of such molecules are estrogens [25], NO [26], cadmium and mercury [27], opiates [28], dopamine [29], and anti-angiogenic agents such as endostatin [30], statins [31], captopril [32] and interferon-alpha [33].

However, as described above and previously reviewed [11], there are many studies that used and showed the efficacy of Rg3 at high μM ranges up to 230 μM (180 μg/mL) [23]. This opens another

window for Rg3 to have a triphasic dose-response. Examples of molecules with triphasic dose-response are vasopressin [34], neurotensin [35] and amphetamine [36].

4. Molecular Mechanisms of Rg3 in Targeting Angiogenesis

When the balance between pro- and anti-angiogenic agents shifts towards pro-angiogenic agents including VEGF, as a fundamental player, and other factors such as b-FGF, epidermal growth factor (EGF), transforming growth factor β (TGF-β), tumor necrosis factor-alpha (TNF-α), angiogenin, angiopoietin, and interleukin 8 (IL-8) [37], several intracellular pathways are triggered leading to activation of endothelial cell proliferation and migration towards the tumor. Migration of endothelial cells is a complex process which requires coordination of several cellular components and changes the dynamic of cellular compartments. Below, the molecules and signaling pathways that are affected following administration of Rg3 are discussed.

4.1. VEGF and its Receptor, VEGFR2

VEGFR2, a receptor tyrosine kinase (RTK), is one of the three subtypes of VEGF receptor. The interaction between VEGF and VEGFR2 is known as the key driver of angiogenesis (Figure 2a). One of the commonly described mechanisms of inhibition of angiogenesis is decreased expression or availability of VEGF and VEGFR2. Rg3 inhibited the protein expression of VEGF in human hepatocellular (HepG2) [38], esophageal (Eca-109) and renal cell carcinoma (786-0) cell lines [39], decreased VEGF-A and -C in anaplastic thyroid and papillary thyroid cancer cell lines [40] and decreased transcripts of VEGF-A, -B and -C in a mouse model of breast cancer [25]. In hypertrophic scar fibroblasts, RRg3 inhibited the transcript and protein expression of VEGF [41]. Likewise, a decreased expression of VEGFR2 was shown in EPCs [17]. Many in vivo studies also showed a decreased expression of VEGF and VEGFR2 (Table 2). The mechanisms involved in such decreased expression of these factors could be explained by the inhibitory action of Rg3 on the expression of hypoxia inducible factor-1α (HIF-1α), cyclooxygenase-2 (COX-2) and nuclear factor-κB (NF-κB) [39]. The VEGF promoter has a hypoxia-responsive element which upon binding to HIF-1α, activates the expression of VEGF [42]. Hypoxia also regulates the expression of COX-2, the expression of which correlates with VEGF [43]. NF-κB is a regulator of various cellular processes that lead to tumorigenesis and metastasis. Angiogenesis is one of these processes. P65 is one of the important members of NF-κB family, the expression of which was inhibited by Rg3 [39].

At least four major downstream intracellular signaling pathways are involved in VEGFR2 activation (reviewed in [44]). The major pathway is the activation of phospholipase Cγ, which can activate a number of downstream signaling molecules and pathways including protein kinase C/Raf/MEK/ERK [45,46]. Activation of this pathway leads to cell proliferation, survival and migration. Another pathway is PI3K/Akt/mTOR pathway which is involved in cell survival and regulation of migration [47]. The third signaling pathway includes SRC and small GTPases that are involved in cell polarization, shape and migration [48]. A fourth signaling pathway involves molecules downstream of VEGFR2 activation: stress kinases such as STATs, G protein-coupled receptor-dependent signaling and p38 MAPK [44]. The specific action of Rg3 on some of the pathways has been elucidated (Figure 2); some of the explored signaling pathways which play roles in angiogenesis are described below.

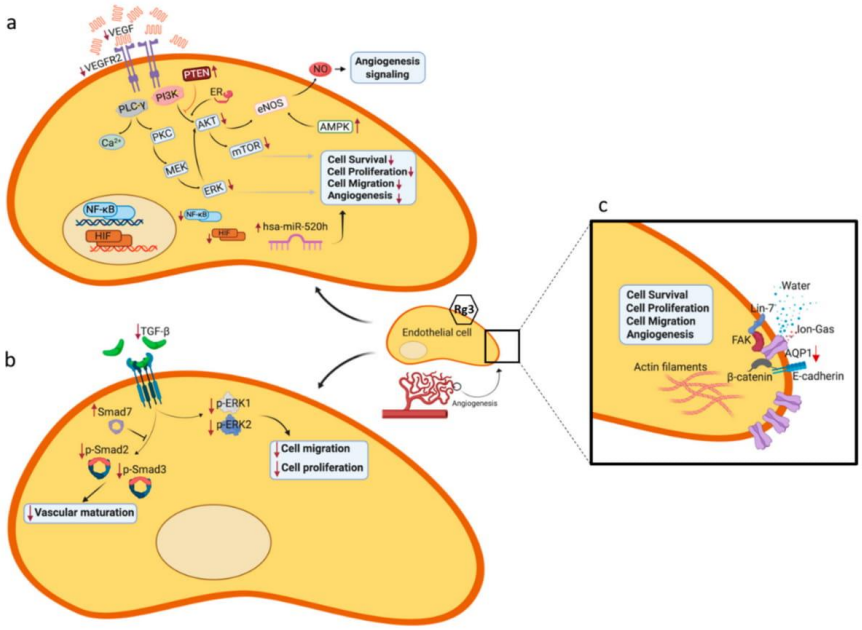

Figure 2. Signaling molecules and pathways that are affected by Rg3 in an endothelial cell. (**a**) VEGF–VEGFR2 interaction and inhibition of the related signaling pathways and molecules, (**b**) decreased expression of TGF-β1 and the related signaling molecules, (**c**) blocking the water transport function of AQP1 and decreased expression of AQP1. Red arrows ↓ and ↑ show the effect of Rg3 on decreased and increased expression of molecules, respectively.

Table 2. Antiangiogenic properties of Rg3 studied in different cancer models.

Cancer	Animal Model	Rg3, Dose and Route of Administration	Other Drugs in Study	Results	Ref
Breast	BALB/c mouse	10 mg/kg/day, p.o.	Low dose capecitabine, 200 mg/kg/day, p.o.	↓ MVD [a] and VEGF expression (especially in the combination group)	[49]
	Nude mouse	5 mg/kg q.a.d., s.c.	Recombinant human endostatin, 10 mg/kg, q.a.d.	↓ VEGF-A, -B, -C (especially in the combination group), proteins involved in autophagy pathway, mTOR, PI3K, Akt, JNK and Beclin-1	[50]
Ovary	Nude mouse	i.p.	Cyclophosphamide	↓ MVD and VEGF expression (combination)	[51]
	Nude mouse	0.3, 1 and 3 mg/kg/d for 20 days, i.p.		↓ number of vessels oriented toward the tumor mass	[52]

Table 2. *Cont.*

Cancer	Animal Model	Rg3, Dose and Route of Administration	Other Drugs in Study	Results	Ref
Uterus	Rats	5 or 10 mg/kg/d for 21 days	Gestrinone	Rg3 (10 mg/kg/d) + gestrinone significantly decreased the expression of VEGF, VEGFR2, p-Akt and p-mTOR, suggesting Rg3 blocks the effect of VEGFR2 via PI3K/Akt/mTOR signaling pathway	[53]
Colorectal cancer	Nude mouse	25 mg/kg/d for 12 days, gastric perfusion		Inhibited the expression of angiogenesis-related genes, MVD and decreased neo-vessel formation	[54]
	Nude mouse	10 mg/kg/d for 30 days, p.o.	Radiotherapy twice weekly (2 Gy) for 2 weeks	↑ effects of radiation on the expression of CD31	[55]
Thyroid	Nude mouse	10 mg/kg/d, intragastric		↓ CD31 in the tumors	[40]
Lung	Mouse	20 mg/kg/day for 18 days, (gastric perfusion)	Gemcitabine, 10 mg/kg, i.p. every 3rd day	↓ VEGF expression, MVD and signals of blood flow and peak systolic velocity of the tumor	[56]
	Mouse	600 μg/kg/day (p.o.) for 23 days		↓ arterial and capillary density, decreased number of CD34+/VEGFR2+ EPCs	[17]
	Wistar rats	1 mg/kg		↓ tumor volume and MVD	[57]
Melanoma	C57BL/6 mouse	1.5 mg/kg every other day for 20 days (i.v.)		↓ MVD	[58]
	C57BL/6 mouse	0.3, 1.0 or 3.0 mg/kg Rg3 (i.p.) for 10 days	5-Fluorouracil, 20 mg/kg	↓ vessel numbers, MVD and VEGF and proliferating cell nuclear antigen (PCNA)	[59]
Liver	A rabbit model of liver VX2 carcinoma	6 mg/kg (i.v.)	TAE [b]	↓ CD31 and VEGF and ↑ Bcl-2 and caspase-3	[38]
	Buffalo rat	1 mg/kg (i.p.)	TAE [b]	↓ MVD, CD31 expression, VEGF overexpression, and VEGFR2 expression and phosphorylation	[60]
	C57BL/6 mouse	10 mg/kg for 10 days		↓ MVD	[61]
Glioma	Rat	10 mg/kg/d for 8 days (p.o.)	LDT [c] 5 mg/kg/d for 8 days MDT [d] 30 mg/kg/d for 3 days	↑ rCBV [e]; Untreated: 90% Rg3: 65% MDT: 64% LDT: 51% LDT + Rg3: 15%. ↓ MVD	[23]

[a] MVD: microvessel density. [b] TAE: transcatheter arterial embolization. [c] LDT: low-dose temozolomide. [d] MDT: maximum-tolerated dose temozolomide. [e] rCBV: relative cerebral blood volume.

4.2. Signaling Pathways Leading to Activation of eNOS

eNOS is one of the important mediators of angiogenesis (Figure 2a) [62]. It was shown that VEGF-induced activation of phosphatidylinositol 3-kinase (PI3K) activates eNOS by phosphorylation at Ser1177 [63]. Akt is one of the major kinases downstream of PI3K, which is activated following VEGF stimulation and plays a role in cell survival [64]. Activated Akt also directly signals activation of eNOS (Figure 2a) [65]. It was shown that Rg3 (300 ng/mL) decreased VEGF-dependent Akt/eNOS signaling in EPCs [18]. The effect of ginsenosides [66] and Rg3 [67] on NO production was shown previously. Controversies on the effect of Rg3 on eNOS and NO production exist: at 10 μg/mL, increased NO production was reported to be independent of eNOS in canine carporal smooth muscle [67], however in human ECV 304 endothelial cells, the same concentration of Rg3 increased expression and phosphorylation of eNOS via estrogen receptor (ER)-mediated activation of phosphatidylinositol 3-kinase (PI3-kinase) [21]. Involvement of eNOS for production of NO in the Rg3-treated cells might be a tissue- and species-dependent factor. What is controversial here is whether Rg3 increases or decreases the activation of eNOS in endothelial cells. It seems that at 300 ng/mL, the activity of eNOS was decreased [18] while at 10 μg/mL, this activity was increased [21]. Once again it seems that the effect of Rg3 is dependent on the range of concentration. At nM ranges, the activity of eNOS was decreased and at μM ranges, the activity increased. Another regulator of this pathway is a tumor suppressor, phosphatase and tensin homolog deleted on chromosome 10 (PTEN). PTEN is an inhibitor of the PI3K/Akt pathway. In a mouse model of hepatocarcinoma, the mice receiving 5 mg/kg SRg3 showed a non-significant increase in PTEN and decrease in pAkt, as evidenced by immunohistochemistry staining of the tumors. These changes were potentiated and statistically significant when SRg3 was co-administered with sorafenib [68].

The other pathway for the activation of eNOS is via the ER-mediated activation of PI3K/Akt in endothelial cells (Figure 2a) [69] and Rg3 at 10 μg/mL activates this pathway [21]. It is not yet examined whether Rg3 has a similar pattern of response at other ranges of concentration. It is noteworthy that the promoter region of VEGF gene has an estrogen response element (ERE) [70] and the expression of VEGF is affected by both ER-α and -β [71]. Rg3 has a steroid backbone and could be a potential ligand for ER.

The mitogen-activated protein kinase (MAPK) pathway is also another regulator of eNOS (Figure 2a). Activation of MAPK signaling pathway is dependent on the extracellular stimuli and leads to cell stress response, cell proliferation, apoptosis, motility and differentiation. The MAPK family has four subgroups; the p38 group of protein kinases, c-jun N-terminal or stress-activated protein kinases (JNK/SAPK), extracellular signal-regulated kinases (ERKs) and ERK/big MAP kinase 1 (BMK1) [72]. It was shown that at 10 μg/mL, Rg3 increased the activities of c-Jun N-terminal kinase (JNK), and p38 MAPK. JNK is responsible for a number of cell functions including angiogenesis. It is responsible for a sustained phosphorylation and activation of VEGFR2 following interaction with VEGF [73] and plays a role in the phosphorylation (Ser1177) and activation of eNOS [74]. Likewise, p38 MAPK is activated by VEGFR2 and is necessary to mediate the shear stress-induced angiogenesis [75]. It also binds to and activates eNOS [76].

The other activator of eNOS is AMP-activated protein kinase (AMPK) (Figure 2a), which is a stress activated kinase. Cellular stresses such as hypoxia activate AMPK [77] followed by phosphorylation (Ser1177) and activation of eNOS [78]. Upstream of AMPK is calmodulin-dependent protein kinase II (CaMK-II). Following exposure of ECV 304 cells with 10 μg/mL Rg3, CaMK-II was phosphorylated and activated leading to activation of AMPK [21]. However, it is not yet clear if Rg3 has a similar mechanism at nM or higher μM concentrations.

4.3. Role of Mammalian Target of Rapamycin (TOR), Angiogenesis and Autophagy

mTOR plays crucial roles in cell growth and metabolism including lipid and protein synthesis, autophagy, mitochondrial metabolism and biogenesis, and angiogenesis. It is one of the conserved proteins belonging to the PI3K related kinase family sand downstream of activation of PI3K/Akt

(Figure 2a) [79]. Activation of PI3K/Akt, both in a hypoxia-dependent and -independent manners, increases the expression of VEGF and regulated the expression of NO and other angiogenic factors. Hence, inhibitors of PI3K/Akt/mTOR pathway inhibit angiogenesis (reviewed in [80]). Cao et al. (2017) studied a rat model of endometriosis that received 10 mg/kg/day Rg3 for 21 days, resulting in blocking the VEGFR2-mediated PI3K/Akt/mTOR signaling pathway. This was evidenced by decreased protein expression of VEGF, phosphorylated Akt and phosphorylated mTOR and transcript expression of VEGF, Akt and mTOR [53]. In mice bearing breast tumors, subcutaneous Rg3 (5 mg/kg) alone or in combination with Endostar, a modified recombinant human endostatin, decreased the transcript expression of mTOR, PI3K, Akt [50], a pathway that not only is involved in the regulation of angiogenesis, but also modulates autophagy. This study also showed a decreased transcript expression JNK and of Beclin-1 [50]. JNK/Beclin-1 is a crucial pathway mediating autophagic cell death.

4.4. Signal Transducer and Activator of Transcription 3 (STAT3)

STAT3 is one of the important members of the STAT family which plays an important role in angiogenesis, being an activator for the transcription of VEGF [81]. Rg3 inhibited the hypoxia-induced phosphorylation of STAT3, ERK1/2 and JNK in esophageal and renal cell carcinoma lines [39].

4.5. TGF-β1

TGF-β1 is a member of TGF-β superfamily of cytokines. Downstream to the activation of TGF-β receptors, activation of Smads and Smad-interacting transcription factors play roles in cellular responses. Besides Smads, ERK is also activated as a part of non-Smad signaling of TGF-β receptors (Figure 2b).

Development of keloid, a hyper-proliferation in a healing wound, requires angiogenesis. Studies in keloid samples showed that Rg3 inhibited the expression of TGF-β1, VEGF and plasminogen activator inhibitor-1 (PAI-1). Smad7, a negative feedback regulator in the TGF-β1/Smad pathway, was increased and the expression levels of p-Smad2 and p-Smad3, which are enhanced by TGF-β1, were markedly decreased, p-ERK1/2 expression was decreased and the protein expression levels of total Smad2/3 and total ERK1/2 remained almost unchanged [82]. In hypertrophic scar fibroblasts RRg3 inhibited the transcript and protein expression of TGF-β1, protein levels of phosphorylated Smad2 and Smad3 and ERK1/2 and transcripts of VEGFR and platelet-derived growth factor and increased the protein level of Smad7 [41].

4.6. Aquaporin 1 (AQP1)

AQP1 is one of the members of water channel family of AQP proteins. It exists as a homotetramer, with every monomer responsible for the transport of water and the central channel between the four monomers responsible for the transport of ion and gases. The role of AQP1 in angiogenesis has already been discussed in the literature (reviewed in [11,83]). AQP1 plays key roles in the migration of cells, contributing to several steps including polarization, protrusion, cell adhesion to extracellular matrix (ECM), degradation of extracellular matrix and cell retraction (reviewed in [84]). Signaling of AQP1 in complex with other proteins such as focal adhesion kinase (FAK), β-catenin, Lin-7 and E-cadherin, facilitates the migration of cells (Figure 2c). Lin-7 is one of the proteins that accumulate at cadherin-catenin junctions [85]. The lin-7/β-catenin complex is also in interaction with AQP1 playing a role in the effects mediated by AQP1. Lin-7 is one of the scaffolding proteins, with the major role of assembling components of a functional complex of receptors, channels, signaling and adhesion molecules [86]. Moreover, at focal adhesion sites, integrins link the extracellular matrix and the actin cytoskeleton. FAK is another scaffolding protein functioning at these sites and regulating the interaction of proteins. It was shown that there is a functional cross talk between AQP1 and FAK. AQP1 regulates the expression of FAK and FAK colocalizes with AQP1 [87]. AQP1 also regulates the expression of β-catenin [87] and was also shown to be related to the expression of MMP-2 and -9 [88]. AQP1 also plays a role in regulating cell proliferation via regulating the expression of key cell cycle proteins

such as cyclin D1 and E1 [89] and transport of oxygen reactive species (ROS), hydrogen peroxide (H_2O_2) [90], the signaling of which plays a role in proliferation, migration and angiogenesis [91]. In addition, increased mitochondrial ROS enhances necroptotic signaling [92] and AQP1, via effluxing ROS to the extracellular space, can potentially inhibit ROS-induced necroptosis thereby increasing cell survival.

AQP1 plays a fundamental role in the proliferation and migration of endothelial cells during angiogenesis; it is abundantly expressed in tumor microvessels and in endothelial cells in culture [83]. AQP1 has been identified as a promoter of angiogenesis [93], disruption of which impairs angiogenesis [94]. The promoter of *Aqp1* has a hypoxia response element, and following hypoxia, not only the transcription of VEGF but also AQP1 was increased [95]. This is in agreement with AQP1 as an anti-angiogenesis target. We have shown that blockers of the AQP1 water channel such as AqB013 [96], AqB050 [97] and bacopaside II [98] inhibit tube formation in endothelial cells. We have also shown that SRg3 stereoselectively inhibited AQP1-mediated transport of water [12]. Decreased expression of AQP1 with Rg3 treatment was also shown in a prostate cancer cell line [99]. This opens new windows for further investigations of the role of AQP1 as a target of Rg3 in inhibiting angiogenesis.

4.7. MicroRNAs (miRs)

One of the anti-angiogenic mechanisms suggested for Rg3 is via miR regulation of angiogenic pathways (Figure 2a). Keung et al. [19] screened human miR and found that in RRg3-treated HUVECs, nine miRs were differentially expressed. Based on microarray data, both hsa-miR-520h and hsa-miR-487b were increased >10 fold and hsa-miR-219, hsa-miR-342, hsa-miR-524-5p, and hsa-miR -197 were increased 2–7 fold. Additionally, hsa-miR-23a, hsa-miR-489, and hsa-miR-377 were down regulated (4 to 35 fold). In validation studies they showed a 3-fold increase in the transcripts of hsa-miR-520h in RRg3-treated cells and suggested EphB2 and EphB4 as target genes for hsa-miR-540h. EphB2 and EphB4 are two proteins of the Eph family, the largest RTK family, which upon activation mediate critical steps in cancer cell migration and angiogenesis. This study also showed that overexpression of hsa-miR-520h inhibited the proliferation and tube-forming capacity of HUVECs by 18 and 35%, respectively. Injection of hsa-miR-520h into the zebra-fish embryos showed that hsa-miR-520h significantly inhibited the neovessel formation. Knock-down of hsa-miR-520h expression significantly reduced the endogenous hsa-miR-520h level in HUVECs, their proliferation and tube-forming capacity [19]. Overall, this study showed that RRg3, potentially, via targeting hsa-miR-520h, suppressed the expression of EphB2 and EphB4 and inhibited angiogenesis.

4.8. CD31 and CD34

Cluster of differentiation (CD) 31 and CD34 are two of the surface molecules that have been studied as a marker of angiogenesis in many studies. These proteins are involved in angiogenesis and migration of endothelial cells. Rg3 decreased expression of CD34 in EPCs [18] and decreased expression of CD31 and CD34 in cultured patient keloid samples, by 50 and 65%, respectively [82]. Several animal studies have also demonstrated decreases in CD31 expression in tumors following treatment with Rg3 (Table 2).

5. Pharmacokinetic Aspects of Administering Rg3

In various in vivo models of cancer, Rg3 has been administered alone or in combination with other treatments to study the anti-angiogenic properties of this potential drug. Table 2 summarizes these studies' doses and routes of administration and the major anti-angiogenic outcomes of the studies. These studies used doses up to 20 mg/kg and the drug was administered either p.o., i.v., intraperitoneally (i.p.) or subcutaneously (s.c.).

Depending on the structure of any drug candidate, route of drug administration might have a major role in the disposition of a drug. Among the four determinants of pharmacokinetics, absorption, distribution, metabolism and elimination, the most important determinant to consider

for administration of Rg3 seems to be metabolism. From this perspective Rg3 might not be the best candidate for oral administration. It is rapidly metabolized in the gastrointestinal tract (GIT), going through partial or complete hydrolysis in the stomach and losing the sugar moieties by the GIT anaerobic microflora, leaving de-glycosylated active anti-cancer metabolites such as ginsenoside Rh2 and protopanaxadiol (PPD) [100–102]. Rg3 is also a substrate for cytochrome P450 members, which are abundant in the liver and GIT and also found in other organs including skin, blood, lungs and kidneys. This means that Rg3 is a potential substrate for metabolism in any of these organs [11]. Oral administration could facilitate Rg3 metabolism. However, there are controversies in the literature in terms of the concentration of Rg3 detected in the blood following oral administration. Plasma detection of Rg3 after oral administration of 10 mg/kg in Sprague-Dawley rats lasted for 12 h [103] and after 50 [104] and 100 mg/kg [105] was not detectable. The absolute bioavailability of Rg3 was calculated to be 2.63% [103]. In addition, Rg3 has a relatively high lipophilicity (estimated log P 4) (PubChem) and a low water solubility at pH 7.4 (estimated log S −4.04) (ChemAxon). These, together with the 8 H-bond donors and 13 oxygens in the structure of Rg3, make it a molecule with low permeability and low bioavailability. This also shows that Rg3 is a violation of Lipinski's "rule of five" which makes it an inappropriate candidate for oral administration [106].

The i.p. administration bypasses the GIT metabolism, but the drug will still be exposed to the liver metabolizing enzymes before distribution in the body. Hence, i.v. and s.c. might result in more delayed metabolism and potentially a more durable action of Rg3 itself compared to the other routes of administration. However, even with a single i.v. administration, Rg3 metabolites, ginsenoside-Rh2 and protopanaxadiol, were almost instantly detected in the blood [100]. We already know that these molecules have anti-tumor and anti-angiogenic properties [107–109]. This raises the question, are the anti-angiogenic effects of Rg3 in vivo due to Rg3, its metabolites, or a combination of all? In that case, Rg3 is potentially not only a drug but also a prodrug.

Half-life of Rg3 following i.v. administration was studied in Sprague-Dawley rats. With 10 mg/kg, Rg3 showed a two-compartment pharmacokinetic model with half-lives of about 12 min and 2 h [103]. With 5 mg/kg, the half-life was reported to be about 14–18.5 min [104,105]. This shows that Rg3 has a generally short half-life in rats. Furthermore, the highest reported C_{max} in human study is about 400 ng/mL [110]. This is a very low concentration, equal to almost 5×10^{-7} nM. At this concentration, in vitro assays fail to show any efficacy of Rg3, and therefore it is possible to conclude that the efficacy of Rg3 is due to a combination of Rg3 and metabolites. This queries the sufficiency of the dosing schedule in many of the animal studies (Table 2). Administration of a single dose per day or even one dose per 3 days seems to be effective, but would they be as effective as administering 3–4 doses per day?

6. Safety of Rg3

Regardless of the route of administration, Rg3 seems to be a safe drug. Acute toxicity testing of 800 and 1600 mg/kg of SRg3 (p.o.) to Sprague-Dawley rats and Kunming mice, respectively, showed no mortality or toxicity [111]. Repeated oral administration of 20, 60 and 180 mg/kg SRg3 to Sprague-Dawley rats for 26 weeks showed no sign or symptoms of toxicity, with a no-observed-adverse-effect level (NOAEL) of 180 mg/kg [111]. Another toxicity study with 7, 20, or 60 mg/kg SRg3 (p.o.) was performed on Beagle dogs for 26 weeks and showed that SRg3 was safe. The only adverse finding was the increased but reversible kidney weight in dogs that received 60 mg/kg SRg3. The NOAEL in this study was found to be 20 mg/kg [112], the human equivalent dose of which is approximately 11 mg/kg. In healthy humans receiving intramuscular injections of 10–60 mg/kg SRg3 as a single dose or 30 mg/kg once every two days for 15 days the drug was well tolerated with no detectable sign or symptoms of toxicity [110]. Furthermore, some clinical trials on non-small cell lung carcinoma [113,114] and advanced hepatocellular carcinoma [115] have used Rg3 as orally administered anti-angiogenic agent, up to 50 mg/day with no reported toxicity [113–115]. Therefore, Rg3 at these doses appears to be safe and well tolerated.

7. Conclusions

From the literature, Rg3 has been shown to inhibit the proliferation and survival of endothelial cells and the expression of various factors involved in angiogenesis. The key driver of this process is the interaction between VEGF and VEGFR2. As discussed in this review paper, several in vitro and in vivo studies showed that Rg3 decreased the expression of these two molecules, and it could be postulated that this is the major mechanism of anti-angiogenic effect of Rg3. In addition, several other mechanisms are suggested including decreased expression of b-FGF, TGF-β1, AQP1, JNK, Beclin-1, MMP-2, MMP-9 and Bcl-2. Rg3 also decreased the activation of various signaling pathways leading to activation of eNOS, including VEGF-induced Akt/eNOS, ER/PI3K/eNOS or AMPK/eNOS and decreased activation of PI3K/Akt/mTOR pathway, STAT3, ERK1/2 and JNK. It also decreased hsa-miR-520h-mediated expression of EphB2 and EphB4. With a few exceptions, studies describe this anti-angiogenic effect at μM range. Yet, some studies show Rg3 is effective at nM range too. This raises the question whether Rg3 has a biphasic or tri-phasic dose–response curve. In either case, higher efficacy of Rg3 in nM range is impressive, considering the low bioavailability following oral administration and high metabolism rate. It seems that administering the drug at μM doses leaves only nM concentrations in the blood, which is sufficient to exert the anti-cancer effects. Whether the metabolites of Rg3 also follow the same pattern is an unanswered question.

Considering the high rate of metabolism of Rg3, which leaves low levels of Rg3 in the blood, a dose-dependent anti-angiogenic effect at nM scale explains the observed in vivo anti-angiogenic effects, which could especially be potentiated by other metabolites of Rg3. Despite various in vivo reports supporting the anti-angiogenic action of Rg3, it should be taken into consideration that Rg3 is potentially a drug and a prodrug, which upon metabolism with active metabolites, ginsenoside Rh2 and PPD, could also contribute to the effects observed for Rg3. Therefore, the in vivo effects observed from this drug candidate could be attributed to a combination of Rg3 and its metabolites.

The final important issue is that Rg3 has two epimers with stereoselective activities, efficacies and pharmacokinetic profiles [100]. These epimers should be considered as two separate drugs; hence, the term Rg3 is vague and might not reflect the true nature and pharmacokinetic profile of the administered drug.

Author Contributions: Conceptualization, M.N. and J.E.H.; Writing—original draft preparation, M.N.; Writing—review and editing, M.N., E.S., A.R.T., T.J.P. and J.E.H.; Illustration, M.N. and J.E.H.; Supervision and mentoring, J.E.H., A.R.T. and T.J.P. All authors have read and agreed to the published version of the manuscript.

Funding: This research was funded by the Margaret Elcombe Hospital Research Foundation Research Grant.

Conflicts of Interest: The authors declare no conflict of interest.

References

1. Miao, X.S.; Metcalfe, C.D.; Hao, C.; March, R.E. Electrospray ionization mass spectrometry of ginsenosides. *J. Mass Spectrom.* **2002**, *37*, 495–506. [CrossRef]
2. Jo, S.K.; Kim, I.S.; Yoon, K.S.; Yoon, H.H.; Yoo, H.H. Preparation of ginsenosides Rg3, Rk1, and Rg5-selectively enriched ginsengs by a simple steaming process. *Eur. Food Res. Technol.* **2015**, *240*, 251–256. [CrossRef]
3. Chen, C.-f.; Chiou, W.-f.; Zhang, J.-t. Comparison of the pharmacological effects of Panax ginseng and Panax quinquefolium. *Acta Pharmacol. Sin.* **2008**, *29*, 1103–1108. [CrossRef] [PubMed]
4. Cheng, L.-Q.; Na, J.R.; Bang, M.H.; Kim, M.K.; Yang, D.-C. Conversion of major ginsenoside Rb1 to 20 (S)-ginsenoside Rg3 by Microbacterium sp. GS514. *Phytochemistry* **2008**, *69*, 218–224. [CrossRef] [PubMed]
5. Yan, Q.; Zhou, W.; Li, X.; Feng, M.; Zhou, P. Purification method improvement and characterization of a novel ginsenoside-hydrolyzing β-glucosidase from Paecilomyces Bainier sp. 229. *Biosci. Biotechnol. Biochem.* **2008**, *72*, 352–359. [CrossRef] [PubMed]
6. Jiang, Y.; Chen, J.; Ma, S.; Liu, K. Isolation and elucidation of alkaline degradation Product from total saponins in leaves and stems of Panax quinquefolium L. *J. Guangzhou Univ. Tradit. Chin. Med.* **2006**, *19*, 142–147.
7. Sun, C.; Gao, W.; Zhao, B.; Cheng, L. Optimization of the selective preparation of 20 (R)-ginsenoside Rg3 catalyzed by d, l-tartaric acid using response surface methodology. *Fitoterapia* **2013**, *84*, 213–221. [CrossRef]

8. Bae, S.H.; Lee, H.-S.; Kim, M.-R.; Kim, S.Y.; Kim, J.-M.; Suh, H.J. Changes of ginsenoside content by mushroom mycelial fermentation in red ginseng extract. *J. Ginseng Res.* **2011**, *35*, 235–242. [CrossRef]
9. Lee, H.S.; Lee, H.J.; Yu, H.J.; Ju, D.W.; Kim, Y.; Kim, C.T.; Kim, C.J.; Cho, Y.J.; Kim, N.; Choi, S.Y. A comparison between high hydrostatic pressure extraction and heat extraction of ginsenosides from ginseng (Panax ginseng CA Meyer). *J. Sci. Food Agric.* **2011**, *91*, 1466–1473. [CrossRef]
10. Lee, S.A.; Jo, H.K.; Im, B.O.; Kim, S.; Whang, W.K.; Ko, S.K. Changes in the contents of prosapogenin in the red ginseng (Panax ginseng) depending on steaming batches. *J. Ginseng Res.* **2012**, *36*, 102–106. [CrossRef]
11. Nakhjavani, M.; Hardingham, J.E.; Palethorpe, H.M.; Tomita, Y.; Smith, E.; Price, T.J.; Townsend, A.R. Ginsenoside Rg3: Potential molecular targets and therapeutic indication in metastatic breast cancer. *Medicines* **2019**, *6*, 17. [CrossRef] [PubMed]
12. Nakhjavani, M.; Palethorpe, H.M.; Tomita, Y.; Smith, E.; Price, T.J.; Yool, A.J.; Pei, J.V.; Townsend, A.R.; Hardingham, J.E. Stereoselective Anti-Cancer Activities of Ginsenoside Rg3 on Triple Negative Breast Cancer Cell Models. *Pharmaceuticals* **2019**, *12*, 117. [CrossRef]
13. Kang, D.-I.; Lee, J.-Y.; Yang, J.-Y.; Jeong, S.M.; Lee, J.-H.; Nah, S.-Y.; Kim, Y. Evidence that the tertiary structure of 20 (S)-ginsenoside Rg3 with tight hydrophobic packing near the chiral center is important for Na+ channel regulation. *Biochem. Biophys. Res. Commun.* **2005**, *333*, 1194–1201. [CrossRef] [PubMed]
14. Mochizuki, M.; Yoo, Y.C.; Matsuzawa, K.; Sato, K.; Saiki, I.; Tono-oka, S.; Samukawa, K.; Azuma, I. Inhibitory effect of tumor metastasis in mice by saponins, ginsenoside-Rb2, 20(R)- and 20(S)-ginsenoside-Rg3, of red ginseng. *Biol. Pharm. Bull.* **1995**, *18*, 1197–1202. [CrossRef] [PubMed]
15. Yue, P.Y.; Wong, D.Y.; Wu, P.K.; Leung, P.Y.; Mak, N.K.; Yeung, H.W.; Liu, L.; Cai, Z.; Jiang, Z.H.; Fan, T.P.; et al. The angiosuppressive effects of 20(R)- ginsenoside Rg3. *Biochem. Pharmacol.* **2006**, *72*, 437–445. [CrossRef] [PubMed]
16. Lee, J.J.; Kwon, H.K.; Jung, I.H.; Cho, Y.B.; Kim, K.J.; Kim, J.L. Anti-cancer Activities of Ginseng Extract Fermented with Phellinus linteus. *Mycobiology* **2009**, *37*, 21–27. [CrossRef] [PubMed]
17. Kim, J.W.; Jung, S.Y.; Kwon, Y.H.; Lee, J.H.; Lee, Y.M.; Lee, B.Y.; Kwon, S.M. Ginsenoside Rg3 attenuates tumor angiogenesis via inhibiting bioactivities of endothelial progenitor cells. *Cancer Biol. Ther.* **2012**, *13*, 504–515. [CrossRef]
18. Kim, J.W.; Jung, S.Y.; Kwon, Y.H.; Lee, S.H.; Lee, J.H.; Lee, B.Y.; Kwon, S.M. Ginsenoside Rg3 inhibits endothelial progenitor cell differentiation through attenuation of VEGF-dependent Akt/eNOS signaling. *Phytother. Res.* **2012**, *26*, 1286–1293. [CrossRef]
19. Keung, M.H.; Chan, L.S.; Kwok, H.H.; Wong, R.N.; Yue, P.Y. Role of microRNA-520h in 20(R)-ginsenoside-Rg3-mediated angiosuppression. *J. Ginseng Res.* **2016**, *40*, 151–159. [CrossRef]
20. Kwok, H.H.; Guo, G.L.; Lau, J.K.; Cheng, Y.K.; Wang, J.R.; Jiang, Z.H.; Keung, M.H.; Mak, N.K.; Yue, P.Y.; Wong, R.N. Stereoisomers ginsenosides-20(S)-Rg(3) and -20(R)-Rg(3) differentially induce angiogenesis through peroxisome proliferator-activated receptor-gamma. *Biochem. Pharmacol.* **2012**, *83*, 893–902. [CrossRef]
21. Hien, T.T.; Kim, N.D.; Pokharel, Y.R.; Oh, S.J.; Lee, M.Y.; Kang, K.W. Ginsenoside Rg3 increases nitric oxide production via increases in phosphorylation and expression of endothelial nitric oxide synthase: Essential roles of estrogen receptor-dependent PI3-kinase and AMP-activated protein kinase. *Toxicol. Appl. Pharmacol.* **2010**, *246*, 171–183. [CrossRef] [PubMed]
22. Li, J.P.; Zhao, F.L.; Yuan, Y.; Sun, T.T.; Zhu, L.; Zhang, W.Y.; Liu, M.X. Studies on anti-angiogenesis of ginsenoside structure modification HRG in vitro. *Biochem. Biophys. Res. Commun.* **2017**, *492*, 391–396. [CrossRef] [PubMed]
23. Sun, C.; Yu, Y.; Wang, L.; Wu, B.; Xia, L.; Feng, F.; Ling, Z.; Wang, S. Additive antiangiogenesis effect of ginsenoside Rg3 with low-dose metronomic temozolomide on rat glioma cells both in vivo and in vitro. *J. Exp. Clin. Cancer Res.* **2016**, *35*, 32. [CrossRef] [PubMed]
24. Duan, S.Z.; Usher, M.G.; Mortensen, R.M. PPARs: The vasculature, inflammation and hypertension. *Curr. Opin. Nephrol. Hypertens.* **2009**, *18*, 128–133. [CrossRef]
25. Calabrese, E.J. Estrogen and related compounds: Biphasic dose responses. *Crit. Rev. Toxicol.* **2001**, *31*, 503–515. [CrossRef]
26. Calabrese, E.J. Nitric oxide: Biphasic dose responses. *Crit. Rev. Toxicol.* **2001**, *31*, 489–501. [CrossRef]

27. Hao, C.; Hao, W.; Wei, X.; Xing, L.; Jiang, J.; Shang, L. The role of MAPK in the biphasic dose-response phenomenon induced by cadmium and mercury in HEK293 cells. *Toxicol. In Vitro* **2009**, *23*, 660–666. [CrossRef]
28. Calabrese, E.J. Opiates: Biphasic dose responses. *Crit. Rev. Toxicol.* **2001**, *31*, 585–604. [CrossRef]
29. Calabrese, E.J. Dopamine: Biphasic dose responses. *Crit. Rev. Toxicol.* **2001**, *31*, 563–583. [CrossRef]
30. Celik, I.; Sürücü, O.; Dietz, C.; Heymach, J.V.; Force, J.; Höschele, I.; Becker, C.M.; Folkman, J.; Kisker, O. Therapeutic efficacy of endostatin exhibits a biphasic dose-response curve. *Cancer Res.* **2005**, *65*, 11044–11050. [CrossRef]
31. Weis, M.; Heeschen, C.; Glassford, A.J.; Cooke, J.P. Statins have biphasic effects on angiogenesis. *Circulation* **2002**, *105*, 739–745. [CrossRef]
32. Volpert, O.V.; Ward, W.F.; Lingen, M.W.; Chesler, L.; Solt, D.B.; Johnson, M.D.; Molteni, A.; Polverini, P.J.; Bouck, N.P. Captopril inhibits angiogenesis and slows the growth of experimental tumors in rats. *J. Clin. Investig.* **1996**, *98*, 671–679. [CrossRef] [PubMed]
33. Slaton, J.W.; Perrotte, P.; Inoue, K.; Dinney, C.P.; Fidler, I.J. Interferon-α-mediated down-regulation of angiogenesis-related genes and therapy of bladder cancer are dependent on optimization of biological dose and schedule. *Clin. Cancer Res.* **1999**, *5*, 2726–2734.
34. Takayasu, M.; Kajita, Y.; Suzuki, Y.; Shibuya, M.; Sugita, K.; Ishikawa, T.; Hidaka, H. Triphasic response of rat intracerebral arterioles to increasing concentrations of vasopressin in vitro. *J. Cereb. Blood Flow Metab.* **1993**, *13*, 304–309. [CrossRef]
35. Oishi, M.; Inagaki, C.; Fujiwara, M.; Takaori, S.; Yajima, H.; Akazawa, Y. Possible mechanisms of the triphasic effects of neurotensin on the rat blood pressure. *Jpn. J. Pharmacol.* **1981**, *31*, 1043–1049. [CrossRef]
36. James, R.C.; Franklin, M.R. The triphasic amphetamine lethal dose curve in mice and its possible relationship to drug metabolism. *Toxicol. Appl. Pharmacol.* **1978**, *44*, 63–73. [CrossRef]
37. Marech, I.; Leporini, C.; Ammendola, M.; Porcelli, M.; Gadaleta, C.D.; Russo, E.; De Sarro, G.; Ranieri, G. Classical and non-classical proangiogenic factors as a target of antiangiogenic therapy in tumor microenvironment. *Cancer Lett.* **2016**, *380*, 216–226. [CrossRef] [PubMed]
38. Yu, Y.; Zhang, C.; Liu, L.; Li, X. Hepatic arterial administration of ginsenoside Rg3 and transcatheter arterial embolization for the treatment of VX2 liver carcinomas. *Exp. Ther. Med.* **2013**, *5*, 761–766. [CrossRef]
39. Chen, Q.J.; Zhang, M.Z.; Wang, L.X. Gensenoside Rg3 inhibits hypoxia-induced VEGF expression in human cancer cells. *Cell. Physiol. Biochem.* **2010**, *26*, 849–858. [CrossRef]
40. Wu, W.; Zhou, Q.; Zhao, W.; Gong, Y.; Su, A.; Liu, F.; Liu, Y.; Li, Z.; Zhu, J. Ginsenoside Rg3 Inhibition of Thyroid Cancer Metastasis Is Associated with Alternation of Actin Skeleton. *J. Med. Food* **2018**, *21*, 849–857. [CrossRef]
41. Tang, M.; Wang, W.; Cheng, L.; Jin, R.; Zhang, L.; Bian, W.; Zhang, Y. The inhibitory effects of 20(R)-ginsenoside Rg3 on the proliferation, angiogenesis, and collagen synthesis of hypertrophic scar derived fibroblasts in vitro. *Iran. J. Basic Med. Sci.* **2018**, *21*, 309–317. [CrossRef] [PubMed]
42. Breen, E.; Tang, K.; Olfert, M.; Knapp, A.; Wagner, P. Skeletal muscle capillarity during hypoxia: VEGF and its activation. *High. Alt. Med. Biol.* **2008**, *9*, 158–166. [CrossRef] [PubMed]
43. Williams, C.S.; Tsujii, M.; Reese, J.; Dey, S.K.; DuBois, R.N. Host cyclooxygenase-2 modulates carcinoma growth. *J. Clin. Investig.* **2000**, *105*, 1589–1594. [CrossRef] [PubMed]
44. Simons, M.; Gordon, E.; Claesson-Welsh, L. Mechanisms and regulation of endothelial VEGF receptor signalling. *Nat. Rev. Mol. Cell Biol.* **2016**, *17*, 611. [CrossRef] [PubMed]
45. Shibuya, M. VEGFR and type-V RTK activation and signaling. *Cold Spring Harb. Perspect. Biol.* **2013**, *5*, a009092. [CrossRef] [PubMed]
46. Nilsson, M.; Heymach, J.V. Vascular endothelial growth factor (VEGF) pathway. *J. Thorac. Oncol.* **2006**, *1*, 768–770. [CrossRef]
47. Zhuang, G.; Yu, K.; Jiang, Z.; Chung, A.; Yao, J.; Ha, C.; Toy, K.; Soriano, R.; Haley, B.; Blackwood, E. Phosphoproteomic analysis implicates the mTORC2-FoxO1 axis in VEGF signaling and feedback activation of receptor tyrosine kinases. *Sci. Signal.* **2013**, *6*, ra25. [CrossRef] [PubMed]
48. Rodrigues, S.F.; Granger, D.N. Blood cells and endothelial barrier function. *Tissue Barriers* **2015**, *3*, e978720. [CrossRef]
49. Zhang, Q.; Kang, X.; Yang, B.; Wang, J.; Yang, F. Antiangiogenic effect of capecitabine combined with ginsenoside Rg3 on breast cancer in mice. *Cancer Biother. Radiopharm.* **2008**, *23*, 647–653. [CrossRef]

50. Zhang, Y.; Liu, Q.Z.; Xing, S.P.; Zhang, J.L. Inhibiting effect of Endostar combined with ginsenoside Rg3 on breast cancer tumor growth in tumor-bearing mice. *Asian Pac. J. Trop. Med.* **2016**, *9*, 180–183. [CrossRef]
51. Xu, T.M.; Xin, Y.; Cui, M.H.; Jiang, X.; Gu, L.P. Inhibitory effect of ginsenoside Rg3 combined with cyclophosphamide on growth and angiogenesis of ovarian cancer. *Chin. Med. J. (Engl.)* **2007**, *120*, 584–588. [CrossRef]
52. Xu, T.M.; Cui, M.H.; Xin, Y.; Gu, L.P.; Jiang, X.; Su, M.M.; Wang, D.D.; Wang, W.J. Inhibitory effect of ginsenoside Rg3 on ovarian cancer metastasis. *Chin. Med. J. (Engl.)* **2008**, *121*, 1394–1397. [CrossRef]
53. Cao, Y.; Ye, Q.; Zhuang, M.; Xie, S.; Zhong, R.; Cui, J.; Zhou, J.; Zhu, Y.; Zhang, T.; Cao, L. Ginsenoside Rg3 inhibits angiogenesis in a rat model of endometriosis through the VEGFR-2-mediated PI3K/Akt/mTOR signaling pathway. *PLoS ONE* **2017**, *12*, e0186520. [CrossRef] [PubMed]
54. Tang, Y.C.; Zhang, Y.; Zhou, J.; Zhi, Q.; Wu, M.Y.; Gong, F.R.; Shen, M.; Liu, L.; Tao, M.; Shen, B.; et al. Ginsenoside Rg3 targets cancer stem cells and tumor angiogenesis to inhibit colorectal cancer progression in vivo. *Int. J. Oncol.* **2018**, *52*, 127–138. [CrossRef] [PubMed]
55. Liu, T.; Duo, L.; Duan, P. Ginsenoside Rg3 Sensitizes Colorectal Cancer to Radiotherapy through Downregulation of Proliferative and Angiogenic Biomarkers. *Evid. Based Complement. Alternat. Med.* **2018**, *2018*, 1580427. [CrossRef]
56. Liu, T.G.; Huang, Y.; Cui, D.D.; Huang, X.B.; Mao, S.H.; Ji, L.L.; Song, H.B.; Yi, C. Inhibitory effect of ginsenoside Rg3 combined with gemcitabine on angiogenesis and growth of lung cancer in mice. *BMC Cancer* **2009**, *9*, 250. [CrossRef] [PubMed]
57. Yu, H.; Teng, L.; Meng, Q.; Li, Y.; Sun, X.; Lu, J.; R, J.L.; Teng, L. Development of liposomal Ginsenoside Rg3: Formulation optimization and evaluation of its anticancer effects. *Int. J. Pharm.* **2013**, *450*, 250–258. [CrossRef] [PubMed]
58. Chen, J.; Peng, H.; Ou-Yang, X.; He, X. Research on the antitumor effect of ginsenoside Rg3 in B16 melanoma cells. *Melanoma Res.* **2008**, *18*, 322–329. [CrossRef]
59. Meng, L.; Ji, R.; Dong, X.; Xu, X.; Xin, Y.; Jiang, X. Antitumor activity of ginsenoside Rg3 in melanoma through downregulation of the ERK and Akt pathways. *Int. J. Oncol.* **2019**, *54*, 2069–2079. [CrossRef]
60. Zhou, B.; Wang, J.; Yan, Z. Ginsenoside Rg3 attenuates hepatoma VEGF overexpression after hepatic artery embolization in an orthotopic transplantation hepatocellular carcinoma rat model. *Onco Targets Ther.* **2014**, *7*, 1945–1954. [CrossRef]
61. Hu, S.; Zhu, Y.; Xia, X.; Xu, X.; Chen, F.; Miao, X.; Chen, X. Ginsenoside Rg3 Prolongs Survival of the Orthotopic Hepatocellular Carcinoma Model by Inducing Apoptosis and Inhibiting Angiogenesis. *Anal. Cell. Pathol. (Amst.)* **2019**, *2019*, 3815786. [CrossRef] [PubMed]
62. Murohara, T.; Asahara, T.; Silver, M.; Bauters, C.; Masuda, H.; Kalka, C.; Kearney, M.; Chen, D.; Symes, J.; Fishman, M. Nitric oxide synthase modulates angiogenesis in response to tissue ischemia. *J. Clin. Investig.* **1998**, *101*, 2567–2578. [CrossRef] [PubMed]
63. Papapetropoulos, A.; García-Cardeña, G.; Madri, J.A.; Sessa, W.C. Nitric oxide production contributes to the angiogenic properties of vascular endothelial growth factor in human endothelial cells. *J. Clin. Investig.* **1997**, *100*, 3131–3139. [CrossRef] [PubMed]
64. Gerber, H.-P.; McMurtrey, A.; Kowalski, J.; Yan, M.; Keyt, B.A.; Dixit, V.; Ferrara, N. Vascular endothelial growth factor regulates endothelial cell survival through the phosphatidylinositol 3′-kinase/Akt signal transduction pathway requirement for Flk-1/KDR activation. *J. Biol. Chem.* **1998**, *273*, 30336–30343. [CrossRef]
65. Michell, B.; Griffiths, J.; Mitchelhill, K.; Rodriguez-Crespo, I.; Tiganis, T.; Bozinovski, S.; de Montellano, P.O.; Kemp, B.; Pearson, R. The Akt kinase signals directly to endothelial nitric oxide synthase. *Curr. Biol.* **1999**, *9*, 845–848. [CrossRef]
66. Kim, N.D.; Kang, S.Y.; Schini, V.B. Ginsenosides evoke endothelium-dependent vascular relaxation in rat aorta. *Gen. Pharmacol.* **1994**, *25*, 1071–1077. [CrossRef]
67. Kang, Y.J.; Sohn, J.-T.; Chang, K.C. Relaxation of canine corporal smooth muscle relaxation by ginsenoside saponin Rg3 is independent from eNOS activation. *Life Sci.* **2005**, *77*, 74–84. [CrossRef] [PubMed]
68. Lu, M.; Fei, Z.; Zhang, G. Synergistic anticancer activity of 20 (S)-Ginsenoside Rg3 and Sorafenib in hepatocellular carcinoma by modulating PTEN/Akt signaling pathway. *Biomed. Pharmacother.* **2018**, *97*, 1282–1288. [CrossRef]

69. Hisamoto, K.; Ohmichi, M.; Kurachi, H.; Hayakawa, J.; Kanda, Y.; Nishio, Y.; Adachi, K.; Tasaka, K.; Miyoshi, E.; Fujiwara, N. Estrogen induces the Akt-dependent activation of endothelial nitric-oxide synthase in vascular endothelial cells. *J. Biol. Chem.* **2001**, *276*, 3459–3467. [CrossRef]
70. Applanat, M.P.; Buteau-Lozano, H.; Herve, M.A.; Corpet, A. Vascular endothelial growth factor is a target gene for estrogen receptor and contributes to breast cancer progression. In *Hormonal Carcinogenesis V*; Springer: Berlin/Heidelberg, Germany, 2008; pp. 437–444.
71. Mueller, M.D.; Vigne, J.-L.; Minchenko, A.; Lebovic, D.I.; Leitman, D.C.; Taylor, R.N. Regulation of vascular endothelial growth factor (VEGF) gene transcription by estrogen receptors α and β. *Proc. Natl. Acad. Sci. USA* **2000**, *97*, 10972–10977. [CrossRef]
72. Zarubin, T.; Jiahuai, H. Activation and signaling of the p38 MAP kinase pathway. *Cell Res.* **2005**, *15*, 11–18. [CrossRef] [PubMed]
73. Shen, K.; Ji, L.; Lu, B.; Wang, Z. c-Jun N-terminal kinase mediated VEGFR2 sustained phosphorylation is critical for VEGFA-induced angiogenesis in vitro and in vivo. *Cell Biochem. Biophys.* **2012**, *64*, 17–27. [CrossRef] [PubMed]
74. Park, J.-H.; Park, M.; Byun, C.J.; Jo, I. c-Jun N-terminal kinase 2 phosphorylates endothelial nitric oxide synthase at serine 116 and regulates nitric oxide production. *Biochem. Biophys. Res. Commun.* **2012**, *417*, 340–345. [CrossRef] [PubMed]
75. Gee, E.; Milkiewicz, M.; Haas, T.L. p38 MAPK activity is stimulated by vascular endothelial growth factor receptor 2 activation and is essential for shear stress-induced angiogenesis. *J. Cell. Physiol.* **2010**, *222*, 120–126. [CrossRef]
76. Chrestensen, C.A.; McMurry, J.L.; Salerno, J.C. MAP kinases bind endothelial nitric oxide synthase. *FEBS Open Bio.* **2012**, *2*, 51–55. [CrossRef] [PubMed]
77. Nagata, D.; Mogi, M.; Walsh, K. AMP-activated protein kinase (AMPK) signaling in endothelial cells is essential for angiogenesis in response to hypoxic stress. *J. Biol. Chem.* **2003**, *278*, 31000–31006. [CrossRef]
78. Morrow, V.A.; Foufelle, F.; Connell, J.M.; Petrie, J.R.; Gould, G.W.; Salt, I.P. Direct activation of AMP-activated protein kinase stimulates nitric-oxide synthesis in human aortic endothelial cells. *J. Biol. Chem.* **2003**, *278*, 31629–31639. [CrossRef]
79. Laplante, M.; Sabatini, D.M. mTOR signaling at a glance. *J. Cell Sci.* **2009**, *122*, 3589–3594. [CrossRef]
80. Karar, J.; Maity, A. PI3K/AKT/mTOR pathway in angiogenesis. *Front. Mol. Neurosci.* **2011**, *4*, 51. [CrossRef]
81. Chen, Z.; Han, Z.C. STAT3: A critical transcription activator in angiogenesis. *Med. Res. Rev.* **2008**, *28*, 185–200. [CrossRef]
82. Tang, M.; Bian, W.; Cheng, L.; Zhang, L.; Jin, R.; Wang, W.; Zhang, Y. Ginsenoside Rg3 inhibits keloid fibroblast proliferation, angiogenesis and collagen synthesis in vitro via the TGFbeta/Smad and ERK signaling pathways. *Int. J. Mol. Med.* **2018**, *41*, 1487–1499. [CrossRef]
83. Tomita, Y.; Dorward, H.; Yool, A.J.; Smith, E.; Townsend, A.R.; Price, T.J.; Hardingham, J.E. Role of aquaporin 1 signalling in cancer development and progression. *Int. J. Mol. Sci.* **2017**, *18*, 299. [CrossRef]
84. De Ieso, M.L.; Yool, A.J. Mechanisms of aquaporin-facilitated cancer invasion and metastasis. *Front. Chem.* **2018**, *6*, 135. [CrossRef]
85. Perego, C.; Vanoni, C.; Massari, S.; Longhi, R.; Pietrini, G. Mammalian LIN-7 PDZ proteins associate with β-catenin at the cell–cell junctions of epithelia and neurons. *EMBO J.* **2000**, *19*, 3978–3989. [CrossRef]
86. Monzani, E.; Bazzotti, R.; Perego, C.; La Porta, C.A. AQP1 is not only a water channel: It contributes to cell migration through Lin7/beta-catenin. *PLoS ONE* **2009**, *4*. [CrossRef]
87. Meng, F.; Rui, Y.; Xu, L.; Wan, C.; Jiang, X.; Li, G. Aqp1 enhances migration of bone marrow mesenchymal stem cells through regulation of FAK and β-catenin. *Stem Cells Dev.* **2014**, *23*, 66–75. [CrossRef]
88. Wei, X.; Dong, J. Aquaporin 1 promotes the proliferation and migration of lung cancer cell in vitro. *Oncol. Rep.* **2015**, *34*, 1440–1448. [CrossRef]
89. Galán-Cobo, A.; Ramírez-Lorca, R.; Toledo-Aral, J.J.; Echevarría, M. Aquaporin-1 plays important role in proliferation by affecting cell cycle progression. *J. Cell. Physiol.* **2016**, *231*, 243–256. [CrossRef]
90. Almasalmeh, A.; Krenc, D.; Wu, B.; Beitz, E. Structural determinants of the hydrogen peroxide permeability of aquaporins. *FEBS J.* **2014**, *281*, 647–656. [CrossRef]
91. Tafani, M.; Sansone, L.; Limana, F.; Arcangeli, T.; De Santis, E.; Polese, M.; Fini, M.; Russo, M.A. The interplay of reactive oxygen species, hypoxia, inflammation, and sirtuins in cancer initiation and progression. *Oxid. Med. Cell. Longev.* **2016**, *2016*. [CrossRef]

92. Schenk, B.; Fulda, S. Reactive oxygen species regulate Smac mimetic/TNFα-induced necroptotic signaling and cell death. *Oncogene* **2015**, *34*, 5796–5806. [CrossRef]
93. Clapp, C.; de la Escalera, G.M. Aquaporin-1: A novel promoter of tumor angiogenesis. *Trends Endocrinol. Metab.* **2006**, *17*, 1–2. [CrossRef] [PubMed]
94. Saadoun, S.; Papadopoulos, M.C.; Hara-Chikuma, M.; Verkman, A. Impairment of angiogenesis and cell migration by targeted aquaporin-1 gene disruption. *Nature* **2005**, *434*, 786–792. [CrossRef]
95. Abreu-Rodríguez, I.; Silva, R.S.; Martins, A.P.; Soveral, G.; Toledo-Aral, J.J.; López-Barneo, J.; Echevarría, M. Functional and transcriptional induction of aquaporin-1 gene by hypoxia; analysis of promoter and role of Hif-1α. *PLoS ONE* **2011**, *6*, e28385. [CrossRef]
96. Dorward, H.S.; Du, A.; Bruhn, M.A.; Wrin, J.; Pei, J.V.; Evdokiou, A.; Price, T.J.; Yool, A.J.; Hardingham, J.E. Pharmacological blockade of aquaporin-1 water channel by AqB013 restricts migration and invasiveness of colon cancer cells and prevents endothelial tube formation in vitro. *J. Exp. Clin. Cancer Res.* **2016**, *35*, 36. [CrossRef]
97. Tomita, Y.; Palethorpe, H.M.; Smith, E.; Nakhjavani, M.; Townsend, A.R.; Price, T.J.; Yool, A.J.; Hardingham, J.E. Bumetanide-derived aquaporin 1 inhibitors, aqb013 and aqb050 inhibit tube formation of endothelial cells through induction of apoptosis and impaired migration in vitro. *Int. J. Mol. Sci.* **2019**, *20*, 1818. [CrossRef]
98. Palethorpe, H.M.; Tomita, Y.; Smith, E.; Pei, J.V.; Townsend, A.R.; Price, T.J.; Young, J.P.; Yool, A.J.; Hardingham, J.E. The aquaporin 1 inhibitor bacopaside II reduces endothelial cell migration and tubulogenesis and induces apoptosis. *Int. J. Mol. Sci.* **2018**, *19*, 653. [CrossRef]
99. Pan, X.-Y.; Guo, H.; Han, J.; Hao, F.; An, Y.; Xu, Y.; Xiaokaiti, Y.; Pan, Y.; Li, X.-J. Ginsenoside Rg3 attenuates cell migration via inhibition of aquaporin 1 expression in PC-3M prostate cancer cells. *Eur. J. Pharmacol.* **2012**, *683*, 27–34. [CrossRef]
100. Peng, M.; Li, X.; Zhang, T.; Ding, Y.; Yi, Y.; Le, J.; Yang, Y.; Chen, X. Stereoselective pharmacokinetic and metabolism studies of 20 (S)-and 20 (R)-ginsenoside Rg3 epimers in rat plasma by liquid chromatography-electrospray ionization mass spectrometry. *J. Pharm. Biomed. Anal.* **2016**, *121*, 215–224. [CrossRef]
101. Yang, L.; Zhang, X.-y.; Li, K.; Li, A.-p.; Yang, W.-d.; Yang, R.; Wang, P.; Zhao, Z.-h.; Cui, F.; Qin, Y. Protopanaxadiol inhibits epithelial–mesenchymal transition of hepatocellular carcinoma by targeting STAT3 pathway. *Cell Death Dis.* **2019**, *10*, 1–13. [CrossRef]
102. Chen, Y.; Zhang, Y.; Song, W.; Zhang, Y.; Dong, X.; Tan, M. Ginsenoside Rh2 Inhibits Migration of Lung Cancer Cells under Hypoxia via mir-491. *Anti-Cancer Agents Med. Chem.* **2019**, *19*, 1633–1641. [CrossRef] [PubMed]
103. Xie, H.-T.; Wang, G.-J.; Sun, J.-G.; Tucker, I.; Zhao, X.-C.; Xie, Y.-Y.; Li, H.; Jiang, X.-l.; Wang, R.; Xu, M.-J. High performance liquid chromatographic–mass spectrometric determination of ginsenoside Rg3 and its metabolites in rat plasma using solid-phase extraction for pharmacokinetic studies. *J. Chromatogr. B* **2005**, *818*, 167–173. [CrossRef] [PubMed]
104. Cai, Z.; Qian, T.; Wong, R.N.; Jiang, Z.-H. Liquid chromatography–electrospray ionization mass spectrometry for metabolism and pharmacokinetic studies of ginsenoside Rg3. *Anal. Chim. Acta* **2003**, *492*, 283–293. [CrossRef]
105. Qian, T.; Cai, Z.; Wong, R.N.; Mak, N.K.; Jiang, Z.-H. In vivo rat metabolism and pharmacokinetic studies of ginsenoside Rg3. *J. Chromatogr. B* **2005**, *816*, 223–232. [CrossRef]
106. Lipinski, C.A.; Lombardo, F.; Dominy, B.W.; Feeney, P.J. Experimental and computational approaches to estimate solubility and permeability in drug discovery and development settings. *Adv. Drug Deliv. Rev.* **1997**, *23*, 3–25. [CrossRef]
107. Li, G.; Wang, Z.; Sun, Y.; Liu, K.; Wang, Z. Ginsenoside 20 (S)-protopanaxadiol inhibits the proliferation and invasion of human fibrosarcoma HT1080 cells. *Basic Clin. Pharmacol. Toxicol.* **2006**, *98*, 588–592. [CrossRef] [PubMed]
108. Chen, X.-J.; Zhang, X.-J.; Shui, Y.-M.; Wan, J.-B.; Gao, J.-L. Anticancer activities of protopanaxadiol-and protopanaxatriol-type ginsenosides and their metabolites. *Evid. Based Complement. Alternat. Med.* **2016**, *2016*. [CrossRef]
109. Huang, Y.; Huang, H.; Han, Z.; Li, W.; Mai, Z.; Yuan, R. Ginsenoside Rh2 inhibits angiogenesis in prostate cancer by targeting CNNM1. *J. Nanosci. Nanotechnol.* **2019**, *19*, 1942–1950. [CrossRef]

110. Zhao, Q.; Li, P.; Jiang, J.; Hu, P. Pharmacokinetics of single ascending doses and multiple doses of 20 (S)-ginsenoside Rg3 in Chinese healthy volunteers. *Eur. J. Drug Metab. Pharmacokinet.* **2016**, *41*, 845–853. [CrossRef]
111. Li, C.; Wang, Z.; Li, G.; Wang, Z.; Yang, J.; Li, Y.; Wang, H.; Jin, H.; Qiao, J.; Wang, H. Acute and repeated dose 26-week oral toxicity study of 20 (S)-ginsenoside Rg3 in Kunming mice and Sprague–Dawley rats. *J. Ginseng Res.* **2020**, *44*, 222–228. [CrossRef]
112. Gao, Y.; Wang, G.; Wang, T.; Li, G.; Lin, J.; Sun, L.; Wu, X.; Sun, X.; Wang, H.; Li, C. A 26-week 20 (S)-ginsenoside Rg3 oral toxicity study in Beagle dogs. *Regul. Toxicol. Pharmacol.* **2020**, *110*, 104522. [CrossRef]
113. Lu, P.; Su, W.; Miao, Z.-h.; Niu, H.-r.; Liu, J.; Hua, Q.-l. Effect and mechanism of ginsenoside Rg3 on postoperative life span of patients with non-small cell lung cancer. *Chin. J. Integr. Med.* **2008**, *14*, 33–36. [CrossRef] [PubMed]
114. Li, Y.; Wang, Y.; Niu, K.; Chen, X.; Xia, L.; Lu, D.; Kong, R.; Chen, Z.; Duan, Y.; Sun, J. Clinical benefit from EGFR-TKI plus ginsenoside Rg3 in patients with advanced non-small cell lung cancer harboring EGFR active mutation. *Oncotarget* **2016**, *7*, 70535. [CrossRef]
115. Zhou, B.; Yan, Z.; Liu, R.; Shi, P.; Qian, S.; Qu, X.; Zhu, L.; Zhang, W.; Wang, J. Prospective study of transcatheter arterial chemoembolization (TACE) with ginsenoside Rg3 versus TACE alone for the treatment of patients with advanced hepatocellular carcinoma. *Radiology* **2016**, *280*, 630–639. [CrossRef]

Sample Availability: Samples of the compounds are not available from the authors.

Publisher's Note: MDPI stays neutral with regard to jurisdictional claims in published maps and institutional affiliations.

1.9 Statement of authorship

Statement of Authorship

Title of Paper	Druggable molecular targets for the treatment of triple negative breast cancer
Publication Status	☑ Published ☐ Accepted for Publication ☐ Submitted for Publication ☐ Unpublished and Unsubmitted work written in manuscript style
Publication Details	Nakhjavani, M., Hardingham, J. E., Palethorpe, H. M., Price, T. J., & Townsend, A. R. (2019). Druggable molecular targets for the treatment of triple negative breast cancer. Journal of breast cancer, 22(3), 341.

Principal Author

Name of Principal Author (Candidate)	Maryam Nakhjavani		
Contribution to the Paper	Conceptualised, designed and prepared the Tables and Figures and substantially wrote the manuscript.		
Overall percentage (%)	70		
Certification:	This paper reports on original research I conducted during the period of my Higher Degree by Research candidature and is not subject to any obligations or contractual agreements with a third party that would constrain its inclusion in this thesis. I am the primary author of this paper.		
Signature		Date	10th Feb 2021

Co-Author Contributions

By signing the Statement of Authorship, each author certifies that:

i. the candidate's stated contribution to the publication is accurate (as detailed above);
ii. permission is granted for the candidate in include the publication in the thesis; and
iii. the sum of all co-author contributions is equal to 100% less the candidate's stated contribution.

Name of Co-Author	Jennifer E Hardingham		
Contribution to the Paper	Conceptualised the work and contributed to designing the paper, Figures and Tables, and writing the paper.		
Signature		Date	10th Feb 2021

Name of Co-Author	Helen M Palethorpe		
Contribution to the Paper	Contributed to drafting and reviewing the paper.		
Signature		Date	8th February 2021

Name of Co-Author	Tim J Price		
Contribution to the Paper	Contributed to drafting and reviewing the paper.		
Signature		Date	11th Feb 2021

Name of Co-Author	Amanda R Townsend		
Contribution to the Paper	Conceptualised and contributed to designing the paper, Figures and Tables, and writing the paper.		
Signature		Date	11th Feb 2021

J Breast Cancer. 2019 Sep;22(3):341-361
https://doi.org/10.4048/jbc.2019.22.e39
pISSN 1738-6756·eISSN 2092-9900

Journal of Breast Cancer JBC

Review Article

Check for updates

Druggable Molecular Targets for the Treatment of Triple Negative Breast Cancer

Maryam Nakhjavani [1,2], **Jennifer E Hardingham** [1,2], **Helen M Palethorpe** [1,2], **Tim J Price** [2,3], **Amanda R Townsend** [2,3]

[1]Molecular Oncology, Basil Hetzel Institute, The Queen Elizabeth Hospital, Woodville South, Australia
[2]Adelaide Medical School, University of Adelaide, Adelaide, Australia
[3]Medical Oncology, The Queen Elizabeth Hospital, Woodville South, Australia

OPEN ACCESS

Received: Apr 8, 2019
Accepted: Aug 20, 2019

Correspondence to
Jennifer E Hardingham
Molecular Oncology, Basil Hetzel Institute, The Queen Elizabeth Hospital, Woodville South, SA 5011, Australia.
E-mail: jenny.hardingham@sa.gov.au

ORCID iDs
Maryam Nakhjavani
https://orcid.org/0000-0002-5357-7167
Jennifer E Hardingham
https://orcid.org/0000-0001-8277-1199
Helen M Palethorpe
https://orcid.org/0000-0003-3803-5113
Tim J Price
https://orcid.org/0000-0002-3922-2693
Amanda R Townsend
https://orcid.org/0000-0003-3563-4719

Conflict of Interest
The authors declare that they have no competing interests.

Author Contributions
Conceptualization: Nakhjavani M. Supervision: Hardingham JE, Townsend AR. Writing - original draft: Nakhjavani M. Writing - review & editing: Hardingham JE, Palethorpe HM, Price TJ, Townsend AR.

ABSTRACT

Breast cancer (BC) is still the most common cancer among women worldwide. Amongst the subtypes of BC, triple negative breast cancer (TNBC) is characterized by deficient expression of estrogen, progesterone, and human epidermal growth factor receptor 2 receptors. These patients are therefore not given the option of targeted therapy and have worse prognosis as a result. Consequently, much research has been devoted to identifying specific molecular targets that can be utilized for targeted cancer therapy, thereby limiting the progression and metastasis of this invasive tumor, and improving patient outcomes. In this review, we have focused on the molecular targets in TNBC, categorizing these into targets within the immune system such as immune checkpoint modulators, intra-nuclear targets, intracellular targets, and cell surface targets. The aim of this review is to introduce and summarize the known targets and drugs under investigation in phase II or III clinical trials, while introducing additional possible targets for future drug development. This review brings a tangible benefit to cancer researchers who seek a comprehensive comparison of TNBC treatment options.

Keywords: Clinical trial; Drug therapy; Triple negative breast neoplasms

INTRODUCTION

Triple negative breast cancer (TNBC) is one subtype of breast cancer (BC) which is defined as a group of BCs lacking the expression of 3 major receptors involved in BC; estrogen receptor (ER), progesterone receptor (PR), and overexpression of human epidermal growth factor receptor 2 (HER2). The overall incidence of TNBC is approximately 15%–20%, with higher rates seen in young women and African-Americans [1]. Compared to other types of BC, patients with TNBC will experience poorer overall survival (OS), and a higher probability of cancer recurrence.

TNBC is a heterogeneous disease which is subcategorized into various subtypes. Lehmann et al. [2] described a classification for TNBC subtypes, based on the microarray data on 587 TNBC cases. He introduced 2 basal-like (BL) subtypes. BL1 subtype showed high expression of cell cycle and DNA damage response genes and BL2 subtype showed high expression of genes involved in growth factor signaling, nerve growth factor, hepatocyte

growth factor receptor, insulin like growth factor 1 receptor pathways, glycolysis and gluconeogenesis, and myoepithelial markers (TP63 and MME). The immunomodulatory subtype was enriched for immune cell processes and immune signaling. The mesenchymal stem-like subtype was characterized by a high expression of genes involved in motility, extracellular matrix, epithelial-to-mesenchymal transition (EMT), and cell differentiation pathways with a lower expression of genes involved in proliferation. The luminal androgen receptor (LAR) subtype is associated with a higher expression of genes responsible for steroid synthesis and androgen/estrogen metabolism. In 2015, Burstein et al. [3] performed RNA and DNA profiling analysis on 198 TNBC tumors and defined a category consisting of 4 TNBC subtypes; BL immunosuppressed, BL immune-activated, LAR and mesenchymal. Regardless of the disease subtype and since TNBC does not express/overexpress ER, PR or HER2, systemic chemotherapy, rather than targeted therapy, has long been the major treatment option for these patients. Complications associated with single or combination chemotherapy regimens, and limitations in efficacy, has made oncologists and cancer researchers more interested in developing and administering targeted therapies to these patients. In recent years, along with the high efficacy of cancer immunotherapy in metastatic and advanced tumors such as lung and melanoma, some researchers have focused their efforts on the classification of TNBC based on immune markers. For example, Jézéquel et al. [4] performed microarray profiling on 107 TNBC patients and described 3 TNBC subtypes: BL with low immune response and high M2-like macrophages, basal-enriched with high immune response and low M2-like macrophages, and LAR. These subtypes have incidence rates of 45%, 33%, and 22%, respectively. Highlighting the importance of immunotherapy today, drugs developed in this area have been included in clinical trials. This review paper highlights the molecular targets in TNBC, with an emphasis on well-known targets with available drugs, therapies which are mostly in phase II and III clinical trials, and discussing plausible targets for future drug development. The authors hope to give a thorough update on the basic and clinical outcomes and on the current status of clinical drug testing.

IMMUNE CHECKPOINT MODULATORS

Programmed cell death protein 1 (PD-1) and its ligand

PD-1 is a surface receptor expressed by T cells, and when engaged with its ligand has an immunosuppressive role. Therefore, PD-1 inhibitors inhibit the activation of this receptor, thereby improving immune function and allowing cancer cells to come under attack. PD-1 has 2 ligands, PD-L1 and PD-L2 (**Figure 1**). Reports have suggested that 40.9% of TNBC patients express PD-L1 [5]. PD-L1 is associated with increased tumor infiltrating lymphocytes (TILs) [6]. This suggests that anti-PD-1 or anti-PD-L1 agents are efficacious in these patients. Registered PD-1 and PD-L1 clinical trials are listed in **Table 1**. Anti-PD-1 drugs include pembrolizumab, nivolumab, toripalimab, spartalizumab, camrelizumab, FAZ053, and PF-06936308. Most studies of these drugs are in phase I clinical trials. Currently, 48 and 19 clinical trials are registered to use pembrolizumab and nivolumab, respectively, as a potential intervention in TNBC patients. Pembrolizumab is widely used in other cancers with a favorable safety profile. Pembrolizumab, as a monotherapy, was studied in a phase II clinical trial, in 170 metastatic TNBC (mTNBC) patients, 61.8% of which were PD-L1-positive. The objective response rate (ORR) in the whole population and in the PD-L1+ population in this study was 5.3% (95% confidence interval [CI], 2.7–9.9) and 5.7% (95% CI, 2.4–12.2). Likewise, the disease control rate in these 2 groups was 7.6% (95% CI, 4.4–12.7) and 9.5% (95% CI, 5.1–16.8), respectively. The median progression-free survival (PFS) and median OS

https://doi.org/10.4048/jbc.2019.22.e39

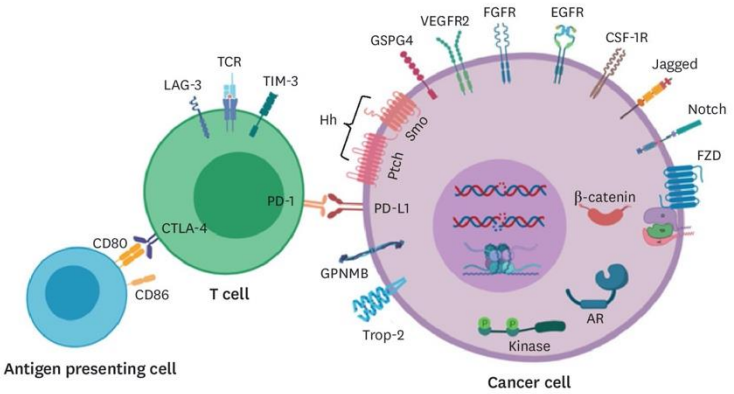

Figure 1. Major druggable targets expressed as proteins or glycoproteins and functioning as receptors, ligands, channels, mitotic protein kinases or nuclear receptors.
TIM-3 = T cell immunoglobulin and mucin-domain containing-3; PD-1 = programmed cell death protein 1; PD-L1 = programmed death-ligand 1; Hh = hedgehog; VEGFR2 = vascular endothelial growth factor receptor 2; FGFR = fibroblast growth factor receptor; EGFR = epidermal growth factor receptor; GPNMB = glycoprotein non-metastatic B; Trop-2 = trophoblast antigen 2; AR = androgen receptor; CSF1R = colony stimulating factor 1 receptor; FZD = frizzled.

in this study was 2 months (95% CI, 1.9–2.0) and 9 months (95% CI, 7.6–11.2), respectively. While the ORR was low, for patients who responded to treatment, disease control was durable [7].

Anti-PD-L1 drugs include atezolizumab, durvalumab, avelumab, and M7824. Atezolizumab is a promising anti-PD-L1 agent, especially in combination with taxane in the treatment of PD-L1 positive mTNBC [5]. Nabpaclitaxel in combination with atezolizumab or placebo in 902 mTNBC patients caused a statistically significant increase in the median PFS in the group receiving atezolizumab (7.2 vs. 5.5 months). In PD-L1+ tumors, the median OS of those receiving atezolizumab and nabpaclitaxel was 25 months, compared with 15.5 months for nabpaclitaxel alone. The results of these studies suggest that anti-PD-1 and anti-PD-L1 drugs may be promising therapies for these patients.

Cytotoxic T lymphocyte-associated protein 4 (CTLA-4)

CTLA-4 is another immune checkpoint protein which is expressed on activated T cells (**Figure 1**). CTLA-4 competes with its homologous molecule, CD28 for binding to CD80 and CD86 on antigen presenting cells. CLTA-4 has a higher affinity for CD80 and CD86, and unlike CD28, CLTA-4 transmits inhibitory signals to the T cell. CTLA-4 is also expressed on regulatory T cells (Tregs) mediating immunosuppressive responses. Therefore, inhibition of CTLA-4 is thought to induce proliferation of T cells leading to a boost of immune responses in the body [8]. Ipilimumab is an anti-CTLA-4 monoclonal antibody and a checkpoint blocker, currently undergoing clinical trial testing in combination with nivolumab (NCT03546686, NCT01928394) or nivolumab and INCAGN01876 (anti-human glucocorticoid-induced tumor necrosis factor [TNF] receptor) (NCT03126110, NCT03241173). Likewise, tremelimumab, a fully human anti-CTLA-4 monoclonal antibody, is under clinical investigations in combination with PF-06936308 (NCT03674827), nab-paclitaxel and carboplatin (NCT02658214), and durvalumab (NCT02527434).

Table 1. Inhibitors of PD-1 and PD-L1 in phase II and III clinical trials

Inhibitor	Other treatments in the study	Status	Identifier
Pembrolizumab*	Bemcentinib	Phase II, R	NCT03184558
	None	Phase II, R	NCT02411656
	Anastrozole, doxorubicin, exemestane, letrozole	Phase II, R	NCT02648477
	Valacyclovir, ADV/HSV-tk, radiation	Phase II, R	NCT03004183
	Tavokinogene telseplasmid	Phase II, R	NCT03567720
	Nab-paclitaxel, epirubicin, cyclophosphamide	Phase II, R	NCT03289819
	Carboplatin, gemcitabine	Phase II, R	NCT02755272
	None	Phase II, R	NCT03145961
	Doxorubicin, cyclophosphamide, paclitaxel, carboplatin, decitabine	Phase II, R	NCT02957968
	Carboplatin, docetaxel, pegfilgrastim	Phase II, R	NCT03639948
	Enobosarm	Phase II, R	NCT02971761
	Carboplatin, nab-paclitaxel	Phase II, R	NCT03121352
	Radiation therapy	Phase III, R	NCT02954874
	None	Phase II, ANR	NCT02447003
	Capecitabine	Phase II, ANR	NCT03044730
	Radiotherapy	Phase II, ANR	NCT02730130
	Imprime PGG	Phase II, ANR	NCT02981303
	Cyclophosphamide	Phase II, ANR	NCT02768701
	Capecitabine, eribulin, gemcitabine, vinorelbine	Phase III, ANR	NCT02555657
	Nab-paclitaxel, paclitaxel, gemcitabine, carboplatin, normal saline solution	Phase III, ANR	NCT02819518
	Carboplatin, paclitaxel, doxorubicin, epirubicin, cyclophosphamide, placebo, filgrastim or pegfilgastrim	Phase III, ANR	NCT03036488
	Cisplatin	Phase II, NR‖	NCT03644589
	Lenvatinib	Phase II, NR	NCT03797326
	Carboplatin	Phase II, S (amendment)	NCT03213041
Nivolumab*	Cabozantinib	Phase II, R	NCT03316586
	Radiation therapy, low dose doxorubicin, cyclophosphamide, cisplatin	Phase II, R	NCT02499367
	Ipilimumab	Phase II, R	NCT03546686
	Capecitabine	Phase II, R	NCT03487666
	Carboplatin	Phase II, R	NCT03414684
	Ipilimumab, capecitabine	Phase II, NR	NCT03818685
	Doxorubicin	Phase II, NR	NCT03815890
Toripalimab*	Nab-paclitaxel, placebo	Phase III, NR	NCT03777579
Camrelizumab*	Apatinib	Phase II, R	NCT03394287
Atezolizumab†	None	Phase II, R	NCT02478099
	Stereotactic radiosurgery	Phase II, R	NCT03483012
	Paclitaxel, carbo/cyclo	Phase II, R	NCT01898117
	Pegylated liposomal doxorubicin, cyclophosphamide, placebo	Phase II, R	NCT03164993
	Placebo, paclitaxel	Phase III, R	NCT03125902
	Placebo	Phase III, R	NCT03281954
	Paclitaxel, dose-dense doxorubicin or dose-dense epirubicin, cyclophosphamide	Phase III, R	NCT03498716
	Nab-paclitaxel, placebo	Phase III, ANR	NCT02425891
	Placebo, nab-paclitaxel, doxorubicin, cyclophosphamide, filgrastim, pegfilgrastim	Phase III, ANR	NCT03197935
	AZD6738, olaparib	Phase II, NR	NCT03740893
	Capecitabine	Phase II, NR	NCT03756298
	Carboplatin, paclitaxel	Phase II, S	NCT02883062
Durvalumab†	Olaparib	Phase II, R	NCT03167619
	Olaparib	Phase II, R	NCT03801369
	Placebo, nab-paclitaxel, epirubicin, cyclophosphamide	Phase II, ANR	NCT02685059
	Tremelimumab	Phase II, ANR	NCT02527434
	Carboplatin, gemcitabine, nab-paclitaxel, personalized synthetic long peptide vaccine, poly ICLC	Phase II, NR	NCT03606967
	AZD6738, olaparib	Phase II, NR	NCT03740893

Pembrolizumab, nivolumab, toripalimab and camrelizumab are anti-PD-1 drugs. Atezolizumab and durvalumab are anti-PD-L1 drugs.
PD-1 = programmed cell death protein 1; PD-L1 = programmed death-ligand 1; ADV/HSV-tk = adenoviral vector-mediated herpes simplex virus tyrosine kinase; R = recruiting; ANR = active, not recruiting; NR = not recruiting; S = suspended.
*Anti-PD-1; †Anti-PD-L1.

Lymphocyte-activation gene 3 (LAG-3)

LAG-3 (**Figure 1**) is another immune checkpoint receptor which, like CTLA-4 and PD-1, is a negative regulator of the activation and proliferation of T cells and a suppressor of Tregs. About 15% of TNBC patients are reported to co-express PD-1 and LAG-3, associated with the presence of TILs [9]. Therefore, inhibition of both LAG-3 and PD-1 may have synergistic antitumor immune effects. Currently, 3 clinical trials investigating anti-LAG-3 antibodies in TNBC patients, usually in combination with an anti-PD-1 drug, are ongoing. These include LAG525 (IMP701), an anti-LAG-3 antibody, in combination with spartalizumab in mTNBC patients (NCT03742349); and TSR-033, another anti-LAG-3 monoclonal antibody, alone or in combination with anti-PD-1 antibody in various solid tumors including TNBC (NCT03250832). the third anti-LAG-3 antibody (INCAGN02385) is in phase I clinical trial in patients with advanced malignancies, including TNBC (NCT03538028).

T cell immunoglobulin and mucin-domain containing-3 (TIM-3)

TIM-3 (**Figure 1**) is another cell surface receptor and immune checkpoint, which together with PD-1 and LAG-3 exhausts $CD8^+$ T cells. TIM-3 is highly expressed in TILs and tumor antigen-specific T cells, playing a role in tumor immunity [10]. Currently, INCAGN02390, an anti-TIM-3 antibody, is in phase I clinical trials in some advanced malignancies, including TNBC (NCT03652077).

Hedgehog (Hh) and neuropilin-2 (NRP-2) signaling pathway

The Hh signaling pathway is involved in the development and differentiation of embryos, angiogenesis and regulating cell fate. Importantly, this signaling pathway is a regulator of immune system, plays a role in TNBC progression [11] and contributes to cancer cell stemness in TNBC [12]. In addition, NRP-2, a VEGF receptor, is expressed in tumour-initiating cells involved in the initiation and genesis of TNBCs. In fact, activation of NRP-2 causes expression of GLI1 which induces another key stem cell factor, BMI-1. BMI-1, in an autocrine loop, enhances the expression of NRP-2. All of these steps could potentially be targeted to delay tumour initiation. *In vitro* studies report the successful use of Hh signaling inhibitors, such as Cyclopamine and Gant61. Vismodegib (NCT02694224) and sonidegib (NCT02027376) are 2 Hh signaling inhibitors which have been approved for use in basal-cell carcinoma, and for clinical trials in TNBC patients by the United States Food and Drug Administration (FDA).

TARGETS WITHIN THE NUCLEUS

Breast cancer susceptibility gene (BRCA) and platinum-based treatment

BRCA1 and *BRCA2* are genes which are responsible for repairing double stranded DNA breaks. Mutations in these 2 genes causes DNA instability, making the cell more susceptible to DNA interacting agents, such as platinum salts. *BRCA* mutation is associated with inherited BC. More than 80% of the tumors with *BRCA1* mutations have TNBC characteristics, and are more aggressive and have higher tumor grade [1]. Platinum-based drugs are increasingly being utilized in the adjuvant and metastatic setting as well as other standard chemotherapeutics (including microtubule inhibitors, anthracyclines and antimetabolites). The results of a phase II clinical trial suggest that platinum monotherapy is especially effective in patients with *BRCA1/2* mutations [13]. Cisplatin in combination with gemcitabine has a favorable safety profile [14] and could be superior to paclitaxel plus gemcitabine, based on a phase III multicenter trial. A recent phase III clinical trial

comparing carboplatin with docetaxel in 376 TNBC patients showed that the ORR between the 2 groups was not significantly different (31.4 vs. 34.0 months; $p = 0.66$). However, in *BRCA* mutated patients, ORR with carboplatin (68%) was twice that of the docetaxel group (33%) ($p = 0.01$) [15]. A randomized phase II clinical trial studied the effects of adding carboplatin and/or bevacizumab to the chemotherapy regimen (paclitaxel, doxorubicin and cyclophosphamide) of 433 stage II and III TNBC patients. The addition of carboplatin resulted in blood toxicities including neutropenia and thrombocytopenia. However, pathologic complete responses (pCRs) in breast (60% vs. 46%; $p = 0.0018$) and breast/axilla (54% vs. 41%; $p = 0.0029$) were significantly increased with carboplatin, while bevacizumab only increased breast pCR (59% vs. 48%; $p = 0.0089$) [16].

Poly-ADP ribose-polymerases (PARP)

PARP is responsible for repairing single stranded DNA breaks. PARP inhibitor (PARPi) agents or PARP trappers inhibit the active site of the enzyme. The PARP/PARPi complex binds to the damaged area, but without the catalytic activity necessary for PARP-dependent DNA damage repair. The stalling PARP on the DNA can induce a double strand break. In healthy cells with normal BRCA function, BRCA ultimately repairs this damage and the cell survives. In cases of *BRCA* mutations, the double stranded breaks persist and the cell eventually dies. Therefore, BRCA mutated patients may benefit from PARPi agents together with platinum-based drugs. There are 5 PARPi agents in phase II or III clinical trials (**Table 2**). The effects of olaparib (300 mg, twice a day) were compared with standard monotherapy in 302 patients with the *BRCA* mutation and HER2 negative metastatic BCs (OLYMPiAD study). Patients treated with olaparib had a significantly longer median PFS (7.0 months) and longer response rate (59.9%) compared to the standard therapy group (4.2 months and 28.8%) ($p < 0.0001$). These patients also had a lower rate of grade 3 or higher adverse events (36.6% vs. 50.5%) and drug discontinuation due to toxic events (4.9% vs. 7.7%) [17]. Olaparib was well-tolerated, however, the median OS of these patients (19.3 months) was not significantly different from the patients on standard therapy (17.1 months) (95% CI, 0.66–1.23; $p = 0.513$) [18]. Olaparib is under investigation as a monotherapy and as a combination therapy with other agents such as immunotherapy drugs, cell cycle and cell growth inhibitors. The completed trial on the combination of olaparib and carboplatin (NCT01445418) on 28 TNBC patients showed this combination is tolerable, with 1 complete response of more than 69 months, 19% partial response (median of 4 months) [19]. The safety, tolerability and efficacy of olaparib (200 mg, twice a day) plus paclitaxel was studied in another phase I clinical trial (NCT00707707) on a total of 19 mTNBC patients. Results from that trial showed that this combination caused

Table 2. A summary of poly-ADP ribose-polymerases inhibitor drugs in clinical trials phase II and III

Inhibitor	Other treatments in the study	Status	Identifier
Olaparib	Durvalumib	Phase II, R	NCT03801369
	Durvalumib	Phase II, R	NCT03167619
	18F-Fluoromisonidazole, cediranib maleate	Phase II, R	NCT02498613
	Paclitaxel, carboplatin, epirubicin, cyclophosphamide	Phase II, R	NCT02789332
	Paclitaxel, carboplatin	Phase II/III, R	NCT03150576
	BKM120, BYL719	Phase II, ANR	NCT01623349
	None	Phase II, ANR	NCT00679783
Veliparib	Cyclophosphamide	Phase II, C	NCT01306032
	Cisplatin, placebo	Phase II, R	NCT02595905
Fluzoparib	Apatinib	Phase I, R	NCT03075462
Rucaparib	Cisplatin	Phase II, ANR	NCT01074970
Talazoparib	None	Phase II, R	NCT02401347

R = recruiting; C = completed; ANR = active, not recruiting.

https://doi.org/10.4048/jbc.2019.22.e39

higher-than-expected neutropenia. However, an encouraging response rate was found in 37% (7) of the patients who had a confirmed partial response, and one patient remained on olaparib monotherapy without disease progression. The authors concluded that further dose adjustments would be required [20].

The EMBRACA clinical trial studied the effects of talazoparib in 431 patients with advanced BC and *BRCA1/2* mutations. Two hundred and eighty-seven patients received 1 mg/day talazoparib and 144 patients received standard therapy. Patients in the talazoparib group had a significantly longer median PFS (8.6 months) compared to the standard therapy group (5.6 months) ($p < 0.001$). The talazoparib group had a higher ORR (62.2%) compared to standard therapy (27.2%) (95% CI, 2.9–8.8; $p < 0.001$) [21]. Talazoparib is currently in a phase II clinical trial recruiting TNBC patients (**Table 2**).

Veliparib is another drug in this group with some completed phase I and II clinical trials. Single agent veliparib was tested in 88 patients with and without *BRCA* mutations and results show that it is well-tolerated and has anti-tumor activity against both tumor types in comparison with other single PARPi agents [22]. A phase I clinical trial (NCT01104259) using a combination of veliparib, cisplatin and vinorelbine tartrate in 50 BRCA mutated TNBC patients, showed a median PFS of 5.5 months (95% CI, 4.1–6.7) [23]. In a phase III clinical trial, veliparib was added to carboplatin in 634 patients, 316 receiving paclitaxel + carboplatin + veliparib, 160 receiving paclitaxel + carboplatin and 158 receiving carboplatin alone. The first group achieved a higher pCR (53%) compared to the paclitaxel alone group (31%), but not compared to paclitaxel + carboplatin (58%). While veliparib did not add to the toxicity profile it did not provide additional benefit beyond the benefit seen with the addition of carboplatin. Importantly, the addition of veliparib + carboplatin to paclitaxel and then doxorubicin + cyclophosphamide improved the pCR in TNBC patients [24]. Other PARPi agents, including niraparib, fluzoparib, rucaparib and E7449, have fewer registered clinical trials.

Histone deacetylase (HDAC)

HDACs, important regulators of gene expression and transcription (**Figure 1**), are upregulated in BC [25]. HDAC inhibitors (HDACi) have shown a various range of effects in laboratory cancer models. Panobinostat is one of these drugs under phase I/II clinical trial in combination with tamoxifen (NCT01194908). A previous clinical trial investigating the effect of panobinostat in combination with letrozole showed that thrombocytopenia was the most common adverse reaction [26]. Romidepsin is also undergoing another clinical trial in locally recurrent or mTNBC. Entinostat was used with azacitidine in a phase II clinical trial study. The results of this study showed that this combination was well-tolerated but TNBC patients did not respond to the therapy [27]. Entinostat alone in combination with atezolizumab (NCT02708680) or azacitidine (NCT01349959) are other examples of HDACi drugs undergoing phase II clinical trials.

p53, checkpoint kinase 1 (ChK1) and ataxia telangiectasia and Rad3 related (ATR)

The tumor suppressor gene *p53* is a well-known oncogene. Studies show that p53 is a nuclear protein which is responsible for DNA repair, triggering apoptosis in cases of irreparable DNA damage or inducing senescence, cell cycle arrest, necrosis or autophagy. Mutations in *p53* are very common in TNBC (60%–70%), and result in the loss of p53 mediated tumor-suppression [28]. Mutated *p53* loses its ability to monitor the G1 checkpoint of cell cycle and as a result, the cell relies more on ChK1 to arrest the cell. ChK1 is downstream of activated ATR, another

coordinator of DNA repair management. The activated ATR-Chk1 pathway affects multiple DNA damage and replication checkpoint responses. Various ATR and/or Chk1/2 inhibitors have been designed and synthesized so far. LY2606368 is a ChK1/2 inhibitor which is being tested in a phase II clinical trial in patients with tumors, including TNBC, aiming to see if this therapy can help shrink tumors (NCT02203513). AZD6738 is an inhibitor of ATR currently in phase II clinical trials to assess the safety and efficacy of olaparib (PARPi) in combination with AZD6738 in TNBC patients (NCT03330847). This drug is also being tested in another phase II clinical trial to compare its effects as a monotherapy to olaparib or durvalumab (anti PD-L1) monotherapy in TNBC patients (NCT03740893).

DNA binding agents

Mithramycin or plicamycin is an antibiotic produced by *Streptomyces* strains. Mithramycin adheres to DNA and inhibits RNA and protein production. Mithramycin has shown efficacy in various cancers, and in *in vitro* and *in vivo* TNBC models. Trabectedin is another antineoplastic alkylating agent. Early studies showed the efficacy of trabectedin in TNBC, however, a phase II clinical trial on TNBC and HER2-overexpressing metastatic BC patients showed no confirmed responses in mTNBC patients [29].

INTRACELLULAR TARGETS AND SIGNALING MEDIATORS

Androgen receptor (AR)

AR is a member of the steroid and nuclear receptor superfamily and a transcription factor (**Figure 1**). The LAR class of TNBC expresses AR. Studies investigating the link between AR and decreased relapse-free survival [2,28], higher mortality rate [30] or a favorable disease-free survival [31,32] are controversial. However, this class of TNBC has become a favorable target for anti-androgen therapy. Bicalutamide, an AR inhibitor, primarily used for metastatic prostate cancer, was well tolerated with a 19% 6-month clinical benefit rate (CBR) (95% CI, 7%–39%) in a phase II trial study in metastatic BC patients [33]. Enzalutamide, an inhibitor of AR nuclear localization, was well tolerated in a phase II clinical trial, resulting in a 35% CBR at 16 weeks and a median PFS of 14% [34]. The use of seviteronel, a dual lyase-selective CYP17 inhibitor and AR antagonist in a phase II trial in AR+TNBC patients was also well tolerated [35], and more studies on the drug are underway. **Table 3** shows a summary of the clinical trials on AR drugs in TNBC patients.

Table 3. Phase II and III clinical trials ongoing on anti-androgen drugs in triple negative breast cancer patients

Treatment	Other treatments	Status/key achievement	Identifier
Bicalutamide	Physician's choice, bicalutamide	Phase III, R	NCT03055312
	Physician's choice, bicalutamide	Phase II, U	NCT02353988
	None	Phase II, T (slow enrolment of patients)	NCT02348281
Enzalutamide	Paclitaxel	Phase IIb, R	NCT02689427
	None	Phase II, ANR	NCT01889238
	None	Phase II, ANR	NCT02750358
Enobosarm	Pembrolizumab	Phase II, R	NCT02971761
	None	Phase II, T (lack of efficacy)	NCT02368691
Seviteronel	None	Phase II, C	NCT02130700
CR1447	None	Phase II, ANR	NCT02067741
Darolutamide	Capecitabine	Phase II, R	NCT03383679
Orteronel	None	Phase II, R	NCT01990209

R = recruiting; U = unknown; T =terminated; ANR = active, not recruiting; C = completed.

https://doi.org/10.4048/jbc.2019.22.e39

Heat shock protein 90 (HSP90)

HSP90 is one of the most common members of HSP class of chaperones which is involved in many important signaling pathways including those that are implicated in BC progression. Owing to its wide range of action on important proteins, inhibition of HSP90 could be very beneficial. The effects of known inhibitors of HSP90 is reviewed in [36]. *In vitro* studies have shown that compared to BL or mesenchymal cell lines, the LAR class of TNBC cell lines are more sensitive to the HSP90 inhibitor, 17-DMAG [2]. In the latest phase II clinical trial on the single agent ganetespib, good tolerability and regression of lung tumor metastases in TNBC patients was observed, yet it failed to meet the expected end point of ORR [37]. Ganetespib is no longer available and hence the other clinical trial on ganetespib was terminated (NCT02637375). A clinical trial of onalespib in combination with talazoparib (PARPi) was withdrawn (NCT02627430), but the organizers of this trial are recruiting for a different clinical trial to test the combination of paclitaxel (NCT02474173) and onalespib (NCT02898207). The future application of this group of drugs remains unclear.

Cyclin-dependent kinases (CDKs)

CDKs are tightly controlled regulators of cell cycle and transcriptional machinery. Aberrant expression of CDKs, such as CDK4 and CDK6, is one of the characteristics of many tumors and in TNBC. Various inhibitors of CDKs have been successfully tested in *in vivo* and *in vitro* TNBC models with promising results. A phase I clinical trial on dinaciclib, a pan-CDK inhibitor, in combination with epirubicine (dinaciclib 20 mg/m^2 in day 1 and epirubicine 75 mg/m^2 on day 2 of a 3-week cycle) in 9 mTNBC patients, was closed due to toxicity issues [38]. Dinaciclib is currently in another phase I clinical trial in combination with pembrolizumab (NCT01676753). However, other agents in this group are in phase II clinical trials: trilaciclib, an inhibitor of CDK4/6 (NCT02978716), ribociclib, an inhibitor of CDK6 and cyclin D1/CDK4 (NCT03090165), PF-06873600 (NCT03519178) and abemaciclib, inhibitors of CDK2/4 (NCT03130439).

Proteins involved in apoptosis

Programmed cell death or apoptosis is a tightly controlled process. Dysregulation in apoptosis results in uncontrolled cell proliferation in cancer. Inhibitors of apoptosis proteins (IAPs) are endogenously produced to inhibit apoptosis. Second mitochondrial-derived activator of caspase (SMAC) is a mitochondrial protein which binds to IAPs, facilitating apoptosis in the cells. The SMAC mimetic LCL161 is an orally bioavailable small molecule which is under investigation for use in TNBC patients. In a study, a TNFα-based gene expression signature (GS) which is predictive of sensitivity to LCL161 was used and evaluated as a clinical assay. The results of this phase II clinical trial on adding LCL161 to paclitaxel in TNBC patients showed that patients who received the combination therapy had a higher (38.2%) pCR compared to the control (17.2%) GS-positive group. This study also revealed an array of adverse effects in the combination group, suggesting the importance of biomarker-driven targeted therapy approach for these patients [39]. LCL161 in combination with PDR001 (anti PD-1) is currently in phase Ib clinical trials in TNBC patients (NCT02890069).

Other intracellular targets are summarized in **Table 4**. These include inducible nitric oxide synthase, bromodomain and extra-terminal, cyclooxygenase-2 and mitotic protein kinases. TNBC has a high proliferation rate. Certain protein kinases were found to be important in the oncogenic transformation of TNBC. Important mitotic protein kinases in TNBC include polo-like kinase, aurora, dual specificity protein kinase TTK, never in mitosis A-related kinases and Src tyrosine kinases. These kinases generally phosphorylate either tyrosine, serine/threonine or all these 3 amino acids, known as dual-specificity protein kinases.

Table 4. Promising molecular targets generally at preclinical or phase I clinical trial studies

Target	Importance/role in TNBC	Examples of drug candidates	References
Intracellular targets			
iNOS	Correlated with aggressiveness and poor prognosis	L-NMMA	[79,80]
BET	Regulation of PD-1/PD-L1 axis	OTX015*	[81]
COX-2	Associated with TNBC and poor prognosis	Indomethacin*, celecoxib*, enteric-coated aspirin*	[82,83]
TGF-β signalling	Plays a role in EMT and metastasis	Zerumbone, silibinin, metformin	[84-86]
Mitotic tyrosine kinases			
PlK	Overexpressed PlK1	BI-2536, BI-6727	[87]
Aurora	Mutated/over-expressed	ENMD-2076*, MLN8237*	[88,89]
TTK	Overexpressed, associated with poor survival and aggressiveness of the breast tumour, poor chemotherapy response and relapse	BOS172722*	[90-92]
NIMA	Over-expressed		[93]
Src	Active in TNBC, affecting cell migration and EMT	Dasatinib*	[94]
Cell surface targets			
Notch and Jagged	Higher expression of Notch-1 and Jag-1, associated with poor prognosis of TNBC	PF-03084014, Notch-1 siRNA	[95]
Aquaporin 1	Highly expressed and correlated with TNBC, poor prognosis, higher tumour grade	AqB013, AqB050	[96-99]
WNT receptors	Upregulated involved in WNT/β-catenin signalling	LGK974*	[100]
CSF-1R	Overexpression is correlated with poor prognosis and more tumour invasiveness and metastasis	MCS110*	[101]
CSPG4	TNBC metastasis and angiogenesis	Novel CFP	[102]

PD-1 = programmed cell death protein 1; PD-L1 = programmed death-ligand 1; iNOS = inducible nitric oxide synthase; BET = bromodomain and extra-terminal; COX-2 = cyclooxygenase-2; TNBC = triple negative breast cancer; TGF-β = transforming growth factor-beta; EMT = epithelial-to-mesenchymal transition; PlK = polo-like kinase; TTK = dual specificity protein kinase; NIMA = never in mitosis A-related kinases; CSPG4 = chondroitin sulfate proteoglycan 4; CFP = cytolytic fusion protein; CSF1R = colony stimulating factor 1 receptor.
*The drugs at clinical trial are marked with asterisk.

Phosphoinositide 3-kinase (PI3K)/AKT/mammalian target of rapamycin (mTOR) pathway

PI3K is a signal transducer downstream of activated receptor tyrosine kinases (RTKs). The signaling pathway of PI3K is in association with AKT and mTOR, known as the PI3K/AKT/mTOR pathway (**Figure 2**). This pathway is activated in 10%–21% of TNBCs [40] and plays a role in cell cycle regulation, cell proliferation and quiescence. Activated mTOR is also implicated in the regulation of cell metabolism and migration. Inhibition of this pathway is achieved by inhibitors of PI3K, AKT or mTOR. Inhibitors of PI3K including CUDC-907, AZD8186, taselisib, BKM120, BYL719, BEZ235, GDC-0941, PQR309 and gedatolisib are in phase I clinical trials for TNBC. Likewise, most of the AKT inhibitors including AZD5363, ONC201, ARQ 092, ritonavir and GSK2141795 are also in phase I or II clinical trials.

The phase II clinical trial on MK2206 was terminated due to toxicity and no significant decline in pAKT [41]. Ipatasertib in combination with paclitaxel increased the PFS (by 1.3 months, $p = 0.037$) in a phase II clinical trial [42] and is currently in 2 other phase II (NCT03337724) and II/III (NCT02162719) clinical trials in combination with paclitaxel. ONC201, an AKT/ERK inhibitor, is in a phase II clinical trial in a methionine-restricted diet (NCT03733119).

Inhibitors of mTOR are an important class of inhibitors in this pathway. Everolimus is an mTOR inhibitor which, in combination with carboplatin in mTNBC patients in a phase II clinical trial, showed efficacy with 36% CBR (95% CI, 21.1%–54.4%), 3 months median PFS (95% CI, 1.6–4.6) and 16.6 months OS (95% CI, 7.3–not reached). Hemotoxicity, as the dose limiting factor and was observed with carboplatin AUC5/6 but not with AUC4 [43]. In a more recent phase II study of cisplatin, paclitaxel with or without everolimus in stage II and

https://doi.org/10.4048/jbc.2019.22.e39

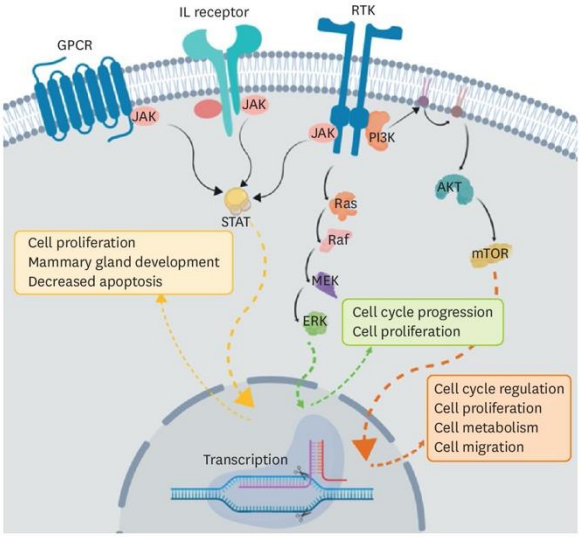

Figure 2. Major druggable signaling pathways with significant roles in triple negative breast cancer.
JAK = Janus kinase; IL = interleukin; RTK = receptor tyrosine kinase; PI3K = phosphoinositide 3-kinase; GPCR = G protein-coupled receptor; mTOR = mammalian target of rapamycin.

III TNBC patients, the combination of paclitaxel and cisplatin was well tolerated with 50% complete responses. Everolimus increased the adverse event profile of this combination and did not improve the desirable clinical responses [44]. Everolimus is currently in another phase II study with paclitaxel, 5-fluorouracil, epirubicin, and cyclophosphamide (NCT00499603). Temsirolimus, another mTOR inhibitor, was well tolerated in combination with cisplatin and erlotinib [45] and was investigated in another phase I study in combination with neratinib (NCT01111825). AZD2014 is also in phase I/II clinical trial (NCT02208375).

RAF-MEK-ERK pathway

TNBC is the only subtype of BC that has a higher expression of various genes involved in the Raf/MEK/ERK pathway [46], highlighting the importance of targeting this signaling pathway in TNBC (**Figure 2**). An analysis of reprogramming of the kinome in 9 TNBC patients showed that targeting MEK in these patients might be a valuable option and pre- and post- administration of trametinib, a MEK1/2 inhibitor, showed that BL and claudin-low tumors responded differently to the treatment, with BL tumors showing more upregulation and activation of RTKs (NCT01467310) [47]. This drug alone or in combination with the an AKT inhibitor, GSK2141795, was tested in a clinical trial (NCT01138085) and showed limited efficacy in 50 TNBC patients. Only 2 patients in the first group had a partial response and one had stable disease after 8 cycles [48]. The same combination is being tested in a different clinical trial (NCT01964924). The other clinical trial still recruiting includes trametinib in combination with spartalizumab (anti-PD-1) (NCT02900664). Trials of selumetinib in combination with chemotherapy agents (NCT02685657), in combination with paclitaxel and durvalumab (NCT03742102), or in combination with the mTOR inhibitor, AZD2014 (NCT02583542) are also recruiting. MEK162, another MEK inhibitor, completed clinical trial testing in combination with BKM120 (NCT01363232) and BEZ235 (NCT01337765), with no posted results.

https://doi.org/10.4048/jbc.2019.22.e39

Janus kinase (JAK)

JAK proteins are a family of 4 tyrosine kinases involved in the JAK-STAT pathway (**Figure 2**). This pathway, along with its various roles, alters the transcription of genes involved in cell proliferation, mammary glands development during the puberty and pregnancy and cancers. Studies have shown that TNBC tumors are enriched with the amplicon of JAK2 [49] and that the subsets of TNBC with amplified JAK2 are more sensitive to the effects of specific inhibitors [50]. Ruxolitinib is an important inhibitor of JAK1 and JAK2, approved by FDA for the treatment of myelofibrosis. Given the effects of this drug and the importance of JAK2 in TNBC, currently, 3 clinical trials focusing on this signaling pathway are currently underway. These include using ruxolitinib combination with pembrolizumab in advanced TNBC patients (NCT03012230), in combination with paclitaxel, doxorubicin or cyclophosphamide (NCT02876302), and in combination with paclitaxel for the treatment of triple negative inflammatory BC (NCT02041429).

CELL SURFACE TARGETS

Vascular endothelial growth factor receptor 2 (VEGFR2)

VEGFR2, an RTK and a key mediator of angiogenesis is implicated in BC pathogenesis. VEGF, the ligand to VEGFR2, has prognostic importance in TNBC. Sixty percent of TNBCs show high VEGF-A expression and the prognosis of this group of patients is even worse, with less than 5 years of survival [51], along with metastasis and poor treatment responses [52]. Mesenchymal stem-like TNBC tumors express higher levels of VEGF-C [53]. The expression of VEGFR2 is linked to TNBC, tumor invasion and metastasis [54]. Inhibition of this pathway would include blocking the activation of the VEGF receptor by neutralizing VEGF (e.g., bevacizumab), blocking the receptor (e.g., ramucirumab), using receptor mimetics (e.g., aflibercept), or using small molecule tyrosine kinase inhibitors that have a wide spectrum of action on RTKs (e.g., sorafenib).

Bevacizumab, a monoclonal antibody, was withdrawn for use in BC by the FDA, following 2 trials showing increased toxicity and no survival benefit in HER2 negative BC [55]. However, it was tested in adjuvant/neoadjuvant settings and clinical trials in TNBC have suggested an improved pCR [16,56], although, the long-term outcomes of adding bevacizumab to chemotherapy regimens is still unclear [16]. The primary results of a phase III clinical trial on invasive BC patients receiving bevacizumab as an adjuvant drug did not improve the OS of the patients [57]. Docetaxel, carboplatin and bevacizumab were administered to stage II/III TNBC patients (phase II). Encouragingly, positive results were observed including positive pCR and clinical response of 42% and 96%, for stage II and stage III TNBC, respectively [58]. Bevacizumab plus chemotherapy (epirubicin, cyclophosphamide, docetaxel) was studied in another phase III clinical trial of 678 TNBC patients in the neoadjuvant setting. The pCR in the combination vs chemotherapy only groups were 39.3% vs. 27.9%, and the OR, 1.73 (95% CI, 2.3–2.42; $p = 0.002$). This study showed a significant improvement in pCR in the patients that received bevacizumab [59].

Bevacizumab was also tested in patients with metastatic tumors. A phase III clinical trial on HER2 negative metastatic breast tumors receiving chemotherapy (capecitabine, anthracycline, taxane) with or without bevacizumab showed that the combination group had a longer median PFS, but this was not statistically significant [60]. The other phase II study on mTNBC patients receiving second-line chemotherapy (taxane, gemcitabine,

capecitabine, or vinorelbine) with bevacizumab showed a median PFS of 6 months in the combination group vs. 2.7 months in the chemotherapy alone group. Likewise, the median OS (17.9 months and 12.6 months, respectively) and ORR (41% and 18%, respectively) was also improved with bevacizumab [61]. Nab-paclitaxel, carboplatin and bevacizumab were administered to mTNBC patients in a phase II study. These combinations showed a median PFS of 9.2 months (95% CI, 7.8–25.1), an ORR of 85% (95% CI, 69–95), a CBR of 94% (95% CI, 80–99), and was well-tolerated [62].

The results of other completed phase II clinical trials including bevacizumab (NCT00608972, NCT00472693, NCT01094184, NCT02456857, and NCT00861705) have not yet been reported. Ramucirumab is a similar drug currently in a phase III clinical trial with docetaxel (NCT00703326). Small tyrosine kinase inhibitors like sorafenib (NCT02624700) and lenvatiniv (NCT03797326) are in phase II clinical trials. Data on the effects of lucitanib has not yet been reported (NCT02202746). In a phase II study on previously treated advanced TNBC patients sunitinib did not improve efficacy in comparison with single-agent standard-of-care [63].

Epidermal growth factor receptor (EGFR)

EGFR has important roles in the survival of many solid tumors, including tumor metastasis, cell cycle progression, cell proliferation, differentiation, angiogenesis and apoptosis. At least 50% of TNBCs overexpress EGFR [64] which is negatively correlated with patient survival [65]. Two classes of EGFR inhibitors are currently available, including small molecule tyrosine kinase inhibitors, such as gefitinib and erlotinib, and monoclonal antibodies, such as cetuximab (SCT200). Gefitinib (NCT01732276) and afatinib (NCT02511847) are both registered for clinical trials (unknown status). Erlotinib in combination with paclitaxel albumin-stabilized nanoparticle formulation and bevacizumab in a phase II study was well-tolerated. The expected PFS was not reached but clinical benefit in most patients was achieved [66].

Cetuximab is an anti-EGFR antibody, which has been trialed in several early phase studies in TNBC with only modest benefit. Ixabepilone alone and in combination with cetuximab was tested in 77 advanced TNBC patients. The combination group had 35.9% ORR (95% CI, 21.2–52.8) vs. 30% (95% CI, 16.6–46.5) in the monotherapy group. Median PFS was equal in both groups (4.1 months) and overall, both groups showed similar clinical results [67]. In another phase II clinical study, cisplatin alone or in combination with cetuximab showed an of ORR 20% (95% CI, 13–29) in the combination group and 10% in the monotherapy group (95% CI, 4–21). Cetuximab improved PFS (3.7 months vs. 1.5 months) and OS (12.9 months vs. 9.4 months). Yet the primary endpoints of the study were not met [68]. Cetuximab plus docetaxel was tested in another phase II clinical trial showing modest activity and acceptable toxicity. The study showed a 24% pCR rate (95% CI, 7.3–40.7) and 22% complete clinical response rate [69]. Cetuximab plus irinotecan was tested in another phase II clinical trial on BC patients with 58% being TNBC. The combination was tolerable but showed low overall activity. The treatment resulted in 11% ORR (95% CI, 1–33), one partial response and one complete response. TNBC patients had 18% response rate vs. no response in non-TNBC. The median time to progression and median OS was 1.4 months (95% CI, 1.0–2.2) and 9.4 months (95% CI, 2.8–16.1), respectively [70].

Fibroblast growth factor receptor (FGFR)

FGFR is another RTKs protein of which there are 5 (FGFR1–5). A total 4% of TNBCs overexpress FGFR2. FGFR1 and FGFR2 are reported to account for about 16 and 13% of TNBC patients [71]. Expression of FGFR2 could be considered as an independent prognostic

factor of OS in TNBC patients [72]. Therefore, small molecule tyrosine kinase inhibitors or monoclonal antibodies (e.g., IM-412) may be applicable in certain types of TNBC [73].

Trophoblast antigen 2 (Trop-2)

Trop-2 is a cell surface receptor and an epithelial glycoprotein-1, involved in various aspects of cancer including cancer cell proliferation, EMT, migration, invasion and metastasis. Overexpression of Trop-2 is common in TNBC [74]. Irinotecan is a prodrug to the topoisomerase I inhibitor, SN-38. Sacituzumab govitecan-hziy (or IMMU-132 or hRS7-SN-38) is a conjugate of SN-38 and humanized anti-trop-2 monoclonal antibody. This drug (10 mg/kg) was studied in a phase I/II clinical trial on 108 TNBC patients who had received 2–10 therapies and was associated with durable objective responses. The response rate was 33.3% (95% CI, 24.6–43.1) of which 1 had a complete response and 33 had partial responses. The median PFS and OS were 5.5 months (95% CI, 4.1–6.3) and 13.0 months (95% CI, 11.2–13.7), respectively, with the CBR of 45.4%. The main adverse reactions were myelotoxic effects [75]. The efficacy of sacituzumab govitecan in mTNBC patients refractory or relapsing after at least 2 prior chemotherapies is currently being tested in a phase III clinical trial. Approximately 150 institutions across the United States and Europe are involved in this clinical trial (NCT02574455). The drug is also being tested in another phase I/II clinical trial in various tumors including TNBC (NCT01631552). The other preclinical compound under investigation, is anti-Trop-2 conjugated with a nano-carrier-linked with doxorubicin.

Glycoprotein non-metastatic B (GPNMB)

GPNMB, or osteoactivin, is a type I transmembrane glycoprotein, which is overexpressed in 40%–60% of BCs [76], associated with triple-negativity [77] and poor patient outcome [77]. CDX-101 or glembatumumab vedotin, an antibody targeting GPNMB, in a phase I/II study on 42 patients with locally advanced or metastatic BC showed an acceptable safety profile [76]. Out of these patients 16 out of 19 were GPNMB+. The overall median PFS was 9.1, 17.9 and 18 weeks for all patients, TNBC patients and GPNMB+ patients, respectively [76]. Yet, despite being well tolerated, the drug alone could not meet the endpoint of ORR in a different phase II study [78]. In this study with 124 patients, more than 25% of the tumors were GPNMB+ and the ORR was 30% (7 of 23) in the glembatumumab vedotin group vs. 9% in the chemotherapy group. In TNBC patients, the ORR was 18% vs. 0%, and in GPNMP overexpressing TNBC patients, it was 40% vs. 0%, respectively. The results of another phase II clinical trial on the effect of CDX-011 in patients with metastatic GPNMB overexpressing TNBC is not yet published.

CONCLUSION

The development targeted therapy of TNBC is still a challenge that is being investigated by many cancer researchers around the world with the hope of finding improved treatment regimens for these patients. Due to the high rate of PD-1 expression in TNBC patients, the immune system has been uncovered as a major contributing factor to TNBC pathogenesis as revealed by newer TNBC classifications, and the success rate of drugs in this category, today, much attention is paid to immune checkpoint modulators, especially anti-PD-1 and anti-PD-L1 agents. Favorable clinical response rates of phase III studies on PARPi and platinum salts are impressive, and due to the high rate of mutations in *p53*, the ongoing clinical trials on CDK and ATR inhibitors might lead to phase III clinical trials. Inhibitors of VEGFR2 are also in phase III clinical trials, and anti-androgen drugs, due to specific application in LAR TNBC patients, are attracting some attention. There are many drugs in phase I, II and III clinical

trials, investigating novel molecules either alone or in combination with other novel agents or standard chemotherapeutics that are promising for improved clinical outcomes. The results of these studies may pave the way for researchers and open new doors for better treatment and improvement in outcomes of TNBC patients. However, there are many completed clinical trials with no accessible published data, placing the outcomes under question.

REFERENCES

1. Andreopoulou E, Schweber SJ, Sparano JA, McDaid HM. Therapies for triple negative breast cancer. Expert Opin Pharmacother 2015;16:983-98.
PUBMED | CROSSREF
2. Lehmann BD, Bauer JA, Chen X, Sanders ME, Chakravarthy AB, Shyr Y, et al. Identification of human triple-negative breast cancer subtypes and preclinical models for selection of targeted therapies. J Clin Invest 2011;121:2750-67.
PUBMED | CROSSREF
3. Burstein MD, Tsimelzon A, Poage GM, Covington KR, Contreras A, Fuqua SA, et al. Comprehensive genomic analysis identifies novel subtypes and targets of triple-negative breast cancer. Clin Cancer Res 2015;21:1688-98.
PUBMED | CROSSREF
4. Jézéquel P, Loussouarn D, Guérin-Charbonnel C, Campion L, Vanier A, Gouraud W, et al. Gene-expression molecular subtyping of triple-negative breast cancer tumours: importance of immune response. Breast Cancer Res 2015;17:43.
PUBMED | CROSSREF
5. Schmid P, Adams S, Rugo HS, Schneeweiss A, Barrios CH, Iwata H, et al. Atezolizumab and nab-paclitaxel in advanced triple-negative breast cancer. N Engl J Med 2018;379:2108-21.
PUBMED | CROSSREF
6. Schalper KA, Velcheti V, Carvajal D, Wimberly H, Brown J, Pusztai L, et al. *In situ* tumor PD-L1 mRNA expression is associated with increased TILs and better outcome in breast carcinomas. Clin Cancer Res 2014;20:2773-82.
PUBMED | CROSSREF
7. Adams S, Schmid P, Rugo HS, Winer EP, Loirat D, Awada A, et al. Pembrolizumab monotherapy for previously treated metastatic triple-negative breast cancer: cohort A of the phase II KEYNOTE-086 study. Ann Oncol 2019;30:397-404.
PUBMED | CROSSREF
8. Buchbinder EI, Desai A. CTLA-4 and PD-1 pathways: similarities, differences, and implications of their inhibition. Am J Clin Oncol 2016;39:98-106.
PUBMED | CROSSREF
9. Bottai G, Raschioni C, Losurdo A, Di Tommaso L, Tinterri C, Torrisi R, et al. An immune stratification reveals a subset of PD-1/LAG-3 double-positive triple-negative breast cancers. Breast Cancer Res 2016;18:121.
PUBMED | CROSSREF
10. Du W, Yang M, Turner A, Xu C, Ferris RL, Huang J, et al. TIM-3 as a target for cancer immunotherapy and mechanisms of action. Int J Mol Sci 2017;18:E645.
PUBMED | CROSSREF
11. Noman AS, Uddin M, Rahman MZ, Nayeem MJ, Alam SS, Khatun Z, et al. Overexpression of sonic hedgehog in the triple negative breast cancer: clinicopathological characteristics of high burden breast cancer patients from Bangladesh. Sci Rep 2016;6:18830.
PUBMED | CROSSREF
12. Habib JG, O'Shaughnessy JA. The hedgehog pathway in triple-negative breast cancer. Cancer Med 2016;5:2989-3006.
PUBMED | CROSSREF
13. Isakoff SJ, Mayer EL, He L, Traina TA, Carey LA, Krag KJ, et al. TBCRC009: a multicenter phase II clinical trial of platinum monotherapy with biomarker assessment in metastatic triple-negative breast cancer. J Clin Oncol 2015;33:1902-9.
PUBMED | CROSSREF
14. Zhang J, Wang Z, Hu X, Wang B, Wang L, Yang W, et al. Cisplatin and gemcitabine as the first line therapy in metastatic triple negative breast cancer. Int J Cancer 2015;136:204-11.
PUBMED | CROSSREF

15. Tutt A, Tovey H, Cheang MC, Kernaghan S, Kilburn L, Gazinska P, et al. Carboplatin in BRCA1/2-mutated and triple-negative breast cancer BRCAness subgroups: the TNT Trial. Nat Med 2018;24:628-37.
PUBMED | CROSSREF

16. Sikov WM, Berry DA, Perou CM, Singh B, Cirrincione CT, Tolaney SM, et al. Impact of the addition of carboplatin and/or bevacizumab to neoadjuvant once-per-week paclitaxel followed by dose-dense doxorubicin and cyclophosphamide on pathologic complete response rates in stage II to III triple-negative breast cancer: CALGB 40603 (Alliance). J Clin Oncol 2015;33:13-21.
PUBMED | CROSSREF

17. Robson M, Im SA, Senkus E, Xu B, Domchek SM, Masuda N, et al. Olaparib for metastatic breast cancer in patients with a germline BRCA mutation. N Engl J Med 2017;377:523-33.
PUBMED | CROSSREF

18. Robson ME, Tung N, Conte P, Im SA, Senkus E, Xu B, et al. OlympiAD final overall survival and tolerability results: olaparib versus chemotherapy treatment of physician's choice in patients with a germline BRCA mutation and HER2-negative metastatic breast cancer. Ann Oncol 2019;30:558-66.
PUBMED | CROSSREF

19. Lee JM, Hays JL, Chiou VL, Annunziata CM, Swisher EM, Harrell MI, et al. Phase I/Ib study of olaparib and carboplatin in women with triple negative breast cancer. Oncotarget 2017;8:79175-87.
PUBMED

20. Dent RA, Lindeman GJ, Clemons M, Wildiers H, Chan A, McCarthy NJ, et al. Phase I trial of the oral PARP inhibitor olaparib in combination with paclitaxel for first- or second-line treatment of patients with metastatic triple-negative breast cancer. Breast Cancer Res 2013;15:R88.
PUBMED | CROSSREF

21. Litton JK, Rugo HS, Ettl J, Hurvitz SA, Gonçalves A, Lee KH, et al. Talazoparib in patients with advanced breast cancer and a germline BRCA mutation. N Engl J Med 2018;379:753-63.
PUBMED | CROSSREF

22. Puhalla S, Beumer JH, Pahuja S, Appleman LJ, Tawbi HA, Stoller RG, et al. Final results of a phase 1 study of single-agent veliparib (V) in patients (pts) with either BRCA1/2-mutated cancer (BRCA+), platinum-refractory ovarian, or basal-like breast cancer (BRCA-wt). J Clin Oncol 2014;32:2570.
PUBMED | CROSSREF

23. Rodler ET, Kurland BF, Griffin M, Gralow JR, Porter P, Yeh RF, et al. Phase I study of veliparib (ABT-888) combined with cisplatin and vinorelbine in advanced triple-negative breast cancer and/or BRCA mutation–associated breast cancer. Clin Cancer Res 2016;22:2855-64.
PUBMED | CROSSREF

24. Loibl S, O'Shaughnessy J, Untch M, Sikov WM, Rugo HS, McKee MD, et al. Addition of the PARP inhibitor veliparib plus carboplatin or carboplatin alone to standard neoadjuvant chemotherapy in triple-negative breast cancer (BrighTNess): a randomised, phase 3 trial. Lancet Oncol 2018;19:497-509.
PUBMED | CROSSREF

25. Cao C, Vasilatos SN, Bhargava R, Fine JL, Oesterreich S, Davidson NE, et al. Functional interaction of histone deacetylase 5 (HDAC5) and lysine-specific demethylase 1 (LSD1) promotes breast cancer progression. Oncogene 2017;36:133-45.
PUBMED | CROSSREF

26. Tan WW, Allred JB, Moreno-Aspitia A, Northfelt DW, Ingle JN, Goetz MP, et al. Phase I study of panobinostat (LBH589) and letrozole in postmenopausal metastatic breast cancer patients. Clin Breast Cancer 2016;16:82-6.
PUBMED | CROSSREF

27. Connolly RM, Li H, Jankowitz RC, Zhang Z, Rudek MA, Jeter SC, et al. Combination epigenetic therapy in advanced breast cancer with 5-azacitidine and entinostat: a Phase II National Cancer Institute/Stand Up to Cancer Study. Clin Cancer Res 2017;23:2691-701.
PUBMED | CROSSREF

28. Hirshfield KM, Ganesan S. Triple-negative breast cancer: molecular subtypes and targeted therapy. Curr Opin Obstet Gynecol 2014;26:34-40.
PUBMED | CROSSREF

29. Blum JL, Gonçalves A, Efrat N, Debled M, Conte P, Richards PD, et al. A phase II trial of trabectedin in triple-negative and HER2-overexpressing metastatic breast cancer. Breast Cancer Res Treat 2016;155:295-302.
PUBMED | CROSSREF

30. Hu R, Dawood S, Holmes MD, Collins LC, Schnitt SJ, Cole K, et al. Androgen receptor expression and breast cancer survival in postmenopausal women. Clin Cancer Res 2011;17:1867-74.
PUBMED | CROSSREF

31. He J, Peng R, Yuan Z, Wang S, Peng J, Lin G, et al. Prognostic value of androgen receptor expression in operable triple-negative breast cancer: a retrospective analysis based on a tissue microarray. Med Oncol 2012;29:406-10.
PUBMED | CROSSREF

32. Tang D, Xu S, Zhang Q, Zhao W. The expression and clinical significance of the androgen receptor and E-cadherin in triple-negative breast cancer. Med Oncol 2012;29:526-33.
PUBMED | CROSSREF

33. Gucalp A, Tolaney S, Isakoff SJ, Ingle JN, Liu MC, Carey LA, et al. Phase II trial of bicalutamide in patients with androgen receptor-positive, estrogen receptor-negative metastatic Breast Cancer. Clin Cancer Res 2013;19:5505-12.
PUBMED | CROSSREF

34. Traina TA, Miller KD, Yardley DA, O'Shaughnessy J, Cortés JT, de Valeriola D, et al. Results from a phase 2 study of enzalutamide (ENZA), an androgen receptor (AR) inhibitor, in advanced AR+ triple-negative breast cancer (TNBC). J Clin Oncol 2015;33:1003.
PUBMED | CROSSREF

35. Bardia A, Dacosta NA, Gabrail NY, Lemon S, Danso MA, Ali HY, et al. Phase (Ph) 1 study of oral seviteronel (VT-464), a dual CYP17-Lyase (L) inhibitor and androgen receptor (AR) antagonist, in patients (pts) with advanced AR+ triple negative (TNBC) or estrogen receptor (ER)+ breast cancer (BC). J Clin Oncol 2016;34:1088.
PUBMED | CROSSREF

36. Zagouri F, Sergentanis TN, Chrysikos D, Papadimitriou CA, Dimopoulos MA, Psaltopoulou T. Hsp90 inhibitors in breast cancer: a systematic review. Breast 2013;22:569-78.
PUBMED | CROSSREF

37. Jhaveri K, Chandarlapaty S, Lake D, Gilewski T, Robson M, Goldfarb S, et al. A phase II open-label study of ganetespib, a novel heat shock protein 90 inhibitor for patients with metastatic breast cancer. Clin Breast Cancer 2014;14:154-60.
PUBMED | CROSSREF

38. Mitri Z, Karakas C, Wei C, Briones B, Simmons H, Ibrahim N, et al. A phase 1 study with dose expansion of the CDK inhibitor dinaciclib (SCH 727965) in combination with epirubicin in patients with metastatic triple negative breast cancer. Invest New Drugs 2015;33:890-4.
PUBMED | CROSSREF

39. Bardia A, Parton M, Kümmel S, Estévez LG, Huang CS, Cortés J, et al. Paclitaxel With Inhibitor of Apoptosis Antagonist, LCL161, for Localized Triple-Negative Breast Cancer, Prospectively Stratified by Gene Signature in a Biomarker-Driven Neoadjuvant Trial. J Clin Oncol 2018:JCO2017748392.
PUBMED | CROSSREF

40. Cossu-Rocca P, Orrù S, Muroni MR, Sanges F, Sotgiu G, Ena S, et al. Analysis of PIK3CA mutations and activation pathways in triple negative breast cancer. PLoS One 2015;10:e0141763.
PUBMED | CROSSREF

41. Kalinsky K, Sparano JA, Zhong X, Andreopoulou E, Taback B, Wiechmann L, et al. Pre-surgical trial of the AKT inhibitor MK-2206 in patients with operable invasive breast cancer: a New York Cancer Consortium trial. Clin Transl Oncol 2018;20:1474-83.
PUBMED | CROSSREF

42. Kim SB, Dent R, Im SA, Espié M, Blau S, Tan AR, et al. Ipatasertib plus paclitaxel versus placebo plus paclitaxel as first-line therapy for metastatic triple-negative breast cancer (LOTUS): a multicentre, randomised, double-blind, placebo-controlled, phase 2 trial. Lancet Oncol 2017;18:1360-72.
PUBMED | CROSSREF

43. Singh J, Novik Y, Stein S, Volm M, Meyers M, Smith J, et al. Phase 2 trial of everolimus and carboplatin combination in patients with triple negative metastatic breast cancer. Breast Cancer Res 2014;16:R32.
PUBMED | CROSSREF

44. Jovanović B, Mayer IA, Mayer EL, Abramson VG, Bardia A, Sanders ME, et al. A randomized phase II neoadjuvant study of cisplatin, paclitaxel with or without everolimus in patients with stage II/III triple-negative breast cancer (TNBC): responses and long-term outcome correlated with increased frequency of DNA damage response gene mutations, TNBC subtype, AR status, and Ki67. Clin Cancer Res 2017;23:4035-45.
PUBMED | CROSSREF

45. Maurer MA, Kalinsky K, Crew K, Jayasena R, Forman J, Lau YK, et al. Abstract 28: Phase I trial of combined temsirolimus, erlotinib, and cisplatin in advanced solid tumors. Cancer Res 2013;73:28.
CROSSREF

46. Hoeflich KP, O'Brien C, Boyd Z, Cavet G, Guerrero S, Jung K, et al. *In vivo* antitumor activity of MEK and phosphatidylinositol 3-kinase inhibitors in basal-like breast cancer models. Clin Cancer Res 2009;15:4649-64.
PUBMED | CROSSREF

47. Johnson GL, Amos KD, Duncan JS, Whittle M, Zawistowki J, Goulet D, et al. Kinome reprogramming response to MEK inhibition: a window-of-opportunity trial in triple-negative breast cancer (TNBC). J Clin Oncol 2013;31:512.
PUBMED | CROSSREF

48. Ramaswamy B, Mrozek E, Lustberg M, Wesolowski R, Layman R, Abdel-Rasoul M, et al. Abstract LB-216: NCI 9455: Phase II study of trametinib followed by trametinib plus AKT inhibitor, GSK2141795 in patients with advanced triple negative breast cancer. Cancer Res 2016;76:LB-216.
CROSSREF

49. Barrett MT, Anderson KS, Lenkiewicz E, Andreozzi M, Cunliffe HE, Klassen CL, et al. Genomic amplification of 9p24.1 targeting JAK2, PD-L1, and PD-L2 is enriched in high-risk triple negative breast cancer. Oncotarget 2015;6:26483-93.
PUBMED | CROSSREF

50. Balko JM, Schwarz LJ, Luo N, Estrada MV, Giltnane JM, Dávila-González D, et al. Triple-negative breast cancers with amplification of JAK2 at the 9p24 locus demonstrate JAK2-specific dependence. Sci Transl Med 2016;8:334ra53.
PUBMED | CROSSREF

51. Bahhnassy A, Mohanad M, Shaarawy S, Ismail MF, El-Bastawisy A, Ashmawy AM, et al. Transforming growth factor-β, insulin-like growth factor I/insulin-like growth factor I receptor and vascular endothelial growth factor-A: prognostic and predictive markers in triple-negative and non-triple-negative breast cancer. Mol Med Rep 2015;12:851-64.
PUBMED | CROSSREF

52. Bahnassy A, Mohanad M, Ismail MF, Shaarawy S, El-Bastawisy A, Zekri AR. Molecular biomarkers for prediction of response to treatment and survival in triple negative breast cancer patients from Egypt. Exp Mol Pathol 2015;99:303-11.
PUBMED | CROSSREF

53. Bender RJ, Mac Gabhann F. Expression of VEGF and semaphorin genes define subgroups of triple negative breast cancer. PLoS One 2013;8:e61788.
PUBMED | CROSSREF

54. Rydén L, Jirström K, Haglund M, Stål O, Fernö M. Epidermal growth factor receptor and vascular endothelial growth factor receptor 2 are specific biomarkers in triple-negative breast cancer. Results from a controlled randomized trial with long-term follow-up. Breast Cancer Res Treat 2010;120:491-8.
PUBMED | CROSSREF

55. Sasich LD, Sukkari SR. The US FDAs withdrawal of the breast cancer indication for Avastin (bevacizumab). 2012;20:381-5.
PUBMED | CROSSREF

56. Chen XS, Yuan Y, Garfield DH, Wu JY, Huang O, Shen KW. Both carboplatin and bevacizumab improve pathological complete remission rate in neoadjuvant treatment of triple negative breast cancer: a meta-analysis. PLoS One 2014;9:e108405.
PUBMED | CROSSREF

57. Cameron D, Brown J, Dent R, Jackisch C, Mackey J, Pivot X, et al. Adjuvant bevacizumab-containing therapy in triple-negative breast cancer (BEATRICE): primary results of a randomised, phase 3 trial. Lancet Oncol 2013;14:933-42.
PUBMED | CROSSREF

58. Kim HR, Jung KH, Im SA, Im YH, Kang SY, Park KH, et al. Multicentre phase II trial of bevacizumab combined with docetaxel-carboplatin for the neoadjuvant treatment of triple-negative breast cancer (KCSG BR-0905). Ann Oncol 2013;24:1485-90.
PUBMED | CROSSREF

59. Gerber B, Loibl S, Eidtmann H, Rezai M, Fasching PA, Tesch H, et al. Neoadjuvant bevacizumab and anthracycline-taxane-based chemotherapy in 678 triple-negative primary breast cancers; results from the geparquinto study (GBG 44). Ann Oncol 2013;24:2978-84.
PUBMED | CROSSREF

60. Robert NJ, Diéras V, Glaspy J, Brufsky AM, Bondarenko I, Lipatov ON, et al. RIBBON-1: randomized, double-blind, placebo-controlled, phase III trial of chemotherapy with or without bevacizumab for first-line treatment of human epidermal growth factor receptor 2-negative, locally recurrent or metastatic breast cancer. J Clin Oncol 2011;29:1252-60.
PUBMED | CROSSREF

61. Brufsky A, Valero V, Tiangco B, Dakhil S, Brize A, Rugo HS, et al. Second-line bevacizumab-containing therapy in patients with triple-negative breast cancer: subgroup analysis of the RIBBON-2 trial. Breast Cancer Res Treat 2012;133:1067-75.
PUBMED | CROSSREF

62. Hamilton E, Kimmick G, Hopkins J, Marcom PK, Rocha G, Welch R, et al. Nab-paclitaxel/bevacizumab/carboplatin chemotherapy in first-line triple negative metastatic breast cancer. Clin Breast Cancer 2013;13:416-20.
PUBMED | CROSSREF

63. Curigliano G, Pivot X, Cortés J, Elias A, Cesari R, Khosravan R, et al. Randomized phase II study of sunitinib versus standard of care for patients with previously treated advanced triple-negative breast cancer. Breast 2013;22:650-6.
PUBMED | CROSSREF

64. Masuda H, Zhang D, Bartholomeusz C, Doihara H, Hortobagyi GN, Ueno NT. Role of epidermal growth factor receptor in breast cancer. Breast Cancer Res Treat 2012;136:331-45.
PUBMED | CROSSREF

65. Cetin I, Topcul M. Triple negative breast cancer. Asian Pac J Cancer Prev 2014;15:2427-31.
PUBMED | CROSSREF

66. Specht J, Gadi V, Gralow J, Korde L, Linden H, Salazar L, Rodler E, Cundy A, Buening B, Baker K. Abstract P4-22-11: Combined targeted therapies for advanced triple negative breast cancer: a phase II trial of nab-paclitaxel and bevacizumab followed by maintenance targeted therapy with bevacizumab and erlotinib. Cancer Res 2017;77:P4-22-11.
PUBMED | CROSSREF

67. Trédan O, Campone M, Jassem J, Vyzula R, Coudert B, Pacilio C, et al. Ixabepilone alone or with cetuximab as first-line treatment for advanced/metastatic triple-negative breast cancer. Clin Breast Cancer 2015;15:8-15.
PUBMED | CROSSREF

68. Baselga J, Gómez P, Greil R, Braga S, Climent MA, Wardley AM, et al. Randomized phase II study of the anti-epidermal growth factor receptor monoclonal antibody cetuximab with cisplatin versus cisplatin alone in patients with metastatic triple-negative breast cancer. J Clin Oncol 2013;31:2586-92.
PUBMED | CROSSREF

69. Nabholtz JM, Chalabi N, Radosevic-Robin N, Dauplat MM, Mouret-Reynier MA, Van Praagh I, et al. Multicentric neoadjuvant pilot phase II study of cetuximab combined with docetaxel in operable triple negative breast cancer. Int J Cancer 2016;138:2274-80.
PUBMED | CROSSREF

70. Crozier JA, Advani PP, LaPlant B, Hobday T, Jaslowski AJ, Moreno-Aspitia A, et al. N0436 (alliance): a phase II trial of irinotecan with cetuximab in patients with metastatic breast cancer previously exposed to anthracycline and/or taxane-containing therapy. Clin Breast Cancer 2016;16:23-30.
PUBMED | CROSSREF

71. Lee HJ, Seo AN, Park SY, Kim JY, Park JY, Yu JH, et al. Low prognostic implication of fibroblast growth factor family activation in triple-negative breast cancer subsets. Ann Surg Oncol 2014;21:1561-8.
PUBMED | CROSSREF

72. Cheng CL, Thike AA, Tan SY, Chua PJ, Bay BH, Tan PH. Expression of FGFR1 is an independent prognostic factor in triple-negative breast cancer. Breast Cancer Res Treat 2015;151:99-111.
PUBMED | CROSSREF

73. Jung SY, Yi JY, Kim MH, Song KH, Kang SM, Ahn J, et al. IM-412 inhibits the invasion of human breast carcinoma cells by blocking FGFR-mediated signaling. Oncol Rep 2015;34:2731-7.
PUBMED | CROSSREF

74. Cardillo TM, Govindan SV, Sharkey RM, Trisal P, Arrojo R, Liu D, et al. Sacituzumab govitecan (IMMU-132), an anti-Trop-2/SN-38 antibody–drug conjugate: characterization and efficacy in pancreatic, gastric, and other cancers. Bioconjug Chem 2015;26:919-31.
PUBMED | CROSSREF

75. Bardia A, Mayer IA, Vahdat LT, Tolaney SM, Isakoff SJ, Diamond JR, et al. Sacituzumab govitecan-hziy in refractory metastatic triple-negative breast cancer. N Engl J Med 2019;380:741-51.
PUBMED | CROSSREF

76. Bendell J, Saleh M, Rose AA, Siegel PM, Hart L, Sirpal S, et al. Phase I/II study of the antibody-drug conjugate glembatumumab vedotin in patients with locally advanced or metastatic breast cancer. J Clin Oncol 2014;32:3619-25.
PUBMED | CROSSREF

77. Rose AA, Grosset AA, Dong Z, Russo C, Macdonald PA, Bertos NR, et al. Glycoprotein nonmetastatic B is an independent prognostic indicator of recurrence and a novel therapeutic target in breast cancer. Clin Cancer Res 2010;16:2147-56.
PUBMED | CROSSREF

78. Yardley DA, Weaver R, Melisko ME, Saleh MN, Arena FP, Forero A, et al. EMERGE: a randomized phase II study of the antibody-drug conjugate glembatumumab vedotin in advanced glycoprotein NMB–expressing breast cancer. J Clin Oncol 2015;33:1609-19.
PUBMED | CROSSREF

79. Bulut AS, Erden E, Sak SD, Doruk H, Kursun N, Dincol D. Significance of inducible nitric oxide synthase expression in benign and malignant breast epithelium: an immunohistochemical study of 151 cases. Virchows Arch 2005;447:24-30.
PUBMED | CROSSREF

80. Granados-Principal S, Liu Y, Guevara ML, Blanco E, Choi DS, Qian W, et al. Inhibition of iNOS as a novel effective targeted therapy against triple-negative breast cancer. Breast Cancer Res 2015;17:25.
PUBMED | CROSSREF

81. Zhu H, Bengsch F, Svoronos N, Rutkowski MR, Bitler BG, Allegrezza MJ, et al. BET bromodomain inhibition promotes anti-tumor immunity by suppressing PD-L1 expression. Cell Reports 2016;16:2829-37.
PUBMED | CROSSREF

82. Zhou L, Li K, Luo Y, Tian L, Wang M, Li C, et al. Novel prognostic markers for patients with triple-negative breast cancer. Hum Pathol 2013;44:2180-7.
PUBMED | CROSSREF

83. Mosalpuria K, Hall C, Krishnamurthy S, Lodhi A, Hallman DM, Baraniuk MS, et al. Cyclooxygenase-2 expression in non-metastatic triple-negative breast cancer patients. Mol Clin Oncol 2014;2:845-50.
PUBMED | CROSSREF

84. Kim S, Lee J, Jeon M, Lee JE, Nam SJ. Zerumbone suppresses the motility and tumorigenecity of triple negative breast cancer cells via the inhibition of TGF-β1 signaling pathway. Oncotarget 2016;7:1544-58.
PUBMED

85. Kim S, Han J, Jeon M, You D, Lee J, Kim HJ, et al. Silibinin inhibits triple negative breast cancer cell motility by suppressing TGF-β2 expression. Tumour Biol 2016;37:11397-407.
PUBMED | CROSSREF

86. Wahdan-Alaswad R, Harrell JC, Fan Z, Edgerton SM, Liu B, Thor AD. Metformin attenuates transforming growth factor beta (TGF-β) mediated oncogenesis in mesenchymal stem-like/claudin-low triple negative breast cancer. Cell Cycle 2016;15:1046-59.
PUBMED | CROSSREF

87. Maire V, Némati F, Richardson M, Vincent-Salomon A, Tesson B, Rigaill G, et al. Polo-like kinase 1: a potential therapeutic option in combination with conventional chemotherapy for the management of patients with triple-negative breast cancer. Cancer Res 2013;73:813-23.
PUBMED | CROSSREF

88. Chang SS, Yamaguchi H, Xia W, Lim SO, Khotskaya Y, Wu Y, et al. Aurora A kinase activates YAP signaling in triple-negative breast cancer. Oncogene 2017;36:1265-75.
PUBMED | CROSSREF

89. Diamond JR, Eckhardt SG, Pitts TM, van Bokhoven A, Aisner D, Gustafson DL, et al. A phase II clinical trial of the Aurora and angiogenic kinase inhibitor ENMD-2076 for previously treated, advanced, or metastatic triple-negative breast cancer. Breast Cancer Res 2018;20:82.
PUBMED | CROSSREF

90. Lips EH, Michaut M, Hoogstraat M, Mulder L, Besselink NJ, Koudijs MJ, et al. Next generation sequencing of triple negative breast cancer to find predictors for chemotherapy response. Breast Cancer Res 2015;17:134.
PUBMED | CROSSREF

91. Al-Ejeh F, Simpson PT, Sanus JM, Klein K, Kalimutho M, Shi W, et al. Meta-analysis of the global gene expression profile of triple-negative breast cancer identifies genes for the prognostication and treatment of aggressive breast cancer. Oncogenesis 2014;3:e100.
PUBMED | CROSSREF

92. Maire V, Baldeyron C, Richardson M, Tesson B, Vincent-Salomon A, Gravier E, et al. TTK/hMPS1 is an attractive therapeutic target for triple-negative breast cancer. PLoS One 2013;8:e63712.
PUBMED | CROSSREF

93. Tsunoda N, Kokuryo T, Oda K, Senga T, Yokoyama Y, Nagino M, et al. Nek2 as a novel molecular target for the treatment of breast carcinoma. Cancer Sci 2009;100:111-6.
PUBMED | CROSSREF

94. Tryfonopoulos D, Walsh S, Collins DM, Flanagan L, Quinn C, Corkery B, et al. Src: a potential target for the treatment of triple-negative breast cancer. Ann Oncol 2011;22:2234-40.
PUBMED | CROSSREF

95. Dickson BC, Mulligan AM, Zhang H, Lockwood G, O'Malley FP, Egan SE, et al. High-level JAG1 mRNA and protein predict poor outcome in breast cancer. Mod Pathol 2007;20:685-93.
PUBMED | CROSSREF

96. Nakhjavani M, Hardingham JE, Palethorpe HM, Tomita Y, Smith E, Price TJ, et al. Ginsenoside Rg3: Potential molecular targets and therapeutic indication in metastatic breast cancer. Medicines (Basel) 2019;6:17.
PUBMED | CROSSREF

97. Dorward HS, Du A, Bruhn MA, Wrin J, Pei JV, Evdokiou A, et al. Pharmacological blockade of aquaporin-1 water channel by AqB013 restricts migration and invasiveness of colon cancer cells and prevents endothelial tube formation *in vitro*. J Exp Clin Cancer Res 2016;35:36.
PUBMED | CROSSREF

98. Tomita Y, Palethorpe HM, Smith E, Nakhjavani M, Townsend AR, Price TJ, et al. Bumetanide-derived aquaporin 1 inhibitors, AqB013 and AqB050 inhibit tube formation of endothelial cells through induction of apoptosis and impaired migration *in vitro*. Int J Mol Sci 2019;20:E1818.
PUBMED | CROSSREF

99. Smith E, Tomita Y, Palethorpe HM, Howell S, Nakhjavani M, Townsend AR, et al. Reduced aquaporin-1 transcript expression in colorectal carcinoma is associated with promoter hypermethylation. Epigenetics 2019;14:158-70.
PUBMED | CROSSREF

100. Liu J, Pan S, Hsieh MH, Ng N, Sun F, Wang T, et al. Targeting Wnt-driven cancer through the inhibition of Porcupine by LGK974. Proc Natl Acad Sci U S A 2013;110:20224-9.
PUBMED | CROSSREF

101. Sapi E. The role of CSF-1 in normal physiology of mammary gland and breast cancer: an update. Exp Biol Med (Maywood) 2004;229:1-11.
PUBMED | CROSSREF

102. Amoury M, Mladenov R, Nachreiner T, Pham AT, Hristodorov D, Di Fiore S, et al. A novel approach for targeted elimination of CSPG4-positive triple-negative breast cancer cells using a MAP tau-based fusion protein. Int J Cancer 2016;139:916-27.
PUBMED | CROSSREF

Chapter 2 Stereoselective activity of the epimers of ginsenoside Rg3

2.1. Background

As reviewed in the previous chapter, the role of Rg3 had been investigated in several cancer models. Rg3 is extracted from any part of the plant *Panax ginseng*, but the most important and common part is the root. The extraction procedure usually includes heating up the ginseng root, which raises the production of several members of the ginsenoside family of saponins, Rg3 being one of them. Depending on the extraction conditions, such as temperature and pressure, the ratio of Rg3 epimers changes. A big concern with reviewing the efficacy of Rg3 published in the literature was that in numerous studies, Rg3 was extracted in experimental settings and without further specification of the extracted epimer or mixture of epimers, or the purity of the molecule extracted, was studied *in vitro* and *in vivo*. As mentioned in several papers reviewed in chapter one, Rg3 epimers showed stereoselectivity action in interaction with ion channels, inhibition of epithelial-mesenchymal transition, antioxidant effect and promoting immune function. Due to this stereoselective action, it is very important to identify the exact molecule that is being studied. In the current chapter, continuing with the search for a better treatment for TNBC, anti-cancer effects of each Rg3 epimer were evaluated and stereoselectivity of epimers was shown.

As reviewed in the previous chapter, AQP1 is highly expressed in TNBC and its expression is correlated with higher tumour grade, poorer prognosis and overall survival of these patients. In this paper, using *in silico* molecular docking studies, the interaction of Rg3 with AQP1 water channel was studied. Following promising results from this *in silico* study, an *in vitro* assay was performed to show the interaction of Rg3 with AQP1 water channel, using oocyte swelling assay.

SRg3-specific blockage of AQP1 was an important finding, leading to further experiments on TNBC cell lines. The experiments showed that only SRg3 inhibited the proliferation of MDA-MB-231, a mesenchymal-like TNBC cell line. However, it was only RRg3 that inhibited the invasion of these cells in a spheroid invasion assay. The epimers also differently inhibited the migration of MDA-MB-231 in circular scratch wound closure and in transwell migration assays. These findings in TNBC models confirmed the stereoselective activities of Rg3.

The findings of this chapter showed the potential of Rg3 epimers as a treatment for TNBC. It also paved the way for optimisation of the combination of both epimers, which is the topic of chapter 3.

This chapter has been published as:

Nakhjavani, M., Palethorpe, H. M., Tomita, Y., Smith, E., Price, T. J., Yool, A. J., Pei, J. V., Townsend, A. R., and Hardingham, J. E. (2019). Stereoselective anti-cancer activities

of ginsenoside Rg3 on triple negative breast cancer cell models. Pharmaceuticals, 12(3), 117.

2.2. Statement of Authorship

Statement of Authorship

Title of Paper	Stereoselective anti-cancer activities of ginsenoside Rg3 on triple negative breast cancer cell models
Publication Status	☑ Published ☐ Accepted for Publication ☐ Submitted for Publication ☐ Unpublished and Unsubmitted work written in manuscript style
Publication Details	Nakhjavani, Maryam, Helen M. Palethorpe, Yoko Tomita, Eric Smith, Timothy J. Price, Andrea J. Yool, Jinxin V. Pei, Amanda R. Townsend, and Jennifer E. Hardingham. "Stereoselective anti-cancer activities of ginsenoside Rg3 on triple negative breast cancer cell models." Pharmaceuticals 12, no. 3 (2019): 117.

Principal Author

Name of Principal Author (Candidate)	Maryam Nakhjavani		
Contribution to the Paper	Conceptualised, designed and performed the experiments, analysed and curated the data, and substantially wrote the manuscript.		
Overall percentage (%)	70		
Certification:	This paper reports on original research I conducted during the period of my Higher Degree by Research candidature and is not subject to any obligations or contractual agreements with a third party that would constrain its inclusion in this thesis. I am the primary author of this paper.		
Signature		Date	10th Feb 2021

Co-Author Contributions

By signing the Statement of Authorship, each author certifies that:

i. the candidate's stated contribution to the publication is accurate (as detailed above);
ii. permission is granted for the candidate in include the publication in the thesis; and
iii. the sum of all co-author contributions is equal to 100% less the candidate's stated contribution.

Name of Co-Author	Helen M. Palethorpe		
Contribution to the Paper	Contributed to designing the experiment and discussion.		
Signature		Date	8th February 2021

Name of Co-Author	Yoko Tomita		
Contribution to the Paper	Contributed to discussion and reviewing.		
Signature		Date	12th Feb 2021

Name of Co-Author	Eric Smith		
Contribution to the Paper	Contributed to drafting and discussion.		
Signature		Date	10th Feb 2021

Name of Co-Author	Timothy J Price		
Contribution to the Paper	Contributed to discussion and reviewing.		
Signature		Date	11th Feb 2021

Name of Co-Author	Andrea J Yool		
Contribution to the Paper	Contributed to designing the experiment, data analysis and discussion.		
Signature		Date	10th Feb 2021

Name of Co-Author	Jinxin V. Pei		
Contribution to the Paper	Contributed to data analysis and discussion.		
Signature		Date	8th Feb 2021

Name of Co-Author	Amanda R. Townsend		
Contribution to the Paper	Contributed to discussion and reviewing.		
Signature		Date	11th Feb 2021

Name of Co-Author	Jennifer E. Hardingham		
Contribution to the Paper	Conceptualised and designed the experiments, analysed and curated the data, contributed to drafting and discussion.		
Signature		Date	10th Feb 2021

pharmaceuticals

MDPI

Article

Stereoselective Anti-Cancer Activities of Ginsenoside Rg3 on Triple Negative Breast Cancer Cell Models

Maryam Nakhjavani [1,2], Helen M. Palethorpe [1,2], Yoko Tomita [1,2,3], Eric Smith [1,2], Timothy J. Price [2,3], Andrea J. Yool [2], Jinxin V. Pei [2], Amanda R. Townsend [2,3] and Jennifer E. Hardingham [1,2,*]

1 Molecular Oncology, Basil Hetzel Institute, The Queen Elizabeth Hospital, Woodville South, SA 5011, Australia
2 Adelaide Medical School, University of Adelaide, Adelaide, SA 5005, Australia
3 Oncology Unit, The Queen Elizabeth Hospital, Woodville South, SA 5011, Australia
* Correspondence: jenny.hardingham@sa.gov.au; Tel.: +61-8-8222-6142

Received: 15 May 2019; Accepted: 29 July 2019; Published: 1 August 2019

Abstract: Ginsenoside Rg3 (Rg3) has two epimers, 20(S)-ginsenoside Rg3 (SRg3) and 20(R)-ginsenoside Rg3 (RRg3), and while Rg3 itself has been reported to have anti-cancer properties, few studies have been reported on the anti-cancer effects of the different epimers. The aim was to investigate the stereoselective effects of the Rg3 epimers on triple negative breast cancer (TNBC) cell lines, tested using cell-based assays for proliferation, apoptosis, cell cycle arrest, migration and invasion. Molecular docking showed that Rg3 interacted with the aquaporin 1 (AQP1) water channel (binding score −9.4 kJ mol^{-1}). The *Xenopus laevis* oocyte expression system was used to study the effect of Rg3 epimers on the AQP1 water permeability. The AQP1 expression in TNBC cell lines was compared with quantitative-polymerase chain reaction (PCR). The results showed that only SRg3 inhibited the AQP1 water flux and inhibited the proliferation of MDA-MB-231 (100 μM), due to cell cycle arrest at G0/G1. SRg3 inhibited the chemoattractant-induced migration of MDA-MB-231. The AQP1 expression in MDA-MB-231 was higher than in HCC1143 or DU4475 cell lines. These results suggest a role for AQP1 in the proliferation and chemoattractant-induced migration of this cell line. Compared to SRg3, RRg3 had more potency and efficacy, inhibiting the migration and invasion of MDA-MB-231. Rg3 has stereoselective anti-cancer effects in the AQP1 high-expressing cell line MDA-MB-231.

Keywords: breast cancer; epimer; stereoselective; Ginsenoside Rg3; triple negative breast cancer

1. Introduction

Ginsenosides are a class of natural triterpenoid saponins with the general structure of an aglycone steroid backbone and a glycoside side chain. They are extracted from the plant *Panax ginseng* Meyer, commonly known as ginseng, and play an important role in the medicinal effects of ginseng extract [1,2]. Ginsenoside Rg3 (Rg3) is one of the extensively studied members of the ginsenoside family, having a variety of biological actions and efficacies, including anti-oxidant properties [3] and protective effects in cardiovascular diseases [4–6], neurological disorders [7–10], diabetes [11–13], immune function and inflammation [14–17], and cancer [18]. Although many papers refer to Rg3 as a single molecule and report the effects of Rg3, rather than a specific epimer, it is noteworthy that Rg3, like other ginsenosides, has two epimers: 20(S)-ginsenoside Rg3 (SRg3) and 20(R)-ginsenoside Rg3 (RRg3). Each of these epimers has distinct pharmacological actions, intracellular targets, effects and efficacies. For example, the SRg3 epimer activates caspases in the human gastric cancer cell line [19] and inhibits Ca^{2+}, Na^{+} and K^{+} ion channels [20], while the RRg3 epimer has antioxidant properties to combat cyclophosphamide-induced cellular stress [3].

The anti-cancer properties of Rg3 have made it a notable drug candidate for many cancer models. Few studies have focused on the anti-cancer effects of Rg3 in breast cancer models, specifically in triple negative breast cancer (TNBC), a subtype of breast cancer with a poor prognosis [21]. Since this subtype of breast tumour lacks the expression or overexpression of an estrogen receptor, progesterone receptor or human epidermal growth factor receptor (HER) 2, there are as yet no targeted therapies for TNBC; chemotherapy regimens, along with their adverse effects, remain the mainstay of treatment in most TNBC patients. Thus, finding a targeted biological agent for TNBC would make a paradigm shift in the treatment of these patients. Previous reported studies have shown that Rg3-induced apoptosis [22] inhibited the activation of NF-κB [23], induced G0/G1 arrest [24] and inhibited chemoinvasion directed by CXCR4 [25] in breast cancer cell lines. However, these studies did not use a specific epimer of Rg3, nor did they specify the ratio of the two epimers.

Aquaporin 1 (AQP1) is a member of the AQP family of water transporters. Like other AQPs, AQP1 is a homo-tetramer. Each monomer, as depicted in Figure 1A, works as a single channel for water transport. The central pore of the tetramer is responsible for gas and ion transport, the latter of which is gated by cGMP. It is already shown that AQP1 plays a role in the growth, angiogenesis and metastasis of tumours [26–29]. AQP1 is highly expressed in mouse models of breast tumour [30], and AQP1 deficiency in such models decreased the number of lung metastases [31]. Furthermore, clinical studies have shown that some TNBC tumours have higher levels of AQP1 expression and an expression correlated with a poorer prognosis [32,33].

To date, no studies have focused on the stereoselectivity of Rg3 epimers on TNBC cell lines, and no studies have shown the interaction between Rg3 epimers and AQP1. The aim of our study was to investigate the stereoselective effects of Rg3 on human TNBC cell lines. In particular, our aim was to investigate whether these two epimers have effects on different functions on TNBC in cell line models, including proliferation, apoptosis, cell cycle, migration and invasion. Furthermore, in line with our previous research focus [28,34–37], we investigated the interaction of Rg3 epimers with AQP1 in in silico models.

2. Results

2.1. Interaction of Rg3 with AQP1

2.1.1. Molecular Docking of Rg3

The in silico molecular docking studies were performed on Rg3 docked within the water channel of AQP1, AQP2, AQP4 and AQP5. The results in Table 1 are the scores based on Gibbs free energy (kJ mol^{-1}).

Table 1. The results of the in silico molecular docking of Rg3 with aquaporin water channels in comparison with other blockers of AQP1. The results are presented as Gibbs free energy (kJ mol^{-1}).

Molecule	Binding Score (kJ mol^{-1})			
	AQP1	**AQP2**	**AQP4**	**AQP5**
Ginsenoside Rg3	−9.4	−6.4	−6.1	−4
Bacopaside I	−9.2 [38]	7.4	−5.2	−6.9
Bacopaside II	−9.3 [38]	2.2	−5.2	−6.4

The modelled binding energetically favoured AQP1 (−9.4 kJ mol^{-1}) at a level comparable to known AQP1-inhibitors such as bacopaside I (−9.2 kJ mol^{-1}) and bacopaside II (−9.3 kJ mol^{-1}) [38]. Figure 1A illustrates the role of the AQP channels in migration and invasion (as reviewed in [39]). We showed that the water channel of the AQP1 monomer was blocked by Rg3 (Figure 1B,C). The H-bonding between the OH group (located on the C4′ of the second sugar molecule) with Gly^{65}

(located in the second transmembrane helices, between loops A and B), with a distance of 3.4 Å, is shown in Figure 1D.

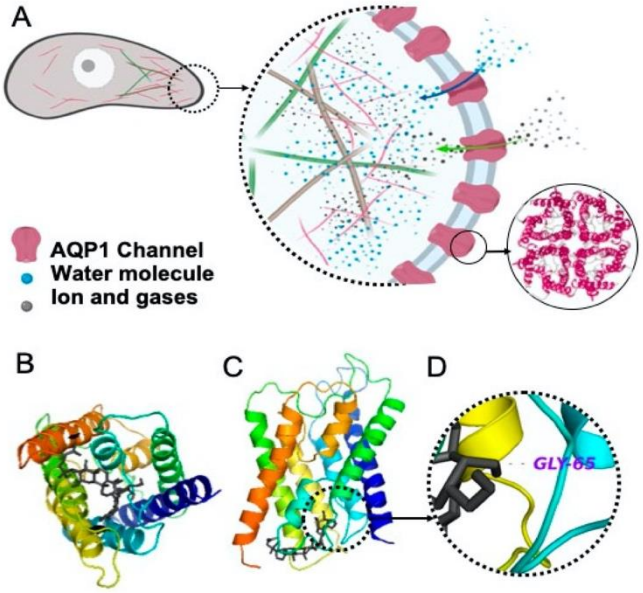

Figure 1. (**A**) The role of aquaporin 1 (AQP1) in cell migration and invasion (as reviewed in [39]). AQPs are redistributed to the leading edge of the migrating cell, leading water, ions and gases inside the cell; hence, along with changes in actin polymerisation, they play a role in the forward movement of the cell. AQP1 is a tetramer. Water passes through the pore of each monomer, and ions and gases pass through the central pore of the tetramer. (**B**) Top view of an AQP1 monomer, being blocked with Rg3, the black structure, (**C**) Side view of an AQP1 monomer, blocked with Rg3, and (**D**) H-bonding between Rg3 and Gly 65.

2.1.2. Stereoselectivity of Rg3 in Inhibiting AQP1 Water Channel

To find out if this interaction of Rg3-AQP1 is stereoselective, a *Xenopus laevis* oocyte expression system expressing human AQP1 was used. Native *Xenopus laevis* oocytes lack water channels, and hence a heterologous expression of human AQP1 on these cells makes them permeable to water. Following exposure to hypotonic media, water penetrates the cells based on osmotic driving forces. Figure 2A shows the result of the double swelling assays. The slope (± standard error) of the swelling rate for untreated, vehicle, RRg3 and SRg3 groups was 0.9 ± 0.1, 0.9 ± 0.2, 1.0 ± 0.2 and 0.4 ± 0.1, respectively. This shows that the rate of swelling in untreated, vehicle or RRg3 treated oocytes was similar, while the rate of swelling for SRg3 treated cells was reduced by almost 2.6 times, indicating the blockage of AQP1 with SRg3.

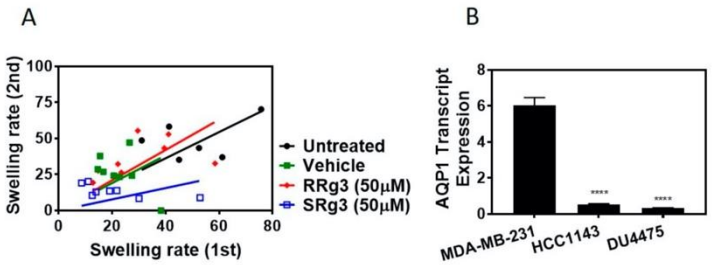

Figure 2. (**A**) Double swelling assay showing the swelling rates for the first and the second swelling on a single oocyte. Eight oocytes per treatment were measured for swelling in a hypotonic medium, before and 2 h after exposure to a vehicle or epimers of Rg3. The results were analysed and presented with a linear regression. (**B**) The AQP1 transcript expression in MDA-MB-231, HCC1143 and DU4475 cell lines. Each data point represents a mean ± SD value of 3 replicates, and comparisons were made with the vehicle control group (**** $p < 0.0001$).

2.2. Rg3 Has Stereoselectivity and Cell Line-Specificity in Inhibition of Proliferation

To study the effect of Rg3 epimers on the proliferation of TNBC cell lines, MDA-MB-231, HCC1143 and the non-adherent DU4475 were tested. Within 3 days of treatment, all of the cell lines showed an increased cell proliferation. Interestingly, only SRg3 at 100 μM had an anti-proliferative effect on MDA-MB-231 in both assays (Figure 3A,B). A crystal violet assay showed that SRg3 (100 μM) inhibited the proliferation of cells by 45%. This indicates a stereoselective activity and cell line specificity of Rg3, since neither of the other cell lines showed an inhibition of proliferation with SRg3 or RRg3. A potential mechanism for the effect of SRg3 on the inhibition of proliferation in MDA-MB-231 was investigated by measuring the AQP1 transcript expression. Since the MDA-MB-231 cells had an 11 and 19 times higher expression of AQP1 compared to the HCC1143 and DU4475 cell lines, respectively ($p < 0.0001$) (Figure 2B), SRg3 may, in part, exert its activity through blocking AQP1.

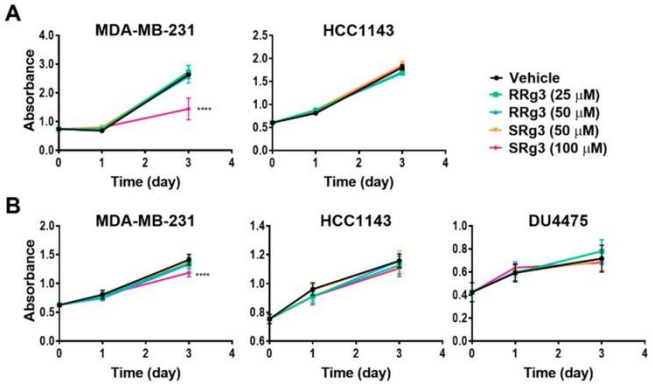

Figure 3. Effect of SRg3 and RRg3 on the proliferation of MDA-MB-231, HCC1143 and DU4475 triple negative breast cancer cell lines, after 3 days, with (**A**) a crystal violet assay on the adherent cell lines and (**B**) an MTS assay. Only 100 μM of SRg3 showed an inhibition of proliferation of MDA-MB-231 in both assays, indicating the cell line selectivity and stereoselective effect of Rg3 for the inhibition of proliferation. Each data point represents a mean ± SD value of 6 replicates, and comparisons are made with the vehicle control group (**** $p < 0.0001$).

2.3. Cytostatic Effect of SRg3 Inhibits Cell Proliferation in MDA-MB-231 Cell Line without Inducing Apoptosis

The MDA-MB-231 cell line was exposed to a concentration of 100 μM SRg3 for 3 days, after which the cells were tested to see if the inhibition of proliferation was due to the induction of apoptosis. As shown in Figure 4A,B, there were no significant differences between the amount of apoptosis induced by vehicle (11.29% ± 3.22) or 100 μM of SRg3 (6.96% ± 1. 81) ($p = 0.11$). Since SRg3 was not inducing apoptosis, the cells were tested to determine if the inhibition of proliferation was due to cell cycle arrest. The percentages of cells in each cell cycle phase for the untreated cells were 51.3% ± 2.9 for G0/G1, 29.8% ± 1.8 for S, and 17.1% ± 1.9 for G2/M (Figure 4C,D). Vehicle-treated cells have similar values, at 52.8 ± 5.1, 27.6 ± 3.0 and 19.8 ± 1.2, respectively. The statistical analysis showed no significant differences between the untreated and vehicle control groups for each phase. However, the cells treated with 100 μM of SRg3 for 3 days showed a significant accumulation of cells in G0/G1 (65.3% ± 3.22) ($p < 0.0001$) and a reduction of cells in the G2/M phase (12.5% ± 1.4) ($p < 0.05$), compared to the vehicle group. Together, these data suggest that 100 μM SRg3 inhibited the MDA-MB-231 proliferation by inducing a G0/G1 cell cycle arrest.

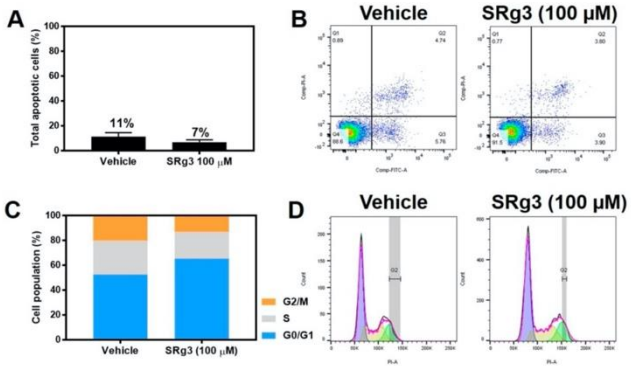

Figure 4. The effect of SRg3 on apoptosis and cell cycle arrest in the MDA-MB-231 cell line. (**A**) Total apoptotic cells (%) induced by vehicle or 100 μM SRg3 after 3 days of exposure; (**B**) Scatter plots of untreated cells or the cells treated with vehicle or SRg3. The left lower quadrant, right lower quadrant, right upper quadrant and left upper quadrant indicate viable cells, early apoptotic cells, late apoptotic cells and necrotic cells, respectively. (**C**) Cell population (%) in each of the G0/G1, S and G2/M phases of the cell cycle. (**D**) Histograms of the untreated, vehicle and SRG3-treated cells, following staining with PI. The violet, yellow and green curves represent events in the G0/G1, S and G2/M phases, respectively. The data presented is representative of 3 repeats.

2.4. Stereoselective Inhibition of Migration of MDA-MB-231 Cell Line

To study if the epimers of Rg3 had any effect on the MDA-MB-231 migration, the cells were pre-treated with Rg3 epimers for 3 days, after which they were seeded for a circular wound closure assay. The results of this assay showed that after 24 h, the untreated and vehicle cells closed the circular wound by about 80% (Figure 5A). The wound closure in the cells treated with 100 μM of SRg3 was 76% ± 3.8, not significantly different to the vehicle ($p = 0.81$), while the wound closure in the cells treated with 50 μM of RRg3 was inhibited by 22 % compared to the vehicle control group ($p = 0.001$).

We showed, using a chemoattractant transwell migration assay, that at 50 and 100 μM of RRg3 and SRg3, the transwell migration of MDA-MB-231 cells was significantly inhibited by 69 and 68%, respectively ($p < 0.0001$).

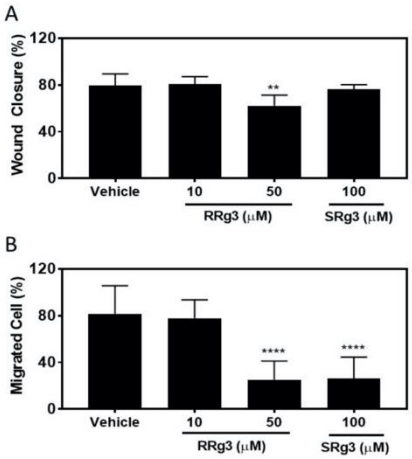

Figure 5. Migration assays on the MDA-MB-231 cell line following exposure to RRg3 and SRg3. (**A**) The percentage of wound closure following exposure of the MDA-MB-231 cell line to RRg3 and SRg3. Data is presented as mean ± SD of 6 repeats, and comparisons are made with the vehicle control group (** $p = 0.001$). (**B**) The transwell migration assay on the MDA-MB-231 cell line following exposure to RRg3 and SRg3. Data are presented as mean ± SD of 3 replicates, and comparisons are made with the vehicle control group (**** $p < 0.0001$).

2.5. Stereoselective Inhibition of Invasion

The ability of epimers of Rg3 to inhibit invasion was tested with a spheroid invasion assay. As shown in Figure 6, 50 μM of RRg3 resulted in inhibition ($p = 0.0001$). The inhibition of invasion was 78% for the spheroids treated with 50 μM RRg3. SRg3 did not inhibit spheroid invasion in this assay.

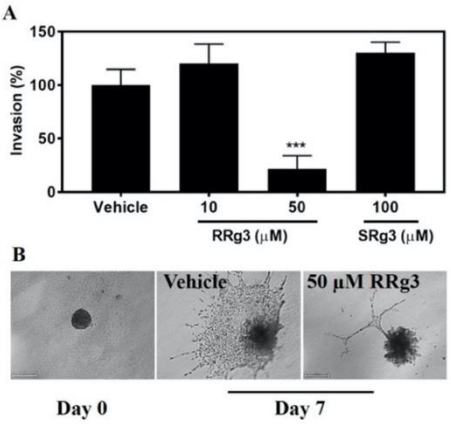

Figure 6. Spheroid invasion assay on the MDA-MB-231 cell line following exposure to RRg3 and SRg3. (**A**) The percentage of increase in the area, as an indicator of invasion to the extracellular matrix, following exposure of the MDA-MB-231 spheroids to RRg3 and SRg3. Data are presented as mean ± SD of 3 replicates, and comparisons are made with the vehicle control group (***) $p = 0.0001$. (**B**) Representative images of the vehicle control and RRg3-treated spheroids after 7 days, indicating the inhibition of spheroid invasion in the RRg3-treated spheroids.

3. Discussion

This is the first study to investigate the stereoselective effects of epimers of Rg3 on TNBC cell lines. To our knowledge, the literature has no comparable studies that define the Rg3 epimers, or the specific ratio of SRg3/RRg3 in breast cancer models. Notably, we showed the stereoselectivity of Rg3 in the inhibition of proliferation in MDA-MB-231, the only cell line that showed sensitivity toward the anti-proliferative effects of SRg3. Neither of the Rg3 epimers inhibited the proliferation of the HCC1143 or DU4475 cell lines. MDA-MB-231 is a basal-like B [40,41] but with claudin-low [42] or mesenchymal-like [41] features, representative of tumours with a worse prognosis and more aggressive nature. Higher levels of AQP1 expression in breast tumours have been correlated with a triple negativity, poorer prognosis of the disease and higher tumour grade [33,43]. We showed that the AQP1 expression in MDA-MB-231 is much higher than in the HCC1143 and DU4475 cell lines. Molecular docking studies showed that Rg3 had a promising binding score with AQP1, comparable with some other blockers of AQP1 such as AqB013 [44], bacopaside I and bacopaside II [38]. Furthermore, for the first time, we showed that SRg3 was the only epimer that inhibited the AQP1 water flux. This stereoselective inhibition of the AQP1 water flux and inhibition of proliferation in the cell line with a higher expression of AQP1 by SRg3 suggests that AQP1 might be one of the important proteins involved in the proliferation of MDA-MB-231. Importantly, it is already reported that the over-expression of AQP1 in MDA-MB-231 significantly increased the proliferation and chemotactic invasion [45].

We also showed that the inhibition of proliferation of MDA-MB-231 by SRg3 was not due to the induction of apoptosis, but rather due to cell cycle arrest at the G0/G1 phase of the cell cycle. This G0/G1-arrest mechanism was comparable with similar studies in prostate [45], melanoma [46] and breast cell lines [24]. None of them, however, have defined a specific epimer in their studies. For example, the study on the breast cancer cell line exposed MCF7 (an estrogen and progesterone receptor positive cell line) to Rg3 and the heated extract of ginseng, containing about 5% Rg3 [24]. We have shown that it is SRg3 that causes G0/G1-arrest in MDA-MB-231. In fact, it has been shown that the over-expression of AQP1 causes a higher level of cyclin D and E, which are crucial for phase transition [47]. Cyclin E is a regulator for G1-S transition, and the blockage of AQP1 or inhibiting the expression of AQP1, as suggested by Pan et al. [45], inhibits the G1-S transition and arrests the cells in G0/G1.

Migration was tested in two assays. While the scratch wound closure assay measures the rate of cells migrating on plastic to close the circular wound, the transwell migration assay measures the ability of cells in suspension to migrate toward a chemoattractant [48]. Both of the epimers inhibited the chemoattractant-induced migration of cells. Notably, SRg3, which inhibited the water transport function of AQP1 in a stereoselective manner, was only effective in the chemoattractant-induced migration of cells as opposed to adherent cells migrating on plastic. This suggests that these epimers might have different mechanisms of action for the inhibition of migration. For example, in ovarian carcinoma cell lines, SRg3 was the only epimer that inhibited migration and invasion via blocking hypoxia-induced epithelial-mesenchymal transition (EMT), the degradation of hypoxia-inducible factor-1α (HIF-1α) and the transcriptional repression of Snail and hence E-cadherin [49]. Importantly, Rg3 decreased the expression of AQP1 in the PC-M3 prostate cancer cell line, causing the inhibition of the chemoattractant-induced migration of these tumour cells [45]. It is already known that AQP1 is involved in the chemotactic migration of the cancer cells [29,50,51]. The chemotactic movement of the cancer cells is an important driver toward metastasis. Cancer cells sense the chemotactic gradient, and polarize into the leading edge to move forward toward the chemotactic agent. AQP1 is found on the leading edge of migrating cells (Figure 1A). AQP1, via directing the water influx and interactions with the actin cytoskeleton at the protrusion site of the migrating cell, plays roles in the migration of cancer cells, as reviewed in [39]. In our studied assays of migration and invasion, the transwell migration assay was the only assay in which the chemoattractant-induced migration of cells was assessed and SRg3, as a stereoselective inhibitor of AQP1, showed inhibitory effects. This suggests that

AQP1, along with other mechanisms, is involved in the chemoattractant-induced migration of highly AQP1-expressing MDA-MB-231 cells.

While SRg3 showed no efficacy in the inhibition of migration in the wound closure migration assay nor in the spheroid invasion assays, RRg3, with a higher potency, inhibited migration and invasion in all of the studied assays. This suggests that RRg3 modulates different targets and pathways. Similar to our results, studies on the lung cancer A549 cell line showed that RRg3 at concentrations < 50 μg/mL did not inhibit the proliferation of the cells, but, in a stereoselective manner, suppressed TGF-β1-induced EMT, through repressing the Snail expression and inhibiting the activation of Smad and non-Smad (p38 MAPK) signalling pathways, hence inhibiting the E-cadherin expression [52]. The RRg3 inhibition of TGF-β1-induced EMT caused the inhibition of migration, invasion and anoikis resistance. RRg3 inhibited the TGF-β1-induced MMP-2 expression and inhibited the activation of Smad2 and p38 MAPK [52]. Other suggested mechanisms for the RRg3 inhibition of EMT and invasion were through the downregulation of fucosyltransferase IV (FUT4) [53]. FUT4 is an enzyme responsible for abnormal fucosylation in cancer cells, associated with the proliferation and metastasis of breast tumour cells [54], and it is also suggested as a biomarker for the diagnosis of breast tumours [55].

This is the first paper to study the stereoselectivity of epimers of Rg3 in TNBC cell lines and demonstrates that SRg3 and RRg3 have distinct effects. Furthermore, this is the first time that the interaction between Rg3 epimers and AQP1 is demonstrated. The effect of Rg3 epimers on the inhibition of proliferation of TNBC cell lines was specific to MDA-MB-231, suggesting that basal-like claudin-low or mesenchymal type tumours, with a high AQP1 expression, might be better candidates for treatment with SRg3. SRg3 had cytostatic effects on the MDA-MB-231 cell line, leading to the inhibition of proliferation. It inhibited the chemoattractant-induced cell migration and, notably, was the only epimer that blocked the AQP1 water channel function. This suggests that the SRg3 blocking of the AQP1-mediated water flux is a potential contributor to the mechanism of inhibition of chemoattractant-induced cell migration and the inhibition of proliferation in this cell line, but may not be the only target of action. Importantly, RRg3 is not cytotoxic to the cells, yet it inhibited the cell migration and invasion of MDA-MB-231, with a higher potency. The distinct and stereoselective actions of each epimer suggest that SRg3 and RRg3 should be considered as separate drug candidates. Although this study was limited to cell lines and in vitro assays, these results will inform the doses of each epimer to be tested in a mouse model of breast cancer.

4. Materials and Methods

4.1. Materials

SRg3 (Sigma-Aldrich, St Louis, MO, USA) and RRg3 (AdooQ Bioseciences Irvine, CA, USA) epimers, both with purities > 98%, were dissolved in dimethyl sulfoxide (DMSO) at 12.7 and 6.5 mM stocks and stored in aliquots at −20 °C. Due to the low water solubility, log S −4.04 (ChemAxon, Cambridge, MA, USA), and relatively high lipophilicity (logP 4) of Rg3, these stocks were found to have the highest stock concentration of Rg3, which did not precipitate out upon dilution in aqueous media. The maximum concentration of DMSO with no observable biological effects in this study was found to be 0.8%. Triple negative breast cancer cell lines; MDA-MB-231 (basal-like with mesenchymal or claudin-low phenotype), HCC1143 (basal-like), and DU4475 (basal-like) were purchased from the American Type Culture Collection (ATCC; Manassas, VA, USA) and used at low passage numbers.

4.2. Molecular Docking of Rg3

The molecular docking of Rg3 on aquaporin (AQP) channels was performed as previously described [38,56]. The crystal structures of the proteins were obtained from the protein data bank of NCBI (RCSB PDB). The structure IDs were as follows: AQP1 (1FQY), AQP2 (4NEF), AQP4 (3GD8), AQP5 (3D9S). The SMILES structure of Rg3 was obtained from PubChem. The three-dimensional structure of Rg3 was prepared in the UCSF Chimera program (version 1.13.1-mac64). The Autodock

Vina algorithm (version 1.1.2_Mac) and UCSF Chimera program were used for in silico molecular docking. Images were prepared in the PyMol Molecular Graphics System, The X Window System, XQuartz 2.7.11. Notably, Autodock uses a stochastic search method to explore the conformational space of the ligand molecule, and this is by the random generation of distinct conformations, leading to finding a global energy minimum, expressed by a score for the Gibbs free energy of protein-ligand binding [57]. Due to this random generation of conformations, it is not practical to study a single epimer with this algorithm.

4.3. Oocyte Expression System and Swelling Assay

The unfertilized oocytes from a native *Xenopus laevis* frog were prepared and maintained, as previously described [38]. Briefly, the oocytes were injected with 3 ng of AQP1 cRNA and incubated at 16–18 °C for 3 days to allow for AQP1 expression. The inhibitory effect of Rg3 epimers on the AQP1 water channel was measured with the double-swelling assay. The swelling rate in hypotonic media (50% saline) for each oocyte was recorded and measured with ImageJ software (Wayne Rashband, National Institutes of Health, Bethesda, MD, USA), before and after a 2 h exposure to normal saline (as the untreated group), vehicle, or 50 μM of RRg3 or SRg3. Each treatment group consisted of 8 oocytes, and the rate of swelling in each group was compared with the vehicle group, using a linear regression analysis, as previously described [38].

4.4. Cell Culture

All of the TNBC cell lines were cultured as recommended by ATCC. The cells were thawed, and cultured in their respective media supplemented with a final concentration of 10% foetal bovine serum (FBS; Corning, Corning, NY, USA), 1% penicillin-streptomycin solution (Life Technologies, Grand Island, NY, USA) and 1% GlutaMax (Life Technologies), and they were incubated at 37 °C, 5% CO_2 in the air.

4.5. Quantitative PCR for Expression of AQP1

The cell lines were seeded at 5×10^5 cells/well in 6-well plates. Following an overnight incubation, RNA was extracted using the PureLink RNA mini kit (Life Technologies), followed by the reverse transcription of 200 ng RNA with the iScript cDNA Synthesis Kit (Bio-Rad Laboratories, Hercules, CA, USA). The duplex TaqMan Gene Expression Assays for aquaporin-1 (AQP1; Hs01028916_m1; Applied Biosystems, Foster City, CA, USA) and the reference gene serine-rich coiled-coil domain-containing protein 2 (CCSER2; HS00982799_mH, Applied Biosystems, Foster City, CA, USA) were used to determine the transcript expression, as previously described [58]. Reactions were performed using the Applied Biosystems ViiA 7 Real-Time PCR System (Life Technologies) with activation for 30 s at 95 °C, followed by 40 cycles of 15 s at 95 °C and 30 s at 60 °C. The AQP1 transcript expression was calculated using the $2^{-\Delta Ct}$ formula.

4.6. Proliferation Assay

The effect of Rg3 epimers on the proliferation of the MDA-MB-231 and HCC1143 adherent cell lines was tested with a crystal violet assay, as described previously [58]. DU4475, a non-adherent cell line, along with the two adherent ones, were also tested with the MTS assay (CellTiter 96® AQueous Non-Radioactive Cell Proliferation Assay, Promega, Madison, WI, USA), as described previously [34]. Briefly, 7×10^3 cells/well were seeded in 96-well plates, incubated overnight and treated with 0–100 μM (final concentration) Rg3 epimers (6 replicates). The absorptions at 595 nm (for the crystal violet assay) and 490 nm (for the MTS assay) were measured at 0, 24 and 72 h of treatment.

4.7. Apoptosis Assay

An apoptosis assay was performed using the Annexin-V-FLUOS staining kit (Roche Diagnostics, Mannheim, Germany), based on the previously described method [34]. Briefly, a density of 1×10^5 cells/well of 6-well plates were seeded in triplicate and incubated overnight. MDA-MB-231 cells were treated with 100 μM SRg3 for 72 h. Paclitaxel (400 nM) was used as a positive control. A control for necrosis was prepared by heating the cells at 63 °C for 30 min. Following the staining of the samples, they were analysed in BD FACSCanto II (BD Biosciences, San Jose, CA, USA) and FlowJo software, v 10.4 (FlowJo, LLC, Ashland, OR, USA).

4.8. Cell Cycle Analysis

MDA-MB-231 cells were seeded at 1×10^5 cells/well of 6-well plates, in triplicate. After an overnight incubation, 100 μM of SRg3 was added to the cells. After 3 days, propidium iodide staining and a cell cycle analysis were performed on the cells, as previously described [59,60]. The samples were analysed with BD FACSCanto II and FlowJo software, v 10.4.

4.9. Scratch Wound Closure Assay

MDA-MB-231 cells were pre-treated with Rg3 epimers for 3 days and then seeded at 8×10^4 cells/well in 96-well plates for a scratch wound closure assay. The cells were exposed to different concentrations of RRg3 and SRg3, and the assay was performed as described previously [61]. Images were taken at time 0 and 24 h using a Nikon microscope, and the wound closure (%) was measured using ImageJ software. The relative wound closure (%) at time 24 h was calculated compared to time 0, with 6 replicates.

4.10. Transwell Migration Assay

MDA-MB-231 cells were pre-treated with either vehicle or Rg3 epimers for 3 days. Then, 1×10^5 cells were suspended in 250 μL of serum-free DMEM containing vehicle or Rg3 epimers and placed in the upper chamber of the Corning® transwells (8 μm pore size). The lower chamber was filled with 750 μL DMEM supplemented with final concentrations of 10% FBS, 1% penicillin-streptomycin solution and 1% GlutaMax. The cells were incubated for 4.5 h, after which the cells on top of the membrane were removed with a cotton swab. The migrated cells on the other side of the membrane were fixed in 10% neutral buffered formalin for 30 min, stained in a crystal violet solution (1% crystal violet in 2% ethanol) for 10 min, and washed in distilled water. The experiment was carried out in triplicate, and the total migrated cells were counted in five fields of view per chamber, at 200× magnification using NIS-Elements (Nikon, Tokyo, Japan). The migration percentage for each treatment group is presented relative to the average vehicle control group.

4.11. Spheroid Invasion Assay

A single cell suspension (3×10^3 cell/well) and 1X Spheroid Formation ECM (Cultrex®, Trevigen Inc., Gaithersburg, MD, USA) (5 μL/well) was prepared, and 50 μL of this suspension was placed in each well of the 96-well ultra-low attachment Costar® plates (Corning Inc., Corning, NY, USA). The plate was centrifuged at 200× *g* for 3 min and incubated in a 37 °C, 5% CO_2 incubator for 72 h. Then, the plate was left on ice for 15 min, and 50 μL of Invasion Matrix (Cultrex®) was added to each well (day 0). The plate was then centrifuged at 300× *g*, 4 °C, 5 min, followed by a 1 h incubation. The spheres were then treated with different concentrations of Rg3. At day 0 and day 7, images were taken of the spheres using a Nikon Eclipse TE2000-U light microscope, and the area of each sphere was measured using NIS-elements software (Nikon, Tokyo, Japan). The invasion (%) of each spheroid was normalized to the mean invasion area of the vehicle group.

4.12. Statistical Analysis

A one-way or two-way analysis of variance (ANOVA) was performed for the data analysis using GraphPad Prism (version 7.02). The data are presented as the mean ± standard deviation (SD). $p < 0.05$ was considered as the level of statistical significance.

Author Contributions: Conceptualization, M.N., H.M.P., A.J.Y. and J.E.H.; Data curation, Y.T., E.S. and J.V.P.; Formal analysis, M.N., H.M.P., A.J.Y. and J.E.H.; Funding acquisition, T.J.P., A.R.T. and J.E.H.; Investigation, M.N.; Methodology, M.N., H.M.P., A.J.Y. and J.V.P.; Resources, T.J.P. and A.R.T.; Supervision, J.E.H.; Writing—original draft, M.N.; Writing—review & editing, H.M.P., Y.T., E.S., T.J.P., A.J.Y., J.V.P., A.R.T. and J.E.H.

Funding: This research was funded by the Margaret Elcombe Hospital Research Foundation Research Grant.

Conflicts of Interest: The authors declare no conflict of interest.

References

1. Yang, M.S.; Wu, M.Y. Chinese ginseng. In *Nutraceuticals*; Elsevier: Amsterdam, The Nederlands, 2016; pp. 693–705.
2. Szczuka, D.; Nowak, A.; Zakłos-Szyda, M.; Kochan, E.; Szymańska, G.; Motyl, I.; Blasiak, J.J.N. American ginseng (panax quinquefolium l.) as a source of bioactive phytochemicals with pro-health properties. *Nutrients* **2019**, *11*, 1041. [CrossRef] [PubMed]
3. Wei, X.; Su, F.; Su, X.; Hu, T.; Hu, S. Stereospecific antioxidant effects of ginsenoside rg3 on oxidative stress induced by cyclophosphamide in mice. *Fitoterapia* **2012**, *83*, 636–642. [CrossRef] [PubMed]
4. Lee, J.-Y.; Lim, K.-M.; Kim, S.-Y.; Bae, O.-N.; Noh, J.-Y.; Chung, S.-M.; Kim, K.; Shin, Y.-S.; Lee, M.-Y.; Chung, J.-H. Vascular smooth muscle dysfunction and remodeling induced by ginsenoside rg3, a bioactive component of ginseng. *Toxicol. Sci.* **2010**, *117*, 505–514. [CrossRef] [PubMed]
5. Sun, M.; Huang, C.; Wang, C.; Zheng, J.; Zhang, P.; Xu, Y.; Chen, H.; Shen, W. Ginsenoside rg3 improves cardiac mitochondrial population quality: Mimetic exercise training. *Biochem. Biophys. Res. Commun.* **2013**, *441*, 169–174. [CrossRef] [PubMed]
6. Park, J.-B.; Kwon, S.K.; Nagar, H.; Jung, S.-B.; Jeon, B.H.; Kim, C.S.; Oh, J.-H.; Song, H.-J.; Kim, C.-S. Rg3-enriched korean red ginseng improves vascular function in spontaneously hypertensive rats. *J. Ginseng Res.* **2014**, *38*, 244–250. [CrossRef] [PubMed]
7. Tian, J.; Fu, F.; Geng, M.; Jiang, Y.; Yang, J.; Jiang, W.; Wang, C.; Liu, K. Neuroprotective effect of 20 (s)-ginsenoside rg3 on cerebral ischemia in rats. *Neurosci. Lett.* **2005**, *374*, 92–97. [CrossRef] [PubMed]
8. Yang, L.; Hao, J.; Zhang, J.; Xia, W.; Dong, X.; Hu, X.; Kong, F.; Cui, X. Ginsenoside rg3 promotes beta-amyloid peptide degradation by enhancing gene expression of neprilysin. *J. Pharm. Pharmacol.* **2009**, *61*, 375–380. [CrossRef] [PubMed]
9. He, B.; Chen, P.; Yang, J.; Yun, Y.; Zhang, X.; Yang, R.; Shen, Z. Neuroprotective effect of 20 (r)-ginsenoside rg3 against transient focal cerebral ischemia in rats. *Neurosci. Lett.* **2012**, *526*, 106–111. [CrossRef] [PubMed]
10. Liu, L.; Anderson, G.A.; Fernandez, T.G.; Dore, S. Efficacy and mechanism of panax ginseng in experimental stroke. *Front. Neurosci.* **2019**, *13*, 294. [CrossRef]
11. Saba, E.; Kim, S.-H.; Kim, S.-D.; Park, S.-J.; Kwak, D.; Oh, J.-H.; Park, C.-K.; Rhee, M.H. Alleviation of diabetic complications by ginsenoside rg3-enriched red ginseng extract in western diet-fed ldl−/−mice. *J. Ginseng Res.* **2018**, *42*, 352–355. [CrossRef]
12. Park, M.W.; Ha, J.; Chung, S.H. 20 (s)-ginsenoside rg3 enhances glucose-stimulated insulin secretion and activates ampk. *Biol. Pharm. Bull.* **2008**, *31*, 748–751. [CrossRef] [PubMed]
13. Kang, K.S.; Yamabe, N.; Kim, H.Y.; Park, J.H.; Yokozawa, T. Therapeutic potential of 20 (s)-ginsenoside rg3 against streptozotocin-induced diabetic renal damage in rats. *Eur. J. Pharmacol.* **2008**, *591*, 266–272. [CrossRef] [PubMed]
14. Kee, J.-Y.; Hong, S.-H. Ginsenoside rg3 suppresses mast cell–mediated allergic inflammation via mitogen-activated protein kinase signaling pathway. *J. Ginseng Res.* **2019**, *43*, 282–290. [CrossRef] [PubMed]
15. Wei, X.; Chen, J.; Su, F.; Su, X.; Hu, T.; Hu, S. Stereospecificity of ginsenoside rg3 in promotion of the immune response to ovalbumin in mice. *Int. Immunol.* **2012**, *24*, 465–471. [CrossRef] [PubMed]

16. Wu, R.; Ru, Q.; Chen, L.; Ma, B.; Li, C. Stereospecificity of ginsenoside rg3 in the promotion of cellular immunity in hepatoma h22-bearing mice. *J. Food Sci.* **2014**, *79*, H1430–H1435. [CrossRef] [PubMed]
17. Yi, Y.-S. Roles of ginsenosides in inflammasome activation. *J. Ginseng Res.* **2019**, *43*, 172–178. [CrossRef] [PubMed]
18. Nakhjavani, M.; Hardingham, J.E.; Palethorpe, H.M.; Tomita, Y.; Smith, E.; Price, T.J.; Townsend, A.R. Ginsenoside rg3: Potential molecular targets and therapeutic indication in metastatic breast cancer. *Medicines* **2019**, *6*, 17. [CrossRef]
19. Park, E.-H.; Kim, Y.-J.; Yamabe, N.; Park, S.-H.; Kim, H.-K.; Jang, H.-J.; Kim, J.H.; Cheon, G.J.; Ham, J.; Kang, K.S. Stereospecific anticancer effects of ginsenoside rg3 epimers isolated from heat-processed american ginseng on human gastric cancer cell. *J. Ginseng Res.* **2014**, *38*, 22–27. [CrossRef]
20. Jeong, S.M.; Lee, J.-H.; Kim, J.-H.; Lee, B.-H.; Yoon, I.-S.; Lee, J.-H.; Kim, D.-H.; Rhim, H.; Kim, Y.; Nah, S.-Y. Stereospecificity of ginsenoside rg 3 action on ion channels. *Mol. Cells* **2004**, *18*, 383–389.
21. Ismail-Khan, R.; Bui, M.M. A review of triple-negative breast cancer. *Cancer Control* **2010**, *17*, 173–176. [CrossRef]
22. Kim, B.-M.; Kim, D.-H.; Park, J.-H.; Na, H.-K.; Surh, Y.-J. Ginsenoside rg3 induces apoptosis of human breast cancer (mda-mb-231) cells. *J. Cancer Prev.* **2013**, *18*, 177–185. [CrossRef] [PubMed]
23. Kim, B.-M.; Kim, D.-H.; Park, J.-H.; Surh, Y.-J.; Na, H.-K. Ginsenoside rg3 inhibits constitutive activation of nf-κb signaling in human breast cancer (mda-mb-231) cells: Erk and akt as potential upstream targets. *J. Cancer Prev.* **2014**, *19*, 23. [CrossRef] [PubMed]
24. Wang, C.-Z.; Aung, H.H.; Zhang, B.; Sun, S.; Li, X.-L.; He, H.; Xie, J.-T.; He, T.-C.; Du, W.; Yuan, C.-S. Chemopreventive effects of heat-processed panax quinquefolius root on human breast cancer cells. *Anticancer Res.* **2008**, *28*, 2545–2551. [PubMed]
25. Chen, X.-P.; Qian, L.-L.; Jiang, H.; Chen, J.-H. Ginsenoside rg3 inhibits cxcr 4 expression and related migrations in a breast cancer cell line. *Int. J. Clin. Oncol.* **2011**, *16*, 519–523. [CrossRef] [PubMed]
26. Yool, A.J.; Brown, E.A.; Flynn, G.A. Roles for novel pharmacological blockers of aquaporins in the treatment of brain oedema and cancer. *Clin. Exp. Pharmacol. Physiol.* **2010**, *37*, 403–409. [CrossRef] [PubMed]
27. Yool, A.J. Functional domains of aquaporin-1: Keys to physiology, and targets for drug discovery. *Curr. Pharm. Des.* **2007**, *13*, 3212–3221. [CrossRef] [PubMed]
28. Dorward, H.S.; Du, A.; Bruhn, M.A.; Wrin, J.; Pei, J.V.; Evdokiou, A.; Price, T.J.; Yool, A.J.; Hardingham, J.E. Pharmacological blockade of aquaporin-1 water channel by aqb013 restricts migration and invasiveness of colon cancer cells and prevents endothelial tube formation in vitro. *J. Exp. Clin. Cancer Res.* **2016**, *35*, 36–45. [CrossRef] [PubMed]
29. Papadopoulos, M.; Saadoun, S.; Verkman, A. Aquaporins and cell migration. *Pflug. Arch.—Eur. J. Physiol.* **2008**, *456*, 693–700. [CrossRef]
30. Endo, M.; Jain, R.K.; Witwer, B.; Brown, D. Water channel (aquaporin 1) expression and distribution in mammary carcinomas and glioblastomas. *Microvasc. Res.* **1999**, *58*, 89–98. [CrossRef]
31. Esteva-Font, C.; Jin, B.-J.; Verkman, A. Aquaporin-1 gene deletion reduces breast tumor growth and lung metastasis in tumor-producing mmtv-pyvt mice. *FASEB J.* **2014**, *28*, 1446–1453.
32. Shi, Z.; Zhang, T.; Luo, L.; Zhao, H.; Cheng, J.; Xiang, J.; Zhao, C. Aquaporins in human breast cancer: Identification and involvement in carcinogenesis of breast cancer. *J. Surg. Oncol.* **2012**, *106*, 267–272. [CrossRef] [PubMed]
33. Otterbach, F.; Callies, R.; Adamzik, M.; Kimmig, R.; Siffert, W.; Schmid, K.W.; Bankfalvi, A. Aquaporin 1 (aqp1) expression is a novel characteristic feature of a particularly aggressive subgroup of basal-like breast carcinomas. *Breast Cancer Res. Treat.* **2010**, *120*, 67–76. [PubMed]
34. Palethorpe, H.; Tomita, Y.; Smith, E.; Pei, J.; Townsend, A.; Price, T.; Young, J.; Yool, A.; Hardingham, J. The aquaporin 1 inhibitor bacopaside ii reduces endothelial cell migration and tubulogenesis and induces apoptosis. *Int. J. Mol. Sci.* **2018**, *19*, 653. [CrossRef] [PubMed]
35. Smith, E.; Tomita, Y.; Palethorpe, H.M.; Howell, S.; Nakhjavani, M.; Townsend, A.R.; Price, T.J.; Young, J.P.; Hardingham, J.E. Reduced aquaporin-1 transcript expression in colorectal carcinoma is associated with promoter hypermethylation. *Epigenetics* **2019**, *14*, 158–170. [CrossRef] [PubMed]

36. Tomita, Y.; Palethorpe, H.M.; Smith, E.; Nakhjavani, M.; Townsend, A.R.; Price, T.J.; Yool, A.J.; Hardingham, J.E. Bumetanide-derived aquaporin 1 inhibitors, aqb013 and aqb050 inhibit tube formation of endothelial cells through induction of apoptosis and impaired migration in vitro. *Int. J. Mol. Sci.* **2019**, *20*, 1818. [CrossRef] [PubMed]
37. Tomita, Y.; Dorward, H.; Yool, A.; Smith, E.; Townsend, A.; Price, T.; Hardingham, J. Role of aquaporin 1 signalling in cancer development and progression. *Int. J. Mol. Sci.* **2017**, *18*, 299. [CrossRef] [PubMed]
38. Pei, J.V.; Kourghi, M.; De Ieso, M.L.; Campbell, E.M.; Dorward, H.S.; Hardingham, J.E.; Yool, A.J. Differential inhibition of water and ion channel activities of mammalian aquaporin-1 by two structurally related bacopaside compounds derived from the medicinal plant bacopa monnieri. *Mol. Pharmacol.* **2016**, *90*, 496–507. [CrossRef] [PubMed]
39. De Ieso, M.L.; Yool, A.J. Mechanisms of aquaporin-facilitated cancer invasion and metastasis. *Front. Chem.* **2018**, *6*, 135.
40. Dai, X.; Cheng, H.; Bai, Z.; Li, J. Breast cancer cell line classification and its relevance with breast tumor subtyping. *J. Cancer* **2017**, *8*, 3131. [CrossRef]
41. Kao, J.; Salari, K.; Bocanegra, M.; Choi, Y.-L.; Girard, L.; Gandhi, J.; Kwei, K.A.; Hernandez-Boussard, T.; Wang, P.; Gazdar, A.F. Molecular profiling of breast cancer cell lines defines relevant tumor models and provides a resource for cancer gene discovery. *PLoS ONE* **2009**, *4*, e6146. [CrossRef]
42. Riaz, M.; van Jaarsveld, M.T.; Hollestelle, A.; Prager-van der Smissen, W.J.; Heine, A.A.; Boersma, A.W.; Liu, J.; Helmijr, J.; Ozturk, B.; Smid, M. Mirna expression profiling of 51 human breast cancer cell lines reveals subtype and driver mutation-specific mirnas. *Breast Cancer Res.* **2013**, *15*, R33. [CrossRef] [PubMed]
43. Mobasheri, A.; Shakibaei, M.; Marples, D. Immunohistochemical localization of aquaporin 10 in the apical membranes of the human ileum: A potential pathway for luminal water and small solute absorption. *Histochem. Cell Biol.* **2004**, *121*, 463–471. [CrossRef] [PubMed]
44. Migliati, E.; Meurice, N.; DuBois, P.; Fang, J.S.; Somasekharan, S.; Beckett, E.; Flynn, G.; Yool, A.J. Inhibition of aquaporin-1 and aquaporin-4 water permeability by a derivative of the loop diuretic bumetanide acting at an internal pore-occluding binding site. *Mol. Pharmacol.* **2009**, *76*, 105–112. [CrossRef] [PubMed]
45. Pan, X.-Y.; Guo, H.; Han, J.; Hao, F.; An, Y.; Xu, Y.; Xiaokaiti, Y.; Pan, Y.; Li, X.-J. Ginsenoside rg3 attenuates cell migration via inhibition of aquaporin 1 expression in pc-3m prostate cancer cells. *Eur. J. Pharmacol.* **2012**, *683*, 27–34. [CrossRef] [PubMed]
46. Shan, X.; Fu, Y.-S.; Aziz, F.; Wang, X.-Q.; Yan, Q.; Liu, J.-W. Ginsenoside rg3 inhibits melanoma cell proliferation through down-regulation of histone deacetylase 3 (hdac3) and increase of p53 acetylation. *PLoS ONE* **2014**, *9*, e115401. [CrossRef] [PubMed]
47. Galán-Cobo, A.; Ramírez-Lorca, R.; Toledo-Aral, J.J.; Echevarría, M. Aquaporin-1 plays important role in proliferation by affecting cell cycle progression. *J. Cell. Physiol.* **2016**, *231*, 243–256. [CrossRef] [PubMed]
48. Justus, C.R.; Leffler, N.; Ruiz-Echevarria, M.; Yang, L.V. In vitro cell migration and invasion assays. *J. Vis. Exp.* **2013**, *752*, 10–24.
49. Liu, T.; Zhao, L.; Zhang, Y.; Chen, W.; Liu, D.; Hou, H.; Ding, L.; Li, X. Ginsenoside 20 (s)-rg3 targets hif-1α to block hypoxia-induced epithelial-mesenchymal transition in ovarian cancer cells. *PLoS ONE* **2014**, *9*, e103887. [CrossRef]
50. Pelagalli, A.; Nardelli, A.; Fontanella, R.; Zannetti, A. Inhibition of aqp1 hampers osteosarcoma and hepatocellular carcinoma progression mediated by bone marrow-derived mesenchymal stem cells. *Int. J. Mol. Sci.* **2016**, *17*, 1102. [CrossRef]
51. Qin, F.; Zhang, H.; Shao, Y.; Liu, X.; Yang, L.; Huang, Y.; Fu, L.; Gu, F.; Ma, Y. Expression of aquaporin1, a water channel protein, in cytoplasm is negatively correlated with prognosis of breast cancer patients. *Oncotarget* **2016**, *7*, 8143. [CrossRef]
52. Kim, Y.-J.; Choi, W.-I.; Jeon, B.-N.; Choi, K.-C.; Kim, K.; Kim, T.-J.; Ham, J.; Jang, H.J.; Kang, K.S.; Ko, H. Stereospecific effects of ginsenoside 20-rg3 inhibits tgf-β1-induced epithelial–mesenchymal transition and suppresses lung cancer migration, invasion and anoikis resistance. *Toxicology* **2014**, *322*, 23–33. [CrossRef] [PubMed]
53. Tian, L.; Shen, D.; Li, X.; Shan, X.; Wang, X.; Yan, Q.; Liu, J. Ginsenoside rg3 inhibits epithelial-mesenchymal transition (emt) and invasion of lung cancer by down-regulating fut4. *Oncotarget* **2016**, *7*, 1619. [CrossRef] [PubMed]

54. Zhao, L.; Feng, X.; Song, X.; Zhou, H.; Zhao, Y.; Cheng, L.; Jia, L. Mir-493-5p attenuates the invasiveness and tumorigenicity in human breast cancer by targeting fut4. *Oncol. Rep.* **2016**, *36*, 1007–1015. [CrossRef] [PubMed]
55. Yan, X.; Lin, Y.; Liu, S.; Yan, Q. Fucosyltransferase iv (fut4) as an effective biomarker for the diagnosis of breast cancer. *BioMed Pharmacother.* **2015**, *70*, 299–304. [CrossRef] [PubMed]
56. Yool, A.J.; Morelle, J.; Cnops, Y.; Verbavatz, J.-M.; Campbell, E.M.; Beckett, E.A.; Booker, G.W.; Flynn, G.; Devuyst, O. Aqf026 is a pharmacologic agonist of the water channel aquaporin-1. *J. Am. Soc. Nephrol.* **2013**, *24*, 1045–1052. [CrossRef] [PubMed]
57. Borrel, A. Development of Computational Methods to Predict Protein Pocket Druggability and profile Ligands Using Structural Data. Ph.D. Thesis, University of Helsinki, Helsinki, Finland, 2016.
58. Smith, E.; Palethorpe, H.M.; Tomita, Y.; Pei, J.V.; Townsend, A.R.; Price, T.J.; Young, J.P.; Yool, A.J.; Hardingham, J.E. The purified extract from the medicinal plant bacopa monnieri, bacopaside ii, inhibits growth of colon cancer cells in vitro by inducing cell cycle arrest and apoptosis. *Cells* **2018**, *7*, 81. [CrossRef] [PubMed]
59. Palethorpe, H.M.; Leach, D.A.; Need, E.F.; Drew, P.A.; Smith, E. Myofibroblast androgen receptor expression determines cell survival in co-cultures of myofibroblasts and prostate cancer cells in vitro. *Oncotarget* **2018**, *9*, 19100–19114. [CrossRef]
60. Palethorpe, H.M.; Drew, P.A.; Smith, E. Androgen signaling in esophageal adenocarcinoma cell lines in vitro. *Dig. Dis. Sci.* **2017**, *62*, 3402–3414. [CrossRef]
61. Kourghi, M.; Pei, J.V.; De Ieso, M.L.; Flynn, G.; Yool, A.J. Bumetanide derivatives aqb007 and aqb011 selectively block the aquaporin-1 ion channel conductance and slow cancer cell migration. *Mol. Pharmacol.* **2016**, *89*, 133–140. [CrossRef]

Chapter 3 Effects of ginsenoside Rg3 on angiogenesis

3.1. Background

Cancer angiogenesis is a complex but highly regulated and organised process, which fulfils a tumour's nutritional requirements and facilitates tumour cells' metastasis to other organs. Some tumours, including breast, show high levels of angiogenesis, hence the administration of anti-angiogenic drugs became a part of cancer treatment regimens for these tumours. However, the administration of the current clinically approved anti-angiogenic treatments is accompanied by serious side effects and drug resistance. Therefore, drug development programs are actively ongoing to introduce safer and more effective drugs.

As described in the first chapter, one important aspect of the anti-cancer efficacy of Rg3 is its anti-angiogenic action. Blood vessels have a single layer of endothelial cells. These cells, via proliferation, migration and invasion are responsible for angiogenesis. Hence, an important part of preclinical *in vitro* assessment of anti-angiogenic candidates focuses on their efficacy in inhibiting these critical steps of angiogenesis in these cells.

As discussed before, AQP1 is highly expressed in endothelial cells and promotes angiogenesis. Blockers of AQP1 have shown anti-angiogenic properties. In the first chapter, anti-angiogenic properties of Rg3 were reviewed and in chapter 2, it was shown that SRg3 blocked AQP1 water channel. Based on these and the stereoselective efficacy of Rg3 epimers, for the first time, I have shown the anti-angiogenic efficacy of an optimised combination of SRg3 and RRg3. The optimisation of the SRg3 and RRg3 combination was found using response surface methodology (RSM) modelling based on loop formation assay. Loop formation assay is an *in vitro* measurement of angiogenesis, which takes into account both the migration and invasion of endothelial cells.

To evaluate the anti-angiogenic efficacy of Rg3, human and murine endothelial cells were used. This would also give an estimation about the sensitivity of human or mouse tumours to the applied drug, and of use in the mouse model of breast cancer. The combination was also tested in migration and proliferation assays to confirm the efficacy of the drug candidate. The mechanism of inhibition of proliferation and mode of cell death was studied.

VEGF, the expression of which is increased in hypoxic conditions, is one of the crucial pro-angiogenic factors and its interaction with VEGFR2 is the key driver of angiogenesis. Therefore, to further study the mechanisms of the drug, the effect of Rg3 on this interaction was studied *in silico* and *in vitro*. In addition, the effect of the drug on the signalling of PI3K/AKT, and expression of AQP1 and FAK was studied. Since hypoxia is one of the important conditions that encourages angiogenesis, these mechanisms were studied in both normoxia and hypoxia.

This chapter was submitted to the "*Angiogenesis*" journal and is currently under review.

3.2. Statement of Authorship

Statement of Authorship

Title of Paper	Anti-angiogenic properties of ginsenoside Rg3 epimers: in vitro assessment of single and combination treatments
Publication Status	☑ Published ☐ Accepted for Publication ☐ Submitted for Publication ☐ Unpublished and Unsubmitted work written in manuscript style
Publication Details	Nakhjavani, M., Smith, E., Yeo, K., Palethorpe, H. M., Tomita, Y., Price, T. J., Townsend, A. R., and Hardingham, J. E. (2021) Anti-angiogenic properties of ginsenoside Rg3 epimers: in vitro assessment of single and combination treatments. Cancers, 13(9), 2223.

Principal Author

Name of Principal Author (Candidate)	Maryam Nakhjavani		
Contribution to the Paper	Conceptualised, designed and performed the experiments, analysed and curated the data, and substantially wrote the manuscript.		
Overall percentage (%)	70		
Certification:	This paper reports on original research I conducted during the period of my Higher Degree by Research candidature and is not subject to any obligations or contractual agreements with a third party that would constrain its inclusion in this thesis. I am the primary author of this paper.		
Signature		Date	10th Feb 2021

Co-Author Contributions

By signing the Statement of Authorship, each author certifies that:

i. the candidate's stated contribution to the publication is accurate (as detailed above);
ii. permission is granted for the candidate in include the publication in the thesis; and
iii. the sum of all co-author contributions is equal to 100% less the candidate's stated contribution.

Name of Co-Author	Eric Smith		
Contribution to the Paper	Contributed to designing the experiment, data analysis, discussion and reviewing the paper.		
Signature		Date	10th Feb 2021

Name of Co-Author	Kenny Yeo		
Contribution to the Paper	Contributed to performing the experiment and discussion.		
Signature		Date	8th Feb 2021

Name of Co-Author	Yoko Tomita		
Contribution to the Paper	Contributed to the discussion and reviewing the paper.		
Signature		Date	12th Feb 2021

Name of Co-Author	Timothy J Price		
Contribution to the Paper	Contributed to the discussion and reviewing the paper.		
Signature		Date	11th Feb 2021

Name of Co-Author	Andrea Yool		
Contribution to the Paper	Contributed to drafting and discussion and reviewing the paper.		
Signature		Date	10th Feb 2021

Name of Co-Author	Amanda R Townsend		
Contribution to the Paper	Contributed to the discussion and reviewing the paper.		
Signature		Date	11th Feb 2021

Name of Co-Author	Jennifer E Hardingham		
Contribution to the Paper	Conceptualised and designed the experiments, contributed in data analysis and curation, and reviewing the paper.		
Signature		Date	10th Feb 2021

cancers

MDPI

Article

Anti-Angiogenic Properties of Ginsenoside Rg3 Epimers: In Vitro Assessment of Single and Combination Treatments

Maryam Nakhjavani [1,2], Eric Smith [1,2,*], Kenny Yeo [1,2], Helen M. Palethorpe [3], Yoko Tomita [1,2,4], Tim J. Price [2,4], Amanda R. Townsend [2,4] and Jennifer E. Hardingham [1,2]

1 Molecular Oncology, Basil Hetzel Institute, The Queen Elizabeth Hospital, Woodville South, SA 5011, Australia; maryam.nakhjavani@adelaide.edu.au (M.N.); a1811332@student.adelaide.edu.au (K.Y.); yoko.tomita@sa.gov.au (Y.T.); jennifer.hardingham@adelaide.edu.au (J.E.H.)
2 Adelaide Medical School, University of Adelaide, Adelaide, SA 5005, Australia; timothy.price@sa.gov.au (T.J.P.); amanda.townsend@sa.gov.au (A.R.T.)
3 Centre for Cancer Biology, University of South Australia and SA Pathology, Adelaide, SA 5000, Australia; helen.palethorpe@unisa.edu.au
4 Oncology Unit, The Queen Elizabeth Hospital, Woodville South, SA 5011, Australia
* Correspondence: eric.smith@adelaide.edu.au; Tel.: +61-8-8222-6142

Simple Summary: Angiogenesis is a critical step in tumour progression and metastasis. The application of current inhibitors of angiogenesis is accompanied by adverse effects. Therefore, there is a need for developing better treatments. *Panax ginseng* is a traditional herbal medicine that has been used by humans for thousands of years. 20(S) ginsenoside-Rg3 and 20(R) ginsenoside-Rg3 are two structurally similar molecules extracted from this plant, with distinct mechanisms of action. In this research, a combination of both of these molecules was optimised (C3) to inhibit angiogenesis, in lab settings. The results showed the role of C3 as a novel anti-angiogenic drug.

Abstract: Tumour angiogenesis plays a key role in tumour growth and progression. The application of current anti-angiogenic drugs is accompanied by adverse effects and drug resistance. Therefore, finding safer effective treatments is needed. Ginsenoside Rg3 (Rg3) has two epimers, 20(S)-Rg3 (SRg3) and 20(R)-Rg3 (RRg3), with stereoselective activities. Using response surface methodology, we optimised a combination of these two epimers for the loop formation of human umbilical vein endothelial cell (HUVEC). The optimised combination (C3) was tested on HUVEC and two murine endothelial cell lines. C3 significantly inhibited the loop formation, migration, and proliferation of these cells, inducing apoptosis in HUVEC and cell cycle arrest in all of the cell lines tested. Using molecular docking and vascular endothelial growth factor (VEGF) bioassay, we showed that Rg3 has an allosteric modulatory effect on vascular endothelial growth factor receptor 2 (VEGFR2). C3 also decreased the VEGF expression in hypoxic conditions, decreased the expression of aquaporin 1 and affected AKT signaling. The proteins that were mostly affected after C3 treatment were those related to mammalian target of rapamycin (mTOR). Eukaryotic translation initiation factor 4E (eIF4E)-binding protein 1 (4E-BP1) was one of the important targets of C3, which was affected in both hypoxic and normoxic conditions. In conclusion, these results show the potential of C3 as a novel anti-angiogenic drug.

Keywords: ginsenoside Rg3; response surface methodology; optimisation; epimer; angiogenesis

Citation: Nakhjavani, M.; Smith, E.; Yeo, K.; Palethorpe, H.M.; Tomita, Y.; Price, T.J.; Townsend, A.R.; Hardingham, J.E. Anti-Angiogenic Properties of Ginsenoside Rg3 Epimers: In Vitro Assessment of Single and Combination Treatments. *Cancers* **2021**, *13*, 2223. https://doi.org/10.3390/cancers13092223

Academic Editor: Domenico Ribatti

Received: 11 March 2021
Accepted: 4 May 2021
Published: 6 May 2021

1. Introduction

Tumour angiogenesis is a critical step in tumour growth, survival, and metastasis. Several pro- and anti-angiogenic factors and signaling pathways contribute to regulate angiogenesis and facilitate tumour growth and metastasis [1–3]. The key driver of angiogenesis is the signaling of vascular endothelial growth factor receptor 2 (VEGFR2). VEGFR2 is activated upon interaction with its major ligand, VEGF. Hence, VEGF; VEGFR2; or the

downstream signaling of VEGFR2, including PI3K/AKT, could be potential key targets in anti-angiogenesis drug development. Currently, the clinically approved anti-angiogenic agents are either antibodies against VEGF such as bevacizumab or small molecule tyrosine kinase inhibitors (TKIs). The administration of bevacizumab in advanced cancer patients could be accompanied by severe and sometimes fatal adverse effects, including hematological disorders, respiratory disorders, perforation and hemorrhage in the gastrointestinal system, and nervous system disorders [4]. TKIs also cause hematological and non-hematological events that may limit the application of treatment [5]. Furthermore, the administration of current anti-angiogenic treatments may also be limited because of drug resistance [6]. Therefore, developing effective less-toxic treatments is a fundamental effort for improving patient outcomes and it is the main aim of this research.

Epimers of ginsenoside Rg3 (Rg3), SRg3, and RRg3 are some of the most important pharmacologically active members of the ginsenosides family of chemicals extracted from *Panax ginseng* [7]. These molecules seem to be suitable anti-angiogenic candidates for drug development studies, because several studies have described their effects of inhibiting angiogenesis, and have shown their potential as anti-cancer agents (reviewed in [8,9]). Furthermore, in vitro and in vivo studies in animals and humans have shown tolerability and a low toxicity profile for these molecules (reviewed in [8,9]). These factors make Rg3 epimers intriguing candidates. In this regard, one important aspect of pharmacology of these epimers is their stereoselective anti-cancer action. We previously showed that these epimers have stereoselective activities for the inhibition of the migration and invasion of triple-negative breast cancer cell lines [10]. In addition, we showed that only SRg3 blocks the water transport function of aquaporin 1 (AQP1) [10], a protein that plays important roles in angiogenesis, tumour growth, and metastasis [11–13]. Furthermore, other studies have shown the stereoselectivity of these epimers on ion channels [14], the relaxation of the swine coronary artery [15], the anti-oxidant effect [16], promotion of immune system [17,18], and the inhibition of epithelial–mesenchymal transition [19]. Considering this stereoselective anti-cancer activity, these epimers should be considered as separate drugs that could be combined.

For the first time, in this research, the concentrations of these epimers in combination was optimised to yield the highest anti-angiogenic efficacy. The optimal combination was determined using response surface methodology (RSM), a statistical and experiment design modelling process, which aims at reducing the number of experiments and costs associated with the experiment design [20]. In recent years, RSM has gained popularity in drug design [21], drug interaction [22], and combination therapy in cancer treatment studies [23]. It describes a three-dimensional dose–response surface, measures drug interactions, and defines the optimised combination of two drugs [24]. In this study, the efficacy of the optimal combination of Rg3 epimers was confirmed in migration and proliferation assays in human and murine endothelial cells. The mode of cell death and several potential intracellular targets of this combination that play roles in angiogenesis were studied. These targets included the expression of VEGF, activation of VEGFR2, signaling of AKT downstream of the activation of VEGFR2, and expression of AQP1. Because of the essential role of hypoxia in driving angiogenesis in a rapidly growing tumour, the role of this combination was studied in both normoxic and hypoxic conditions. [25].

2. Materials and Methods

2.1. Reagents, Cell Lines, and Cell Culture

Human umbilical vein endothelial cell (HUVEC) and its media, endothelial cell growth medium-2 (EBM-2; Clonetics, Lonza, Belgium), were purchased from Lonza, Belgium. Murine endothelial cell lines, 2H-11 and 3B-11, and human triple-negative breast cancer cell line MDA-MB-231 were purchased from the American Type Culture Collection (Manassas, VA, USA) and maintained in Dulbecco's Modified Eagle Medium (DMEM; Life Technologies, Carlsbad, CA, USA), supplemented with 10% fetal bovine serum (Corning, Corning, NY, USA), 50 U/mL penicillin, and 50 µg/mL (Life Technologies). The cells were used

within the first 10 passages. SRg3 (>98%) and RRg3 (>98%) (ChemFaces®, Wuhan, China) were dissolved in dimethyl sulfoxide (DMSO, HYBRI-MAX, Sigma-Aldrich, St. Louis, MO, USA). Aliquots of SRg3 and RRg3 at 6.5 and 12.7 mM, respectively, as the maximum concentrations of Rg3 epimers in aqueous media, were stored at −20 °C. The concentration of DMSO in the experiments did not exceed 0.8%, as described previously [10].

2.2. Response Surface Methodology (RSM)

To develop the RSM, the central composite design technique was employed with three levels, namely: low, mid, and high values corresponding to −1, 0, and +1, respectively, for the input parameters. The input parameters were the concentration of SRg3 and RRg3, which ranged from 0–100 μM for SRg3 and 0–50 μM for RRg3. Table 1 represents the values corresponding to low, mid, and high bounds of concentrations for the Rg3 epimers. The design matrix used in the RSM analysis is shown in Supplementary Table S1. To optimise the combination of concentrations, the RSM model reduced the total experiments to 13 iterations, with loop formation being the "main measurable target parameter".

Table 1. Low, mid, and high values used for response surface methodology (RSM) model.

Parameter	Index	Concentration (μM)		
		Lowest value (−1)	Centre Value (0)	Highest Value (+1)
SRg3	A	0	50	100
RRg3	B	0	25	50

Following optimising the combination, two other combinations were used to confirm the validity of the RSM model. These two combinations (C1 and C2) are as follows, which were tested along with the optimised combination (C3). Combination 1 (C1): SRg3 (12.5 μM) + RRg3 (6.25 μM). Combination 2 (C2): SRg3 (25 μM) + RRg3 (12.5 μM).

2.3. Proliferation Assay

A crystal violet assay was performed as previously described [26]. Briefly, cells were seeded at 800 cells per well of a 96-well plate and were cultured overnight. Single or combination concentrations of Rg3 epimers were added to the wells, and the absorbance was read at 595 nm at 3 time points, on days 0, 1, and 3, in order to assess the effect of the Rg3 epimers on the proliferation of the endothelial cell lines. The experiment included six replicates and the data are shown as mean ± standard deviation (SD).

2.4. Flow Cytometric Analysis of Cell Death

The cells were seeded at 5×10^4 cells per well on six-well plates overnight and were then exposed to Rg3 combinations for three days. Then, the samples were collected and stained using the Annexin-V-FLUOS staining kit (Roche Diagnostics, Mannheim, Germany), as previously described [10]. The samples were analysed in the BD FACSCanto II (BD Biosciences, San Jose, CA, USA) and FlowJo software, v 10.4 (FlowJo, LLC, Ashland, OR, USA). The experiment was performed in triplicate and the data are shown as mean ± SD.

2.5. Flow Cytometric Analysis of Cell Cycles

The cells were seeded at 5×10^4 cells per well on six-well plates, cultured overnight, and then exposed to C3 for 3 days. The cells were collected, fixed, stained, and analysed using BD FACSCanto II and FlowJo software, v10.4, as previously described [10]. The experiment was performed in triplicate and the data are shown as mean ± SD.

2.6. Migration Assay

A migration assay was performed based on the previously described method [27]. Briefly, HUVECs, 2H-11, and 3B-11 cells, either not pretreated or pretreated for 3 days with Rg3 epimers, were seeded in 96-well plates at 3.5×10^4, 1.2×10^4, and 4×10^4 cells

per well, respectively, and were incubated overnight. A circular scratch was made in the cell monolayer. The area of the circular wound was measured based on a time of 0 and 10 h (murine endothelial cells), or 16 h (HUVEC), using ImageJ software (version 1.53a, National Health of Institute, Bethesda, MD, USA). The experiment included six replicates per treatment and the data are shown as mean ± SD.

2.7. Loop Formation Assay

A loop formation assay was optimised based on the cell proliferation index, viability, and cell number, and was performed as previously described [28]. Endothelial cells were seeded at 1.5×10^4 cells per well of a µ-plate (Ibidi, Martinsried, Germany) coated with Matrigel® (Corning) according to the manufacturer's protocol. The number of loops formed was counted at 16 h for HUVEC and 4 h for 2H-11 and 3B-11. The results are presented relative to the vehicle control. The experiment was performed in triplicate and the data are shown as mean ± SD.

2.8. Molecular Docking

For the molecular docking of Rg3 on the VEGF receptors, the SMILES structures of Rg3, sorafenib, and lenvatinib were obtained from PubChem. The crystal structure of VEGFR2 (2XIR and 3V2A) and VEGFR1 (5EX3) were from the protein data bank of NCBI (RCSB PDB). The UCSF Chimera program (version 1.15-mac64) and Autodock Vina algorithm (version 1-1-1-mac-catalina-64bit) were used to build the 3D structure of Rg3 and perform the molecular docking. The prediction of the Gibbs free energy of the protein-ligand binding was based on the flexible ligand docking simulations run within the docking grids on the interaction site of each protein, as previously described [10].

2.9. VEGFR2 Specific Interaction

To study the interaction between Rg3 epimers and VEGFR2, a VEGF bioassay kit (Promega, Madison, WI, USA) was used. It is a bioluminescent assay using KDR/NFAT-RE HEK293 cells. Upon activation of VEGFR2, intracellular signals triggered NFAT-RE-mediated luminescence. The experiment was performed according to the manufacturer's protocol. Briefly, the cells were seeded in white, flat-bottom 96-well assay plates (Delta Surface ™, Thermo Scientific, Roskilde, Denmark). Serial dilutions of SRg3 and RRg3 at final maximum concentrations of 100 and 50 µM were used alone or in combination with VEGF-A (recombinant VEGF, Promega, Madison, WI, USA) at a constant final concentration of 35 ng/mL (80% effective concentration). Bevacizumab (Avastin®, a maximum final concentration of 6 µg/mL) and VEGF-A (a maximum final concentration of 0.1 µg/mL) were used as the controls. The cells were incubated with the drugs for 6 h before a 10 min incubation with the Bio-Glo™ Reagent. Bioluminescence was measured using a FLUOstar Optima microplate reader (BMG LABTECH, Offenburg, Germany). The relative luminescence units (RLU) in each well were subtracted from the background. The experiment was performed in duplicate. GraphPad Prism (version 9.0.0 for Mac, GraphPad Software, San Diego, CA, USA, www.graphpad.com (accessed on 11 March 2021)) was used for plotting the dose–response curves (non-linear regression using log(inhibitor) vs. normalised response) and calculating the half inhibitory concentration (IC_{50}).

2.10. Quantitative PCR for the Expression of AQP1

The cells were seeded at 0.5×10^5 cells per well on six-well plates and were incubated overnight. Then, the cells were treated with Rg3 for 3 days at a normoxic (21% O_2) or hypoxic (0.1% O_2) condition. PureLink RNA mini kit (Life Technologies) was used to extract RNA and 20 ng RNA was used for reverse transcription using iScript cDNA Synthesis Kit (Bio-Rad Laboratories, Hercules, CA, USA). The duplex TaqMan Gene Expression Assays for aquaporin-1 (AQP1; Hs01028916_m1; Life Technologies) and the reference gene CCSER2 (HS00982799_mH, Life Technologies) was used in the study. Three biological repli-

cates were used. Reactions were performed in triplicate and were analysed as previously described [10].

2.11. Enzyme-Linked Immunosorbent Assay (ELISA) for the Expression of VEGF-A

HUVEC and MDA-MB-231 cells were seeded on six-well plates at 1×10^5 cells per well on a 96-well plate. After overnight culture, the cells were exposed to C3 for three days. The expression of VEGF in these cells was compared in normoxic and hypoxic conditions. Following treatment, the supernatants were collected and centrifuged to pellet any debris. The cells were then lysed with a RIPA Lysis and Extraction Buffer (Pierce Biotechnology, Rockford, IL, USA) and the total protein was measured using Bio-Rad protein assay (Bio-Rad Laboratories). VEGF production was measured using the human VEGF-A ELISA Kit (RayBiotech, Norcross, GA, USA). The experiment was performed in duplicate, and the results are shown as mean ± SD.

2.12. Western Blotting for the Expression of Proteins Involved in Migration and Invasion

The total cell lysates were prepared and quantified as described above. Western blot was performed as previously described [28]. The anti-aquaporin-1 antibody [EPR20325] (ab219055, Abcam, Cambridge, UK, 1:1000) and goat anti-rabbit IgG H&L (ab6721, Abcam, 1:3000) were used as the primary and secondary antibodies, respectively. The experiments were repeated three times and the results are shown as mean ± SD.

2.13. AKT Pathway Phosphorylation Array

To assess the effect of Rg3 on the signaling of AKT, a Human/Mouse AKT Pathway Phosphorylation Array C1 (RayBiotech) was used. The HUVEC cells were pretreated with Rg3 or a vehicle (DMSO) for three days at normoxic and hypoxic conditions, and then the protein was collected using lysis buffer, protein inhibitor, and phosphatase inhibitor, as per the manufacturer's protocol. The protein concentration was determined using Bio-Rad Protein Assay Dye Reagent Concentrate (Bio-Rad Laboratories, Hercules, CA, USA). The density of each dot was measured using Image Lab™ Software (version 6.1). The results are shown as the mean ± SD of the two replicates.

2.14. Statistical Analysis

The results were analysed using parametric one-way or two-way analysis of variance using GraphPad Prism (version 9.0.0 for mac, GraphPad Software, San Diego, CA, USA, www.graphpad.com). The results are presented as mean ± SD for two to eight replicates, with $p < 0.05$.

3. Results

3.1. Optimisation of Concentration Combination of SRg3 and RRg3

The results of the response surface methodology modelling are depicted in Figure 1. Parameters A (SRg3), B (RRg3), and the combination of both (AB), all have significant effects (Figure 1a). Notably, AA is defined as a high concentration of SRg3, which is included as a reference. For further analysis, the Pareto chart analysis for the loop formation data (Figure 1b) reflects the effectiveness of each parameter and shows the critical parameters that needed to be investigated in this study. This chart shows that the concentration of SRg3 (A), RRg3 (B), and the combination of both drugs (AB) are key parameters playing a major role in the anti-angiogenic effects. The highest effect is sourced from SRg3, followed by the combination of both drugs and RRg3. Accordingly, the key parameter requiring optimisation is the combination of both drugs (AB), which shows a plausible efficacy and reduces the concentration needed of each if used singly. Both the Pareto analysis and standardised effect plots showed that the combination parameter is a key factor determining the efficacy of loop formation. By optimising the concentrations, the optimum region for a concentration of both drugs to give the minimum loop formation was identified, and is shown in a contour plot (Figure 1c) and surface plot (Figure 1d).

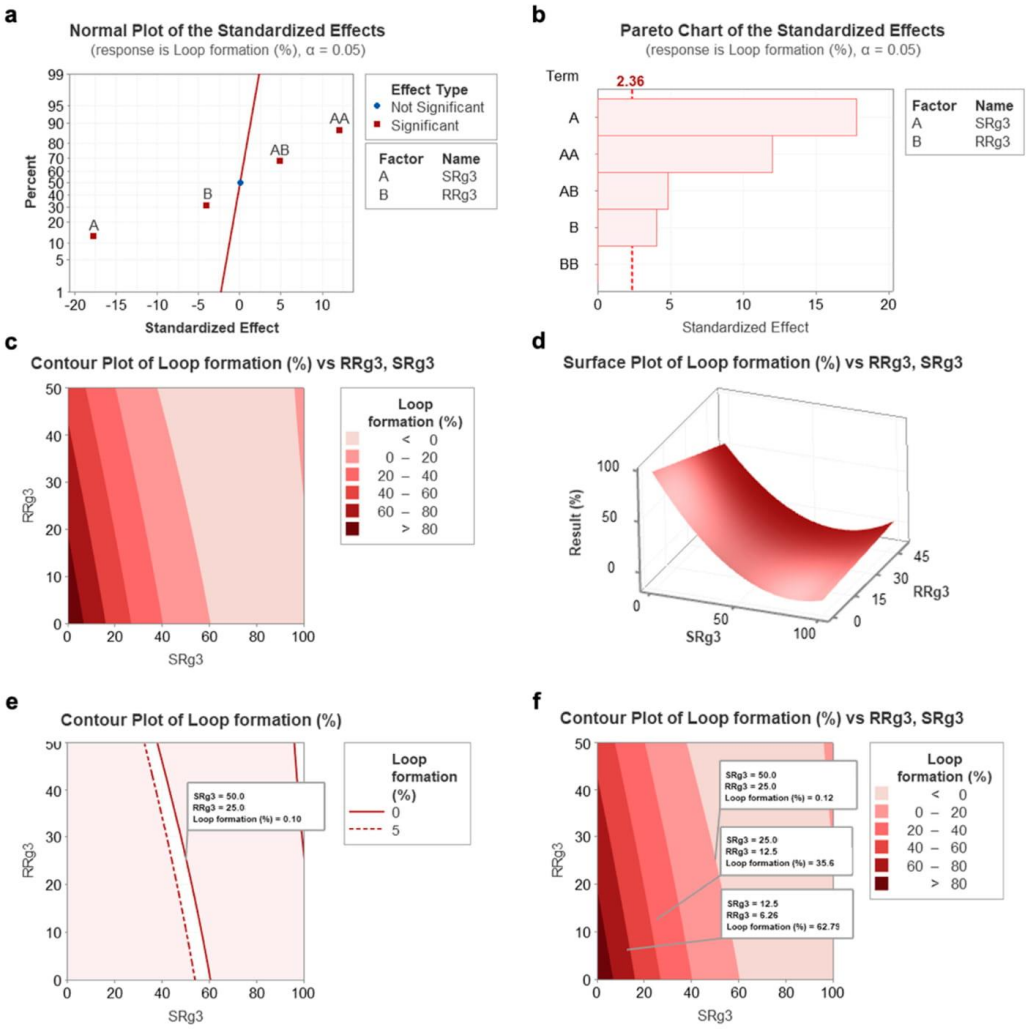

Figure 1. The calculated results of the response surface methodology developed using the central composite design technique for the optimisation of SRg3 and RRg3 drugs. (**a**) Standardised effect chart showing the critical parameters that need to be investigated, (**b**) Pareto chart analysis for loop formation data that reflects the effectiveness of each parameter, (**c**) contour plot, (**d**) surface plot for the percentage of loop formation following a combination of SRg3 or RRg3, (**e**) contour plot highlighting the area with the best efficacy for the combination, and (**f**) contour plot showing the predicted responses of two other combination treatments. A and B stand for SRg3 and RRg3, respectively, and AB represents the combination of SRg3 and RRg3. AA and BB show a mathematical expression of high concentrations of SRg3 and RRg3, respectively.

Notably, AA is defined as a high concentration of SRg3, which is included as a reference. For further analysis, the Pareto chart analysis for the loop formation data (Figure 1b) reflects the effectiveness of each parameter and shows the critical parameters that need to be investigated in this study. This chart shows that the concentration of SRg3 (A), RRg3 (B), and the combination of both drugs (AB) are key parameters playing a

major role in the anti-angiogenic effects. The highest effect is sourced from SRg3, followed by the combination of both drugs and then RRg3. Accordingly, the key parameter requiring optimisation is the combination of both drugs (AB), which shows a plausible efficacy and reduces the concentration needed of each if used singly. Both the Pareto analysis and standardised effect plots showed that the combination parameter is a key factor determining the efficacy of loop formation. By optimising the concentrations, the optimum region for a concentration of both drugs to give the minimum loop formation was identified and is shown in a contour plot (Figure 1c) and surface plot (Figure 1d).

Accordingly, different areas, shown with different colours (Figure 1c), show the percentage of loop formation in response to the combination of concentrations of SRg3 and RRg3. As represented in Figure 1e, by narrowing down the identified region of the result to 0–5% loop formation, the response of the combination of 50 μM SRg3 + 25 μM RRg3 (C3) was minimised to 0.1%, in which loop formation was almost completely suppressed. Notably, a concentration of 50 μM SRg3 is a concentration that blocks AQP1 water channels [10], which, in combination with 25 μM RRg3, gives a minimum loop formation. To validate the results of this RSM model, two other combinations (C1 and C2) were considered and tested for loop formation. Figure 2a shows the results of the validation of the RSM model on HUVEC cells. As shown in Figure 1f, C1 and C2 are predicted to provide responses of 60–80% and 20–40% loop formation, respectively. In Figure 2a it is shown that C1 and C2 give mean responses of 74% and 22%, which is within the predicted regions in Figure 1f. Therefore, the identified concentration of C3 was used to conduct the rest of the experiments.

3.2. Effect of Rg3 on Loop Formation and Migration of Endothelial Cells

To show the effects of Rg3 epimers alone and in combination, loop formation and migration assays were performed at two-time points: on non-pretreated cells and three-day pretreated cells (Figure 2). In the non-pretreated state, HUVECs were the most sensitive of the three cell types to inhibitory effects of single and combination of Rg3 epimers, with C3 being the most effective combination to completely inhibit loop formation (Figure 2a–c) and cell migration (Figure 2d–f). In these cells, in this state, a dose–response relationship was observed for a single or combination of Rg3 epimers. The loop formation with RRg3 at 25 μM and 50 μM ($p = 0.0001$) was 76% and 50%, respectively. Loop formation with 50 μM SRg3 was inhibited by 74% ($p < 0.0001$) and was completely inhibited with 100 μM SRg3 ($p < 0.0001$).

With combinations of C1 and C2, loop formation was reduced to 74% ($p = 0.0348$) and 21% ($p < 0.0001$), while C3 completely inhibited loop formation ($p < 0.0001$). In this state, the murine 2H-11 and 3B-11 cell lines were less sensitive to the inhibitory effects of Rg3 and the treatment required more time to show an inhibitory action in these cell lines. 2H-11 was more sensitive to the effects of RRg3, and at 25 μM and 50 μM, loop formation was 63% and 45% ($p = 0.0023$), respectively (Figure 2b). However, only SRg3 inhibited loop formation in 3B-11. With 50 μM and 100 μM SRg3, 40% ($p = 0.0005$) and 21% ($p < 0.0001$) loop formation occurred, respectively (Figure 2c). Although the combinations did not significantly inhibit the loop formation of murine endothelial cell lines in the non-pretreated state, a dose–response pattern was observed with these treatments.

To study the time-dependency of the effects of Rg3, a three-day pretreatment was performed. Following this pretreatment of cells with Rg3, the inhibitory effects of treatment were exacerbated in all of the tested cells. In HUVEC, RRg3 at 25 and 50 μM inhibited loop formation by 35 and 70%, respectively ($p < 0.0001$), and RRg3 completely inhibited loop formation ($p < 0.0001$). With C1, only 35% loop formation occurred, and no loops formed with C2 and C3 ($p < 0.0001$). In the pretreated state, the effect of single and combination drugs increased in both murine cell lines. In 2H-11, 25 and 50 μM RRg3 decreased loop formation by an average of 59% ($p = 0.0004$) and 96% ($p < 0.0001$), respectively. SRg3 at 50 and 100 μM inhibited loop by 53% ($p < 0.0026$) and 83% ($p < 0.0001$), respectively. C1, C2 and C3, inhibited loop formation by 68%, 78% and 100% ($p < 0.0001$), respectively.

In pretreated 3B-11 cells, all single drugs inhibited loop formation by more than 90% ($p < 0.0001$), and C2 and C3 inhibited it by 73 and 100% ($p < 0.0001$), respectively. These results showed that Rg3 has a time- and dose-dependent effect on the inhibition of loop formation for endothelial cells.

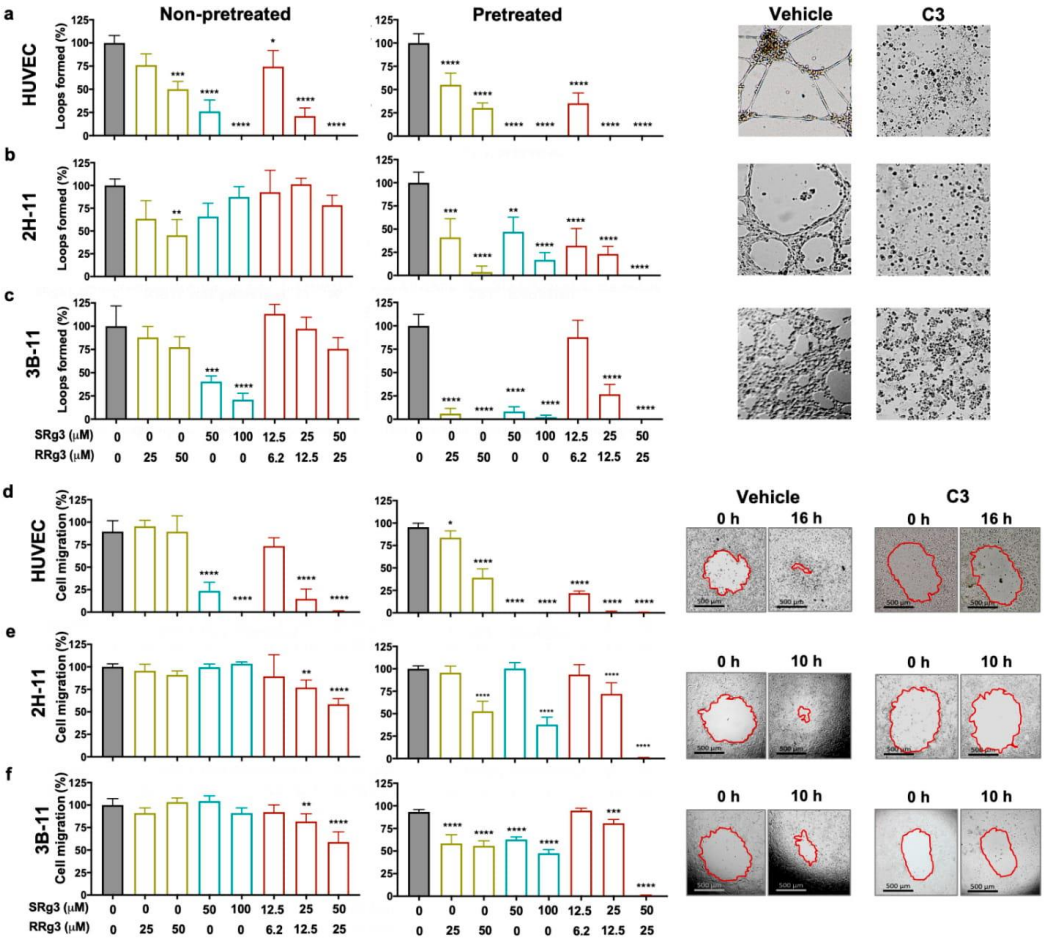

Figure 2. Effect of Rg3 epimers on loop formation (**a**–**c**) and migration (**d**–**f**) of human umbilical vein endothelial cell (HUVEC), 2H-11, and 3B-11 cells. Analysis of the loop formation and migration was performed at two timepoints; non-pretreated cells and 3-day pre-treated cells. Treatments are shown on the x axis, and (**a**–**c**) show the results of the loop formation in the HUVEC, 2H-11, and 3B-11 cell lines, respectively, at peak loop formation timepoints—16 h for HUVEC and 4 h for 2H-11 and 3B-11 cells. The experiments were done in triplicate and the results are presented as mean ± standard deviation (SD; $p < 0.05$). (**d**–**f**) show the results of cell migration in HUVEC, 2H-11 and 3B-11 cell lines, respectively. Results are presented as mean ± SD of 3 and 6 replicates for loop formation and migration assays, respectively ($p < 0.05$). The images represent the pre-treated cells. C3 represents a combination of 50 μM SRg3 + 25 μM RRg3. * $p < 0.05$, ** $p < 0.01$, *** $p < 0.001$ and **** $p < 0.0001$.

In the migration assay, the efficacy of single or a combination of Rg3 epimers was studied in non-pretreated or 3-day pretreated cells (Figure 2d–f). The trend of cells' response in this assay was similar to the results of loop formation assay. Similar to the inhibitory effects of Rg3 on loop formation, HUVEC was the most sensitive cell to the anti-migration effects of Rg3 (Figure 2d).

In non-pretreated HUVEC, only SRg3 inhibited cell migration by 66% and 80% for 50 and 100 μM, respectively ($p < 0.0001$; Figure 2d). C1, C2, and C3 inhibited loop formation dose-dependently by 16%, 75% ($p < 0.0001$), and 89% ($p < 0.0001$), respectively (Figure 2d). 2H-11 and 3B-11 were not sensitive to single epimers, but the C2 ($p < 0.001$) and C3 ($p<0.0001$) significantly inhibited cell migration. A three-day exposure of the cells with the drugs increased the effects of single drugs. In HUVEC, the inhibitory effects of RRg3 increased and both concentrations of SRg3 completely inhibited migration ($p < 0.0001$). In 2H-11, the inhibitory effects of higher concentrations of SRg3 and RRg3 increased, while in 3B-11, the effects of all single epimers were increased. In both cell lines, C3 almost completely inhibited cell migration (Figure 2e,f). This experiment also showed time- and dose-dependent inhibition of migration by Rg3 epimers and confirmed the results of Rg3 in the loop formation assay.

3.3. Anti-Proliferative Effects of Rg3 in Endothelial Cells

As shown in Figure 3a, HUVEC was the most sensitive cell type to the anti-proliferative effects of Rg3. At equimolar concentrations, RRg3 was a less potent inhibitor of cell proliferation in HUVEC, while SRg3, C2, and C3 almost completely inhibited cell proliferation ($p < 0.0001$), and C1 had no significant inhibitory action. 2H-11 and 3B-11 were more sensitive to the combination of SRg3 and RRg3 compared with single epimers. In these two cell lines, C3 was the most effective inhibitor of cell proliferation (Figure 3a).

The induction of cell death was studied by staining the cells with annexin V and propidium iodide (PI; Figure 3b). In HUVEC cells, C2 and C3 induced about 29% ($p = 0.0003$) and 92% ($p < 0.0001$), respectively, cell death after three days of treatment. The cell death induced by C3 was associated with G0/G1 arrest in HUVEC ($p < 0.0001$; Figure 3c). Further studies showed that C2 and C3 induced the activation of caspase 3/7 in HUVEC by 536% and 980%, respectively (Figure 3d), with subsequent increases in the number of PI-positive cells (Figure 3e), consistent with late apoptosis. Interestingly, single epimers of Rg3 did not induce caspase activation in HUVEC. This shows that SRg3 and RRg3 in C2 and C3 combinations play a synergistic role in the induction of apoptosis in this cell.

In contrast, in murine 2H-11 and 3B-11 endothelial cells, C2 and C3 did not induce significant cell death (Figure 3b), while the cells were arrested in S phase (Figure 3c). Induction of cell cycle arrest in the S-phase was by 42% ($p = 0.0006$) and 63% ($p = 0.0001$) in 2H-11 and 3B-11, respectively. Therefore, it seems that the major mechanism of the inhibition of proliferation in these two cell lines is via the induction of cell cycle arrest.

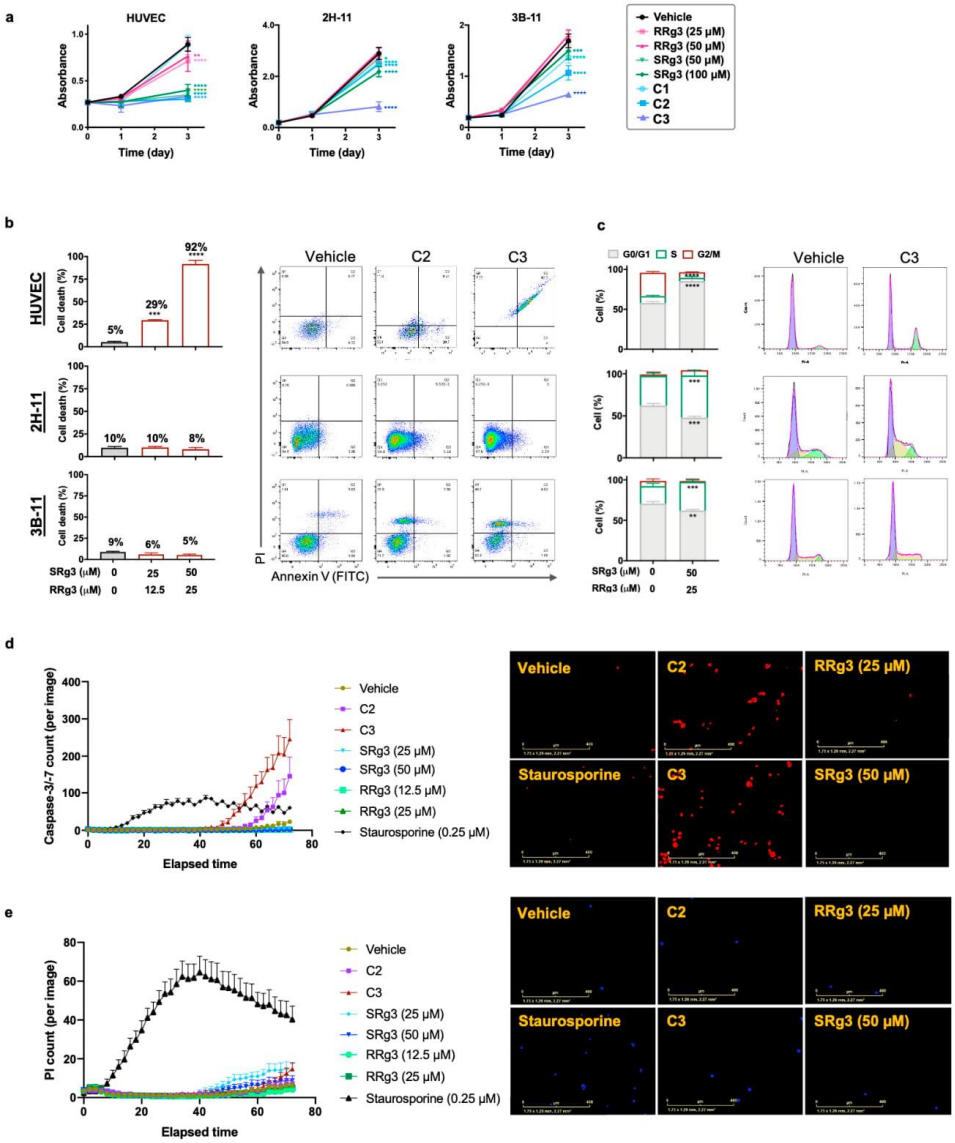

Figure 3. HUVEC, 2H-11, and 3B-11 cells were exposed to 0.8% dimethyl sulfoxide (DMSO) as a vehicle control or at concentrations of 25 and 50 μM RRg3; 50 and 100 μM SRg3; or three combinations of RRg3 + SRg3 at 6.2 + 12.5 (C1), 12.5 + 25 (C2), and 25 + 50 μM (C3). (**a**) The effect of single or combination Rg3 epimers on the proliferation of these cells in a three-day time frame. Each data point represents mean ± SD of six replicates. (**b**) The flow cytometric analysis of the induction of cell death and (**c**) cell cycle arrest in these cells by C2 and C3. Each data point represents mean ± SD of three replicates. (**d**) Activation of caspase 3/7, shown by red spots and (**e**) propidium iodide (PI) staining of cells shown by blue spots in HUVEC cells. Images are at 72 h and scale bars show 400 μm. Each data point represents mean ± SD of eight replicates. Statistical analyses were performed between the Rg3 and vehicle-treated cells ($p < 0.05$). * $p < 0.05$, ** $p < 0.01$, *** $p < 0.001$ and **** $p < 0.0001$.

3.4. The Effect of Rg3 on VEGF, VEGFR2, and Their Interaction

To further investigate the role of Rg3 epimers in angiogenesis, molecular docking was performed on two of the receptors VEGF—VEGFR1 and VEGFR2. As a comparable reference, molecular docking was also performed on two small-molecule TKIs—sorafenib and lenvatinib—which are known to interact with and inhibit VEGFR activity [29]. Human VEGFR2 includes an extracellular site with seven immunoglobulin (Ig)-like domains, and an intracellular tyrosine kinase domain, which are connected with a short transmembrane and a juxta-membrane domain (Figure 4a) [30]. The results of the molecular docking between Rg3 epimers and VEGFR1 and VEGFR2 predicted good binding scores between TKIs and the ATP-binding pocket of these receptors (Table 2). Molecular docking of SRg3 and RRg3 at this site of VEGFR2 predicted that both epimers have a strong binding with this site of the receptor, with scores of −9.0 and −8.9 kJ/mol, respectively. These scores are comparable with the binding scores of sorafenib (−9.9 kJ/mol) and lenvatinib (−9.1 kJ/mol; Table 2).

Table 2. Binding score (kJ/mol) of Rg3 epimers and growth factor receptors and the number of hydrogen binding (H-bond) predicted by Chimera program and Autodock vina algorithm.

Molecule	Binding Score (kJ/mol) (Number of H-Bonds)		
	VEGFR1	VEGFR2 [1]	VEGFR2 [2]
SRg3	4.8 (0)	−9.0 (8)	−7.2 (3)
RRg3	−7.4 (6)	−8.9 (5)	−7.0 (5)
Sorafenib	−4.9 (0)	−9.9 (0)	–
Lenvatinib	−8.9 (0)	−9.1 (0)	–

[1] Interaction with ATP-binding pocket; [2] interaction with vascular endothelial growth factor (VEGF)-binding site.

As shown in Figure 4a and summarised in Table 2, 8 and 5 H-bonds were predicted between VEGFR2 and the two epimers, SRg3 and RRg3, respectively. In both cases, Asn108, Asp180, Arg27, and Arg179 were suggested as potential H-bond residues. Although the ATP-binding cassette of VEGFR2 plays an important role in the activation of the receptor, the VEGF binding site in the extracellular side of the receptor is a key interaction site between VEGF and VEGFR2 to facilitate the intercellular signal transduction. Out of the 7 Ig-like domains, the first three domains, especially 2 and 3, mediate VEGF binding [31]. We performed a molecular docking on domains 2 and 3 of VEGFR2 and each of the Rg3 epimers. The results of this in silico study predicted binding scores of −7.2 and −7.0 kJ/mol for SRg3 and RRg3, respectively. These scores, together with the number of H-bond interactions with the receptor, were 3 and 5 H-bonds for SRg3 and RRg3, respectively, indicating strong binding. For both epimers, glycine, asparagine, and valine were the predicted amino acid residues to make H-bonds with each epimer at different positions of the domains, and provide affinity positions for H-bonds (Figure 4a).

To investigate the interaction between Rg3 and VEGFR2, in vitro, a VEGF bioassay was conducted. Figure 4b,c shows two dose–response curves of VEGF in a stimulatory state and a bevacizumab inhibitory state, respectively. VEGF, as the activator of the receptor, shows a stimulatory dose–response curve (Figure 4b) with a half effective concentration (EC_{50}) of 0.001 ng/mL (Table 3). The anti-VEGF monoclonal antibody, bevacizumab, antagonised the action of VEGF (Figure 4c) with the IC_{50} of 0.11 µg/mL (Table 3).

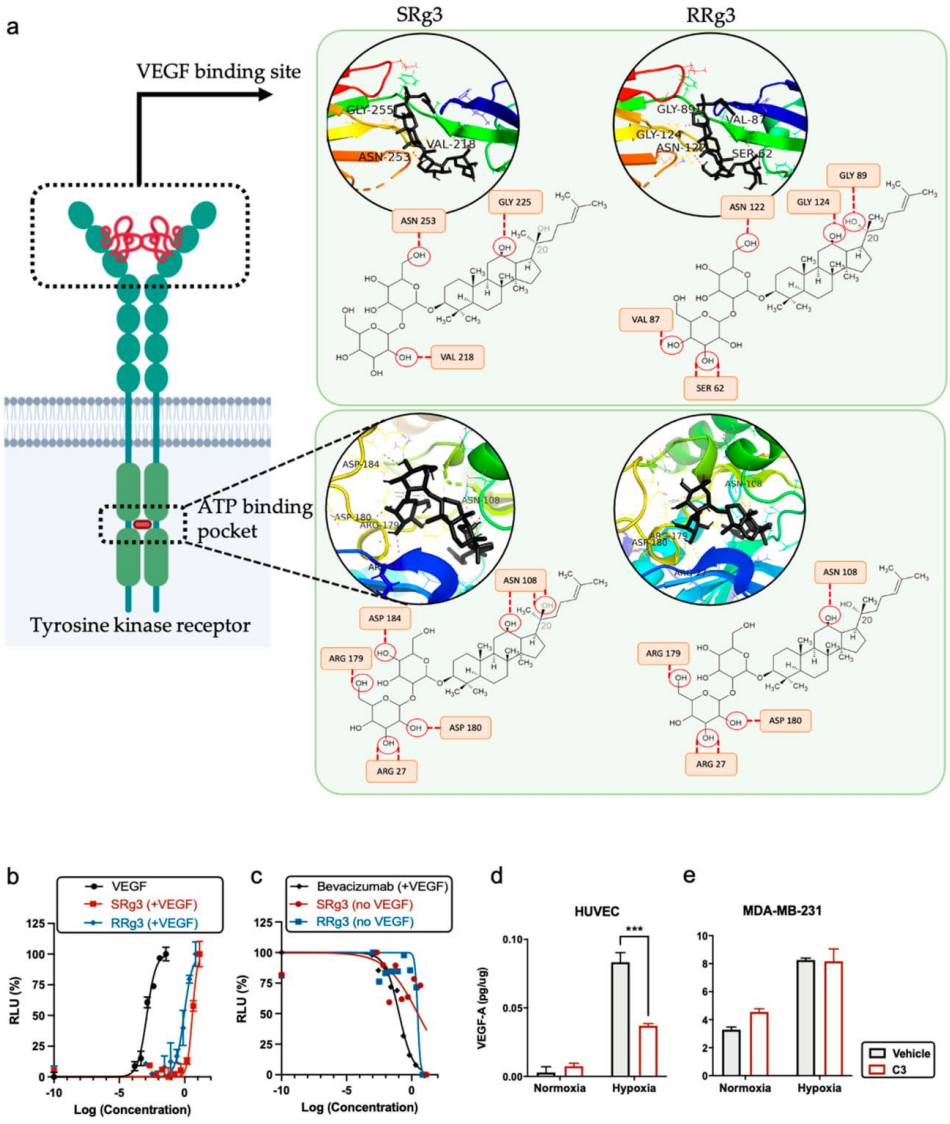

Figure 4. (**a**) A demonstration of the interaction between SRg3 and RRg3 (in black) with VEGFR2 at VEGF binding site or ATP-binding pocket. The interaction sites were predicted using molecular docking performed by AutoDock Vina algorithm. The predicted H-bonds between Rg3 and amino acid residues are shown with dashed lines. Dose–response curve of (**b**) VEGF, SRg3, and RRg3 in the presence of 35 ng/mL VEGF (stimulatory dose–response state) and (**c**) bevacizumab in the presence of 35 ng/mL VEGF, SRg3, and RRg3 alone (inhibitory dose–response state). Expression of VEGF in the presence of Rg3 in normoxic or hypoxic conditions in (**d**) HUVEC and (**e**) MDA-MB-231. The experiment was performed in duplicate, and the results are shown as mean ± SD, with $p < 0.05$. RLU—relative light units. *** $p < 0.001$.

To test the activity of Rg3 on VEGFR2, the bioassay was performed in two states: (i) in the presence of high levels (EC_{80}) of VEGF, which is a condition that encourages angiogenesis and highly activates VEGFR2, and (ii) in the absence of VEGF to test whether the molecules alone have any stimulatory or inhibitory effect on the receptor. In the presence of an EC_{80} value of VEGF (35 ng/mL), Rg3 epimers shifted the VEGF dose–response curve to the right. This means that Rg3 epimers reduced the efficacy of VEGF for the activation of VEGFR2. The EC_{50} values of SRg3 and RRg3 in this state were about 28 and 6.5 µM (Table 3). This means that RRg3 is almost four-fold more potent than SRg3 at reducing the efficacy of VEGF. SRg3, although less potent, more effectively shifted the VEGF dose–response curve to the right (Figure 4b).

Table 3. Calculated IC_{50} and EC_{50} values for VEGF (ng/mL), bevacizumab (µg/mL), SRg3 (µM), and RRg3 (µM) alone or in combination with 35 ng/mL VEGF, in interaction with VEGFR2. The experiment was performed in duplicate using the VEGF bioassay system (Promega) and was analysed using Prism software.

Compound	IC_{50}	EC_{50}	95% CI [1]	R Squared
VEGF	–	0.001	0.001–0.002	0.9781
Bevacizumab	0.11	–	0.08–0.15	0.9644
SRg3	21.23	–	3.25–8008	0.3391
RRg3	20.67	–	15.06–30.82	0.6963
SRg3 + VEGF	–	27.95	23.79–32.44	0.9670
RRg3 + VEGF	–	6.52	4.84–8.66	0.9411

[1] CI—confidence interval

To test whether the Rg3 epimers had any stimulatory effect on VEGFR2, the dose response curve was studied in the absence of VEGF. In this state, Rg3 epimers showed an almost steady response, except for the highest concentration (Figure 4c), and the regression analysis approach was not a plausible technique to fit a non-linear sigmoidal dose–response function, which resulted in poor R squared values (Table 3). However, the overall trend of their effect was inhibitory, as at the highest concentrations used (100 and 50 µM for SRg3 and RRg3, respectively), the response was minimised (Figure 4c). The decreased bioluminescence detected at the highest tested concentrations could be due to the cytotoxicity of the molecules, rather than the inhibitory effect of the drugs on the receptor.

Given the observed effects of Rg3 in this system and the results obtained from the molecular docking, it seems probable that Rg3 is an allosteric modulator of VEGFR2. In the absence of VEGF, as the primary ligand, SRg3 and RRg3 had a minimum activity on the receptor, while in the presence of VEGF, Rg3 epimers decreased the efficacy of VEGF-VEGFR2 interactions potentially by changing the conformation of the receptor. Furthermore, the efficacy of C3 on the VEGF expression in normoxic and hypoxic conditions in HUVEC and MDA-MB-231 cells was studied (Figure 4d,e). C3 did not have any significant effect on VEGF expression in MDA-MB-231 (Figure 5e), but in hypoxic HUVEC cells, when the expression of VEGF was significantly increased in vehicle-treated cells, Rg3 decreased this expression ($p = 0.0008$; Figure 4d).

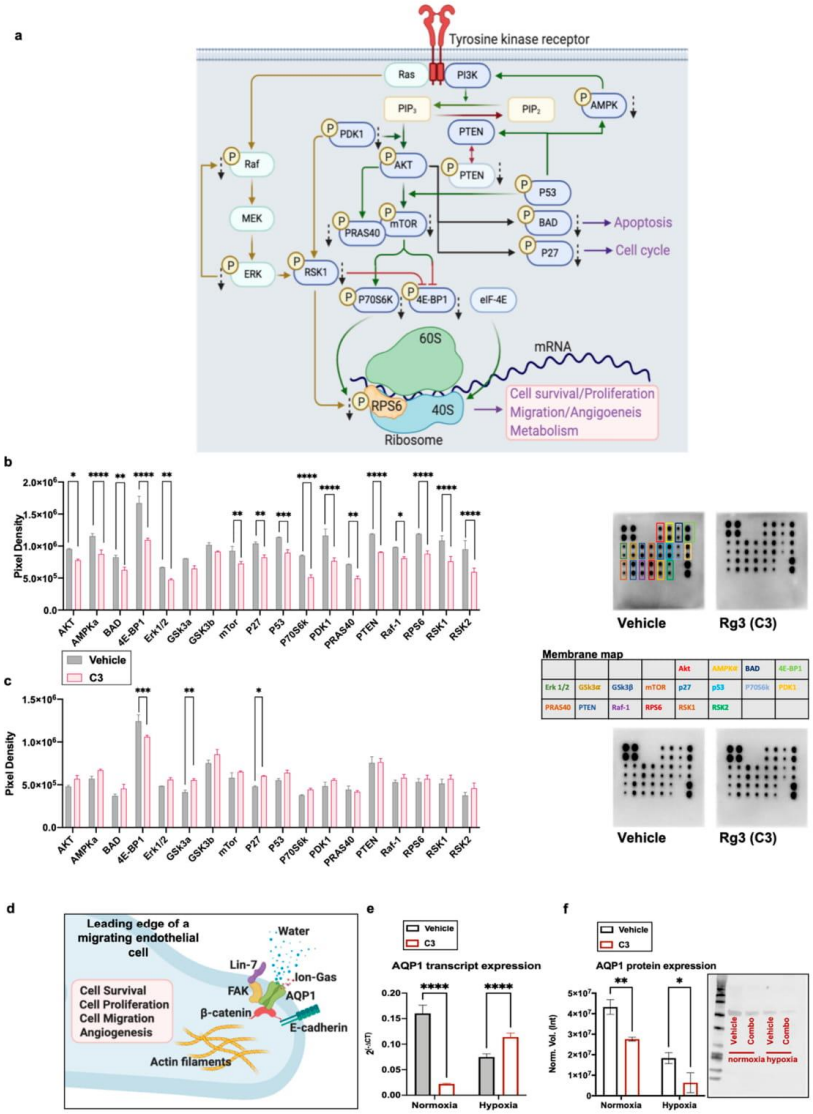

Figure 5. (**a**) A schematic diagram of the signaling of the downstream activation of a receptor tyrosine kinase, leading to cell survival, proliferation, migration, angiogenesis, and metabolism (created with BioRender.com (accessed on 11 March 2021)). The effects of C3 (50 μM SRg3 + 25 μM RRg3) on the phosphorylation of signaling proteins in PI3K/AKT signaling in HUVEC cells grown in (**b**) normoxia and (**c**) hypoxia (1% O_2) conditions. The cells were exposed with C3 for three days. The data show the mean ± SD of two replicates with $p < 0.05$. (**d**) A schematic diagram of the role of AQP1 localised in the leading edge of an endothelial cell facilitating cell migration (reviewed in [9]) (created with BioRender.com). The cells were exposed with C3 for thee days in normoxic or hypoxic (1% O_2) conditions. Expression levels of (**e**) AQP1 transcripts measured with QT-PCR or (**f**) proteins detected using the Western blotting technique in normoxic and hypoxic conditions are shown. The data represent the mean ± SD of three replicates with $p < 0.05$. * $p < 0.05$, ** $p < 0.01$, *** $p < 0.001$ and **** $p < 0.0001$.

3.5. Effect of Rg3 on the AKT Signalling Pathway and AQP1

Signaling of PI3K/AKT and its interaction with the Raf/MEK/ERK signal transduction pathway (Figure 5a) regulates several proteins controlling cell survival, proliferation, migration, and metabolism. To test whether C3 treatment has any effects on the signaling of AKT, a protein array was performed. C3 affected the phosphorylation of proteins downstream of the activation of AKT in both normoxia and hypoxia, although the effects in normoxia were more extensive (Figure 5). In normoxic conditions, Rg3 combined with C3 affected the phosphorylation of several proteins important in the signaling of AKT. The phosphorylation of AKT was decreased ($p = 0.017$) and regulators for the activation of AKT, including AMP-activated protein kinase (AMPK), phosphatase and tensin homolog (PTEN), and phosphoinositide-dependent kinase-1 (PDK1), were decreased ($p < 0.0001$) (Figure 5b). C3 also decreased the phosphorylation of the BCL2 associated agonist of cell death (BAD; $p = 0.0048$; Figure 5b), which plays important roles in AKT-mediated cell survival. C3 decreased the phosphorylation of cyclin-dependent kinase inhibitor 1B ($p27^{kip1}$; $p = 0.0015$; Figure 5b), hence keeping it in its active form, which could cause $p27^{kip1}$-mediated G1 arrest. With C3, the activation of p53 also decreased ($p = 0.0003$), which could also affect the activation of mTOR.

This experiment showed that C3 decreased the phosphorylation of mTOR ($p = 0.0045$), PRAS40 ($p = 0.0012$), P70S6K ($p < 0.0001$), 4E-BP1 ($p < 0.0001$), and RPS6 ($p < 0.0001$). These proteins play roles in the translation function of migrating cells. Furthermore, C3 decreased the phosphorylation of Raf ($p = 0.0187$), ERK 1/2 ($p = 0.0066$), RSK1, and RSK2 ($p < 0.0001$). In hypoxic conditions, the C3 affected proteins included 4E-BP1 ($p = 0.0003$), glycogen synthase kinase-3a (GSK3a; $p = 0.0086$), and $p27^{kip1}$ ($p = 0.0323$).

AQP1 in combination with other proteins at the leading edge of a migrating cell facilitates cell migration (Figure 5d). We showed that in normoxic conditions, the levels of AQP1 transcript ($p < 0.0001$) and protein ($p = 0.0268$) were significantly decreased. In hypoxic conditions, although the transcript levels were increased, the protein levels were decreased ($p = 0.0195$; Figure 5e,f). In addition, in a mouse endothelial cell line, 3B-11, a significantly decreased expression of the AQP1 transcript was observed (Supplementary Figure S1). However, we did not detect any significant changes in the activation of focal adhesion kinase (FAK), as another player in the AQP1-facilitated migration in HUVECs (Supplementary Figure S2). Therefore, it seems that AQP1 is a more important protein in the C3-induced inhibition of migration in HUVECs. Furthermore, preliminary testing showed that in C2 treated HUVEC, the expression of the AQP1 transcript and protein and the activation of AKT were reduced (Supplementary Figure S3).

4. Discussion

A few studies have investigated the mechanisms of action of Rg3 as an anti-angiogenic agent. Keung et al. (2016) showed that RRg3 exerted its anti-angiogenic effects via an increased expression of hsa-miR-520h, which targeted ephrin type-B receptor 2 (EphB2) and EphB4 as a mediator of cancer migration and angiogenesis [32]. In addition, it was shown that an unspecified epimer of Rg3 (64 μM) decreased the protein and transcript expression of VEGF, basic fibroblast growth factor (b-FGF), matrix metalloproteinase-2 (MMP-2), and MMP-9 [33]. Because of the stereoselective activity of Rg3 epimers, for the first time, in this study, C3 was introduced as an optimised combination of SRg3 and RRg3 and a novel anti-angiogenic agent. This combination showed time- and dose-dependent anti-angiogenic properties in vitro. HUVECs were more sensitive to these effects of Rg3 than to the murine endothelial cell lines.

To further investigate the mechanisms involved in the anti-angiogenic properties of Rg3 and more specifically C3, (i) the effects of Rg3 on the VEGF–VEGFR2 interaction and (ii) the anti-angiogenic mechanisms Rg3 combination (C3) were studied. Molecular docking predicted good biding scores and VEGFR2, comparable to the binding of known TKIs. We showed that Rg3 has no stimulatory action on VEGFR2. The antiangiogenic effects observed by Rg3 are not comparable with a drug such as bevacizumab. Bevacizumab is a

monoclonal antibody against VEGF, while Rg3 has several mechanisms, one of which is via the interaction with the activation of VEGFR2. For the first time, we showed that the interaction between Rg3 and VEGFR2 decreased the efficacy of VEGF on the system, working as an allosteric modulator. Allosteric modulators are of special interest in pharmacology. Since the introduction and successful treatment profile of benzodiazepines as allosteric ligands of γ-aminobutyric acid-A ($GABA_A$) receptors, versus the toxic direct-acting agonists of this receptor, much more attention has been paid to finding and registering allosteric drugs for various diseases (reviewed in [34]). Allosteric modulators offer several advantages over orthosteric ligands, such as subtype selectivity within receptor families and less adverse side effects [34,35]. Of special interest are tyrosine kinases, which play roles in several human diseases such as cancer. The ATP-binding pocket of kinases is a highly conserved part, and this results in a low selectivity and, consequently, off-target and side effects for the inhibitors designed for this target. Other types of inhibitors either bind at the ATP site extending into an adjacent allosteric pocket, specifically bind to the allosteric pockets near the ATP pocket, or bind to allosteric sites more remote from the ATP pocket [34]. The fact that Rg3 has been administered to humans without any reported serious side effects (reviewed in [8,9]) could be evidence for the safety of Rg3 allosterism. This research provided evidence of the anti-VEGFR2 action of Rg3 epimers as one of the anti-angiogenic mechanisms of these molecules. To confirm the interaction site of Rg3 with VEGFR2, further experiments are required in future research.

This research also provided evidence of the effectiveness of C3 in hypoxic conditions. This is especially important because of the importance of hypoxia in driving tumour invasiveness [36]. Hypoxia is a common feature of rapidly growing tumours, which affects tumour metabolism, metastasis, and resistance to chemotherapy [37], and is linked to a poor prognosis for several tumours (reviewed in [38]). Hypoxia leads to VEGF expression to encourage angiogenesis in the tumour. Increased VEGF expression promotes endothelial cell proliferation and migration, inhibits apoptosis in these cells, and facilitates the degradation of the extracellular matrix and endothelial cell migration and invasion [39]. Some solid tumours such as breast cancers overexpress VEGF and its receptors. This led to the development of anti-angiogenic drugs for these patients [40]. Our group is interested in developing novel treatments for breast cancer, in which VEGF expression is an independent prognostic factor and a possible target of treatment [41]. Both endothelial and breast cancer cells have an autocrine VEGF signaling pathway that supports angiogenesis and cancer progression [42]. Hence, we measured VEGF expression in both HUVEC and MDA-MB-231, in hypoxic and normoxic conditions, and showed that C3 significantly decreased VEGF expression only in hypoxic HUVEC cells and not in MDA-MB-231. Whether C3 has efficacy on other breast cancer cell lines should be further assessed. However, the responding cells, endothelial cells, play key roles in angiogenesis.

Downstream of the activation of VEGFR2, several signaling pathways are activated, including PI3K/AKT/mTOR signaling, the activation of which is one of the hallmark signaling pathways in cancer and angiogenesis [43,44]. Therefore, inhibitors of mTOR signaling have gained plenty of attention in cancer treatment. Currently, 70 trials of the inhibitors of mTOR signaling are recruiting in several tumour types, such as breast, lung, colorectal, and hematological tumours (https://clinicaltrials.gov/ (accessed on 11 March 2021)). In addition to several cellular functions, the activation of mTOR also plays roles in VEGF production and angiogenesis [45]. Inhibitors of this pathway, inhibiting either PI3K/mTOR or mTOR alone, show anti-angiogenic properties (reviewed in [46]). For example, rapamycin, an inhibitor of mTORC1, also inhibits VEGF production and angiogenesis [47]. As reviewed before, in leukemic and ovarian cancer models, Rg3 affected PI3K/AKT signaling [8]. Therefore, we examined the effects of C3 on this signaling pathway in normoxic and hypoxic conditions. In the normoxic condition, except GSK3, all other tested proteins were affected with C3. The proteins that showed more than 30% decreased phosphorylation were those that were related to mTORC1 function, including PRAS40 (a component and substrate of mTORC1); P70S6K, which phosphorylates and activates

RSP6, a component of 40S ribosomal subunit; and 4E-BP1, which, upon phosphorylation, releases eIF-4E, as one of the key components of ribosomal translation initiation for regulators of mTOR function including PDK1 and RSKs. PRAS40, when dephosphorylated, inhibits mTOR signaling, consequently decreasing ribosomal transcription via affecting the activation of 4E-BP1 and P70S6k, both of which play roles in tumour angiogenesis [48,49].

Decreased phosphorylation of 4E-BP1 was also observed both in hypoxic and normoxic HUVEC cells exposed to C3, thus implicating 4E-BP1 as having an important role in C3 mediated anti-angiogenic effects. In particular, as mTORC1, via mechanisms involving 4E-BP1, drives VEGF signaling in hypoxic conditions [50], it could be considered that the decreased expression of VEGF observed in these cells was mediated through mTORC1/4E-BP1. The leading edge of migrating cells is where many fundamental biological and biochemical processes occur to facilitate cell migration, including 4E-BP1, PRAS40, mRNAs, and translation initiation factors [51,52]. Therefore, one major mechanism of C3 could be via the inhibition of the translational function of mTOR.

Additionally, hypoxia-induced-endothelial cell proliferation requires functional mTOR complexes [53]. C3, via the decreased phosphorylation of 4E-BP1, could decrease the functionality of mTORC1 and hence play a contributing role in the decreased proliferation of these cells. C3, in hypoxic conditions, caused minor increased levels of p-$p27^{Kip1}$, which is a negative regulator of G1 cell cycle progression. It has been shown that GSK3 stabilises the levels of $p27^{Kip1}$ and decreases cell proliferation [54] and hence, the observed minor increased levels of $p27^{Kip1}$ could be a consequence of the deactivation of GSK3.

GSK3 is a constitutively active kinase, an activator of AKT, mTORC1, and mTORC2, which is in feedback and crosstalk with PI3K/AKT/mTOR. Phosphorylation on SER-21 (GSK3a) and SER-9 (GSK3b) is initiated by the growth factor activation of AKT/mTOR and inhibits GSK3 function [55], and C3 increased this phosphorylation to decrease the activation of this signaling. This could further decrease the functionality of mTORC1 and mTORC2. This is especially important, as mTORC2 is an essential cellular energy production element, which promotes cancer progression via lipid formation and fueling the PI3K/AKT/mTOR pathway [56]. It also plays roles in driving angiogenesis multiple myeloma, where mTORC2 inhibitors restrict angiogenesis in this tumour model [57]. mTORC2 is one of the molecular targets that is in advanced stages of translational application, and whether C3 has any inhibitory action on mTORC2 needs to be further investigated.

Some AQPs such as AQP1, AQP4, and AQP5 localise at the leading edge of migrating cells [58]. AQP1, for example, polarises at the leading edge, a phenomenon that is associated with an increased turnover of cell membrane protrusions and enhanced cell migration (reviewed in [12]). AQP1 was recognised as a pro-angiogenic factor [59], which, independent of VEGF, was required for the hypoxia-induced tube forming capacity of human retinal vascular endothelial cells [60]. AQP1-deficient cells were shown to have impaired migration and tube formation [61]. We have also shown that blockers of AQP1 impair angiogenesis [27,28]. In addition, using the molecular docking and oocyte swelling assay, we showed that Rg3 blocked AQP1 [10]. Therefore, it could be concluded that the blockage of AQP1 could contribute to the immediate inhibition of the loop formation observed. After a three-day pretreatment with C2 and C3, the protein expression of AQP1 was decreased. FAK, another important contributor to endothelial cell migration via VEGFR2-signalling or complexing with AQP1 (reviewed in [13]), did not seem to be involved in the mechanism of action of C3, which further highlights the role of AQP1 in this process.

5. Conclusions

In conclusion, we showed that Rg3 had a time- and dose-dependent inhibition of the migration and invasion of endothelial cells. The optimised combination of SRg3 and RRg3 inhibited the proliferation, migration, and invasion of endothelial cells. SRg3 and RRg3 potentiated each other's action in activating caspase 3/7 and inducing apoptosis, which was the major anti-angiogenic mechanism. This action was measured after 3 days of exposure with the treatment. Besides the induction of apoptosis, other inhibitory mechanisms were

also involved that assisted with the anti-angiogenic action of Rg3. As our studies showed, these molecules were allosteric modulators of VEGFR2, and therefore potentially had far fewer off-target effects with less clinical side effects expected. A reduced expression of VEGF and AQP1, and decreased PI3K/AKT/mTOR signaling are suggested mechanisms of this drug. Further studies are needed to confirm the anti-angiogenic effects of C3 in vivo.

Supplementary Materials: The following are available online at https://www.mdpi.com/article/10.3390/cancers13092223/s1, Figure S1: Quantitative PCR for transcript expression of AQP1 in murine 3B-11 cell line following exposure with C3 for 3 days. Figure S2: Western blot analysis of activation of focal adhesion kinase (FAK) in HUVEC exposed to vehicle (V) or C3 (50 μM SRg3 + 25 μM RRg3), in normoxia or hypoxia conditions. Figure S3: HUVEC was exposed to vehicle (V) or C2 (25 μM SRg3 + 12.5 μM RRg3) for 3 days. Table S1: Design table developed for the RSM model.

Author Contributions: Conceptualization, M.N. and J.E.H.; methodology, M.N., E.S., H.M.P., K.Y. and Y.T.; software, M.N.; formal analysis, M.N., E.S. and K.Y.; investigation, M.N., E.S., J.E.H. and A.R.T.; resources, A.R.T., J.E.H. and T.J.P.; data curation, J.E.H. and A.R.T.; writing—original draft preparation, M.N.; writing—review and editing, E.S., H.M.P., Y.T., K.Y., A.R.T., T.J.P. and J.E.H.; visualization, M.N.; supervision, J.E.H. and A.R.T.; project administration, J.E.H.; funding acquisition, A.R.T., J.E.H. and T.J.P. All authors have read and agreed to the published version of the manuscript.

Funding: This research was funded by the Margaret Elcombe Hospital Research Foundation Research Grant.

Institutional Review Board Statement: Not applicable.

Informed Consent Statement: Not applicable.

Data Availability Statement: All of the data are available in the paper or as Supplementary Data.

Conflicts of Interest: The authors declare no conflict of interest.

References

1. Ollauri-Ibáñez, C.; Astigarraga, I. Use of antiangiogenic therapies in pediatric solid tumors. *Cancers* **2021**, *13*, 253. [CrossRef] [PubMed]
2. Maennling, A.E.; Tur, M.K.; Niebert, M.; Klockenbring, T.; Zeppernick, F.; Gattenlöhner, S.; Meinhold-Heerlein, I.; Hussain, A.F. Molecular targeting therapy against EGFR family in breast cancer: Progress and future potentials. *Cancers* **2019**, *11*, 1826. [CrossRef] [PubMed]
3. He, B.; Ganss, R. Modulation of the vascular-immune environment in metastatic cancer. *Cancers* **2021**, *13*, 810. [CrossRef] [PubMed]
4. Taugourdeau-Raymond, S.; Rouby, F.; Default, A.; Jean-Pastor, M.-J. Bevacizumab-induced serious side-effects: A review of the French pharmacovigilance database. *Eur. J. Clin. Pharmacol.* **2012**, *68*, 1103–1107. [CrossRef]
5. Hartmann, J.T.; Haap, M.; Kopp, H.-G.; Lipp, H.-P. Tyrosine kinase inhibitors-a review on pharmacology, metabolism and side effects. *Curr. Drug Metab.* **2009**, *10*, 470–481. [CrossRef]
6. Haibe, Y.; Kreidieh, M.; El Hajj, H.; Khalifeh, I.; Mukherji, D.; Temraz, S.; Shamseddine, A. Resistance mechanisms to anti-angiogenic therapies in cancer. *Front. Oncol.* **2020**, *10*. [CrossRef]
7. Yun, U.-J.; Lee, I.H.; Lee, J.-S.; Shim, J.; Kim, Y.-N. Ginsenoside Rp1, A ginsenoside derivative, augments anti-cancer effects of Actinomycin D via downregulation of an AKT-SIRT1 pathway. *Cancers* **2020**, *12*, 605. [CrossRef]
8. Nakhjavani, M.; Hardingham, J.E.; Palethorpe, H.M.; Tomita, Y.; Smith, E.; Price, T.J.; Townsend, A.R. Ginsenoside Rg3: Potential molecular targets and therapeutic indication in metastatic breast cancer. *Medicines* **2019**, *6*, 17. [CrossRef]
9. Nakhjavani, M.; Smith, E.; Townsend, A.R.; Price, T.J.; Hardingham, J.E. Anti-angiogenic properties of ginsenoside Rg3. *Molecules* **2020**, *25*, 4905. [CrossRef]
10. Nakhjavani, M.; Palethorpe, H.M.; Tomita, Y.; Smith, E.; Price, T.J.; Yool, A.J.; Pei, J.V.; Townsend, A.R.; Hardingham, J.E. Stereoselective anti-cancer activities of ginsenoside Rg3 on triple negative breast cancer cell models. *Pharmaceuticals* **2019**, *12*, 117. [CrossRef]
11. Nico, B.; Ribatti, D. Aquaporins in tumor growth and angiogenesis. *Cancer Lett.* **2010**, *294*, 135–138. [CrossRef]
12. Papadopoulos, M.; Saadoun, S.; Verkman, A. Aquaporins and cell migration. *Pflügers Arch. Eur. J. Physiol.* **2008**, *456*, 693–700. [CrossRef]
13. Tomita, Y.; Dorward, H.; Yool, A.J.; Smith, E.; Townsend, A.R.; Price, T.J.; Hardingham, J.E. Role of aquaporin 1 signalling in cancer development and progression. *Int. J. Mol. Sci.* **2017**, *18*, 299. [CrossRef]
14. Jeong, S.M.; Lee, J.-H.; Kim, J.-H.; Lee, B.-H.; Yoon, I.-S.; Lee, J.-H.; Kim, D.-H.; Rhim, H.; Kim, Y.; Nah, S.-Y. Stereospecificity of Ginsenoside Rg 3 Action on Ion Channels. *Mol. Cells* **2004**, *18*, 383–389.

15. Kim, J.-H.; Lee, J.-H.; Jeong, S.M.; Lee, B.-H.; Yoon, I.-S.; Lee, J.-H.; Choi, S.-H.; Kim, D.-H.; Park, T.-K.; Kim, B.-K. Stereospecific effects of ginsenoside Rg3 epimers on swine coronary artery contractions. *Biol. Pharm. Bull.* **2006**, *29*, 365–370. [CrossRef]
16. Wei, X.; Su, F.; Su, X.; Hu, T.; Hu, S. Stereospecific antioxidant effects of ginsenoside Rg3 on oxidative stress induced by cyclophosphamide in mice. *Fitoterapia* **2012**, *83*, 636–642. [CrossRef]
17. Wei, X.; Chen, J.; Su, F.; Su, X.; Hu, T.; Hu, S. Stereospecificity of ginsenoside Rg3 in promotion of the immune response to ovalbumin in mice. *Int. Immunol.* **2012**, *24*, 465–471. [CrossRef]
18. Wu, R.; Ru, Q.; Chen, L.; Ma, B.; Li, C. Stereospecificity of Ginsenoside Rg3 in the promotion of cellular immunity in hepatoma H22-bearing mice. *J. Food Sci.* **2014**, *79*, H1430–H1435. [CrossRef]
19. Kim, Y.-J.; Choi, W.-I.; Jeon, B.-N.; Choi, K.-C.; Kim, K.; Kim, T.-J.; Ham, J.; Jang, H.J.; Kang, K.S.; Ko, H. Stereospecific effects of ginsenoside 20-Rg3 inhibits TGF-β1-induced epithelial–mesenchymal transition and suppresses lung cancer migration, invasion and anoikis resistance. *Toxicology* **2014**, *322*, 23–33. [CrossRef]
20. Myers, R.H.; Montgomery, D.C.; Anderson-Cook, C.M. *Response Surface Methodology: Process and Product Optimization Using Designed Experiments*; John Wiley & Sons: Hoboken, NJ, USA, 2016.
21. Razura-Carmona, F.F.; Pérez-Larios, A.; González-Silva, N.; Herrera-Martínez, M.; Medina-Torres, L.; Sáyago-Ayerdi, S.G.; Sánchez-Burgos, J.A. Mangiferin-loaded polymeric nanoparticles: Optical characterization, effect of anti-topoisomerase I., and cytotoxicity. *Cancers* **2019**, *11*, 1965. [CrossRef]
22. Liou, J.-Y.; Tsou, M.-Y.; Ting, C.-K. Response surface models in the field of anesthesia: A crash course. *Acta Anaesthesiol. Taiwanica* **2015**, *53*, 139–145. [CrossRef] [PubMed]
23. Zafar, S.; Akhter, S.; Ahmad, I.; Hafeez, Z.; Rizvi, M.M.A.; Jain, G.K.; Ahmad, F.J. Improved chemotherapeutic efficacy against resistant human breast cancer cells with co-delivery of Docetaxel and Thymoquinone by Chitosan grafted lipid nanocapsules: Formulation optimization, in vitro and in vivo studies. *Colloids Surf. B Biointerfaces* **2020**, *186*, 110603. [CrossRef] [PubMed]
24. Lee, J.J.; Kong, M.; Ayers, G.D.; Lotan, R. Interaction index and different methods for determining drug interaction in combination therapy. *J. Biopharm. Stat.* **2007**, *17*, 461–480. [CrossRef] [PubMed]
25. Malfettone, A.; Silvestris, N.; Paradiso, A.; Mattioli, E.; Simone, G.; Mangia, A. Overexpression of nuclear NHERF1 in advanced colorectal cancer: Association with hypoxic microenvironment and tumor invasive phenotype. *Exp. Mol. Pathol.* **2012**, *92*, 296–303. [CrossRef] [PubMed]
26. Smith, E.; Palethorpe, H.; Tomita, Y.; Pei, J.; Townsend, A.; Price, T.; Young, J.; Yool, A.; Hardingham, J. The purified extract from the medicinal plant bacopa monnieri, bacopaside II, inhibits growth of colon cancer cells in vitro by inducing cell cycle arrest and apoptosis. *Cells* **2018**, *7*, 81. [CrossRef]
27. Tomita, Y.; Palethorpe, H.M.; Smith, E.; Nakhjavani, M.; Townsend, A.R.; Price, T.J.; Yool, A.J.; Hardingham, J.E. Bumetanide-derived aquaporin 1 inhibitors, AqB013 and AqB050 inhibit tube formation of endothelial cells through induction of apoptosis and impaired migration in vitro. *Int. J. Mol. Sci.* **2019**, *20*, 1818. [CrossRef]
28. Palethorpe, H.; Tomita, Y.; Smith, E.; Pei, J.; Townsend, A.; Price, T.; Young, J.; Yool, A.; Hardingham, J. The aquaporin 1 inhibitor bacopaside II reduces endothelial cell migration and tubulogenesis and induces apoptosis. *Int. J. Mol. Sci.* **2018**, *19*, 653. [CrossRef]
29. Jiao, Q.; Bi, L.; Ren, Y.; Song, S.; Wang, Q.; Wang, Y.-s. Advances in studies of tyrosine kinase inhibitors and their acquired resistance. *Mol. Cancer* **2018**, *17*, 1–12. [CrossRef] [PubMed]
30. Thieltges, K.M.; Avramovic, D.; Piscitelli, C.L.; Markovic-Mueller, S.; Binz, H.K.; Ballmer-Hofer, K. Characterization of a drug-targetable allosteric site regulating vascular endothelial growth factor signaling. *Angiogenesis* **2018**, *21*, 533–543. [CrossRef]
31. Brozzo, M.S.; Bjelić, S.; Kisko, K.; Schleier, T.; Leppänen, V.-M.; Alitalo, K.; Winkler, F.K.; Ballmer-Hofer, K. Thermodynamic and structural description of allosterically regulated VEGFR-2 dimerization. *Blood* **2012**, *119*, 1781–1788. [CrossRef]
32. Keung, M.-H.; Chan, L.-S.; Kwok, H.-H.; Wong, R.N.-S.; Yue, P.Y.-K. Role of microRNA-520h in 20 (R)-ginsenoside-Rg3-mediated angiosuppression. *J. Ginseng Res.* **2016**, *40*, 151–159. [CrossRef] [PubMed]
33. Li, J.-P.; Zhao, F.-L.; Yuan, Y.; Sun, T.-T.; Zhu, L.; Zhang, W.-Y.; Liu, M.-X. Studies on anti-angiogenesis of ginsenoside structure modification HRG in vitro. *Biochem. Biophys. Res. Commun.* **2017**, *492*, 391–396. [CrossRef] [PubMed]
34. Wenthur, C.J.; Gentry, P.R.; Mathews, T.P.; Lindsley, C.W. Drugs for allosteric sites on receptors. *Annu. Rev. Pharmacol. Toxicol.* **2014**, *54*, 165–184. [CrossRef] [PubMed]
35. Grover, A.K. Use of allosteric targets in the discovery of safer drugs. *Med Princ. Pract.* **2013**, *22*, 418–426. [CrossRef]
36. Muz, B.; de la Puente, P.; Azab, F.; Azab, A.K. The role of hypoxia in cancer progression, angiogenesis, metastasis, and resistance to therapy. *Hypoxia* **2015**, *3*, 83–92. [CrossRef]
37. Walsh, J.C.; Lebedev, A.; Aten, E.; Madsen, K.; Marciano, L.; Kolb, H.C. The clinical importance of assessing tumor hypoxia: Relationship of tumor hypoxia to prognosis and therapeutic opportunities. *Antioxid. Redox Signal.* **2014**, *21*, 1516–1554. [CrossRef]
38. Luo, D.; Liu, H.; Lin, D.; Lian, K.; Ren, H. The clinicopathologic and prognostic value of hypoxia-inducible factor-2α in cancer patients: A systematic review and meta-analysis. *Cancer Epidemiol. Prev. Biomark.* **2019**, *28*, 857–866. [CrossRef]
39. Ma, Q.; Reiter, R.J.; Chen, Y. Role of melatonin in controlling angiogenesis under physiological and pathological conditions. *Angiogenesis* **2020**, *23*, 91–104. [CrossRef]
40. Ramjiawan, R.R.; Griffioen, A.W.; Duda, D.G. Anti-angiogenesis for cancer revisited: Is there a role for combinations with immunotherapy? *Angiogenesis* **2017**, *20*, 185–204. [CrossRef]
41. Carpini, J.D.; Karam, A.K.; Montgomery, L. Vascular endothelial growth factor and its relationship to the prognosis and treatment of breast, ovarian, and cervical cancer. *Angiogenesis* **2010**, *13*, 43–58. [CrossRef]

42. Weigand, M.; Hantel, P.; Kreienberg, R.; Waltenberger, J. Autocrine vascular endothelial growth factor signalling in breast cancer. Evidence from cell lines and primary breast cancer cultures in vitro. *Angiogenesis* **2005**, *8*, 197–204. [CrossRef] [PubMed]
43. Masłowska, K.; Halik, P.K.; Tymecka, D.; Misicka, A.; Gniazdowska, E. The Role of VEGF receptors as molecular target in nuclear medicine for cancer diagnosis and combination therapy. *Cancers* **2021**, *13*, 1072. [CrossRef] [PubMed]
44. Tian, T.; Li, X.; Zhang, J. mTOR signaling in cancer and mTOR inhibitors in solid tumor targeting therapy. *Int. J. Mol. Sci.* **2019**, *20*, 755. [CrossRef] [PubMed]
45. Chen, M.C.; Hsu, W.L.; Chang, W.L.; Chou, T.C. Antiangiogenic activity of phthalides-enriched Angelica Sinensis extract by suppressing WSB-1/pVHL/HIF-1α/VEGF signaling in bladder cancer. *Sci. Rep.* **2017**, *7*. [CrossRef]
46. Karar, J.; Maity, A. PI3K/AKT/mTOR pathway in angiogenesis. *Front. Mol. Neurosci.* **2011**, *4*, 51. [CrossRef]
47. Guba, M.; von Breitenbuch, P.; Steinbauer, M.; Koehl, G.; Flegel, S.; Hornung, M.; Bruns, C.J.; Zuelke, C.; Farkas, S.; Anthuber, M. Rapamycin inhibits primary and metastatic tumor growth by antiangiogenesis: Involvement of vascular endothelial growth factor. *Nat. Med.* **2002**, *8*, 128–135. [CrossRef]
48. Mi, C.; Ma, J.; Wang, K.S.; Zuo, H.X.; Wang, Z.; Li, M.Y.; Piao, L.X.; Xu, G.H.; Li, X.; Quan, Z.S.; et al. Imperatorin suppresses proliferation and angiogenesis of human colon cancer cell by targeting HIF-1α via the mTOR/p70S6K/4E-BP1 and MAPK pathways. *J. Ethnopharmacol.* **2017**, *203*, 27–38. [CrossRef]
49. Saraswati, S.; Kumar, S.; Alhaider, A.A. α-santalol inhibits the angiogenesis and growth of human prostate tumor growth by targeting vascular endothelial growth factor receptor 2-mediated AKT/mTOR/P70S6K signaling pathway. *Mol. Cancer* **2013**, *12*, 1–18. [CrossRef]
50. Dodd, K.M.; Yang, J.; Shen, M.H.; Sampson, J.R.; Tee, A.R. mTORC1 drives HIF-1α and VEGF-A signalling via multiple mechanisms involving 4E-BP1, S6K1 and STAT3. *Oncogene* **2015**, *34*, 2239–2250. [CrossRef]
51. Herbert, S.P.; Costa, G. Sending messages in moving cells: mRNA localization and the regulation of cell migration. *Essays. Biochem.* **2019**, *63*, 595–606.
52. Willett, M.; Brocard, M.; Davide, A.; Morley, S.J. Translation initiation factors and active sites of protein synthesis co-localize at the leading edge of migrating fibroblasts. *Biochem. J.* **2011**, *438*, 217–227. [CrossRef]
53. Li, W.; Petrimpol, M.; Molle, K.D.; Hall, M.N.; Battegay, E.J.; Humar, R. Hypoxia-induced endothelial proliferation requires both mTORC1 and mTORC2. *Circ. Res.* **2007**, *100*, 79–87. [CrossRef]
54. Stein, J.; Milewski, W.M.; Hara, M.; Steiner, D.F.; Dey, A. GSK-3 inactivation or depletion promotes β-cell replication via down regulation of the CDK inhibitor, p27 (Kip1). *Islets* **2011**, *3*, 21–34. [CrossRef]
55. Hermida, M.A.; Kumar, J.D.; Leslie, N.R. GSK3 and its interactions with the PI3K/AKT/mTOR signalling network. *Adv. Biol. Regul.* **2017**, *65*, 5–15. [CrossRef]
56. Guri, Y.; Colombi, M.; Dazert, E.; Hindupur, S.K.; Roszik, J.; Moes, S.; Jenoe, P.; Heim, M.H.; Riezman, I.; Riezman, H. mTORC2 promotes tumorigenesis via lipid synthesis. *Cancer Cell* **2017**, *32*, 807–823. [CrossRef]
57. Lamanuzzi, A.; Saltarella, I.; Desantis, V.; Frassanito, M.A.; Leone, P.; Racanelli, V.; Nico, B.; Ribatti, D.; Ditonno, P.; Prete, M. Inhibition of mTOR complex 2 restrains tumor angiogenesis in multiple myeloma. *Oncotarget* **2018**, *9*, 20563. [CrossRef]
58. De Ieso, M.L.; Yool, A.J. Mechanisms of aquaporin-facilitated cancer invasion and metastasis. *Front. Chem.* **2018**, *6*, 135. [CrossRef]
59. Nicchia, G.P.; Stigliano, C.; Sparaneo, A.; Rossi, A.; Frigeri, A.; Svelto, M. Inhibition of aquaporin-1 dependent angiogenesis impairs tumour growth in a mouse model of melanoma. *J. Mol. Med.* **2013**, *91*, 613–623. [CrossRef]
60. Kaneko, K.; Yagui, K.; Tanaka, A.; Yoshihara, K.; Ishikawa, K.; Takahashi, K.; Bujo, H.; Sakurai, K.; Saito, Y. Aquaporin 1 is required for hypoxia-inducible angiogenesis in human retinal vascular endothelial cells. *Microvasc. Res.* **2008**, *75*, 297–301. [CrossRef] [PubMed]
61. Saadoun, S.; Papadopoulos, M.C.; Hara-Chikuma, M.; Verkman, A.S. Impairment of angiogenesis and cell migration by targeted aquaporin-1 gene disruption. *Nature* **2005**, *434*, 786–792. [CrossRef]

Supplementary data

Supplementary Table S1. Design table developed for the RSM model.

Run*	SRg3 (A)	RRg3 (B)
1	0	0
2	0	0
3	-1	1
4	0	1
5	-1	-1
6	0	0
7	1	-1
8	0	0
9	0	-1
10	-1	0
11	0	0
12	1	1
13	1	0

*See Table 1 for values corresponding to the bounds -1, 0 and 1.

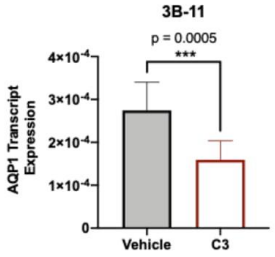

Supplementary Figure S1. Quantitative PCR for transcript expression of AQP1 in murine 3B-11 cell line following exposure with C3 for 3 days. PureLink RNA mini kit (Life Technologies, Grand Island, NY, USA) was used to extract RNA and 20 ng RNA was used for reverse transcription using iScript cDNA Synthesis Kit (Bio-Rad Laboratories, Hercules, CA, USA). The duplex TaqMan Gene Expression Assays for aquaporin-1 (AQP1; Mm01326465_g1; Applied Biosystems, Foster City, CA, USA) was used for the mouse endothelial cell line with *Eef2* (Eef2; Mm01171434_g1; Applied Biosystems, Foster City, CA, USA) as the reference gene. Reactions were performed in triplicate and analyzed as previously described [28].

1

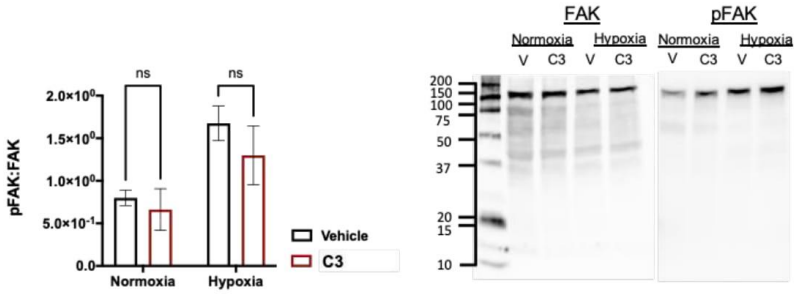

Supplementary Figure S2. Western blot analysis of activation of focal adhesion kinase (FAK) in HUVEC exposed to vehicle (V) or C3 (50 μM SRg3 + 25 μM RRg3), in normoxia or hypoxia conditions. Western blot was performed as previously described [28]. The antibodies used for immunostaining include anti-VEGF Receptor 2 antibody [EPRER16Y] (ab134191, Abcam, Cambridge, UK), anti-AQP1 antibody [EPR20325] (ab219055, Abcam, Cambridge, UK, 1:1000), anti-FAK antibody [EP6954] (ab40794, Abcam, Cambridge, UK, 1:1000), anti-phospho FAK antibody [EP2]60Y] phosphor Y397 (ab 81298, Abcam, Cambridge, UK, 1:1000). Goat anti-rabbit IgG H&L (HRP) (ab6721, Abcam, Cambridge, UK, 1:3000) was used as the secondary antibody. The experiments were repeated 3 times and the results are shown as mean ± SD.

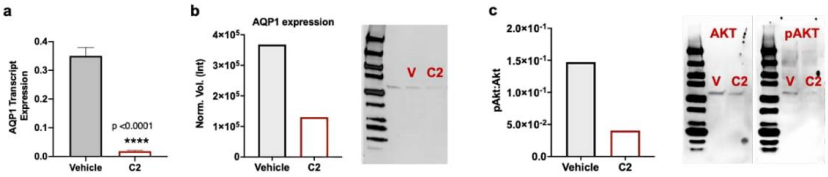

Supplementary Figure S3. HUVEC was exposed to vehicle (V) or C2 (25 μM SRg3 + 12.5 μM RRg3) for 3 days. (**a**) Quantitative PCR for transcript expression of AQP1 shown as mean ± SD of three experiments, (**b**) western blot protein expression of AQP1 and (**c**) activation of AKT in these cells. Anti-AQP1 antibody [EPR20325] (ab219055, Abcam, Cambridge, UK, 1:1000), anti-AKT antibody [E.32.10] (Invitrogen, Rockford, USA) and anti-phospho AKT antibody [104A282] (Invitrogen, Rockford, USA) were used.

Appendix A

To perform the circular wound migration assay, HUVECs, 2H-11, and 3B-11 cells, either not pretreated or pretreated for 3 days with Rg3 epimers, were seeded in 96-well plates at 3.5×10^4, 1.2×10^4, and 4×10^4 cells per well, respectively, and were incubated overnight. Then, to inhibit cell proliferation, the cells were exposed with culture media containing 2% FBS and 1 μg/mL mitomycin C and incubated overnight. The following day, when a confluent monolayer was achieved, circular wounds were made using suction through a sterile p10 pipette tip. Using ImageJ software (version 1.53a, National Health of Institute, Bethesda, MD, USA), the area of each circular wound was measured at two timepoints, based on a time of 0 and 10 h (murine endothelial cells), or 16 h (HUVEC). Cell migration was calculated for each well as a percentage of the initial wound area at time 0. The experiment included six replicates per treatment and the data are shown as mean ± SD.

Chapter 4 Effects of ginsenoside Rg3 on triple negative breast cancer models

4.1. Background

As reviewed in chapter 1 and investigated in chapter 2, Rg3 epimers have potential to be studied as a treatment for TNBC and especially metastatic TNBC. TNBC has a high potential of developing metastasis and therefore, to inhibit metastasis, two general options are considered: (1) to inhibit angiogenesis and (2) to inhibit migration of cancer cells. Anti-angiogenic properties of Rg3 were reviewed in chapter 1 and further investigated in chapter 3. Given the stereoselective activities of Rg3 epimers, the efficacy of the combination of Rg3 epimers, C3, was evaluated *in vitro* in chapter 3, which provided further evidence of the potential of C3 for application in TNBC.

The main question in this chapter was whether C3 had any efficacy on TNBC models. To answer this question, two TNBC cell lines were chosen, one derived from a metastatic site with more mesenchymal characteristics and one from a primary tumour with more epithelial characteristics. First, an RSM model was developed and the efficacy of C3 in TNBC cell migration in 2D and 3D models was evaluated. Then, to study the efficacy of this treatment in a more relevant model to human breast tumour, mammospheres were used. The efficacy of C3 on mammosphere formation and stem cell markers was studied. Stem cell markers studied in this research were CD44 and CD24, the ratio of which plays important roles in invasiveness of this disease and metastasis.

Furthermore, using *in silico* molecular docking, a screening of interaction of Rg3 epimers with a number of receptor tyrosine kinases was performed to find potential targets. Then, the effect of C3 on the PI3K/AKT signalling of TNBC mammospheres was studied using a protein array. Since the results indicated that C3 affected mTOR signalling, the interaction of Rg3 with rapamycin binding site of mTOR and Rheb, an activator of mTOR, was studied. Furthermore, it was investigated whether C3 affected the expression of AQP1 and FAK in TNBC mammospheres.

Subsequently, the efficacy of C3 was evaluated in an *in vivo* orthotopic mouse model of metastatic TNBC. This model was based on using immunodeficient Nod *scid* gamma (NSG) mice, which are capable of growing human TNBC cells. An almost complete lack of immune system in this model and use of a highly metastatic cell line (MDA-MB-231-Luc) makes this model a highly aggressive model, in which the cells spontaneously metastasise to distant organs. The growth of the primary and secondary tumours was monitored using IVIS spectrum. The dose of the drug was extrapolated from C3, based on the total body volume of water in an average mouse of 18 g. To bypass the first-pass effect, the drug was injected subcutaneously.

Following the promising results of the first animal study, a second dose-escalation study was designed and performed.

This chapter was submitted to "*Pharmacological Research*" journal and is currently under review.

4.2. Statement of Authorship

Statement of Authorship

Title of Paper	Anti-cancer effects of an optimised combination of ginsenoside Rg3 epimers on triple negative breast cancer models
Publication Status	☐ Published ☐ Accepted for Publication ☑ Submitted for Publication ☐ Unpublished and Unsubmitted work written in manuscript style
Publication Details	Nakhjavani, M., Smith, E., Palethorpe, H. M., Tomita, Y., Yeo, K., Price, T. J., Townsend, A. R., and Hardingham, J. E. Anti-cancer effects of an optimised combination of ginsenoside Rg3 epimers on triple negative breast cancer models. Submitted to Pharmaceuticals.

Principal Author

Name of Principal Author (Candidate)	Maryam Nakhjavani		
Contribution to the Paper	Conceptualised, designed and performed the experiments, analysed and curated the data, and substantially wrote the manuscript.		
Overall percentage (%)	70		
Certification:	This paper reports on original research I conducted during the period of my Higher Degree by Research candidature and is not subject to any obligations or contractual agreements with a third party that would constrain its inclusion in this thesis. I am the primary author of this paper.		
Signature		Date	10th Feb 2021

Co-Author Contributions

By signing the Statement of Authorship, each author certifies that:

i. the candidate's stated contribution to the publication is accurate (as detailed above);
ii. permission is granted for the candidate in include the publication in the thesis; and
iii. the sum of all co-author contributions is equal to 100% less the candidate's stated contribution.

Name of Co-Author	Eric Smith		
Contribution to the Paper	Contributed to performing the experiment, data analysis, discussion and reviewing the paper.		
Signature		Date	10th Feb 2021

Name of Co-Author	Helen M Palethorpe		
Contribution to the Paper	Contributed to designing the experiment, discussion and reviewing the paper.		
Signature		Date	8th Feb 2021

Name of Co-Author	Yoko Tomita		
Contribution to the Paper	Contributed to the discussion and reviewing the paper.		
Signature		Date	12th Feb 2021

Name of Co-Author	Kenny Yeo		
Contribution to the Paper	Contributed to the discussion and reviewing the paper.		
Signature		Date	8th Feb 2021

Name of Co-Author	Tim J Price		
Contribution to the Paper	Contributed to the discussion and reviewing the paper.		
Signature		Date	11th Feb 2021

Name of Co-Author	Amanda R Townsend		
Contribution to the Paper	Contributed to the discussion and reviewing the paper.		
Signature		Date	11th Feb 2021

Name of Co-Author	Jennifer E Hardingham		
Contribution to the Paper	Conceptualised and designed the experiments, contributed to data analysis and curation, discussion and reviewing the paper.		
Signature		Date	10th Feb 2021

Article

Anti-cancer effects of an optimised combination of ginsenoside Rg3 epimers on triple negative breast cancer models

Maryam Nakhjavani [1,2], Eric Smith [1,2*], Helen M Palethorpe [3], Yoko Tomita [1,2,4], Kenny Yeo [1,2], Tim J Price [2,4], Amanda R Townsend [2,4] and Jennifer E Hardingham [1,2]

[1] Molecular Oncology, Basil Hetzel Institute, The Queen Elizabeth Hospital, Woodville South, SA 5011, Australia; maryam.nakhjavani@adelaide.edu.au; yoko.tomita@adelaide.edu.au
[2] Adelaide Medical School, University of Adelaide, Adelaide, SA 5005, Australia; jenny.hardingham@sa.gov.au, a1811332@student.adelaide.edu.au
[3] Centre for Cancer Biology, University of South Australia and SA Pathology, Adelaide, SA, Australia; helen.palethorpe@unisa.edu.au
[4] Oncology Unit, The Queen Elizabeth Hospital, Woodville South, SA 5011, Australia; amanda.townsend@sa.gov.au; timothy.price@sa.gov.au
***** Correspondence: eric.smith@adelaide.edu.au; Tel.: +61-8-8222-6142

Abstract: Key problems of chemotherapies, as the mainstay of treatment for triple-negative breast cancer (TNBC), are toxicity and development of tumour resistance leading to the low survival rate of these patients. Using response surface methodology (RSM), we previously optimised the combination of epimers of ginsenoside Rg3 (Rg3) for anti-angiogenic action. Here, we show that the optimised combination (C3), derived from an RSM model of migration of TNBC cell line MDA-MB-231, inhibited migration of MDA-MB-231 and a second TNBC cell line, HCC1143, in 2D and 3D migration assays ($p < 0.0001$). C3 significantly inhibited mammosphere formation efficiency in both cell lines, while it did not cause significant cell death. The combination significantly decreased the $CD44^+$ stem cell marker in the mammospheres. Molecular docking showed that Rg3 epimers had a better binding score with IGF-1R than with EGFR, HER-2 or PDGFR. In addition, this *in silico* screening predicted an mTOR inhibitory function of Rg3. C3 affected the signalling of AKT as phosphorylation of 4E-BP1, P70S6K, PTEN and RPS6 in MDA-MB-231 mammospheres was decreased and phosphorylation of PRAS40, PTEN, Raf-1, RPS6 and RSK1 was decreased in HCC1143. The combination was then tested in a mouse model of metastatic TNBC. A dose of 23 mg/kg SRg3 + 11 mg/kg RRg3 or an escalated dose of 46 mg/kg SRg3 + 23 mg/kg RRg3 was administered to NSG mice bearing MDA-MB-231-Luc cells. Calliper and IVIS spectrum measurement of the primary and secondary tumour showed that the treatment shrunk the primary tumour and decreased the load of metastasis in mice. In conclusion, this combination of Rg3 epimers showed promising results as a potential treatment option for TNBC patients.

Keywords: Ginsenoside Rg3, Epimer, Triple negative breast cancer, Metastasis, Response surface methodology, Nod *scid* gamma mice

1. Introduction

Triple-negative breast cancer (TNBC) is a subtype of breast cancer for which limited targeted therapy is available. Chemotherapy is the mainstay of the treatment

for TNBC. Administration of various chemotherapies can be limited by toxicities and the development of tumour resistance [1]. Despite using selected chemotherapy regimens, these patients have a higher rate of developing visceral metastases [2] with a median overall survival of 13.3 months [3].

Cancer cells undergo epithelial to mesenchymal transition (EMT), and acquire cancer stem cell characteristics [4], one of the mechanisms by which cells become resistant to chemotherapies (reviewed in [5]). Different subtypes and stages of breast cancer have their unique expression of stem cell markers such as CD44, CD24 and aldehyde dehydrogenase (ALDH) [4, 6] and the search for drugs which reduce cancer stemness is an essential investigation in drug discovery and development programs. Phosphatidylinositol 3-kinase /protein kinase B/mammalian target of rapamycin (PI3K/AKT/mTOR) pathway is one of the several self-renewal pathways existing in breast cancer cells [4] and inhibitors of this pathway may reduce 'stemness' of cancer cells. Targeting this pathway is therefore important in overcoming drug resistance [7, 8], cell survival, and metastasis in this cancer [9, 10]. Several clinical studies are ongoing to evaluate the efficacy of the inhibitors of this pathway in TNBC patients (reviewed in [11]).

Natural products have always been a major source of therapeutic drugs. About 70% of the current cancer treatments are derived from or imitate natural products [12]. Natural inhibitors of PI3K/AKT signal transduction pathway have been under investigation for the treatment of breast cancer [13]. Ginsenoside Rg3 (Rg3) is a member of the ginsenosides family of molecules extracted from *Panax ginseng*. The molecule has two epimers, 20(S)-Rg3 (SRg3) and 20(R)-Rg3 (RRg3). We have previously discussed the potential of these molecules as a treatment for metastatic breast cancer [14, 15]. Besides, studies showed that Rg3 decreased the activation of PI3K/AKT pathway in several tumour models such as leukemia, ovarian, and lung carcinoma (reviewed in [14]). Based on this background, Rg3 might be a potential candidate for the treatment of metastatic TNBC (mTNBC). We previously showed that the epimers of Rg3 have stereoselectivity in their anti-cancer actions [16] such that only SRg3 inhibited the proliferation of MDA-MB-231 and blocked aquaporin 1 (AQP1) water channel, which plays important roles in the proliferation, migration, and invasion of cancer cells and in angiogenesis. Furthermore, it was only RRg3 that inhibited the invasion of MDA-MB-231 cells. SRg3 and RRg3 inhibited the migration of TNBC cells in wound closure and transwell migration assays with different manners [16]. Based on these findings, SRg3 and RRg3 could be considered as two different drugs. Therefore, we determined the optimal concentration of SRg3 and RRg3 using response surface methodology (RSM) modelling. RSM is one of the well-established methods of studying drug combinations which is especially important and helpful in cancer treatment studies [17-19]. The optimisation, which was based on the anti-angiogenic effects of the molecules [20], showed that a combination of 50 μM SRg3 + 25 μM RRg3 had the best efficacy in inhibition of loop formation and cell migration of endothelial cells. This treatment induced cell death and cell cycle arrest in human and murine endothelial cell lines, decreased the expression of vascular endothelial growth

factor (VEGF), AQP1 and phosphorylation of several proteins downstream of activation of AKT.

The current study aimed at investigating the efficacy of this combination on TNBC cell lines and in a murine model of mTNBC. The optimised combination of both molecules was assessed using RSM to confirm that the combination is effective in inhibiting TNBC cell migration. Next, the efficacy of the treatment was studied on mammospheres, as a more relevant model of human breast tumour and the effects of the treatment on stem cell markers and PI3K/AKT signalling pathway was investigated. Lastly, the *in vivo* efficacy of the treatment was studied in an orthotopic model of murine mTNBC.

2. Materials and Methods

2.1. Materials

SRg3 and RRg3 (both with a purity of > 98% by HPLC) were purchased from ChemFaces®, Wuhan, China. Stocks of SRg3 and RRg3 were prepared in dimethyl sulfoxide (DMSO D2650, HYBRI-MAX, Sigma-Aldrich, Steinheim, Germany) and stored at -20°C, as previously described [16]. TNBC cell lines; MDA-MB-231 (basal-like with mesenchymal or claudin-low phenotype) and HCC1143 (basal-like with epithelial phenotype) and MCF-12A (immortalised normal human breast epithelial cell line) were purchased from American type culture collection (ATCC). Luciferase-expressing MDA-MB-231-Luc cells were purchased from CellBank Australia. All cells were mycoplasma-free. As previously described, cells were tested for mycoplasma using MycoAlert Detection Kit (Lonza) and/or a custom PCR-based assay [21, 22].

2.2. Cell culture of adherent cells

MDA-MB-231 cells were grown in Dulbecco's Modified Eagle Medium (DMEM; Life Technologies, CA, USA) and HCC1143 cells were grown in Roswell Park Memorial Institute (RPMI) 1640 medium (Life Technologies, Carlsbad, CA, USA). Media was supplemented with 10% foetal bovine serum (FBS; Corning, Corning, NY, USA) and 1% penicillin-streptomycin solution (Life Technologies). MCF-12A cells were grown in MammoCult™ media supplemented with 5% FBS (Corning), 10% MammoCult™ proliferation supplement, 0.5% hydrocortisone and 0.2% heparin (all from Stem Cell Technologies, Vancouver, Canada). MDA-MB-231-Luc cells were cultured in L-15 media supplemented with 15% FBS and 1% penicillin-streptomycin (Life Technologies). A week before the animal experiment, the cells were harvested, washed in Dulbecco's phosphate-buffered saline (DPBS, Gibco, Thermo Fisher Scientific, Waltham, MA, USA) and grown as mammospheres in MammoCult™ media (described below).

2.3. Circular scratch migration assay

The experiment was performed as previously described [16]. Briefly, three-day pre-treated MDA-MB-231 and HCC-1143 cells were seeded in 96-well cell culture plates (Corning® Costar®, Corning, NY, USA), at 4×10^4 and 8×10^4 cells/well, respectively. Following overnight incubation, a circular scratch was made on a

monolayer of cells and images at time 0 and 24 h were taken using a Nikon microscope. The migration (%) of the cells was measured based on the area of the circular wound measured with ImageJ software (version 1.53a, National Health of Institute, Bethesda, MD, USA). The experiment was replicated 6 times and results represented as mean ± standard deviation (SD).

2.4. Response surface methodology (RSM)

To confirm that the effective combination of Rg3 epimers on endothelial cells was effective on TNBC cells, an RSM model was developed for the migration of MDA-MB-231, as previously described (Supplementary Table 1 and Table 2) [20]. The tested combinations were 12.5 μM SRg3 and 6.2 μM RRg3 (C1), 25 μM SRg3 and 12.5 μM RRg3 (C2), and 50 μM SRg3 and 25 μM RRg3 (C3).

2.5. Transwell migration assay

The experiment was performed as previously described [16]. A total of 1×10^5 of pre-treated MDA-MB-231 and HCC-1143 cells were collected in 250 μL of serum-free media containing vehicle control or Rg3 combinations. The cells were added to the upper chamber of Corning® transwell plates (8 μm pore size) with complete media in the lower chamber. The experiment was performed in triplicate and the results were represented as mean ± SD.

2.6. Proliferation assay

Crystal violet assay (CVA) was used to study the effect of Rg3 on the proliferation of TNBC cells, as previously described [16]. Briefly, MDA-MB-231, HCC1143 and MCF-12A cells were seeded at 5×10^3 cells/well of 96-well flat-bottom cell culture plates. After overnight incubation, the cells were exposed to the vehicle or Rg3 combinations. On days 0 (drug exposure day), 1 and 3, cells were stained with crystal violet and the absorbance was measured at 595 nm using FLUOstar Optima microplate reader (BMG Labtech, Offenburg, Germany). Each treatment replicated 6 times and the data were shown as mean ± SD.

2.7. Culture of mammospheres

Mammospheres were grown in MammoCult™ Human Medium Kit (Stem Cell Technologies, Vancouver, Canada) as recommended by the manufacturer. The media was supplemented with MammoCult™ proliferation supplement, hydrocortisone and heparin at final concentrations of 10%, 0.5% and 0.2%, respectively. Briefly, the cells were harvested, washed and resuspended in complete MammoCult media at the density of 4×10^3 cell/cm^2 in 6-well ultra-low attachment plates (Corning® Costar®). Following a 7-day period, mammospheres were collected in a tube, centrifuged at 350 x g, 10 min, 4°C, and dissociated using 100 μL TrypLE™ Express (phenol red-free, Gibco, Thermo Fisher Scientific, Waltham, MA, USA) and pipetting. Then, 1 mL of cold DPBS supplemented with 2% FBS was added to the cells. The cells were then centrifuged at 350 x g, 10 min, 4° C. Supernatant was then removed, and single cells

were suspended in MammoCult media, counted and seeded in 6-well ultra-low attachment plates exposed with vehicle or C3 for 3 days.

2.8. Mammosphere formation efficiency (MFE)

Mammospheres, exposed to vehicle or Rg3, were collected, counted, seeded in 24-well ultra-low attachment plates at the density of 4000 cell/cm^2. They were exposed to the vehicle or Rg3 for 4 days. Then, MFE was calculated as per the equation MFE (%) = number of mammospheres per well / number of seeded cells per well × 100, as previously described [23].

2.9. Cell viability analysis

Cells were grown and exposed to the drugs, as described in the previous paragraph. Single cells were prepared, and cell viability was measured using CellDrop™ FL Fluorescence Cell Counter (DeNOVIX). The experiment was performed in triplicate and the results are expressed as mean ± SD.

2.10. Expression of stem cell markers

Mammospheres were grown, treated with C3, collected and dissociated into single cells as before. Then the cells were washed in cold fluorescence-activated cell sorting buffer (FACS, 2% FBS, 0.05% sodium azide in DPBS), counted and 1 × 10^6 cell/mL FACS was prepared. The antibodies used to study the expression of CD44 and CD24 markers were as follows: APC mouse anti-human CD44 (BD Pharmingen™, BD Biosciences, CA, USA), APC mouse IgG2b, κ isotype control (BD Pharmingen™, BD Biosciences, CA, USA), PE mouse anti-human CD24 (BD Pharmingen™, BD Biosciences, CA, USA) and PE mouse IGg2a, κ isotype control (BD Pharmingen™, BD Biosciences, CA, USA). APC-Cy7 (100 μL per tube) was used to select for live cells. Incubation with antibodies or isotype controls was for 30 min in darkness at 4°C. Cells were washed twice in 1 mL FACS buffer and resuspended in 100 μL of FACS buffer. Expression of ALDH was studied using ALDEFLUOR™ Kit (Stem Cell Technologies), based on the manufacturer's protocol. An aliquot of 1 × 10^5 cells/tube was prepared on ice for 30 min staining with 20 μL antibody or isotype control. Prior to analysis, the cells were washed twice in 1 mL FACS buffer and resuspended in 100 μL of FACS buffer. The experiments were performed in triplicate and the results are expressed as mean ± SD.

2.11. AKT pathway phosphorylation array

A Human/Mouse AKT Pathway Phosphorylation Array C1 (RayBiotech, Norcross, GA, USA) was used to evaluate the effect of C3 on the signalling of AKT. This array measures the expression of 18 phosphorylated proteins in this signalling pathway. Mammospheres were grown from both TNBC cell lines, exposed to drugs and collected as described above. Mammospheres were washed twice in cold DPBS. Protein was extracted with a protein inhibitor cocktail and phosphatase inhibitors included as recommended by the manufacturer. Bio-Rad Protein Assay Dye Reagent Concentrate (Bio-Rad, Hercules, CA, USA) was used for the determination of protein levels. Image Lab™ Software (version 6.1) was used to measure the density of each dot. The results are shown as the mean ± SD of two replicates.

2.12. In silico molecular docking

The interaction of Rg3 with four tyrosine kinase receptors was studied via molecular docking. The SMILES structure of Rg3 isomers, sorafenib, lenvatinib and rapamycin were obtained from PubChem. The crystal structure of epidermal growth factor receptor (EGFR) (3W33), human epidermal growth factor receptor-2 (HER-2) (3PP0), insulin-like growth factor-1 receptor (IGF-1R) (1JQH), and platelet derived growth factor receptor (PDGFR) (5GRN), the FKBP12 rapamycin-binding (FRB) (1FAP) and Ras homolog enriched in brain (Rheb) (6BSX) were obtained from the protein data bank of NCBI (RCSB PDB). The UCSF Chimera program (version 1.15-mac64) and Autodock Vina algorithm (version 1.1.2_Mac) were used to make the 3D structure of Rg3, perform the molecular docking. The Gibbs free energy of protein-ligand binding (kJ/mol) was predicted based on the flexible ligand docking simulations within the docking grids on defined interaction sites of each specific protein, as previously described [16].

2.13. Developing the mouse model of mTNBC

Female Nod *scid* gamma (NSG) mice (6-8 weeks old) were purchased from Animal Resources Centre (Canning Vale, WA, Australia). Five days prior to commencement of the study, the mice were acclimatized to the animal housing facility, in pathogen-free conditions. Throughout the study, the mice were weighed and checked on a daily basis for general well-being or any signs of toxicity. The experiments were performed according to the guidelines for the ethical use of animals in research and were approved by the Animal Ethics Committees of the University of Adelaide (M-2019-068, 01/08/2019). To prepare MDA-MB-231-Luc cells for injection into mice, they were grown as mammospheres for 7 days. On the day of cell inoculation, the cells were collected, centrifuged at 350 x g, for 5 min at 4°C and washed twice in DPBS. The cells were counted and 1×10^6 cells (viability > 95%) were resuspended in 50 μL cold DPBS. A total of 100 μL of cells in a 1:1 ratio of Matrigel (Corning® Matrigel® Basement Membrane Matrix, Phenol red-free, LDEV-free)/DPBS were injected into the 4th right mammary fat pad (MFP), using aseptic technique.

2.14. Drug administration and toxicity assessment

Drugs were dissolved in DMSO and stored at -20°C as aliquots. Before injection to mice, an aliquot was thawed, mixed with 70% DPBS and 20% Cremophor EL® (Millipore Corp., Billerica, MA USA). The vehicle group received a combination of 10% DMSO, 20% Cremophor EL and 70% DPBS. Doses administered to mice were an extrapolation of *in vitro* results considering the total body water volume (10.35 mL) in a mouse of an average weight of 18 g. In the first study (study A) the mice received a combination of 50 μM SRg3 and 25 μM RRg3, equivalent to 23 and 11 mg/kg (combo A), respectively. Based on the encouraging results of this study, study B was designed in which the mice received a combination of 100 μM SRg3 and 50 μM RRg3, equivalent to 45 and 23 mg/kg (combo B), respectively. Drug administration started on day 12 in study A and day 5 in study B. Study A and B lasted for 40 and 23 days, respectively.

The drugs were injected subcutaneously three times a week. To assess the toxicity of the treatment, the mice were daily checked for any adverse changes including changes in body weight, changes in behaviour, fur condition, movement, posture, breathing and hydration level.

2.15. IVIS imaging and tumour size measurement

To non-invasively monitor the growth of the tumour and development of metastasis, the IVIS® Spectrum Imaging system (PerkinElmer, Boston, Massachusetts, USA) was used. The mice were anaesthetized and given a subcutaneous injection of 100 μL of luciferin solution (Xenolight™ D-luciferin potassium salt, PerkinElmer) at 150 mg/kg, 20 min before imaging. Mice were imaged once a week. Living Image® software (version 4.7.3; Perkin Elmer) was used to quantify the photons emitted from the mice as photons/sec/cm^2. Furthermore, calliper measurement was used to measure the volume of the primary tumour using the equation: (shortest diameter of the tumour)^2 × longest diameter of the tumour / 2.

2.16. H&E staining and proliferative area measurement

At the end of the experiment, the mice were humanely euthanized. Primary tumours and organs including lungs and lymph nodes were fixed in formalin neutral buffered, 10%, histological tissue fixative (Sigma-Aldrich) for 2 days, dehydrated and wax infiltrated (Excelsior AS™ Tissue Processor, Thermo Scientific™) and embedded in paraffin (HistoStar™ Embedding Workstation, Thermo Scientific™). Then, 4-μm thick tissue sections were prepared using a Microm HM 325 Microtome. Tissue slides were then stained for H&E, imaged using a NanoZoomer 2.0-HT slide scanner and viewed with NDP.view2 software (Hamamatsu Photonics, Shizuoka, Japan). The area of necrotic tissue relative to the whole cross-sectional area of the tumours was measured using ImageJ.

2.17. Statistical analysis

GraphPad Prism (version 9.0.0 for mac, GraphPad Software, San Diego, California USA, www.graphpad.com) was used to perform student's t-test, one- or two-way analysis of variance. The significance cut-off was considered to be $p < 0.05$.

3. Results

3.1. RSM for the effect of Rg3 on cell migration

The RSM contour plot (Figure 1a) shows the regions of optimised concentrations of SRg3 and RRg3 for migration (%) in MDA-MB-231 cell line. Different regions with different colours in the contour plot show the predicted percentage of cell migration in response to the combination of SRg3 and RRg3. Figure 1b shows the 3D surface plot of the combination of SRg3 and RRg3 in this cell line. The optimum region in which minimum migration is achieved is shown with dashed line circles. Based on the RSM modelling, in this region, the concentration of the two drugs is optimised to achieve the maximum inhibition of migration. Previously, we showed that the combination of 50 μM SRg3 and 25 μM RRg3 was the optimised combination for inhibition of loop

formation in HUVEC cells [20]. Based on this RSM, this combination gives 22.5% cell migration in MDA-MB-231 (Figure 1c). As shown in Figure 2a, the average cell migration achieved with C3 was about 15%, which falls into the predicted region in the RSM model.

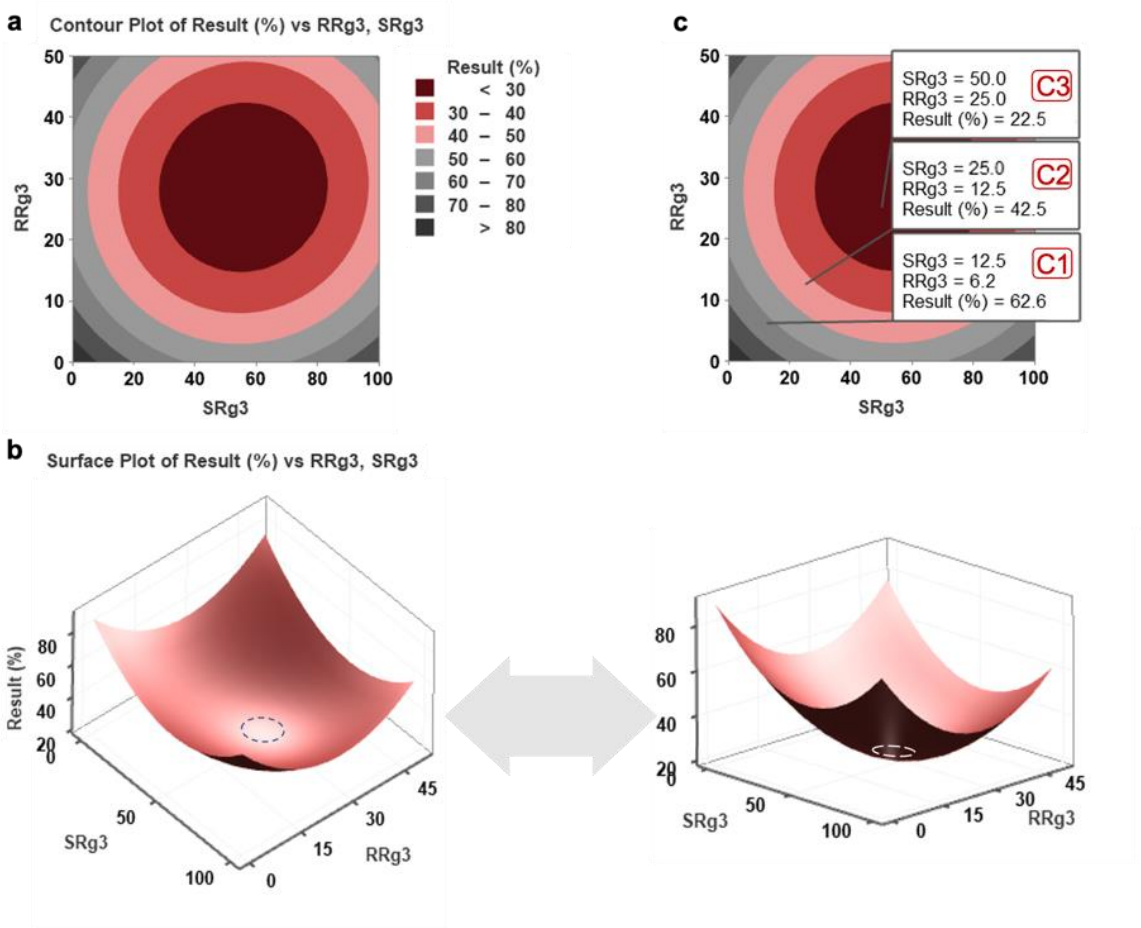

Figure 1. The calculated (**a**) contour plot and (**b**) 3D surface plots (viewed from two angles) for cell migration based on the response surface methodology model developed to optimise and confirm the efficacy of SRg3 + RRg3 drugs in combination in MDA-MB-231 cell line. Dashed circles show the optimised minimal response area. (**c**) shows the predicted cell migration (%) with different combinations of SRg3 and RRg3. Results (%) is the percentage of expected migration.

3.2. Rg3 inhibits migration but not proliferation in TNBC cell lines

The effect of individual or combinations of Rg3 epimers on the migration of TNBC cells was tested in a circular scratch-wound (2D) and a transwell (3D) migration assay (Figure 2).

After a three-day pre-treatment with individual or combinations of Rg3 epimers, MDA-MB-231, compared to HCC1143, showed more sensitivity to the anti-migratory effects of Rg3 only in the 2D assay. In MDA-MB-231, each of the three tested combinations, C3, C2 and C1, significantly inhibited cell migration to 15%, 38% and 52% of vehicle control, respectively (Figure 2a). This was similar to the predicted RSM

model of <30%, 40-50% and 60-70% for C3, C2 and C1, respectively (Figure 1b). In HCC1143, 50 and 100 μM SRg3 inhibited cell migration by about 30% ($p < 0.05$) and among the combinations, only C3 significantly inhibited the 2D migration of cells ($p < 0.0001$) (Figure 2a). These results also indicated that with C1 and C2 average cell migration was about 62% and 48%, respectively, which fall into the appropriate regions predicted by RSM (Figure 1b). These regions are 60-70% for C1 and 40-50% for C2, respectively (Figure 1b). C3 inhibited cell migration by about 85% and 92% in MDA-MB-231 and HCC1143 cell lines, respectively.

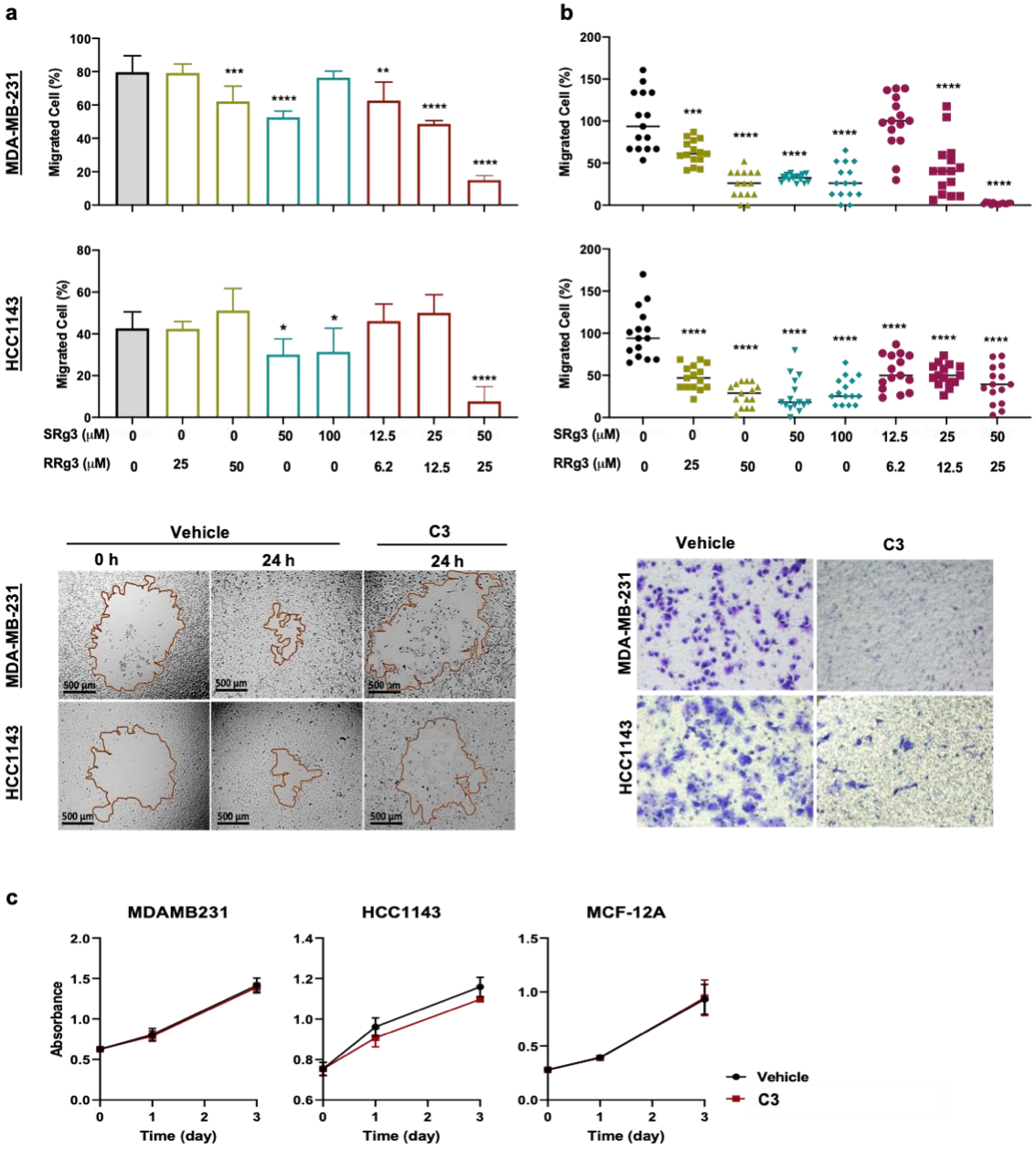

Figure 2. Effects of SRg3, RRg3 and the combination of both on (**a**) circular scratch migration and (**b**) transwell migration assays on MDA-MB-231 and HCC1143. Datapoints show mean ± standard deviation (SD) of 6 (**a**) and 3 (**b**) replicates. (**c**) Anti-proliferative effect of C3 (50 μM SRg3 + 25 μM RRg3) on TNBC cell lines (MDA-MB-231 and HCC1143) and a normal breast cell line (MCF-12A). Each data point represents 6 replicates and shown as mean ± SD.

All comparisons are with the vehicle-treated cells, $p < 0.05$. * $p < 0.05$, ** $p < 0.01$, *** $p < 0.001$ and **** $p < 0.0001$.

The transwell assay showed that in both cell lines, single epimers significantly inhibited cell migration ($p \leq 0.0002$) (Figure 2b). All three combinations in HCC1143 and C2 and C3 in MDA-MB-231 showed efficacy in inhibition of 3D migration of cells ($p < 0.0001$). In MDA-MB-231, C3 showed the highest efficacy by almost completely inhibiting cell migration across the membrane ($p < 0.0001$). Figure 2c shows the anti-proliferative effects of C3 on the TNBC cell lines and a normal breast epithelial cell line. As shown in this figure, this treatment did not inhibit the proliferation of these cell lines.

3.3. Rg3 decreases MFE in TNBC 3D models, via decreasing 'stemness' of the cells

The cells in the presence of vehicle formed mammospheres and in the presence of C3, mostly remained as single cells. MFE was significantly reduced in MDA-MB-231 ($p = 0.0003$) and HCC1143 ($p < 0.0001$) (Figure 3a). Viability of both MDA-MB-231 and HCC1143 cells were not significantly decreased (Figure 3b). Flow cytometric analysis of apoptosis (Supplementary Figure 1a) and cell cycle (Supplementary Figure 1b) showed that there were no significant changes in the percentage of apoptotic cells or induction of cell cycle arrest.

The expression of CD44/CD24 (Figure 3c and 3d) and ALDH (Figure 3e) was studied in both TNBC mammospheres. Cancer stem cells play important roles in driving initiation, progression, metastasis and recurrence and CD44, CD24 and ALDH are widely known breast cancer stem cell markers [6]. It was shown that a high ratio of cells expressing CD44 to CD24 was correlated with strong tumorigenicity of breast cancer and ALDH was correlated with the metastatic capacity of the tumour. These markers were correlated with breast cancer malignancy [6]. The $CD44^{+}/CD24^{-/low}$ phenotype was also correlated with poorer prognosis in TNBC patients and together with $ALDH^{+}$ are expressed in axillary lymph node (aLN) metastasis [6, 24]. MDA-MB-231 and HCC1143 cell lines have mesenchymal and epithelial characteristics, respectively, which is also reflected in the expression of $CD44^{+}/CD24^{-/low}$ phenotype in mammospheres. Figure 3c and 3d show that compared to HCC1143, MDA-MB-231 had higher expression of $CD44^{+}/CD24^{-}$ phenotype as mammospheres. Exposure to C3, decreased the expression of $CD44^{+}/CD24^{-}$ phenotype in MDA-MB-231 mammospheres by 35% ($p = 0.001$) (Figure 3c). MDA-MB-231 showed a more significant decrease in the ratio of cells expressing CD44 to CD24 ($p = 0.001$); a double negative subpopulation was also observed (Figure 3c and 3d).

Likewise, with HCC1143 mammospheres, upon exposure to C3, a double-negative subpopulation of cells was created and the ratio of cells expressing CD44 to CD24 was significantly decreased ($p = 0.02$) (Figure 3d). In both mammospheres, expression of CD44 was significantly decreased (Figure 3e). MDA-MB-231 cells express low levels of ALDH [25] and that expression was not altered by C3. Expression of ALDH in HCC1143 was only slightly decreased by C3 treatment ($p < 0.05$) (Figure 3e). Therefore,

decreased expression of CD44⁺ phenotype and decreased ratio of CD44 to CD24 might play a more important role in the anti-cancer effects of C3.

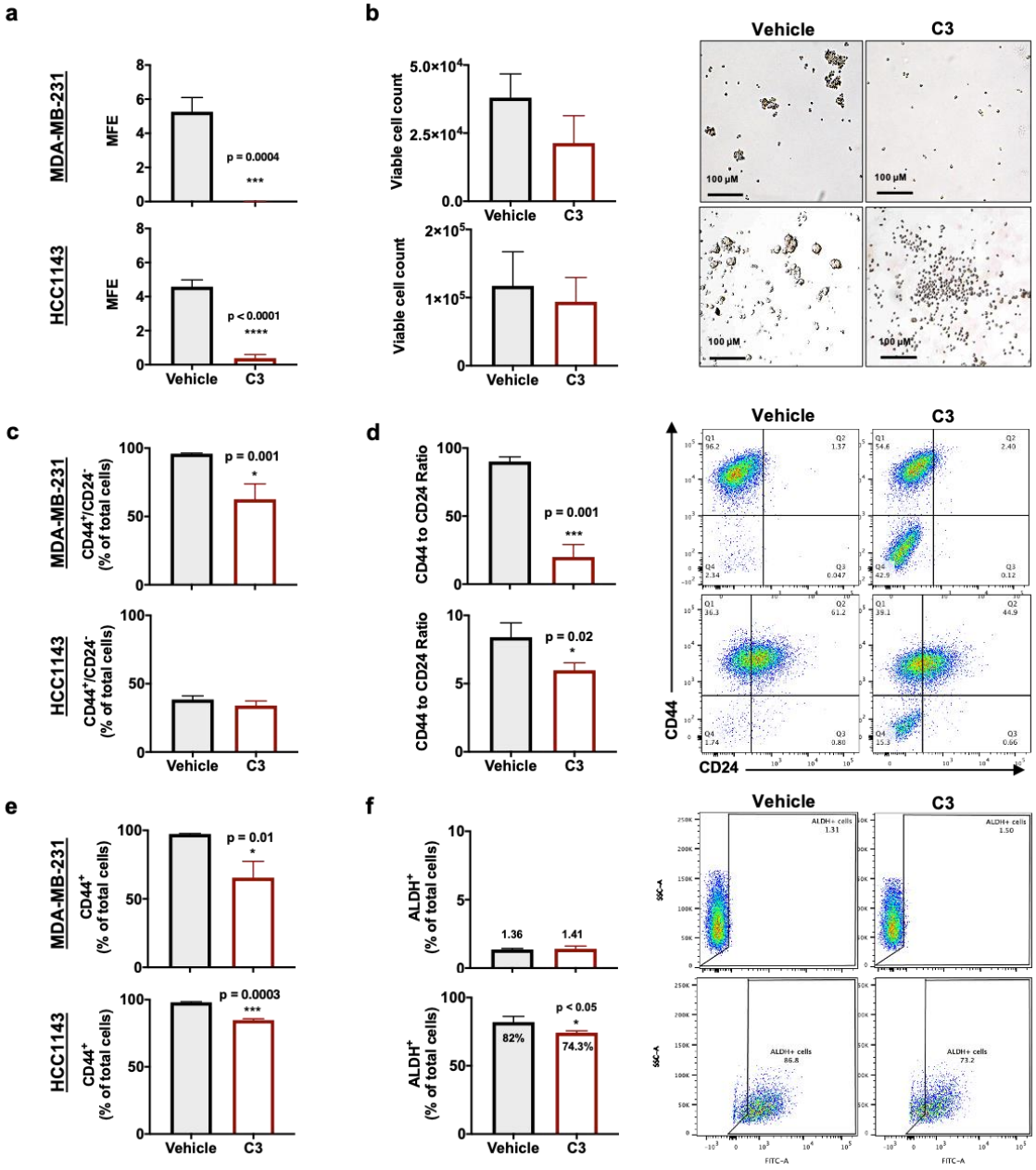

Figure 3. (**a**) Mammosphere formation efficiency (MFE) and (**b**) viability of MDA-MB-231 and HCC1143 grown as mammospheres and exposed to C3 (50 µM SRg3 + 25 µM RRg3). Expression of (**c**) CD44⁺/CD24⁻ phenotype, (d) ratio of CD44 and CD24 expressing cells, (**e**) CD44⁺ expression and (**e**) expression of ALDH in mammospheres exposed to combination of SRg3 + RRg3. Each datapoint represents mean ± SD of three replicates. Statistical comparisons are between the treated and vehicle groups, $p < 0.05$.

3.4. Effect of Rg3 on Akt/mTOR signalling

Receptors tyrosine kinases (RTKs) such as EGFR and IGF-1R are overexpressed in TNBC, are considered to be prognostic and predictive markers [26-28], and are potential targets for treatment. Activation of RTKs triggers multiple signalling

pathways which guarantees cell cycle progression, proliferation, survival, migration and angiogenesis (Figure 4a). We had previously shown that Rg3 interacts with VEGFR2, *in silico* and *in vitro*, and functions as an allosteric modulator of the receptor [20]. In this study, we screened the interaction of Rg3 with some other RTKs.

Table 1 shows the binding scores of Rg3 epimers with EGFR, HER-2, IGF-1R and PDGFR. The binding scores were compared with those of two known tyrosine kinase inhibitors (TKIs), sorafenib and lenvatinib.

As shown in Table 1, both TKIs are predicted to have good binding scores with the receptors. With Rg3 epimers, the best scores belonged to the interaction of SRg3 and RRg3 with IGF-1R, being -8 and -7.5 kJ/mol, respectively. Figure 4b and 4c show the interaction of SRg3 and RRg3 with ATP-binding pocket of IGF-1R, respectively. As shown in these Figures, Rg3 molecules are predicted to be well placed in the ATP-binding pocket of the receptor.

Table 1. Binding score (kJ/mol) between Rg3 epimers and tyrosine kinase receptors, FRB site of mTOR or Rheb, and the number of hydrogen bonds (H-bonds) predicted by Chimera program and Autodock vina algorithm.

	Binding score (kJ/mol) (number of H-bonds)					
Molecule	EGFR	HER-2	IGF-1R	PDGFR	FRB	Rheb
SRg3	-6.9 (2)	2.7 (0)	-8.0 (2)	-2.8 (1)	-7.0 (1)	-8.0 (3)
RRg3	-6.9 (2)	2.7 (1)	-7.5 (0)	-2.8 (1)	-7.2 (1)	-8.0 (4)
Sorafenib	-9.6 (0)	-10.8 (1)	-8.9 (1)	-11.2 (1)	n.d.*	n.d.
Lenvatinib	-10.4 (1)	-9.6 (1)	-7.9 (1)	-10.1 (1)	n.d.	n.d.
Rapamycin	n.d.	n.d.	n.d.	n.d.	-7.6 (0)	n.d.

* not determined

Following activation of a RTK, different downstream signalling pathways might be activated. PI3K/AKT and Ras/Raf/MEK/ERK are two such pathways which are in crosstalk. PI3K phosphorylates and activates AKT. AKT has several targets, the action of which leads to cell survival, migration, proliferation and angiogenesis. One of the important targets of AKT is mammalian target of rapamycin complex 1 (mTORC1), which is sensitive to and regulated by several signals including nutrients and growth factors [29].

Two key substrates of mTORC1 are eukaryotic translation initiation factor 4E (eIF4E)-binding protein 1 (4E-BP1) and P70 ribosomal protein S6 kinase (P70S6K). They are crucial factors in translation initiation that predominantly mediate the translational functions of mTORC1. mTORC1, via phosphorylation of 4E-BP1, inactivates this protein, releasing p-4E-BP1 from eIF-4E. Activated eIF-4E, then initiates translation (Figure 4a). mTORC1 also phosphorylates and activates P70S6K. Activated P70S6K phosphorylates and activates ribosomal protein S6 (RPS6), a component of S40 ribosomal subunit, which plays an important role in global translation and cell growth and glucose homeostasis (Figure 4a) [30]. The effect of C3 on the phosphorylation of proteins downstream of the activation of AKT on two TNBC mammosphere models is shown in Figure 4d-e. Mammospheres, originated from two

different TNBC cell lines with mesenchymal (MDA-MB-231) or epithelial (HCC1143) characteristics reacted differently to C3.

In MDA-MB-231, the expression of phosphorylated forms of 4E-BP1 ($p < 0.0001$), RPS6 ($p = 0.0001$), P70S6K ($p = 0.0032$) and phosphatase and tensin homolog (PTEN) ($p = 0.0109$) were significantly decreased (Figure 4d). PTEN is a tumour suppressor gene, an inhibitor of the activation of PI3K and its subsequent signalling (Figure 4a). In this study, phosphorylation of Ser380, which inactivates PTEN was measured. It was shown that C3 significantly decreased the levels of inactive phosphorylated PTEN ($p = 0.0109$), which would improve the tumour suppressor function. In MDA-MB-231, C3 also reduced mTOR-initiated ribosomal translation via decreased phosphorylation of 4E-BP1, P70S6K and RPS6.

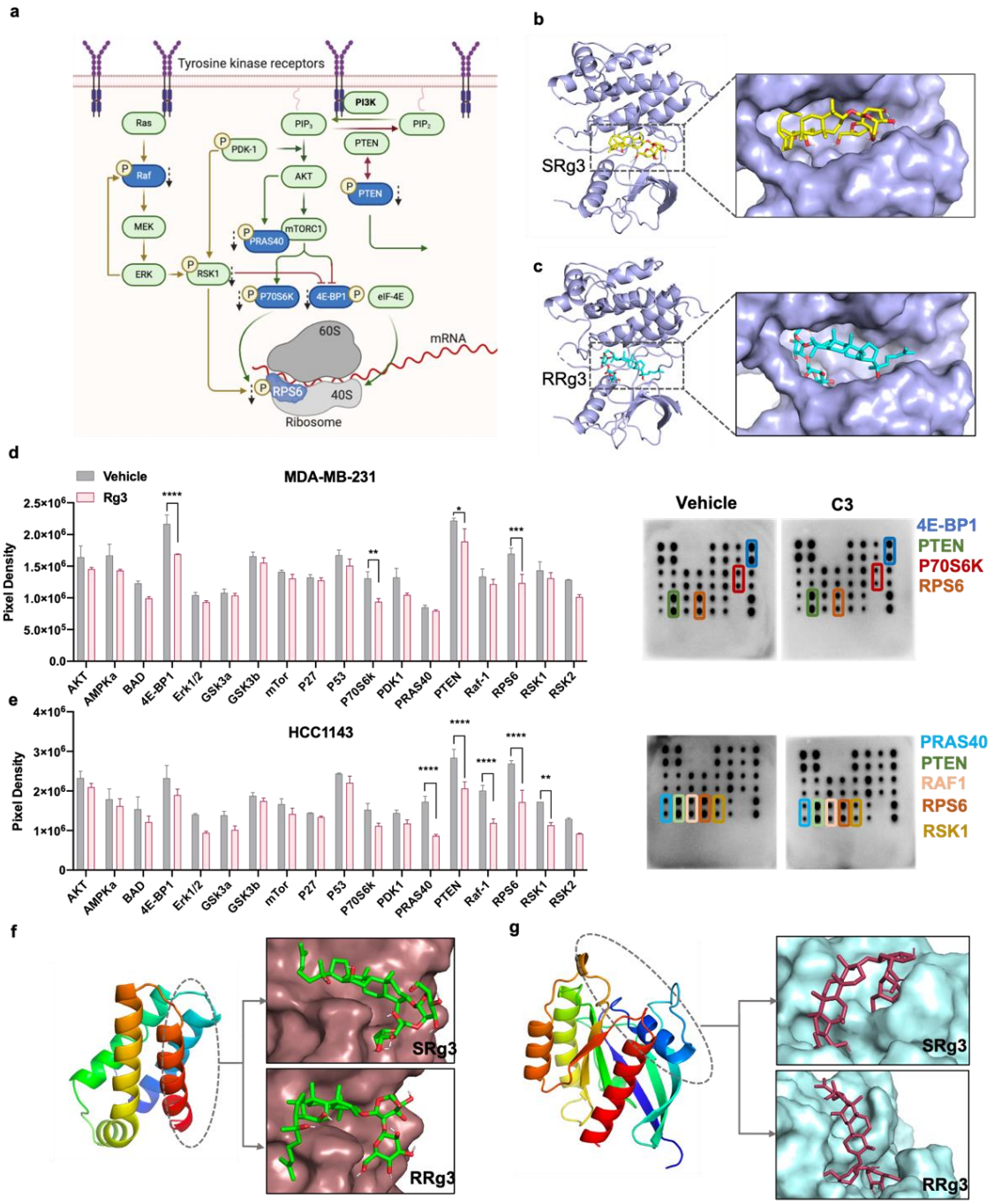

Figure 4. (**a**) An Illustration of signalling of PI3K/AKT/mTOR and Ras/Raf/MEK/ERK signalling pathways. Dashed black arrows show where

Rg3 is affecting and affected proteins are shown in blue. Interaction of (**b**) SRg3 and (**c**) RRg3 with ATP-binding pocket of IGF-1R. The effects of C3 (50 μM SRg3 + 25 μM RRg3) on the expression of phosphorylated proteins downstream of activation of AKT signalling in (**d**) MDA-MB-231 and (**e**) HCC1143 cell lines. The data show mean ± SD of two replicates. Statistical comparisons are between the treated and vehicle groups, $p < 0.05$, (**f**) FKBP12 rapamycin-binding site of mTOR binding to SRg3 and RRg3 and (**g**) Rheb protein binding to SRg3 and RRg3. * $p < 0.05$, ** $p < 0.01$, *** $p < 0.001$ and **** $p < 0.0001$.

Similar to MDA-MB-231, C3 treatment of HCC1143 mammospheres reduced the levels of the phosphorylated forms of PTEN ($p < 0.0001$) and RPS6 ($p < 0.0001$). In addition, the expression of phosphorylated forms of proline-rich AKT substrate of 40 kDa (PRAS40) ($p < 0.0001$), Raf-1 ($p < 0.0001$), and ribosomal S6 kinase (RSK1) ($p = 0.0038$) were also decreased (Figure 4e). PRAS40 is a substrate of AKT and a component and substrate of mTORC1 (Figure 4a). AKT mediated phosphorylation of PRAS40 at Thr246, studied in this assay, inactivates PRAS40 in a way that mTORC1 restores its function [29]. Hence, decreased phosphorylation of PRAS40 decreases the activation of mTORC1.

RSK1 is a member of the family of 90 kDa RSKs. RSKs are activated downstream of activation of Ras/Raf/MEK/ERK pathway. The signalling of Ras/Raf/MEK/ERK plays roles in cell proliferation, survival, migration and angiogenesis. It is in interaction with the signalling of the AKT pathway. Upon activation, RSKs play roles in regulating several cellular functions including cell proliferation, survival and motility [31], via interaction with phosphorylation of 4E-BP1 and RPS6 [32]. Raf-1 is a proto-oncogene and a serine/threonine protein kinase that is activated downstream of activation of Ras, leading to activation of MEK and ERK. Phosphorylation at SER-301 of Raf-1, studied in this assay, is a result of ERK-mediated feedback phosphorylation of Raf-1 [33].

Considering the changes in the phosphorylation of proteins downstream of activation of mTOR, we performed molecular docking to find out if Rg3 epimers have any good binding with mTORC1. In this preliminary screening, we tested two sites of the complex, the FRB and Rheb. The FRB site is one of the functional domains of mTOR kinase, where rapamycin binds. At this site, SRg3 and RRg3 have binding score of -7 and -7.2 kJ/mol, respectively, which are comparable to the binding score of rapamycin, -7.6 kJ/mol (Table 1). Furthermore, SRg3 and RRg3 had binding scores of -8.0 kJ/mol with Rheb. Rheb is a GTP-binding protein that upon insulin and growth factor stimulation, binds to and activates mTORC1. Molecular docking showed that Rg3 has a good binding score with Rheb and hence, could decrease the signalling of mTOR axis, the inhibition of which is important in cancer treatment [34, 35].

3.5. In vivo evaluation of the efficacy of Rg3 combo

To evaluate the *in vivo* efficacy of C3 two *in vivo* studies were conducted. With combo A (23 mg/kg SRg3 + 11.5 mg/kg RRg3) weekly IVIS imaging demonstrated that

the treatment significantly decreased the growth rate of the primary tumour ($p = 0.0004$) (Figure 5a). This result was confirmed with calliper measurements (Figure 5b). This treatment also significantly decreased the total body tumour burden ($p < 0.0001$) (Figure 5c) and thoracic tumour load ($p = 0.0066$) (Figure 5d). Lung metastases were confirmed with *ex vivo* imaging (Figure 5e) and H&E staining (Figure 5f).

Treatment with C3 significantly reduced the number of metastatic aLNs (Figure 5g). Five of 8 mice in the vehicle group showed an enlarged contralateral (left) aLN, whilst only one mouse in the treatment group had an affected left aLN. Mice in both groups had an enlarged ipsilateral (right) aLNs. *Ex vivo* imaging (Figure 5h) and H&E staining (Figure 5i) confirmed the presence of tumour in the metastatic aLNs.

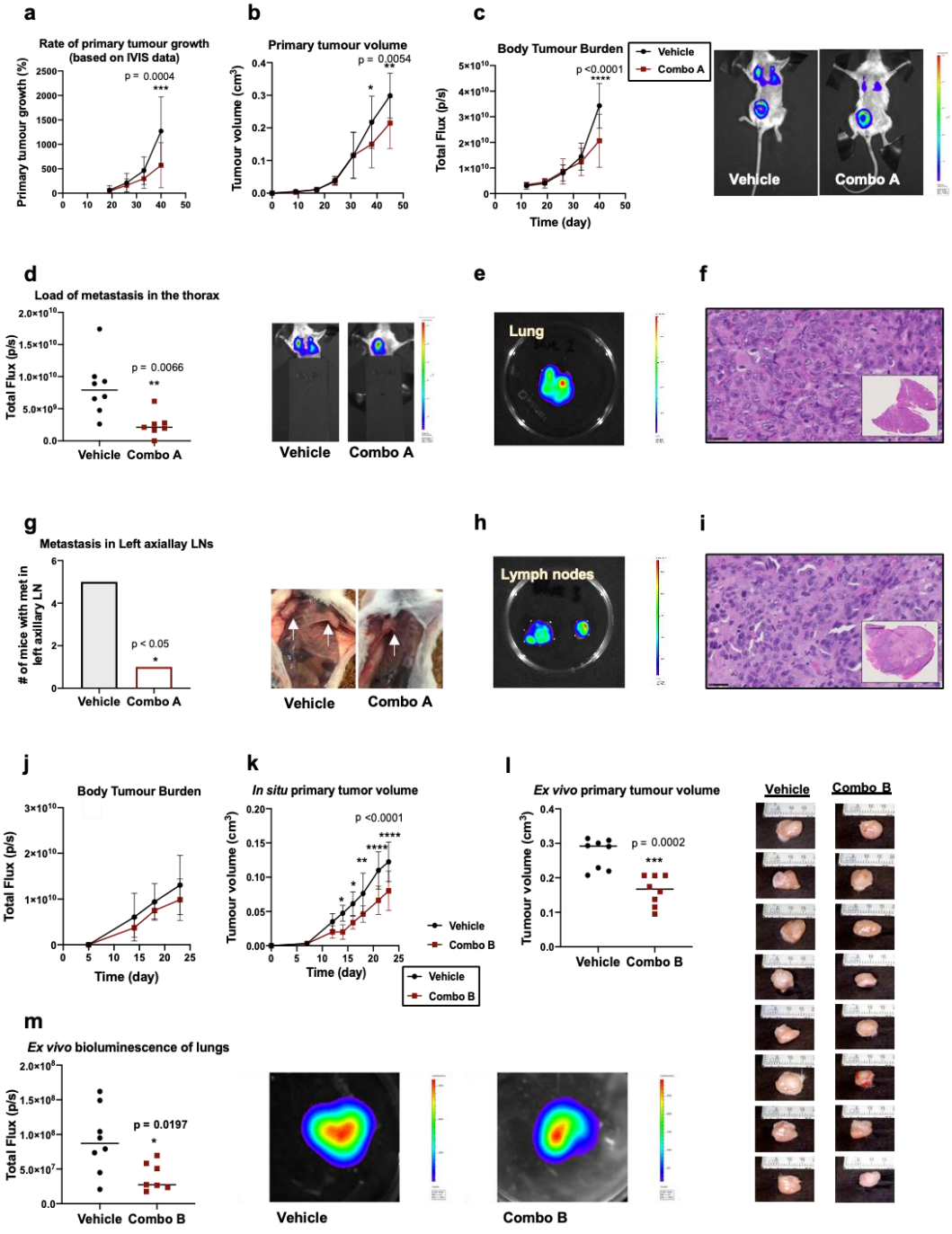

Figure 5. Outcomes of administration of combo A and B to a metastatic model of TNBC in NSG mice. Administration of combo A (**a**) decreased the rate of primary tumour growth measured with IVIS spectra, (**b**) primary tumour

volume measured with a calliper, (**c**) body burden of the tumour, (**d**) the load of metastasis in the thorax and (**g**) number of enlarged left axillary lymph nodes, indicated with white arrows. (**e**) and (**h**) show representative *ex vivo* IVIS images of lung and lymph nodes and (**f**) and (**i**) are the results of histology on lung and lymph node, respectively, showing tumour cells in the tissues. Black arrows show the region in the tissue that is magnified. The scale bar shows 25 μm. Administration of combo B to mice, (**j**) decreased, though not significantly, the average body burden of the tumour, (**k**) primary tumour volume measured with a calliper *in situ*, or (**l**) *ex vivo*. (**m**) The treatment also significantly decreased the load of tumour in the lungs of mice, (**n**) there were no significant differences between the groups in terms of necrotic or viable area, black arrow shows the necrotic area and dashed arrow shows the proliferative region and the scale bar shown 2.5 mm. Each treatment group included 8 mice. All IVIS scales show count values between 600-60000. The data are presented in (**a-c**), (**j-n**) are mean ± SD with $p < 0.05$. * $p < 0.05$, ** $p < 0.01$, *** $p < 0.001$ and **** $p < 0.0001$.

Next, we doubled the doses to 46 mg/kg SRg3 and 23 mg/kg RRg3 (combo B). Administration of a higher dose of Rg3 to mice caused a lessening trend in the average total flux of the whole body (Figure 5j), which started as early as the second dose. However, this decrease in total body flux was not statistically significant. The escalated dose also significantly decreased the size of the primary tumour. A significant difference between the treatment and the vehicle group was noticed as early as day 14 ($p = 0.01$). Tumour volume measurements on days 16 ($p = 0.01$), 18 ($p = 0.0056$), 21 ($p < 0.0001$) and 23 ($p < 0.0001$) confirmed the decreased size in the treatment group (Figure 5k).

Ex vivo measurement confirmed the treatment significantly decreased the primary tumour volume ($p = 0.0002$) (Figure 5l). *Ex vivo* imaging of the excised lungs also showed a significant decrease in the bioluminescence photons detected in the treatment group lungs ($p = 0.0197$) (Figure 5m). Furthermore, there were no significant differences between the groups in terms of necrotic or proliferative areas (Figure 5n). In these two studies, no signs or symptoms of drug toxicity were observed. There were no significant differences between the two groups in terms of weight loss, fur condition, posture and behaviour (Supplementary Figure 3).

4. Discussion

The objective of this research was to study and introduce a plausible treatment option for TNBC and mTNBC. In our previous studies, we showed that epimers of Rg3 have stereoselective activities [16] and then using an RSM model, the combination of these two epimers was optimised for its anti-angiogenic effects, *in vitro* [20]. In the current study, first, the validity of the optimised combination was tested in MDA-MB-231 and it was shown that the combination (C3) exerted a high anti-migration effect in the circular scratch migration assay. The validity of the RSM model was also tested with two other combinations (C1 and C2). In both migration assays, C3 showed high

efficacy in inhibiting cell migration of both TNBC cell lines, while it had no anti-proliferative effect on them. Then the efficacy of C3 was tested in mammospheres, which better mimic the *in vivo* drug responses of human breast tumour. Formation of mammosphere is related to 'stemness' of the cancer cells [36]. The treatment significantly inhibited MFE. As tested in this study, one contributing reason for the decreased MFE could be the decreased 'stemness' of the cells.

In this study, combined expression of CD44 and CD24 were studied. CD44 and CD24 are markers that are more expressed on progenitor-like cells and more differentiated cells, respectively. In breast cancer cells with $CD44^+$ phenotype, genes that are involved in cell motility and angiogenesis were highly expressed, the cells were more mesenchymal, motile, and predominately estrogen receptor negative. In breast cancer patients, $CD44^+/CD24^-$ phenotype related to triple negativity and unfavourable prognosis [37] worse clinical behaviour [38] and distant metastasis [39]. These cells expressed higher levels of pro-invasive genes and had highly invasive properties [40]. Studies also showed that downregulation of CD44 reduced doxorubicin resistance of $CD44^+/CD24^-$ breast cancer cells [41]. It was previously shown that 50 μM SRg3 decreased the $CD44^+/CD24^-$ subpopulation in MDA-MB-231 [42]. In our study, RRg3 was added as a co-treatment and the combination caused a double negative subpopulation of cells. In addition, it was previously reported that Rg3 inhibited EMT via inactivating P38 MAPK and Smad2, increased expression of E-cadherin and Snail and decreased expression of vimentin (reviewed in [14]). Decreased expression of CD44 might be another contributing factor to this phenomenon, because CD44 also plays roles in EMT [43].

The mechanism by which expression of these stem cell markers is decreased in these cells might be via inhibition of PI3K/AKT pathway. It has been shown that inhibitors of this signalling pathway, such as quercetin [44] decreased $CD44^+/CD24^-$ phenotype and hence breast cancer 'stemness'. Previously, Rg3 was shown to affect the PI3K/AKT signalling and decreased the activation of Akt, mTOR, GSK-3β, 4E-BP1, Src, and P70S6K (reviewed in [14]). In the present study, it was shown that C3 affects AKT/mTOR signalling in both TNBC cell lines tested. Rg3 also was predicted to have a good binding score with IGF-1R and could be a blocker of mTOR activation via blocking the interaction site of Rheb with mTOR. mTOR regulates several cellular functions including cell adhesion, changes in extracellular matrix and migration [45]. C3 may have exerted its anti-cancer actions by affecting the regulatory function of mTOR.

We previously showed that in endothelial cells, C3 was an inhibitor of AKT signalling, with the highest efficacy on p-mTOR and its substrates, p-4E-BP1 and p-P70S6K. Consistent with those results, in MDA-MB-231, both of these proteins were affected. 4E-BP1 plays a role in the mTOR-initiated translation of factors involved in metastasis such as matrix metalloproteinase-9, fibroblast growth factor, vascular endothelial growth factor, C-MYC and cyclin D1 [45]. Along with these roles, 4E-BP1 was introduced as an oncogene in breast cancer [46], playing a role in the proliferation of breast cancer cells [47]. Furthermore, mTORC1/4E-BP1 regulated neural stem cell renewal capacity [48], a pathway which also might play a role in stem cell renewal in breast cancer and needs further investigation.

p-P70S6K plays roles in cell growth and cell cycle progression and is also identified as an important factor in breast cancer survival and predicting response to treatment [49]. This protein may also play roles in metastasis as overexpression of p-P70S6K was linked to metastasis in gastric carcinoma [50]. It is also responsible for the phosphorylation of protein S6. RPS6 is involved in the regulation of cell size and glucose homeostasis [30]. Hyperphosphorylation of this protein via AKT/mTOR/p70S6K pathway was relevant to the progression of non-small cell lung carcinoma (NSCLC) [51]. In both of our tested cell lines, the levels of p-RPS6 were significantly reduced, which might indicate the importance of this protein in the Rg3-induced effects observed in both cell lines and potential of involvement of IGF-1R and glucose metabolism. The role of Rg3 with IGF-1 was previously studied and it was shown that Rg3 decreased the expression of IGF-1 causing a reduced cell proliferation in multiple myeloma and breast tumours (reviewed in [14]). This could further highlight the role of Rg3 in IGF-1R signalling.

p-PRAS40 is an important component and regulator of mTORC1. The expression of p-PRAS40 has been reported to be prognostic in gastric cancer [52]and prostate cancer [53] patients. Raf-1 and RSK1 are activated downstream of activation of Ras/Raf/MEK/ERK pathway. RSKs, via enhancing proliferation, migration and invasion, have multiple roles in breast cancer [54]. RSK inhibitors were developed to bypass the side effects of MEK inhibitors, as RSKs have fewer but important targets which play roles in metastasis. The fact that 85% of these patients have activated RSKs makes them a good therapeutic target in TNBC [55].

In addition, the leading edge of migrating cells has a crucial role in cell migration and is a centre for local translation of required proteins for cell migration [56] for which mTOR plays a central role [57]. AQP1 together with other proteins important in cell migration such as focal adhesion kinase (FAK), work in complex at the leading edge to facilitate cell migration. Our preliminary testing has shown that C3 caused decreased activation of FAK and minor decreased expression of AQP1 in MDA-MB-231 and HCC1143 mammospheres (Supplementary Figure 2). A decreased level of AQP1 expression was previously noted in endothelial cells exposed to C3 [20].

The efficacy of C3 was also evaluated in an mTNBC mouse model. Previously some studies reported the efficacy of Rg3 in mice breast cancer models (reviewed in [14]). In these studies, orally administered Rg3 promoted the anti-cancer effects of paclitaxel and capecitabine, and improved mice survival (reviewed in [14]). Although many studies suggested anti-migration mechanisms for Rg3 epimers and anti-metastatic efficacy of Rg3 was shown in melanoma and colon cancer models (reviewed in [14]), until now, no studies have investigated the efficacy of Rg3 on an mTNBC mouse model. For the first time, we have evaluated the efficacy of Rg3 combination in a highly aggressive orthotopic mouse model of mTNBC. Furthermore, we changed the route of administration from oral to subcutaneous injection, hence, bypassing the gastrointestinal metabolism, first-pass effect and low bioavailability of Rg3 (reviewed in [14]). The primary and the increased dosing both showed efficacy in this mouse model. Reduction in tumour size was more meaningful with the escalated dosing, however, the percentage of necrotic tissue between the two groups was not

significantly different. Mollard *et al*. (2016), in a simulation study, showed that in this mTNBC mouse model, necrotic tissue had an almost constant ratio against total tissue volume [58]. Consistent with that, combo B did not change the ratio between necrotic and proliferative tissues in the vehicle or treated groups, however, primary tumour shrinkage was observed. This could mean that the treatment reduced the rate of proliferation in the primary tumour, which caused tumour shrinkage. Previously, we showed that at 100 μM SRg3, the proliferation of MDA-MB-231 was inhibited [16]. Furthermore, epimers of ginsenoside Rh2 and protopanaxadiol were suggested as potential active metabolites of Rg3, detected after intravenous injection to rats (reviewed in [14]), and these molecules have shown anticancer effects in MDA-MB-231 [59, 60]. Therefore, the effects observed in this study might be a result of the combination of Rg3 and its metabolites. Further studies are required to investigate it. For the first time, we reported the anti-metastatic efficacy of combination Rg3 epimers in an mTNBC mouse model. Reduced metastatic load observed in this study is very impressive. Whether this treatment targets angiogenesis *in vivo* requires further investigation. Furthermore, the treatment was tolerable in mice and no signs of toxicity were observed. Single epimers administered to human have not shown toxicities (reviewed in [14, 20]) and therefore, it is not expected that the tested combination be any more toxic.

5. Conclusions

In conclusion, the optimised combination of SRg3 + RRg3 showed efficacy in inhibition of migration of TNBC cell lines, inhibited the MFE, reduced the 'stemness' of these cells and inhibited phosphorylation of proteins downstream of AKT/mTOR signalling. *In silico* studies suggest that Rg3 might be a potential mTORC1 inhibitor. Furthermore, in an mTNBC mouse model, the treatment shrunk the primary tumour and reduced the load of metastasis in mice, which introduces this drug as a potential treatment for TNBC.

Funding: This work was kindly supported by the Margaret Elcombe Hospital Research Foundation Research Grant.

Conflicts of Interest: The authors declare no conflict of interest.

Appendix A. Supplementary data

The central composite design technique (CCD) was employed with three levels; low, mid, and high values corresponding to -1, 0 and +1 for input parameters which are concentration of SRg3 and RRg3. In the present study, the concentration ranged from (0-100 μM) for SRg3 and (0-50 μM) for RRg3 were selected. Supplementary Table 1 represents the values corresponding to low, mid, and high bounds of concentrations for Rg3 epimers.

Supplementary Table 1. Low, mid and high values used for RSM model.

Parameter	Index	Concentration (μM)		
		Lowest value (-1)	Centre Value (0)	Highest Value (+1)
SRg3	A	0	50	100
RRg3	B	0	25	50

Supplementary Table 2 represents the designed matrix used in the RSM analysis and the response (percent of cell migration). To optimize the combination of concentrations, the RSM model has reduced the total experiments to 13 iterations, with cell migration being the "main measurable target parameter".

Supplementary Table 2. Design Matrix developed for the RSM model.

Run*	A	B	SRg3 (A)	RRg3 (B)	Response (%)
1	-1	-1	0	0	79.23
2	0	0	50	25	18.40
3	0	0	50	25	14.19
4	0	0	50	25	15.55
5	1	0	100	25	57.24
6	0	0	50	25	12.09
7	-1	1	0	50	64.33
8	-1	0	0	25	79.23
9	0	-1	50	0	72.40
10	1	1	100	50	53.45
11	0	1	50	50	63.92
12	0	0	50	25	16.14
13	0	-1	100	0	75.09

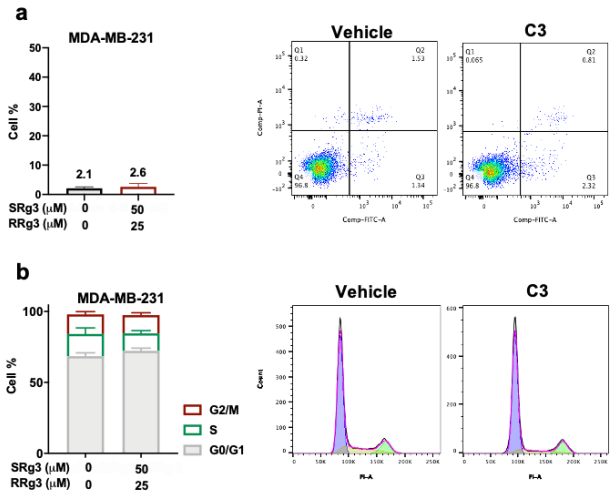

Supplementary Figure 1. MDA-MB-231 cells were grown as mammospheres and exposed to C3 (50 μM SRg3 + 25 μM RRg3). (**a**) shows induction of apoptosis and (**b**) shows cell cycle arrest in these mammospheres exposed to vehicle or drug. The experiment was performed in triplicate and results are shown as mean ± SD.

Apoptosis This assay was performed on mammospheres using Annexin-V-FLUOS staining kit (Roche Diagnostics, Mannheim, Germany) as previously described [61]. Changes in the cell cycle of cells grown as mammospheres were studied using propidium iodide staining and BD FACSCanto™ II analysis, as previously described [62]. The experiment was performed using the BD FACSCanto™ II (BD Biosciences, San Jose, CA, USA) and FlowJo software, v 10.4 (FlowJo, LLC, Ashland, OR, USA).

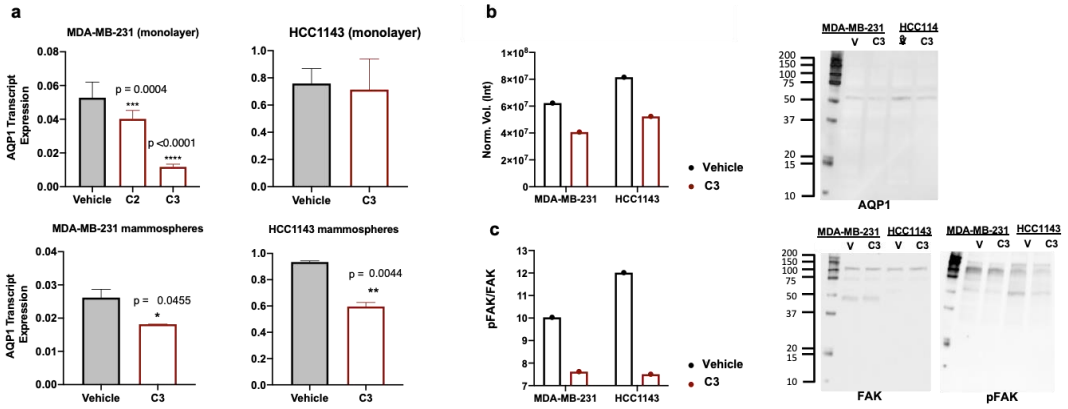

Supplementary Figure 2. (**a**) Expression of AQP1 transcripts in MDA-MB-231 and HCC1143 cells grown as monolayer or mammospheres. The experiment was performed in duplicate and the results are presented as mean ± SD. PureLink RNA mini kit (Life Technologies, Grand Island, NY, USA) was used to extract RNA and 20 ng RNA was used for reverse transcription using iScript cDNA Synthesis Kit (Bio-Rad Laboratories, Hercules, CA, USA). The duplex TaqMan Gene Expression Assays for aquaporin-1 (AQP1; Hs01028916_m1; Applied Biosystems, Foster City, CA, USA) and the reference genes were CCSER2 (HS00982799_mH, Applied Biosystems, Foster City, CA, USA).

Protein expression of (**b**) AQP1 and (**c**) activation of FAK in MDA-MB-231 and HCC1143 mammospheres exposed to vehicle control (V) or C3 (50 μM SRg3 + 25 μM RRg3). Total cell lysates were prepared and quantified. The experiments were repeated 2 times with 20 or 50 μg proteins. The antibodies used for immunostaining include anti-AQP1 antibody [EPR20325] (ab219055, Abcam, Cambridge, UK, 1:1000), anti-FAK antibody [EP6954] (ab40794, Abcam, Cambridge, UK, 1:1000), anti-phospho FAK antibody [EP2]60Y] phosphor Y397 (ab 81298, Abcam, Cambridge, UK, 1:1000). Goat anti-rabbit IgG H&L (HRP) (ab6721, Abcam, Cambridge, UK, 1:3000) was used as the secondary antibody.

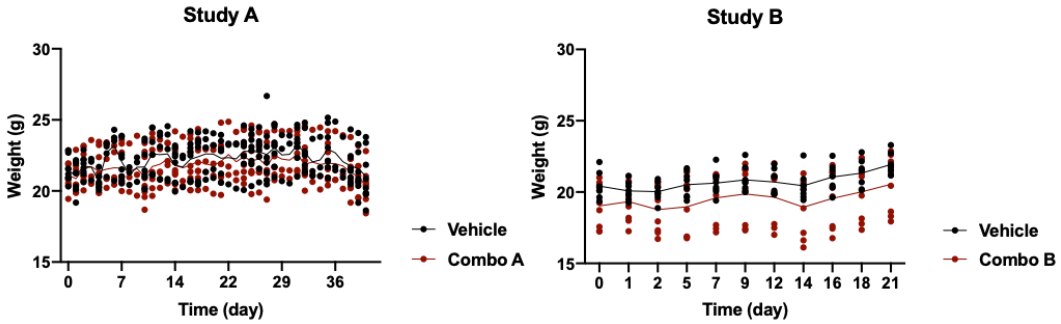

Supplementary Figure 3. Weight pattern of mice in the vehicle- or Rg3-treated groups in study A and B. There were no significant differences between the groups in terms of changes in body weight.

References

[1] K.G.K. Deepak, R. Vempati, G.P. Nagaraju, V.R. Dasari, N. S, D.N. Rao, R.R. Malla, Tumor microenvironment: Challenges and opportunities in targeting metastasis of triple negative breast cancer, Pharmacol. Res. 153 (2020) 104683. https://doi.org/10.1016/j.phrs.2020.104683

[2] A.C. Garrido-Castro, N.U. Lin, K. Polyak, Insights into molecular classifications of triple-negative breast cancer: improving patient selection for treatment, Cancer Discov. 9(2) (2019) 176-198. 10.1158/2159-8290.CD-18-1177

[3] F. Kassam, K. Enright, R. Dent, G. Dranitsaris, J. Myers, C. Flynn, M. Fralick, R. Kumar, M. Clemons, Survival outcomes for patients with metastatic triple-negative breast cancer: implications for clinical practice and trial design, Clin. Breast Cancer 9(1) (2009) 29-33. DOI: 10.3816/CBC.2009.n.005

[4] X. Zeng, C. Liu, J. Yao, H. Wan, G. Wan, Y. Li, N. Chen, Breast cancer stem cells, heterogeneity, targeting therapies and therapeutic implications, Pharmacol. Res. 163 (2021) 105320. https://doi.org/10.1016/j.phrs.2020.105320

[5] S.R. Martins-Neves, A.-M. Cleton-Jansen, C.M.F. Gomes, Therapy-induced enrichment of cancer stem-like cells in solid human tumors: Where do we stand?, Pharmacol. Res. 137 (2018) 193-204. https://doi.org/10.1016/j.phrs.2018.10.011

[6] W. Li, H. Ma, J. Zhang, L. Zhu, C. Wang, Y. Yang, Unraveling the roles of CD44/CD24 and ALDH1 as cancer stem cell markers in tumorigenesis and metastasis, Sci. Rep. 7(1) (2017) 1-15. doi: 10.1038/s41598-017-14364-2

[7] P. Jabbarzadeh Kaboli, F. Salimian, S. Aghapour, S. Xiang, Q. Zhao, M. Li, X. Wu, F. Du, Y. Zhao, J. Shen, C.H. Cho, Z. Xiao, Akt-targeted therapy as a promising strategy to overcome drug resistance in breast cancer – A comprehensive review from chemotherapy to immunotherapy, Pharmacol. Res. 156 (2020) 104806. https://doi.org/10.1016/j.phrs.2020.104806
[8] A. Alwhaibi, A. Verma, M.S. Adil, P.R. Somanath, The unconventional role of Akt1 in the advanced cancers and in diabetes-promoted carcinogenesis, Pharmacol. Res. 145 (2019) 104270. https://doi.org/10.1016/j.phrs.2019.104270
[9] Y. Wu, Y. Zhang, X. Qin, H. Geng, D. Zuo, Q. Zhao, PI3K/AKT/mTOR pathway-related long non-coding RNAs: roles and mechanisms in hepatocellular carcinoma, Pharmacol. Res. 160 (2020) 105195. https://doi.org/10.1016/j.phrs.2020.105195
[10] O. Tetsu, J. Phuchareon, D.W. Eisele, M.J. Hangauer, F. McCormick, AKT inactivation causes persistent drug tolerance to EGFR inhibitors, Pharmacol. Res. 102 (2015) 132-137. https://doi.org/10.1016/j.phrs.2015.09.022
[11] M. Nakhjavani, J.E. Hardingham, H.M. Palethorpe, T.J. Price, A.R. Townsend, Druggable Molecular Targets for the Treatment of Triple Negative Breast Cancer, J. Breast Cancer 22(3) (2019) 341-361. 10.4048/jbc.2019.22.e39
[12] K. Banik, A.M. Ranaware, V. Deshpande, S.P. Nalawade, G. Padmavathi, D. Bordoloi, B.L. Sailo, M.K. Shanmugam, L. Fan, F. Arfuso, G. Sethi, A.B. Kunnumakkara, Honokiol for cancer therapeutics: A traditional medicine that can modulate multiple oncogenic targets, Pharmacol. Res. 144 (2019) 192-209. https://doi.org/10.1016/j.phrs.2019.04.004
[13] Y. Safdari, M. Khalili, M.A. Ebrahimzadeh, Y. Yazdani, S. Farajnia, Natural inhibitors of PI3K/AKT signaling in breast cancer: Emphasis on newly-discovered molecular mechanisms of action, Pharmacol. Res. 93 (2015) 1-10. https://doi.org/10.1016/j.phrs.2014.12.004
[14] M. Nakhjavani, J.E. Hardingham, H.M. Palethorpe, Y. Tomita, E. Smith, T.J. Price, A.R. Townsend, Ginsenoside Rg3: Potential molecular targets and therapeutic indication in metastatic breast cancer, Medicines 6(1) (2019) 17. 10.3390/medicines6010017
[15] M. Nakhjavani, E. Smith, A.R. Townsend, T.J. Price, J.E. Hardingham, Anti-Angiogenic Properties of Ginsenoside Rg3, Molecules 25(21) (2020) 4905. 10.3390/molecules25214905
[16] M. Nakhjavani, H.M. Palethorpe, Y. Tomita, E. Smith, T.J. Price, A.J. Yool, J.V. Pei, A.R. Townsend, J.E. Hardingham, Stereoselective anti-cancer activities of ginsenoside Rg3 on triple negative breast cancer cell models, Pharmaceuticals 12(3) (2019) 117. doi: 10.3390/ph12030117
[17] O.A. Abozaid, F.S. Moawed, M.A. Farrag, R.S. Kawara, Synergistic Effect of Benzethonium Chloride Combined with Endoxan against Hepatocellular Carcinoma in Rats through Targeting Apoptosis Signaling Pathway, Asian Pac. J. Cancer Prev. 21(6) (2020) 1709. 10.31557/APJCP.2020.21.6.1709
[18] W. Zhao, K. Sachsenmeier, L. Zhang, E. Sult, R.E. Hollingsworth, H. Yang, A new bliss independence model to analyze drug combination data, J. Biomol. Screen. 19(5) (2014) 817-821. 10.1177/1087057114521867

[19] C.H. Chui, R.S.M. Wong, G.Y.M. Cheng, F.Y. Lau, S.H.L. Kok, C.H. Cheng, F. Cheung, W.K. Tang, I.T.N. Teo, A.S.C. Chan, Antiproliferative ability of a combination regimen of crocodile egg extract, wild radix ginseng and natural Ganoderma lucidum on acute myelogenous leukemia, Oncol. Rep. 16(6) (2006) 1313-1316. 10.3892/OR.16.6.1313
[20] M. Nakhjavani, E. Smith, K. Yeo, H.M. Palethorpe, Y. Tomita, T.J. Price, A.R. Townsend, J.E. Hardingham, Anti-angiogenic properties of ginsenoside Rg3 epimers; in vitro assessment of single and combination treatments, Angiogenesis (Submitted).
[21] E. Smith, H.M. Palethorpe, Y. Tomita, J.V. Pei, A.R. Townsend, T.J. Price, J.P. Young, A.J. Yool, J.E. Hardingham, The Purified Extract from the Medicinal Plant Bacopa monnieri, Bacopaside II, Inhibits Growth of Colon Cancer Cells In Vitro by Inducing Cell Cycle Arrest and Apoptosis, Cells 7(7) (2018). 10.3390/cells7070081
[22] S. Paltoglou, R. Das, S.L. Townley, T.E. Hickey, G.A. Tarulli, I. Coutinho, R. Fernandes, A.R. Hanson, I. Denis, J.S. Carroll, S.M. Dehm, G.V. Raj, S.R. Plymate, W.D. Tilley, L.A. Selth, Novel Androgen Receptor Coregulator GRHL2 Exerts Both Oncogenic and Antimetastatic Functions in Prostate Cancer, Cancer Res 77(13) (2017) 3417-3430. 10.1158/0008-5472.Can-16-1616
[23] Y. Lombardo, A. de Giorgio, C.R. Coombes, J. Stebbing, L. Castellano, Mammosphere formation assay from human breast cancer tissues and cell lines, J. Vis. Exp. (97) (2015) e52671. 10.3791/52671
[24] W. Zou, Y. Yang, R. Zheng, Z. Wang, H. Zeng, Z. Chen, F. Yang, J. Wang, Association of CD44 and CD24 phenotype with lymph node metastasis and survival in triple-negative breast cancer, Int. J. Clin. Exp. Pathol. 13(5) (2020) 1008.
[25] T. Hiraga, S. Ito, H. Nakamura, Side population in MDA-MB-231 human breast cancer cells exhibits cancer stem cell-like properties without higher bone-metastatic potential, Oncol. Rep. 25(1) (2011) 289-296.
[26] H. Masuda, D. Zhang, C. Bartholomeusz, H. Doihara, G.N. Hortobagyi, N.T. Ueno, Role of epidermal growth factor receptor in breast cancer, Breast Cancer Res. Treat. 136(2) (2012) 331-345. 10.1007/s10549-012-2289-9
[27] A. Bahhnassy, M. Mohanad, S. Shaarawy, M.F. Ismail, A. El-Bastawisy, A.M. Ashmawy, A.R. Zekri, Transforming growth factor-β, insulin-like growth factor I/insulin-like growth factor I receptor and vascular endothelial growth factor-A: Prognostic and predictive markers in triple-negative and non-triple-negative breast cancer, Mol. Med. Rep. 12(1) (2015) 851-864. 10.3892/mmr.2015.3560
[28] T. Toyama, H. Yamashita, N. Kondo, K. Okuda, S. Takahashi, H. Sasaki, H. Sugiura, H. Iwase, Y. Fujii, Frequently increased epidermal growth factor receptor (EGFR) copy numbers and decreased BRCA1 mRNA expression in Japanese triple-negative breast cancers, BMC Cancer. 8(1) (2008) 309. 10.1186/1471-2407-8-309
[29] C.-W. Wu, K.B. Storey, Regulation of the mTOR signaling network in hibernating thirteen-lined ground squirrels, J. Exp. Biol. 215(10) (2012) 1720-1727. 10.1242/jeb.066225
[30] I. Ruvinsky, N. Sharon, T. Lerer, H. Cohen, M. Stolovich-Rain, T. Nir, Y. Dor, P. Zisman, O. Meyuhas, Ribosomal protein S6 phosphorylation is a determinant of cell size and glucose homeostasis, Genes Dev. 19(18) (2005) 2199-2211. 10.1101/gad.351605

[31] Y. Romeo, X. Zhang, P.P. Roux, Regulation and function of the RSK family of protein kinases, Biochem. J. 441(2) (2012) 553-569. 10.1042/BJ20110289
[32] R. Anjum, J. Blenis, The RSK family of kinases: emerging roles in cellular signalling, Nat. Rev. Mol. Cell Biol. 9(10) (2008) 747-758.
[33] M. Hekman, A. Fischer, L.P. Wennogle, Y.K. Wang, S.L. Campbell, U.R. Rapp, Novel C-Raf phosphorylation sites: serine 296 and 301 participate in Raf regulation, FEBS Lett. 579(2) (2005) 464-468. DOI: 10.1016/j.febslet.2004.11.105
[34] T.M. Cardillo, P. Trisal, R. Arrojo, D.M. Goldenberg, C.-H. Chang, Targeting both IGF-1R and mTOR synergistically inhibits growth of renal cell carcinoma in vitro, BMC cancer 13(1) (2013) 1-14. https://doi.org/10.1186/1471-2407-13-170
[35] S.-E. Lamhamedi-Cherradi, B.A. Menegaz, V. Ramamoorthy, D. Vishwamitra, Y. Wang, R.L. Maywald, A.S. Buford, I. Fokt, S. Skora, J. Wang, IGF-1R and mTOR blockade: novel resistance mechanisms and synergistic drug combinations for Ewing sarcoma, J. Natl. Cancer Inst. 108(12) (2016). 10.1093/jnci/djw182
[36] P. Ji, Y. Zhang, S.-J. Wang, H.-L. Ge, G.-P. Zhao, Y.-C. Xu, Y. Wang, CD44hiCD24lo mammosphere-forming cells from primary breast cancer display resistance to multiple chemotherapeutic drugs, Oncology reports 35(6) (2016) 3293-3302.
[37] A. Giatromanolaki, E. Sivridis, A. Fiska, M.I. Koukourakis, The CD44+/CD24− phenotype relates to 'triple-negative'state and unfavorable prognosis in breast cancer patients, Med. Oncol. 28(3) (2011) 745-752. 10.1007/s12032-010-9530-3
[38] M. Shipitsin, L.L. Campbell, P. Argani, S. Weremowicz, N. Bloushtain-Qimron, J. Yao, T. Nikolskaya, T. Serebryiskaya, R. Beroukhim, M. Hu, Molecular definition of breast tumor heterogeneity, Cancer Cell. 11(3) (2007) 259-273. 10.1016/j.ccr.2007.01.013
[39] B.K. Abraham, P. Fritz, M. McClellan, P. Hauptvogel, M. Athelogou, H. Brauch, Prevalence of CD44+/CD24−/low cells in breast cancer may not be associated with clinical outcome but may favor distant metastasis, Clin. Cancer Res. 11(3) (2005) 1154-1159.
[40] C. Sheridan, H. Kishimoto, R.K. Fuchs, S. Mehrotra, P. Bhat-Nakshatri, C.H. Turner, R. Goulet, S. Badve, H. Nakshatri, CD44+/CD24-breast cancer cells exhibit enhanced invasive properties: an early step necessary for metastasis, Breast Cancer Res. 8(5) (2006) R59. 10.1186/bcr1610
[41] P. Van Phuc, P.L.C. Nhan, T.H. Nhung, N.T. Tam, N.M. Hoang, V.G. Tue, D.T. Thuy, P.K. Ngoc, Downregulation of CD44 reduces doxorubicin resistance of CD44+ CD24− breast cancer cells, Onco Targets Ther 4 (2011) 71. 10.2147/OTT.S21431
[42] J. Oh, H.-J. Yoon, J.-H. Jang, D.-H. Kim, Y.-J. Surh, The standardized Korean Red Ginseng extract and its ingredient ginsenoside Rg3 inhibit manifestation of breast cancer stem cell–like properties through modulation of self-renewal signaling, J. Ginseng Res. 43(3) (2019) 421-430. 10.1016/j.jgr.2018.05.004
[43] H. Xu, Y. Tian, X. Yuan, H. Wu, Q. Liu, R.G. Pestell, K. Wu, The role of CD44 in epithelial–mesenchymal transition and cancer development, Onco Targets Ther. 8 (2015) 3783. 10.2147/OTT.S95470
[44] X. Li, N. Zhou, J. Wang, Z. Liu, X. Wang, Q. Zhang, Q. Liu, L. Gao, R. Wang, Quercetin suppresses breast cancer stem cells (CD44+/CD24−) by inhibiting the PI3K/Akt/mTOR-signaling pathway, Life Sci. 196 (2018) 56-62. 10.1016/j.lfs.2018.01.014

[45] C. Lu, L. Makala, D. Wu, Y. Cai, Targeting translation: eIF4E as an emerging anticancer drug target, Expert Rev. Mol. Med. 18 (2016). 10.1017/erm.2015.20
[46] A.C. Rutkovsky, E.S. Yeh, S.T. Guest, V.J. Findlay, R.C. Muise-Helmericks, K. Armeson, S.P. Ethier, Eukaryotic initiation factor 4E-binding protein as an oncogene in breast cancer, BMC Cancer. 19(1) (2019) 1-15. 10.1186/s12885-019-5667-4
[47] B. Pons, V. Peg, M.Á. Vázquez-Sánchez, L. López-Vicente, E. Argelaguet, L. Coch, A. Martínez, J. Hernández-Losa, G. Armengol, S. Ramon y Cajal, The effect of p-4E-BP1 and p-eIF4E on cell proliferation in a breast cancer model, Int. J. Oncol. 39(5) (2011) 1337-1345. 10.3892/ijo.2011.1118
[48] Nathaniel W. Hartman, Tiffany V. Lin, L. Zhang, Grace E. Paquelet, David M. Feliciano, A. Bordey, mTORC1 Targets the Translational Repressor 4E-BP2, but Not S6 Kinase 1/2, to Regulate Neural Stem Cell Self-Renewal In Vivo, Cell Rep. 5(2) (2013) 433-444. https://doi.org/10.1016/j.celrep.2013.09.017
[49] L. Guo, J. Abraham, D. Flynn, V. Castranova, X. Shi, Y. Qian, Individualized survival and treatment response predictions for breast cancers using phospho-EGFR, phospho-ER, phospho-HER2/neu, phospho-IGF-IR/In, phospho-MAPK, and phospho-p70S6K proteins, Int. J Biol. Marker. 22(1) (2007) 1-11. 10.5301/jbm.2008.3686
[50] L. Xiao, Y.C. Wang, W.S. Li, Y. Du, The role of mTOR and phospho-p70S6K in pathogenesis and progression of gastric carcinomas: an immunohistochemical study on tissue microarray, J. Exp. Clin. Cancer Res. 28(1) (2009) 152. 10.1186/1756-9966-28-152
[51] B. Chen, Z. Tan, J. Gao, W. Wu, L. Liu, W. Jin, Y. Cao, S. Zhao, W. Zhang, Z. Qiu, Hyperphosphorylation of ribosomal protein S6 predicts unfavorable clinical survival in non-small cell lung cancer, J. Exp. Clin. Cancer Res. 34(1) (2015) 126. 10.1186/s13046-015-0239-1
[52] Y.-Z. Lu, A.-M. Deng, L.-H. Li, G.-Y. Liu, G.-Y. Wu, Prognostic role of phospho-PRAS40 (Thr246) expression in gastric cancer, Arch. Med. Res. 10(1) (2014) 149. doi: 10.5114/aoms.2013.36927
[53] M. Shipitsin, C. Small, E. Giladi, S. Siddiqui, S. Choudhury, S. Hussain, Y.E. Huang, H. Chang, D.L. Rimm, D.M. Berman, Automated quantitative multiplex immunofluorescence in situ imaging identifies phospho-S6 and phospho-PRAS40 as predictive protein biomarkers for prostate cancer lethality, Proteome Sci. 12(1) (2014) 40. 10.1186/1477-5956-12-40
[54] H. Zhao, T.A. Martin, E.L. Davies, F. Ruge, H. Yu, Y. Zhang, X. Teng, W.G. Jiang, The Clinical Implications of RSK1-3 in Human Breast Cancer, Anticancer Res. 36(3) (2016) 1267-1274.
[55] K.A. Ludwik, J.P. Campbell, M. Li, Y. Li, Z.M. Sandusky, L. Pasic, M.E. Sowder, D.R. Brenin, J.A. Pietenpol, G.A. O'Doherty, Development of a RSK inhibitor as a novel therapy for triple-negative breast cancer, Mol. Cancer Ther. 15(11) (2016) 2598-2608. doi: 10.1158/1535-7163.MCT-16-0106
[56] S.P. Herbert, G. Costa, Sending messages in moving cells: mRNA localization and the regulation of cell migration, Essays. Biochem. 63(5) (2019) 595-606. 10.1042/EBC20190009

[57] M. Willett, M. Brocard, A. Davide, S.J. Morley, Translation initiation factors and active sites of protein synthesis co-localize at the leading edge of migrating fibroblasts, Biochem. J. 438(1) (2011) 217-227. 10.1042/BJ20110435
[58] S. Mollard, R. Fanciullino, S. Giacometti, C. Serdjebi, S. Benzekry, J. Ciccolini, In vivo bioluminescence tomography for monitoring breast tumor growth and metastatic spreading: comparative study and mathematical modeling, Sci. Rep. 6 (2016) 36173. doi: 10.1038/srep36173
[59] S. Choi, T.W. Kim, S.V. Singh, Ginsenoside Rh2-mediated G 1 phase cell cycle arrest in human breast cancer cells is caused by p15 Ink4B and p27 Kip1-dependent inhibition of cyclin-dependent kinases, Pharm. Res. 26(10) (2009) 2280-2288.
[60] J.H. Kwak, J.Y. Park, D. Lee, J.Y. Kwak, E.H. Park, K.H. Kim, H.-J. Park, H.Y. Kim, H.J. Jang, J. Ham, Inhibitory effects of ginseng sapogenins on the proliferation of triple negative breast cancer MDA-MB-231 cells, Bioorganic Med. Chem. Lett. 24(23) (2014) 5409-5412.
[61] H.M. Palethorpe, E. Smith, Y. Tomita, M. Nakhjavani, A.J. Yool, T.J. Price, J.P. Young, A.R. Townsend, J.E. Hardingham, Bacopasides I and II act in synergy to inhibit the growth, migration and invasion of breast cancer cell lines, Molecules 24(19) (2019) 3539. 10.3390/molecules24193539
[62] Y. Tomita, H.M. Palethorpe, E. Smith, M. Nakhjavani, A.R. Townsend, T.J. Price, A.J. Yool, J.E. Hardingham, Bumetanide-derived aquaporin 1 inhibitors, AqB013 and AqB050 inhibit tube formation of endothelial cells through induction of apoptosis and impaired migration in vitro, Int. J. Mol. Sci. 20(8) (2019) 1818.

Chapter 5 Efficacy of the metabolites of ginsenoside Rg3

5.1. Background

As reviewed in chapter 1, a fundamental challenge with the administration of Rg3, which is more evident in oral administration, is its extensive metabolism. In fact, Rg3 could be considered as not only a drug, but also a prodrug. The major active metabolites of Rg3 are deglycosylated epimers of ginsenoside Rh2 (S-Rh2 and R-Rh2) and protopanaxadiol (S-PPD and R-PPD). In this chapter, the efficacy of these molecules in inhibition of proliferation of a TNBC cell line and a human endothelial cell were studied. The mode of cell death in both cell types and the possibility of two programmed cell death types, apoptosis and necroptosis, was investigated using live cell imaging and discussed.

Furthermore, the effect of epimers on loop formation and their potential anti-angiogenic effects is discussed. The interaction of the epimers with VEGFR2 was studied using *in silico* molecular docking and *in vitro* studies. *In silico* molecular docking was also used to screen for the interaction of these molecules with AQPs to see whether these molecules have the potential to block AQP water transport.

This chapter was submitted to "*Journal of Ginseng Research*" and is currently under review.

5.2. Statement of Authorship

Statement of Authorship

Title of Paper	Differential anticancer activities of the active metabolites of ginsenoside Rg3
Publication Status	☐ Published ☑ Accepted for Publication ☐ Submitted for Publication ☐ Unpublished and Unsubmitted work written in manuscript style
Publication Details	Nakhjavani, M., Smith, E., Yeo, K., Tomita, Y., Price, T. J., Yool, A. J., Townsend, A. R., and Hardingham, J. E. Differential anticancer activities of the active metabolites of ginsenoside Rg3. Accepted for publication in Journal of Ginseng Research.

Principal Author

Name of Principal Author (Candidate)	Maryam Nakhjavani		
Contribution to the Paper	Conceptualised, designed and performed the experiments, analysed and curated the data, and substantially wrote the manuscript.		
Overall percentage (%)	70		
Certification:	This paper reports on original research I conducted during the period of my Higher Degree by Research candidature and is not subject to any obligations or contractual agreements with a third party that would constrain its inclusion in this thesis. I am the primary author of this paper.		
Signature		Date	10th Feb 2021

Co-Author Contributions

By signing the Statement of Authorship, each author certifies that:

i. the candidate's stated contribution to the publication is accurate (as detailed above);
ii. permission is granted for the candidate in include the publication in the thesis; and
iii. the sum of all co-author contributions is equal to 100% less the candidate's stated contribution.

Name of Co-Author	Eric Smith		
Contribution to the Paper	Contributed to designing the experiment, data analysis, discussion and reviewing the paper.		
Signature		Date	10th Feb 2021

Name of Co-Author	Kenny Yeo		
Contribution to the Paper	Contributed to performing the experiment and discussion.		
Signature		Date	8th Feb 2021

Name of Co-Author	Yoko Tomita		
Contribution to the Paper	Contributed to the discussion and review ing the paper.		
Signature		Date	12th Feb 2021

Name of Co-Author	Timothy J Price		
Contribution to the Paper	Contributed to the discussion and review ing the paper.		
Signature		Date	11th Feb 2021

Name of Co-Author	Andrea Yool		
Contribution to the Paper	Contributed to drafting and discussion and review ing the paper.		
Signature		Date	10th Feb 2021

Name of Co-Author	Amanda R Tow nsend		
Contribution to the Paper	Contributed to the discussion and review ing the paper.		
Signature		Date	11th Feb 2021

Name of Co-Author	Jennifer E Hardingham		
Contribution to the Paper	Conceptualised and designed the experiments, contributed in data analysis and curation, and review ing the paper.		
Signature		Date	10th Feb 2021

Article

Differential anticancer activities of the active metabolites of ginsenoside Rg3

Maryam Nakhjavani [1], Eric Smith [1,2*], Kenny Yeo [1,2], Yoko Tomita [1,2,3], Timothy J. Price [2,3], Andrea Yool [2], Amanda R. Townsend [2,3] and Jennifer E. Hardingham [1,2,]

[1] Molecular Oncology, Basil Hetzel Institute for Translational Health Research, The Queen Elizabeth Hospital, Woodville South, SA 5011, Australia; maryam.nakhjavani@adelaide.edu.au; yoko.tomita@adelaide.edu.au

[2] Adelaide Medical School, University of Adelaide, Adelaide, SA 5005, Australia; jenny.hardingham@sa.gov.au, andrea.yool@adelaide.edu.au, a1811332@student.adelaide.edu.au

[3] Medical Oncology Unit, The Queen Elizabeth Hospital, Woodville South, SA 5011, Australia; amanda.townsend@sa.gov.au; timothy.price@sa.gov.au

* Correspondence: eric.smith@adelaide.edu.au; Tel.: +61 8 8222 6142

Abstract

Epimers of ginsenoside Rg3 (Rg3) have low bioavailability and are prone to deglycosylation, which produces epimers of ginsenoside Rh2 (S-Rh2 and R-Rh2) and protopanaxadiol (S-PPD and R-PPD). This study aimed to compare the efficacy and potency of these molecules as anti-cancer agents. Crystal violet staining was used to study the anti-proliferatory action of the molecules on MDA-MB-231 and HUVEC cells and compare their potency. Cell death and cell cycle were studied using flow cytometry and the mode of cell death was studied using live cell imaging. Anti-angiogenic effects of the drug were studied using loop formation assay. Molecular docking showed the interaction of these molecules with vascular endothelial growth factor receptor-2 (VEGFR2) and aquaporin (AQP) water channels. VEGF bioassay was used to study the interaction of Rh2 with VEGFR2, *in vitro*. HUVEC was the more sensitive cell line to the anti-proliferative effects of S-Rh2, S-PPD and R-PPD. The molecules induced necroptosis/necrosis in MDA-MB-231 and apoptosis in HUVEC. S-Rh2 was the most potent inhibitor of loop formation. *In silico* molecular docking predicted a good binding score between Rh2 or PPD and the ATP-binding pocket of VEGFR2. VEGF bioassay showed that Rh2 was an allosteric modulator of VEGFR2. In addition, SRh2 and PPD had good binding scores with AQP1 and AQP5, both of which play roles in cell migration and proliferation. The combination of these molecules might be responsible for the anti-cancer effects observed by Rg3.

Keywords: Ginsenoside Rg3, Ginsenoside Rh2, Protopanaxadiol, Epimer, Triple negative breast cancer, Angiogenesis

1. Introduction

Ginsenoside Rg3 (Rg3) is one of the best studied members of the ginsenoside family of molecules extracted from *Panax ginseng*. Like other ginsenosides, Rg3 has two epimers; 20(S)-ginsenoside Rg3 (SRg3) and 20(R)-ginsenoside Rg3 (RRg3). Several

studies have reported the anticancer properties of epimers of Rg3 (reviewed in [1, 2]). Orally administered Rg3 is a registered drug in China [3] and has been evaluated as a single drug in clinical trials in lung [4] and liver cancer patients [5] or in combination with other chemotherapies [3, 6]. However, several *in vitro* and *in vitro* animal studies have suggested an extensive metabolism of Rg3 in the gastrointestinal tract (reviewed in [1]). For example, low bioavailability of less than 3% was reported in Sprague–Dawley rats [7]. Furthermore, after oral administration of 3.2 mg/kg of Rg3 [8] and RRg3 [9] in healthy people, t_{max} (time required to reach the maximum plasma concentration) was about 40 minutes and C_{max} was about 16 and 1 ng/mL, respectively. These data suggested that metabolites of Rg3 could contribute to the oral efficacy of Rg3. While deglycosylation and oxygenation are reported as two major metabolic pathways of Rg3, deglycosylation is a more important pathway as it leads to the formation of the active metabolites ginsenoside Rh2 (Rh2) and protopanaxadiol (PPD) (Figure 1). Peng *et al.* (2016) showed that after oral or intravenous administration of SRg3 and RRg3, the respective deglycosylated epimers are detected in rats' plasma, namely 20(S)-ginsenoside Rh2 (S-Rh2), 20(R)-ginsenoside Rh2 (R-Rh2), 20(S)-protopanaxadiol (S-PPD) and 20(R)-protopanaxadiol (R-PPD) (Figure 1) [10].

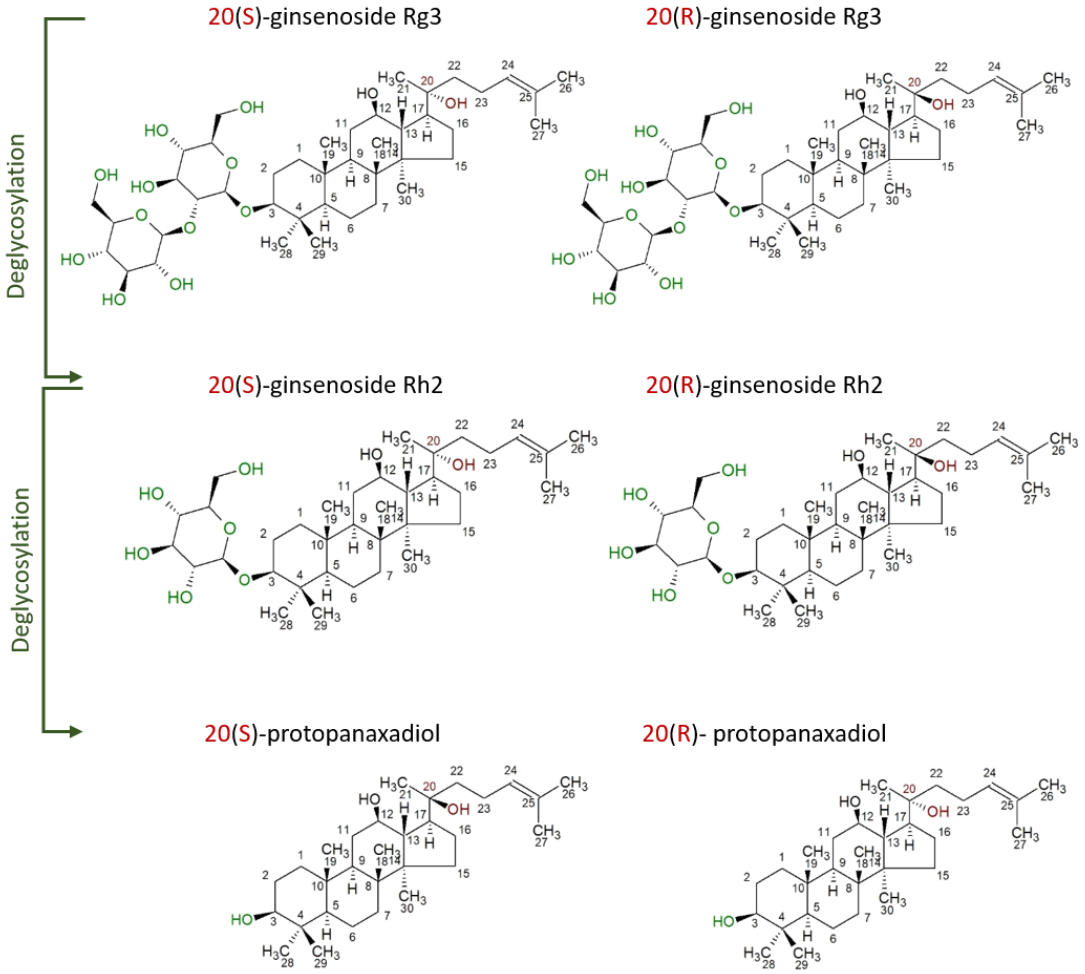

Figure 1. The structure of epimers of ginsenoside Rg3 and their metabolites. Deglycosylation of 20(S)- and 20(R)-ginsenoside Rg3 produces 20(S)- and 20(R)-ginsenoside Rh2 and 20(S)- and 20(R)-protopanaxadiol. The stereocenter on C_{20} is highlighted with a red colour and heteroatoms of the sugar molecules are shown in green.

Our group has been interested in finding novel treatments for metastatic triple-negative breast cancer patients. We have shown the stereoselective activities of SRg3 and RRg3 in inhibition of the proliferation, migration and invasion of triple negative breast cancer cell lines [11]. Aquaporins (AQPs) have been shown to play roles in cell proliferation, migration, invasion and angiogenesis (reviewed in [2, 12]). AQP1, AQP4 and AQP5 localize at the leading edge of migrating cells and facilitate cell migration. Using molecular docking, we showed that Rg3 blocks AQP1 water channel with a good binding score (-9.4 kJ/mol), and *in vitro*, using oocyte swelling assay we showed that only SRg3, stereoselectively, blocked the water transport function of AQP1 [11].

Continuing with the screening of ginsenosides as potential treatment options for metastatic triple-negative breast cancer, given the *in vivo* efficacy of Rg3 in lung and liver cancer, the aim of the current research was to investigate the anticancer properties of epimers of Rh2 and PPD, as potentially active metabolites of Rg3, which could contribute to the effects observed by this drug.

2. Materials and Methods

2.1. Cell lines, reagents and cell culture

MDA-MB-231 was purchased from American Type Culture Collection (ATCC; Manassas, VA, USA) and grown in Dulbecco's modified Eagle's medium (DMEM; Life Technologies, Carlsbad, CA, USA) supplemented with 10% foetal bovine serum (FBS) (Corning, NY, USA) and 1% penicillin-streptomycin (pen strep; Life Technologies, Carlsbad, CA, USA). Human umbilical vein endothelial cells (HUVECs) and its media, EBM-2 Endothelial Cell Growth Medium-2 were both from Lonza (Lonza, Basel, Switzerland). 20(S)- and 20(R)- epimers of ginsenoside Rh2 and protopanaxadiol were from ChemFaces Biochemical Co. (Wuhan, China). Drugs were dissolved in dimethyl sulfoxide (DMSO D2650, HYBRI-MAX, Sigma-Aldrich, St Louis, MO, USA). Stocks of 50 mM of the molecules was prepared and 25 mM aliquots were kept at -20°C to avoid freeze-thawing cycles. Concentrations of 0-100 μM of ginsenosides were used with maximum of 0.2% DMSO as the vehicle control. Cell lines were mycoplasma-free, as determined using the MycoAlert Detection Kit (Lonza) and/or a custom PCR-based assay, as described previously [13, 14].

2.2. Proliferation Assay

To test the efficacy of the ginsenosides on cell proliferation, crystal violet assay (CVA) was used, as previously described [11]. Briefly, MDA-MB-231 and HUVEC cells were seeded at 3×10^3 and 0.8×10^3 cells/well of 96-well plates. On days 0, 1 and 3, CVA was performed and the absorbance of each well was read using FLUOstar Optima microplate reader (BMG Labtech, Offenburg, Germany) at 595 nm. The experiment included 6 replicates and the data are shown as mean ± standard deviation (SD).

2.3. Cell viability and half-maximal inhibitory concentration (IC_{50}) calculation

Based on CVA data on day 3, cell viability and dose-response curves were plotted using non-linear regression using log(inhibitor) vs. normalized response using

GraphPad Prism (version 9.0.0 for Mac, GraphPad Software, San Diego, California USA, www.graphpad.com) to calculate IC_{50}.

2.4. Loop formation assay

As previously described [15], 10 µL of Matrigel® (Corning® Matrigel® Basement Membrane Matrix, LDEV-free, cat# 354234, NY, USA) was used to coat each well of an Angiogenesis 96 Well µ-Plate (Ibidi, Martinsried, Germany). HUVEC was seeded at 1.5×10^4 cells/well and exposed to the vehicle or 1, 10, 50 and 100 µM of ginsenosides. The number of formed loops in each well was counted after 8 h. The experiment was performed in triplicate. The data are presented as mean ± SD.

2.5. Flow cytometric analysis of cell death

The assay was performed as previously described [11, 16]. Briefly, MDA-MB-231 and HUVEC cells were seeded at 1×10^5 and 0.5×10^5 cells/well of six-well plates and incubated overnight and then exposed with the drugs or vehicle for 3 days. Cells were harvested, stained using Annexin-V-FLUOS Staining Kit (Roche Diagnostics, Mannheim, Germany) and analysed using a BD FACSCanto II (BD Biosciences, San Jose, CA, USA), capturing 10,000 single-cell events per sample. Data were analysed using FlowJo software v10.4.0 (FlowJo, LLC, Ashland, OR, USA). The experiment was performed in triplicate and the data are presented as mean ± SD.

2.6. Flow cytometric analysis of cell cycle

The assay was performed as previously described [11, 16]. Briefly, MDA-MB-231 and HUVEC cells were seeded at 1×10^5 and 0.5×10^5 cells/well of six-well plates and incubated overnight. Cells were exposed to the drugs or vehicle. After a 3-day exposure, the cells were harvested, washed twice and resuspended ice-cold Dulbecco's phosphate buffered saline (DPBS, Gibco, Thermo Fisher Scientific, Waltham, MA, USA) with drop-wise addition of an equal volume of 100% ice-cold ethanol. The cells were fixed at -20°C for 2 h, washed and resuspended in 100 µL of propidium iodide (PI) staining solution consisting of 25 µg/mL PI (Sigma-Aldrich, St Louis, MO, USA), 40 µg/mL bovine pancreas ribonuclease A (Sigma-Aldrich), and 0.25% Triton X-100 (Sigma-Aldrich) in DPBS. The stained cells were analysed with a BD FACSCanto II, capturing 10,000 single-cell events per sample. Data were analysed using FlowJo. The experiment was performed in triplicate and the data are presented as mean ± SD. The sub-G1 population was considered as cell death. To calculate cell cycle arrest in each phase, the sub-G1 population was excluded.

2.7. Studying mode of cell death using IncuCyte

MDA-MB-231 and HUVEC cells were seeded at 6.6×10^3 and 1.5×10^3 cells/well of 96-well flat-bottomed plates. Following overnight incubation, the cells were treated with Rh2 and PPD epimers or vehicle, containing 1:1000 dilution of Caspase-3/7 Green Detection Reagent (CellEvent™, Thermo Fisher Scientific) to detect apoptosis. To detect necrosis, 2.5 µg/mL PI was used. Drozitumab 100 ng/mL and staurosporine 0.25 µM (Sigma-Aldrich) were used as positive controls for apoptosis in MDA-MB-231 and HUVEC, respectively [17, 18]. Drozitumab was freshly prepared by combining equal

volumes of 100 ng/μL of drozitumab (Genentech, South San Francisco, CA, USA) with 100 ng/μL of affinity purified goat anti-human IgG Fcγ fragment (Jackson Immunoresearch Laboratories West Grove, PA, USA), incubating for 30 min at 4° C, and then diluting in culture medium for a final concentration of 100 ng/mL of drozitumab [18]. The number of positive cells for activation of caspase 3/7 or staining with PI was determined using an IncuCyte S3 Live-Cell Analysis System (Sartorius, Goettingen, Germany), acquiring four images per well every 2 h for 48 h.

2.8. Molecular docking

Crystal structures of VEGFR2 (2XIR and 3V2A), AQP1 (1FQY), AQP2 (4NEF), AQP4 (3GD8) and AQP5 (3D9S) were obtained from the protein data bank of NCBI (RCSB PDB). Canonical SMILES structures of Rh2 [19] and PPD [20] available on PubChem were used to prepare the 3D structure of each molecule in the UCSF Chimera program (version 1.15-mac64). The molecular docking was performed as previously described [11, 21], using UCSF Chimera program and Autodock Vina algorithm (version 1.1.2_Mac_Catalina_64bit). The energies of interaction were predicted based on the flexible ligand docking simulations run within the docking grids on the intracellular side of the monomeric pores.

2.9. VEGF bioassay

VEGF Bioassay (Promega, Madison, WI, USA) was used to study the effects of S-Rh2 on the activation of VEGFR2. This bioluminescent kit includes KDR/NFAT-RE HEK293 cells, in which activation of VEGFR2 triggers NFAT-RE-mediated luminescence. According to the manufacturer's protocol, the cells were seeded in white, flat-bottom 96-well assay plates (Delta Surface ™, Thermo Scientific, Roskilde, Denmark). Cells received serial dilutions of S-Rh2 at a maximum final concentration of 100 μM, alone or in combination with VEGF-A (recombinant VEGF, Promega) at a constant final concentration of 35 ng/mL (80% effective concentration). Controls included bevacizumab and VEGF-A at the maximum final concentration of 6 μg/mL and 0.1 μg/mL, respectively. After 6 h of incubation, the cells were exposed to Bio-Glo™ Reagent, incubated for 10 minutes and then the luminescence was read using the Optima plate reader. The relative luminescence units (RLU) in each well were subtracted from the background. The experiment was performed in duplicate.

2.10. Statistical analysis

One-way or two-way analysis of variance (ANOVA) was performed using GraphPad Prism version 9.0.0 for Mac, GraphPad Software, San Diego, California USA, www.graphpad.com.

3. Results

3.1. Rh2 and PPD inhibit the proliferation of HUVEC and MDA-MB-231

The results of the anti-proliferative effects of epimers of Rh2 and PPD are shown in Figure 2, and the associated IC_{50} are presented in Table 1. In MDA-MB-231, 50 μM

(p = 0.007) and 100 μM (p = 0.0009) S-Rh2 significantly inhibited cell proliferation and in HUVEC, 12.5, 25, 50 and 100 μM (p < 0.0001) significantly inhibited cell proliferation. The IC_{50} for S-Rh2 was 59 μM in MDA-MB-231, while the IC_{50} in HUVEC was 9 μM, showing that HUVEC was more sensitive to the anti-proliferation effects of S-Rh2.

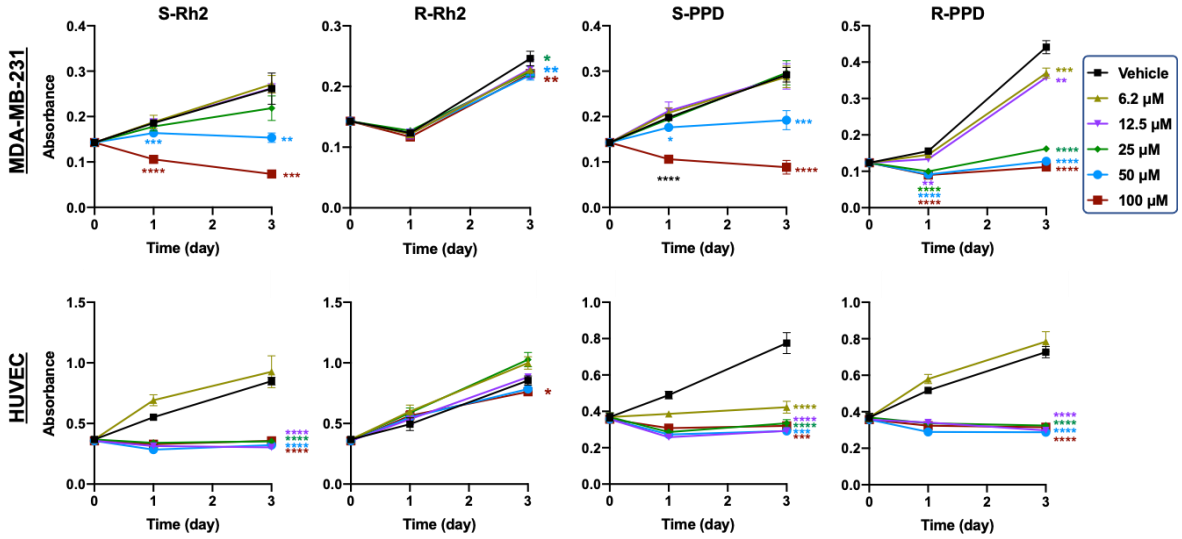

Figure 2. Crystal violet assay on MDA-MB-231 and HUVEC cells exposed to 0-100 μM of S-Rh2, R-Rh2, S-PPD or R-PPD for up to 3 days. Each data point represents mean ± SD of 6 replicates. * p = 0.01, ** p = 0.007, *** p < 0.001, **** p < 0.0001.

R-Rh2 showed much less inhibitory action on MDA-MB-231 and HUVECs (Figure 2) and IC_{50} values could not be calculated for this molecule, indicating that S-Rh2 is the active form of Rh2 responsible for its anti-proliferative action in these cells. Similar to S-Rh2, S-PPD was more effective on HUVECs. All of the tested concentrations of S-PPD significantly inhibited the proliferation of HUVECs (p < 0.0001), while in MDA-MB-231, only 50 μM (p = 0.0002) and 100 μM (p < 0.0001) significantly inhibited the proliferation (Figure 2).

Table 1. The calculated half-maximal inhibitory concentration (IC_{50}) causing reduced survival of MDA-MB-231 and HUVEC cells treated with S-Rh2, S-PPD or R-PPD, at 72 h.

	IC_{50} (μM) (95% log confidence interval)		
	S-Rh2	S-PPD	R-PPD
MDA-MB-231	59 (1.625-1.940)	50 (1.691-1.712)	16 (1.183-1.247)
HUVEC	9 (8.619-8.644)	5 (0.7334-0.7334)	9 (0.9696-0.9696)

IC_{50} values of S-PPD in MDA-MB-231 and HUVECs were 50 and 5 μM, respectively (Table 1). This showed that HUVECs were more sensitive to the anti-proliferation effects of S-PPD. R-PPD, compared to S-PPD, was more potent on MDA-MB-231. All tested concentrations of R-PPD significantly inhibited the proliferation of this cell line (p < 0.0001) (Figure 2). The IC_{50} of R-PPD in MDA-MB-231 and HUVEC was 16 μM and 9 μM, respectively (Table 1). R-PPD, at any concentration above 12.5 μM significantly (p < 0.0001) inhibited the proliferation of HUVEC (Figure 2). Altogether, the above data suggested that HUVEC was more sensitive than MDA-MB-

231 to the anti-proliferative effects of these molecules. Except for R-Rh2, all the other molecules showed effective inhibition of proliferation. In HUVEC, S-Rh2, S-PPD and R-PPD showed similar efficacies. In contrast, MDA-MB-231 was more sensitive to R-PPD than S-Rh2 and S-PPD.

3.2. Rh2 and PPD epimers induce cell death and cell cycle arrest

In MDA-MB-231, the pattern of distribution of dead cells was different from HUVEC. Although a high proportion of MDA-MB-231 and HUVEC cells were located in quadrant (Q) 3 of the flow cytometry plot, annexin V-positive, MDA-MB-231 cells also had a distinct population in Q2 annexin V-/PI-positive, late apoptosis or necroptosis/necrosis (Figure 3). In these cells, 50 μM S-Rh2 did not induce cell death (Figure 3a) but increased cell cycle arrest in S phase by 34% (Figure 3b). At 100 μM ($p = 0.0004$) S-Rh2 induced approximately 80% cell death (Figure 3a) and increased cell cycle arrest in S phase by 99% ($p < 0.0001$) in the remaining 20% cells (Supplementary Figure 1). To determine whether the cells were undergoing apoptosis or necrosis, caspase 3/7 reagent was used to detect the activation of apoptosis or with PI to detect loss of cell membrane integrity (Figure 4). At 50 and 100 μM S-Rh2, no activation of caspase 3/7 was observed (Figure 4a). In contrast, at 100 μM a rapid increase in PI staining was observed, consistent with the observed cell death. These findings suggest that the annexin V-positive MDA-MB-231 cells observed following S-Rh2 treatment are not due to induction of apoptosis but are likely to be the result of a loss in membrane integrity. Necroptosis is a caspases-independent programmed cell death, in which similar to apoptotic cells, phosphatidylserine in the cell membrane is flipped and cell rupture results in the release of DAMPs recruiting immune cells to also prompt a non-inflammatory cell death [22, 23]. *In vitro* and in the absence of immune cells and phagocytosis, the cell membrane of late necroptotic cells becomes leaky and the cells become positive for both annexin V and PI [24]. The rapidly increased PI staining induced by 100 μM S-Rh2 in MDA-MB-231 might indicate a necroptotic/necrosis phenomenon or a combination of both.

In HUVEC, 50 and 100 μM S-Rh2 rapidly (within 2 h) induced activation of caspase 3/7 (Figure 4c) and loss of membrane integrity (Figure 4d). The count of positively stained cells reduced over time and examination of the images revealed that this was due to progressive disintegration of the positive cells. After 3 days of treatment, the majority of the remaining cells (71% for 50 and 100 μM) were annexin V-positive/PI-negative (Figure 3c). These remaining cells had arrested at S phase and the G2/M population had disappeared (Figure 3d, Supplementary Figure 1). Overall, results showed that S-Rh2 was an inducer of necrosis in MDA-MB-231 and apoptosis in HUVEC.

In both cell types, R-Rh2 caused a minimal increase in annexin V/PI staining (Figure 3a and 3c), indicating a minimum induction of cell death, consistent with the results of proliferation assay (Figure 2) and the caspase 3/7 and PI experiments (Figure 4). It induced cell cycle arrest in S phase by about 40% ($p < 0.0001$) in MDA-MB-231 and cell cycle arrest in G0/G1 phase in HUVEC by about 3% ($p < 0.01$) suggesting that

cell cycle arrest is a dominant mechanism of this molecule in inhibition of proliferation (Supplementary Figure 1).

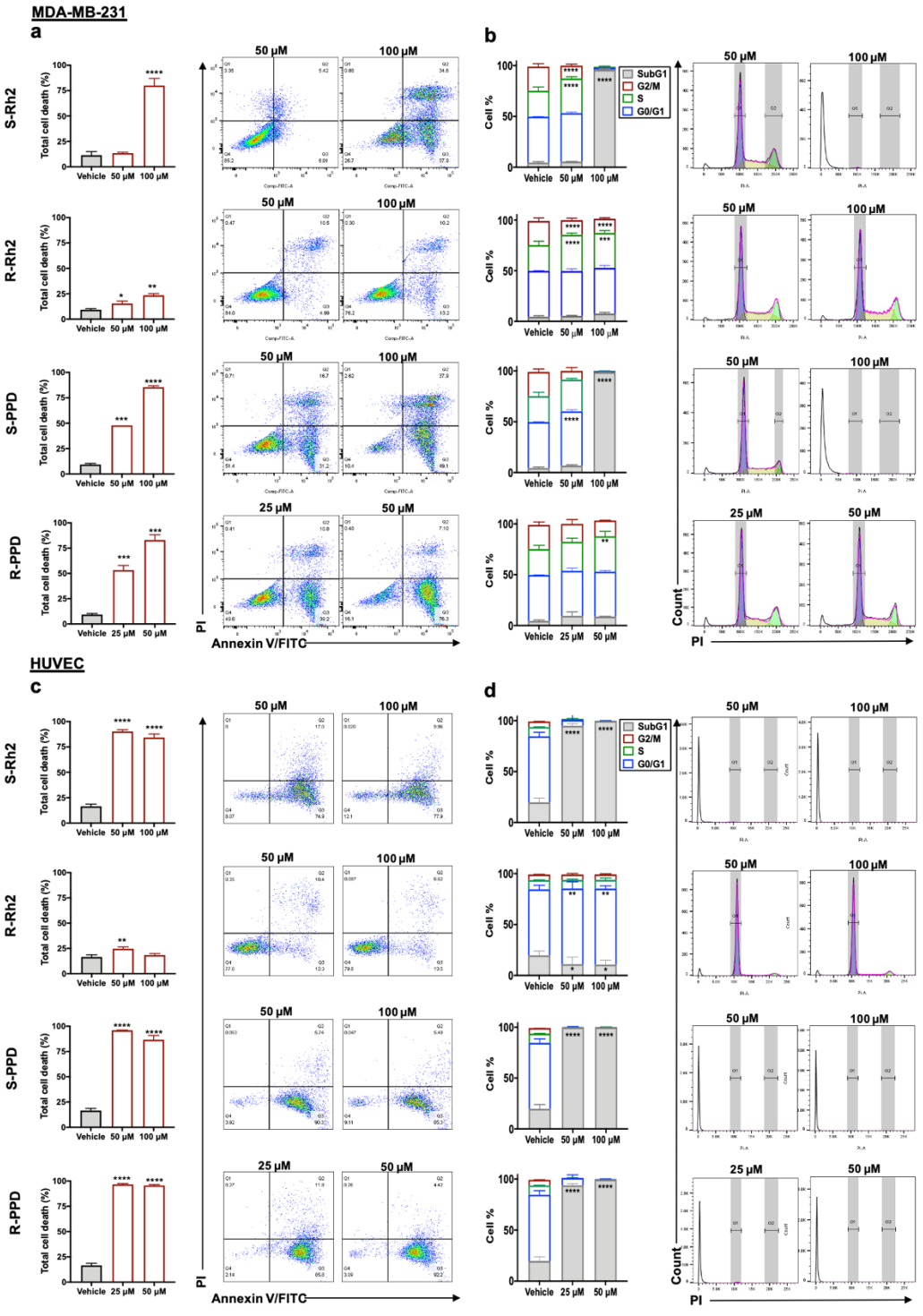

Figure 3. Analysis of (**a**) cell death and (**b**) cell cycle arrest in MDA-MB-231 cell line and (**c**) cell death and (**d**) cell cycle arrest in HUVEC following a three-day exposure to S-Rh2, R-Rh2, S-PPD, and R-PPD. Each data point represents mean ± SD of three replicates. All comparisons are between the treatments and the vehicle control cells, $p < 0.05$. * $p < 0.05$, ** $p < 0.01$, *** $p < 0.001$ and **** $p < 0.0001$.

In MDA-MB-231, 50 and 100 μM S-PPD induced a significant increase in the proportion of cells that stained annexin-positive (Figure 3a). S-PPD did not induce caspase 3/7 activation in MDA-MB-231 (Figure 4a). Instead, it significantly increased the PI count within 4 h with 100 μM ($p < 0.0001$) and 12 h with 50 μM ($p = 0.0002$) (Figure 4b), suggesting that it induced a necroptotic/necrotic cell death.

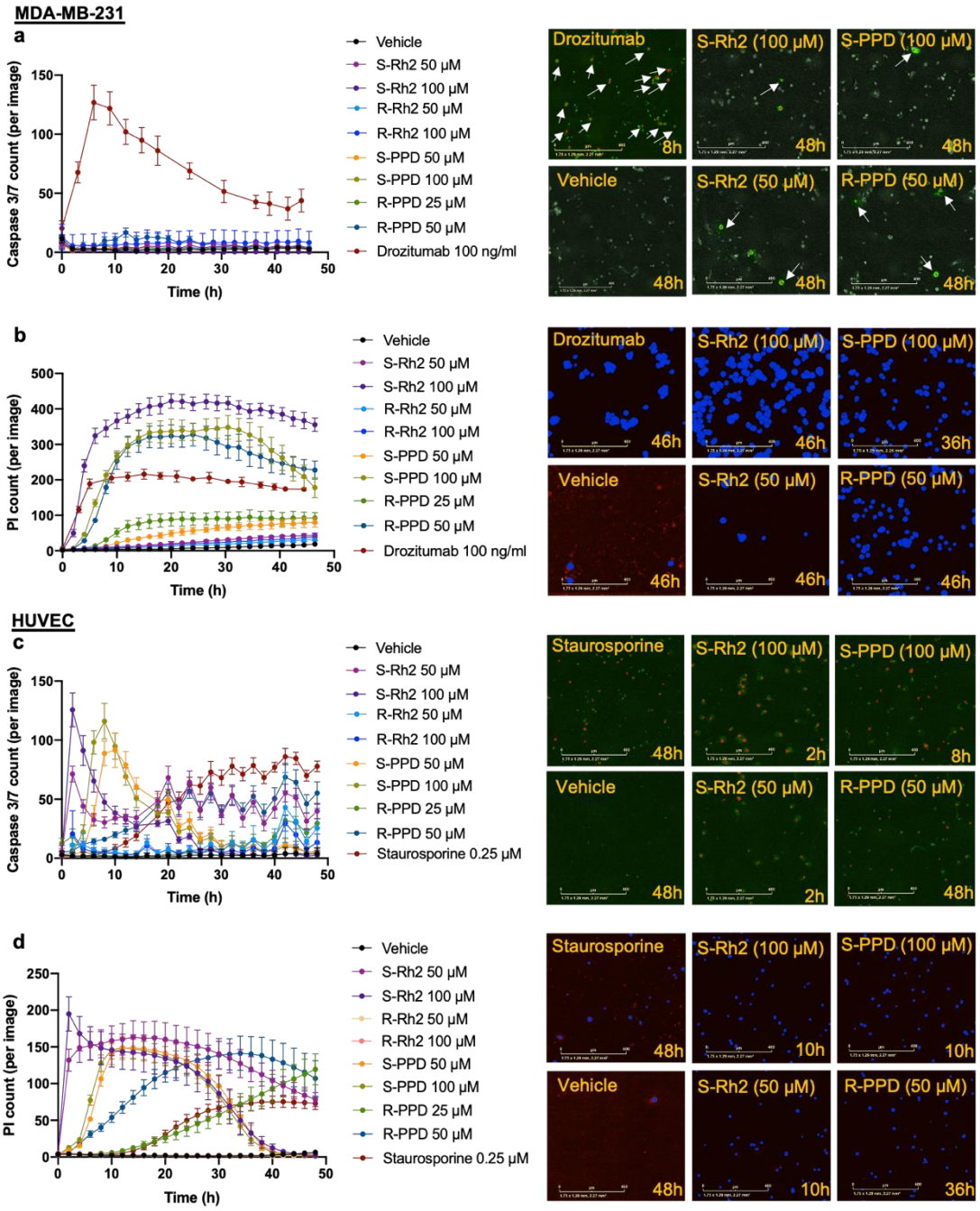

Figure 4. Mode of cell death in MDA-MB-231 and HUVEC cells exposed to Rh2 and PPD epimers. (**a**) and (**c**) show activation of caspase 3/7 in MDA-MB-231 cells, and HUVEC respectively. White arrows pointing at red dots show activation of caspase 3/7 in cells. (**b**) and (**d**) show staining of cells PI in MDA-MB-231 and HUVEC cells, respectively. Blue spots indicate cells positive for PI. Staurosporine or drozitumab were used as positive controls. Scale bars show 400 μm. Each data point represents mean ± SD of 8 replicates.

In HUVEC, a significant increase in annexin V-positive/PI-negative cells (Figure 3c), and an increase in the caspase 3/7-positive cell count, which peaked at 8 h with 100 μM and 10 h with 50 μM (Figure 4c), was observed. The increase in the caspase 3/7 cell count was closely followed by a significant increase in PI-positive cell count (Figure 4d).

R-PPD was the most potent anti-proliferative molecule in MDA-MB-231 (Table 1). At 25 μM ($p = 000.9$) and 50 μM ($p = 0.0001$), R-PPD, in a concentration-dependent manner, induced 53% and 83% cell death (Figure 3a) and 30% cell cycle arrest in S phase (Supplementary Figure 1). Similar to other studied epimers, R-PPD did not induce activation of caspase 3/7 in MDA-MB-231 (Figure 4a) but increased PI staining, dose-dependently (Figure 4b). This could indicate that R-PPD is also an inducer of necroptotic/necrotic cell death in this cell line. In HUVEC, R-PPD induced 95% cell death at both tested concentrations ($p < 0.0001$), and 15% cell cycle arrest in G0/G1 (Supplementary Figure 1), accompanied by a gradual increase in caspase 3/7 activation and PI count, indicating apoptosis. Overall, these findings suggest that S-Rh2, S-PPD and R-PPD induced necroptosis/necrosis in MDA-MB-231 and induced apoptosis in HUVEC. These molecules induce S-phase arrest in MDA-MB-231 and G0/G1 arrest in HUVEC.

3.3. S-Rh2 is the most potent inhibitor of loop formation

Figure 5 shows the results of loop formation assay following exposure with ginsenosides. Vehicle treated HUVEC formed clear loops with elongated cells. Among the four tested molecules, S-Rh2 was the most potent in inhibiting loop formation. At 100 μM, cell migration was completely inhibited, and no loops were formed ($p < 0.0001$), which could be due to the rapid cell death induced by this drug (Figure 4c and 4d). At lower concentrations of S-Rh2 loop formation was also significantly inhibited ($p < 0.0001$). The results indicate that the mechanism by which S-Rh2 inhibits loop formation might be different at different concentrations. At 1 μM, though the concentration was very low, the cells made deformed and unusual loops. This low concentration, after two days of exposure, increased the activation of caspase 3/7 (Supplementary Figure 2). At 10 μM no significant induction of cell death was observed in the cells (Supplementary Figure 2) and the cells survived on Matrigel. As shown in Figure 4c and 4d, 50 μM SRh2 induced significant cell death in HUVEC within the first 2 hours, which could be considered as the major anti-loop formation mechanism of this drug. Based on the number of loops formed, a dose-dependent reduction in loop formation was observed in the 10-100 μM range ($p < 0.0001$).

R-Rh2 did not show any biologically relevant inhibition of proliferation (Figure 2) but showed some level of inhibition of loop formation at 10 ($p = 0.0003$), 50 ($p = 0.0001$) and 100 μM ($p < 0.0001$). However, unlike S-Rh2, at 1 μM R-Rh2 had no efficacy on loop formation. S-PPD and R-PPD showed a U-shaped dose-response curve in loop formation assay, showing inhibition of loop formation only in lower concentrations.

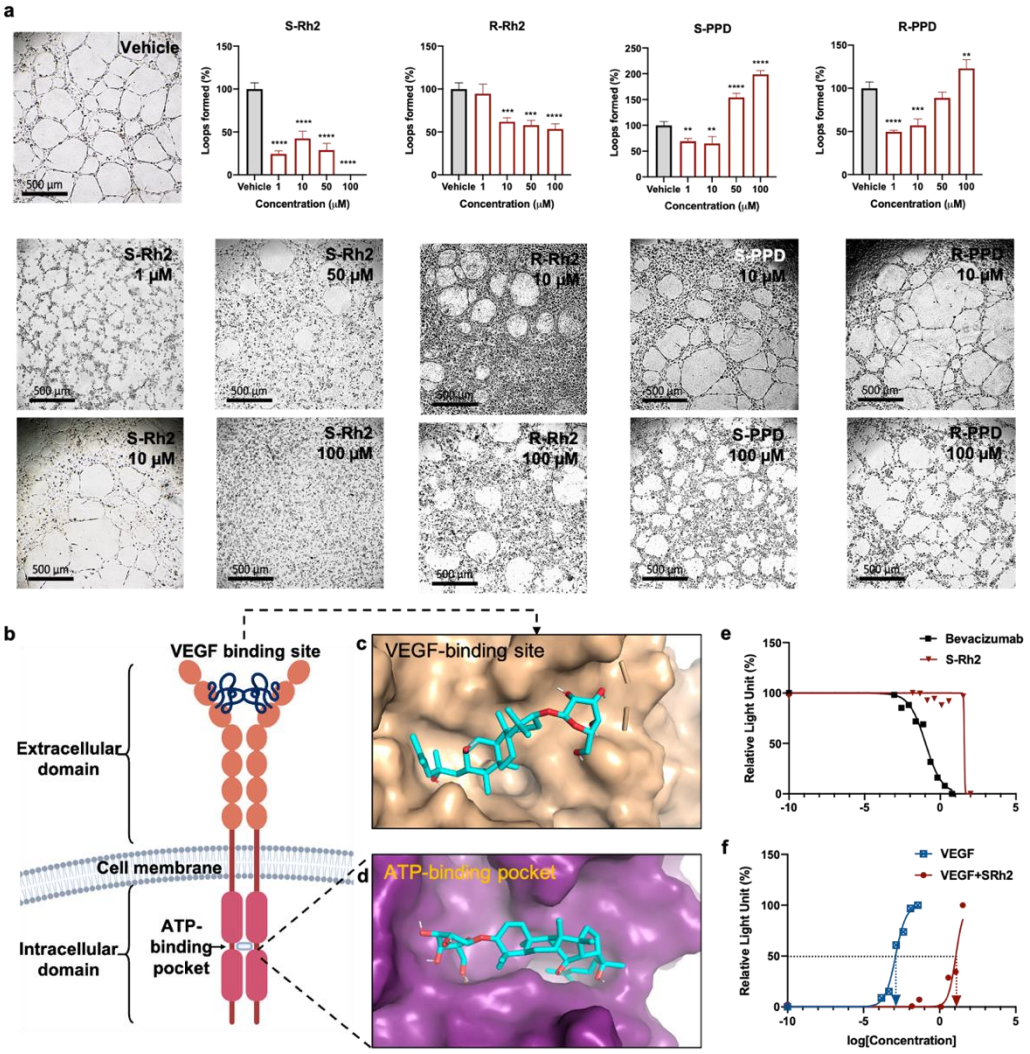

Figure 5. (**a**) Loop formation assay in HUVEC cells following exposure to S-Rh2, R-Rh2, S-PPD, and R-PPD, (**b**) schematic structure of VEGFR2 showing the extracellular domain, VGEF binding site, a transmembrane domain, intracellular domain and the ATP-binding pocket of VEGFR2. Molecular docking of S-Rh2 with (**c**) VEGF-binding site and (**d**) the ATP-binding pocket of VEGFR2, and the dose-response curves relating to the action of (**d**) bevacizumab, (**e**) VEGF and S-Rh2 with or without VEGF in the VEGF bioassay system are shown. Each data point represents mean ± SD of two or three replicates. All comparisons are between the treatments and the vehicle control cells, $p < 0.05$.

3.4. VEGFR2 and AQP1 as potential targets of Rh2

To screen for the possible targets of Rh2 and PPD, molecular docking was performed. A key driver of angiogenesis is the interaction between VEGF and VEGFR2, so the interaction of Rh2 and PPD with VEGFR2 was studied. VEGFR2 has two major binding sites, the ATP-binding pocket and the VEGF-binding site (Figure 5b), both of which were studied in this molecular docking. As shown in Table 2, both Rh2 and PPD were predicted to have a better interaction with the ATP-binding pocket than with the receptor. PPD was predicted to have a better binding score with this site

of VEGFR2. However, given the U-shaped dose-response curve of PPD on loop formation of HUVECs, it is difficult to conclude whether this interaction is inhibitory or stimulatory.

Table 2. Binding scores (number of H bonds) of Rh2 and PPD with different aquaporin water channels, ATP-binding pocket or the VEGF-binding site of VEGFR2.

Molecules	Binding score (kJ/mol) (number of H-bonding)					
	VEGFR2*	VEGFR2**	AQP1	AQP2	AQP4	AQP5
Rh2	-7.6 (1)	-7.1 (2)	-8.1 (2)	-5.2 (1)	-6.3 (3)	-8.1 (4)
PPD	-8.2 (1)	-6.9 (1)	-8.4 (0)	-6.9 (0)	-5.6 (0)	-7.7 (1)

*ATP-binding pocket of the receptor **VEGF binding site of the receptor

Figure 5c and 5d show the interaction sites of Rh2 with VEGF-binding site and the ATP-binding pocket of VEGFR2, respectively. To test the interaction of S-Rh2 with VEGFR2 *in vitro*, a VEGF bioassay was performed. In this assay, upon the activation of VEGFR2 with its ligand, the cells luminesce and in the presence of an inhibitor such as bevacizumab, the luminescence is inhibited. In this assay, bevacizumab, which was used in the presence of VEGF, showed an IC_{50} of 0.11 μg/mL (Figure 5e). S-Rh2 was used with no VEGF to see if it has a stimulatory action on the receptor. In this state, a steady luminescence was detected except at 100 μM. Since Rh2 is highly cytotoxic at 100 μM, the reduced luminescence from the cells at this concentration could be due to cell death. S-Rh2 alone did not affect the activation of the receptor, but in the presence of VEGF, S-Rh2 shifted the dose-response curve of VEGF to right (Figure 5f), indicating that S-Rh2 potentially acted as an allosteric modulator of the receptor, binding to the allosteric site, changing the conformation of the receptor and as a result, decreasing the affinity and potency of VEGF on this receptor.

Furthermore, molecular docking was performed with four members of the aquaporin family, AQP1, AQP2, AQP4 and AQP5. AQPs have a homo-tetramer structure where each monomer is responsible for the transport of water. Each monomer consists of six transmembrane domains (M1-M6) and three loops (B, D and E) (Figure 7a). Loops B and E are responsible for water transport function of the channel [25]. Figure 7b-7e shows the molecular docking of Rh2 and PPD into AQP1 and AQP5. Rh2 had good binding scores with both AQP1 and AQP5, with binding scores of -8.1 kJ/mol (Table 2). With AQP1, Rh2 made two H-bonds at HIS-67 and VAL-72 (Figure 7b) of loop B (water pore) [25]. With AQP5, it made 4 H-bonds at M2, loop B (Pro 795, Arg-819 (2), and GLN-814. PPD had a better binding score with AQP1 (-8.4 kJ/mol) (Table 2). However, molecular docking showed no H-bonds between the two molecules which might suggest a loose binding compared to that of Rh2. With AQP5, PPD showed a single H-bond with ASN-961 in M6.

As shown in Figure 7, both Rh2 and PPD showed a better blocking of AQP1. The surface views suggest that both Rh2 and PPD fit inside the water channel and completely block the passage of water. In the case of AQP5, though the binding scores and number of H-bonds are encouraging, the molecules seem to attach to one side of the water channel and leaving the water passage open (Figure 7c and 7d). Functional assays are required to confirm these *in silico* findings.

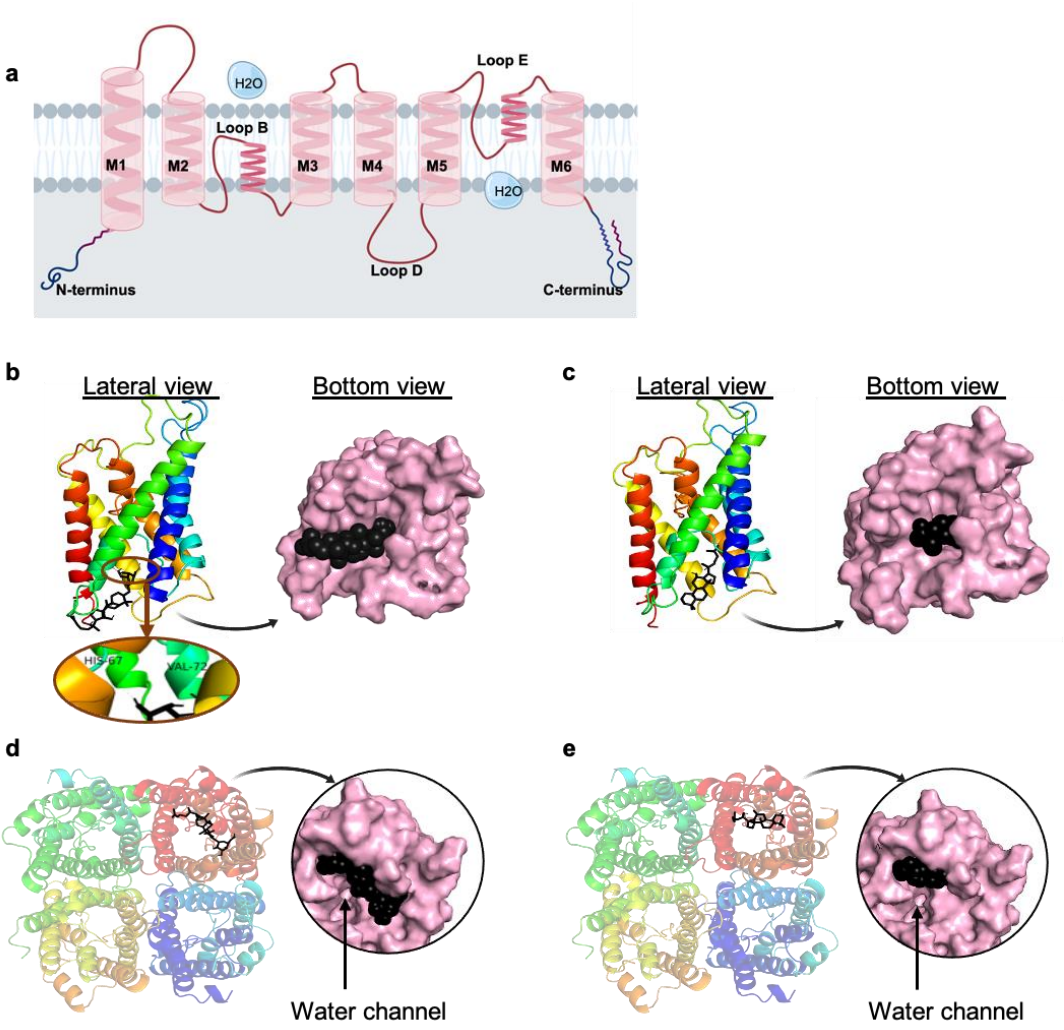

Figure 7. (**a**) Schematic structure of a monomer AQP1 showing transmembrane domains (M1-M6), loops B and E responsible for water transport and loop D. Molecular docking of (**b**) Rh2 and (**c**) PPD in AQP1 and molecular docking of (**d**) Rh2 and (**e**) PPD in AQP5. Rh2 makes two H-bonds with HIS-67 and VAL-72 of loop B (water pore).

4. Discussion

Ginsenoside Rg3 has long been a candidate for investigation as an anticancer drug. Several studies have shown that Rg3 epimers have stereoselective activities [11, 26, 27]. Also, preclinical studies have shown the efficacy of Rg3 for the treatment of breast cancer [11, 28, 29]. In China, Rg3 is a registered anti-angiogenic agent. Several studies have shown that oral or parenteral administration of Rg3 leads to the metabolism of Rg3 (reviewed in [1]), leaving mainly active metabolites in the body. Peng *et al.* (2016) showed that following either of the routes of administration of Rg3 epimers, two major deglycosylated metabolites were produced; SRg3 produced S-Rh2 and S-PPD, and RRg3 produced R-Rh2 and R-PPD [30]. In this study, looking for treatment options for triple negative breast cancer, we looked at the potential of metabolites of Rg3 as anti-cancer agents.

These molecules have been a subject of several studies. S-Rh2 showed efficacy against acute promyelocytic leukemia [31], T-cell acute lymphoblastic leukemia [32] and colon cancer models [33], *in vitro*. There is a lack of literature on the anticancer efficacy of R-Rh2: it was shown that only S-Rh2 and not R-Rh2 inhibited the proliferation of prostate cancer cell lines [35]. Similar to that result, we showed that in MDA-MB-231 and HUVEC, S-Rh2 had a more profound anti-proliferative effect. PPD has also been a subject of some studies. S-PPD induced apoptotic cell death in endometrial cancer cells [36], fibrocarcinoma cells [37], colorectal adenocarcinoma cells [38, 39], breast, prostate and osteosarcoma cell lines [39]. Injection of 30 mg/kg PPD (every 2 days for 3 weeks) to a xenograft mouse model of colorectal cancer showed a significant decrease in tumour size in this model [39]. In colorectal cancer cells, PPD showed anti-proliferative effects via induction of G1/S cell cycle arrest and targeting MAPK and NF-κB signalling [39]. This was in agreement with our finding showing S-PPD induced G1 cell cycle arrest in MDA-MB-231.

We have shown that S-Rh2 is a more potent anti-proliferative molecule compared to its R counterpart. This is similar to the effects observed with SRg3, being the only epimer that inhibited the proliferation of MDA-MB-231 [11]. We have shown that except for R-Rh2, three other ginsenosides have anti-proliferative effects in the tested TNBC cell line. In this cell line, the most potent molecule was R-PPD with an IC_{50} of 16 μM. Choi *et al.* (2009) studied the effects of Rh2 (unspecified epimer) on two breast cancer cell lines, MCF-7 and MDA-MB-231 [40]. In their studies, in a 48-h exposure to 40 μM Rh2, a slight increase in G1 population of cells was observed. They showed that the Rh2-induced cell cycle arrest was via p15 and p27-dependent inhibition of kinase activities of G1-S specific Cdks/cyclin complexes [40]. Their result may not be completely comparable with ours due to lack of specification of the epimer used and the difference in the exposure time. However, it is possible to conclude that in lower concentrations and shorter exposure times (such as 48 h), S-Rh2 might induce cell cycle arrest and this cell cycle arrest might lead to cell death in longer exposure times (such as 72 h in our experiment).

The anti-proliferative concentrations of these molecules significantly increased annexin V/PI staining, as an indicator of cell death. Kwak *et al.* (2014) showed that S-PPD at a short-time exposure and a low concentration (2.5 and 5.8 μM, 24 h) induced apoptosis in MDA-MB-231 via activation of caspase-8, -3 and poly ADP-ribose polymerase [41]. We looked at the mechanism of cell death induced by higher concentrations of all four molecules. At high concentrations, in MDA-MB-231, S-Rh2, S-PPD and R-PPD induced cell death as indicated by both annexin V positive and annexin V/PI positive subpopulations. For the first time, we showed that the mechanism of cell death induced in MDA-MB-231 at these concentrations is not apoptosis, but a necroptotic/necrotic cell death. The R enantiomer of alkanin, known as shikonin, was the first reported inducer of necroptosis [42, 43] and these ginsenosides, if confirmed with complementary experiments, could be another group of natural inducers of necroptosis.

Similar to apoptotic cells, in necroptotic cells phosphatidylserine is flipped to the outer bilayer cell membrane [44] and hence, the cells are stained positive for annexin V. Necroptosis is a regulated process, which unlike apoptosis, is caspase 3/7

independent. The induction of necroptosis is usually dependent on the activation of tumour necrosis factor (TNF) receptor superfamily, interferon receptors, T-cell receptors and Toll-like receptors [45]. Genotoxic stress and anti-cancer agents such as shikonin are also amongst the inducers of necroptosis [45]. Shikonin was shown to overcome cancer drug resistance [43, 46] and inhibit osteosarcoma-induced lung metastasis [47] via induction of necroptosis. The role of necroptosis in cancer treatment has been widely discussed in recent years. It is important to remember that different types of programmed cell death, including apoptosis, necroptosis and autophagy, might coexist with one playing a dominant role. This paper shows for the first time that, in MDA-MB-231, these molecules do not induce apoptosis but are potential inducers of necroptosis/necrosis.

Our results demonstrated that HUVECs were a more sensitive target for the anti-proliferative action of these molecules, a finding relevant to their anti-angiogenic activity. We showed that S-PPD and R-PPD have IC_{50} values of about 5 and 11 μM in HUVECs, respectively, which are close to the values reported by Usami *et al.* (S-PPD: 5 μM and R-PPD: 14 μM) [48]. We showed that both epimers are strong inducers of apoptosis in HUVECs, however, with different rates. S-PPD induces the activation of caspase 3/7 more rapidly; a process that is more gradual with R-PPD. Wang *et al.* showed that S-PPD induces apoptosis via endoplasmic reticulum stress by activating protein kinase R-like endoplasmic reticulum kinase (PERK)-eIF2α signalling pathway [49]. They used up to 20 μM S-PPD and concluded that high concentrations of S-PPD could be used for the treatment of angiogenesis-related diseases. Our results with the loop formation assay showed that S-PPD and R-PPD have U-shaped dose-response curves. This U-shaped dose-response curve was also reported for Rg3 epimers. As reviewed before [2], Rg3 at nM concentrations had anti-angiogenic properties, at low μM ranges, such as 10-15 μM, had proangiogenic effects and at high μM concentrations showed anti-angiogenic effects. It should also be considered that the observed effects on loop formation are a cells' immediate response to these agents. With pretreated cells, it is expected that the anti-loop formation effects of drugs be much increased. As shown in the proliferation assay, in a three-day exposure, low and high concentrations of the drugs considerably inhibited proliferation. Therefore, it could be concluded that, the molecules are very potent anti-angiogenic agents. We also tested the anti-proliferative effects of these four molecules at nM and low μM ranges in HUVECs (Supplementary Figure 3). Unlike the reported effects for Rg3 (reviewed in [2]), these molecules do not have anti-proliferative effects at such low concentrations in HUVEC, although, after 2 days of exposure to 1 μM S-Rh2, evidence of activation of caspase 3/7 is observed (Supplementary Figure 2).

Our results showed that Rh2 had a better immediate anti-angiogenic action. Amongst the four molecules, S-Rh2 was the most potent molecule in inhibition of loop formation. An unspecified epimer of Rh2 was studied by Zhang *et al.* [50] for its anti-angiogenic properties. They showed that Rh2 inhibited the proliferation of HUVECs only at high doses (>125 μM), but pretreatment of cells with 1 and 10 μM Rh2 significantly inhibited the VEGF-induced cell proliferation and migration. They showed that 10 μM Rh2 decreased the activation of GRB2-associated-binding protein

1 (Gab1), vascular endothelial growth factor receptor 2 (VEGFR2), protein kinase B (PKB or AKT) and extracellular signal-regulated kinase 1/2 (ERK 1/2) [50]. We showed that 10 μM S-Rh2 caused small levels of decrease in the expression of AQP1 and activation of focal adhesion kinase (FAK) (Supplementary Figure 4), which could contribute to the anti-angiogenic properties of this drug. Also, preliminary data show that at this concentration, S-Rh2 caused a non-significant reduction in the size of MDA-MB-231 mammospheres (Supplementary Figure 5). This effect, which might indicate a looser cell-cell connection in these mammospheres, could be further exacerbated in higher concentrations.

To investigate potential targets of these molecules, we performed molecular docking on some of the candidate proteins. The interaction between VEGF-VEGFR2 plays a crucial role in induction of angiogenesis. For the first time, using molecular docking we showed that there is a good binding score between these molecules and VGEFR2. VEGF bioassay showed that Rh2 shifted the dose-response curve of VEGF to the right. The extracellular domain of VEGFR2 consists of seven immunoglobulin (Ig) homology domains; D1 to D7 are located at the N-terminus to the closest to the cell membrane, respectively. D2-3 domains have the highest affinity for VEGF and D4-7 reduce binding affinity by about 10 fold, playing role in regulating the activation and function of the receptor [51]. The intracellular domain of VEGFR2 is responsible for the kinase activity and downstream signalling. Small-molecule kinase inhibitors such as sunitinib compete with ATP and interact with the ATP-binding pocket of the intracellular domain [52]. Adjacent to this orthosteric ATP-binding site, there is an allosteric site [53]. Despite the good binding score of Rh2 and PPD with ATP-binding pocket of VEGFR2, S-Rh2 alone did not stimulate or inhibit the receptor. The only exception was the highest concentration used (100 μM) which is a cytotoxic concentration. In the presence of VEGF, S-Rh2 shifted the dose-response of VEGF to the right. This is typical of allosteric modulators. Unlike orthosteric ligands that bind to their agonist-binding site and initiate downstream signalling, allosteric ligands bind to distinct sites distant from the orthosteric site, change the conformation of the receptor and change the efficacy of the orthosteric ligands or function of the receptor [53]. Our preliminary studies have not shown whether S-Rh2 changes the affinity of VEGF or the function of the receptor, but we have shown that S-Rh2 in the presence of high concentrations of VEGF (EC_{75}), reduced the activation of VEGFR2. This could be particularly important in the hypoxic regions of a tumour when angiogenesis is occurring, and high levels of VEGF exist.

AQPs were another target of screening in this study. AQPs are primarily responsible for the transport of water across the cell membrane. AQP1, AQP2, AQP4 and AQP5, the AQPs for which a human crystal structure is published, were investigated in this study. Molecular docking showed that Rh2 and PPD have good binding with AQP1 and AQP5, both of which play roles in cancer. AQP1 and AQP5 play roles in proliferation, migration, invasion and angiogenesis (reviewed in [2, 12]). Both of these AQPs localize at the leading edge of a migrating cell and facilitate cell migration. Despite the good binding score of these ginsenosides with AQP5, the water transport function of AQP5 channel might not be effectively blocked by these molecules. Based on molecular docking data, Rh2 and PPD seem to be a better blocker

of AQP1 water channel. In comparison, Rg3 had a better binding score with AQP1 (-9.4 kJ/mol) [11]. The binding score of Rh2 and PPD is also weaker than those of other known blockers of AQP1 with saponin structure, such as bacopaside I and II [54]. Using oocyte expression assay, we showed that Rg3 epimers have stereoselectivity in blocking AQP1 water channel; SRg3 is a selective blocker of AQP1 [11]. Whether the epimers of Rh2 and PPD have a similar stereoselectivity needs further investigations. Also, in molecular docking studies, Rg3 was more selective for AQP1 and did not show a good binding score with AQP5. Considering the current results of molecular docking, it is possible to conclude that upon administration of Rg3 and production of its metabolites, these ginsenoside could work together and contribute to the observed anti-cancer activities of Rg3. Blocking the water channel function of AQP1 may have an immediate role in inhibition of loop formation and anti-angiogenic effects of Rh2.

In conclusion, we have shown that metabolites of Rg3 are more potent anti-proliferative agents than Rg3. They are potential inducers of S-phase arrest and necroptosis in MDA-MB-231 and inducers of G0/G1 arrest and apoptosis in HUVEC. S-Rh2 was a most potent anti-angiogenic agent and it was shown that S-Rh2 had allosteric modulatory action on VEGFR2 function. Rh2 and PPD have the potential of blocking AQP1 and AQP5. Altogether, these data suggest that metabolites of Rg3 could potentially increase the anti-cancer properties of Rg3, *in vivo*. Single or combination of these molecules could be considered as potential anti-cancer treatment options for future studies.

Funding: This research was funded by the Margaret Elcombe Hospital Research Foundation Research Grant.

Conflicts of Interest: The authors declare no conflict of interest.

Appendix A. Supplementary data

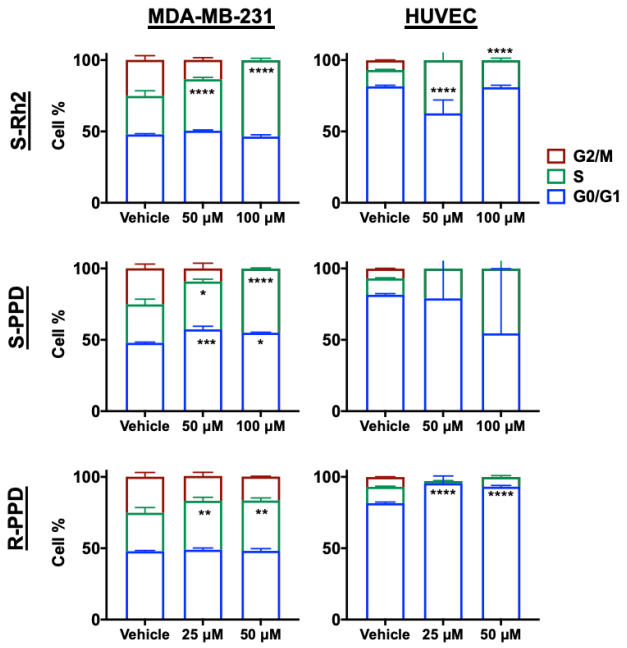

Supplementary Figure 1. The effect of Rh2 and PPD epimers on cell cycle, excluding the sub-G1 cells. The experiment was performed in triplicate and the data are shown as mean ± SD of three replicates. All comparisons are between the treatments and the vehicle control cells, $p < 0.05$. * $p < 0.05$, ** $p < 0.01$, *** $p < 0.001$ and **** $p < 0.0001$.

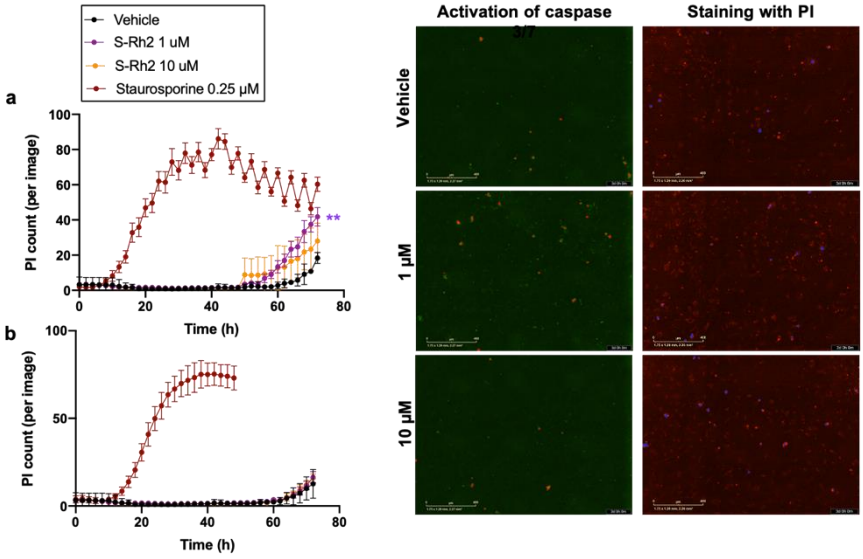

Supplementary Figure 2. Effect of 1 and 10 µM S-Rh2 on the (**a**) activation of caspase 3/7 (red spots) or (**b**) staining with PI (blue spots) in HUVEC cells in a 3-day study. After 2 days of exposure, a significant increase in the activation of caspase 3/7 is observed with 1 µM S-Rh2. Each datapoint represents mean ± SD of 8 replicates. All comparisons are between the treatments and the vehicle control cells, ** $p = 0.0068$.

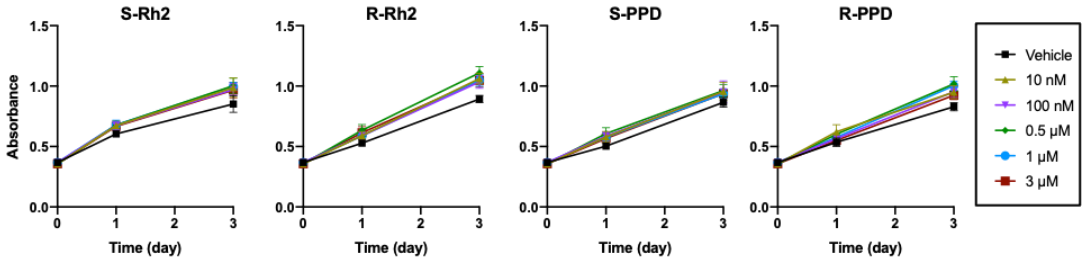

Supplementary Figure 3. The effect of low concentrations of Rh2 and PPD epimers on the proliferation of HUVEC cells. Each datapoint represents mean ± SD of 6 replicates. All comparisons are between the treatments and the vehicle control cells, $p < 0.05$.

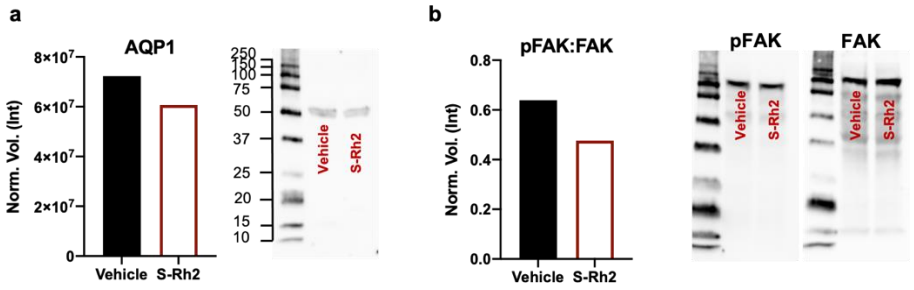

Supplementary Figure 4. (a) Expression of AQP1 and (b) activation of focal adhesion kinase (FAK) following a 3-day exposure with 10 μM S-Rh2. Total cell lysates were prepared, and 50 μg total protein was used for Western blotting. The antibodies used for immunostaining included anti-AQP1 antibody [EPR20325] (ab219055, Abcam, Cambridge, UK, 1:1000), anti-FAK antibody [EP6954] (ab40794, Abcam, Cambridge, UK, 1:1000), anti-phospho FAK antibody [EP2]60Y] phosphor Y397 (ab 81298, Abcam, Cambridge, UK, 1:1000) Goat anti-rabbit IgG H&L (HRP) (ab6721, Abcam, Cambridge, UK, 1:3000) was used as the secondary antibody.

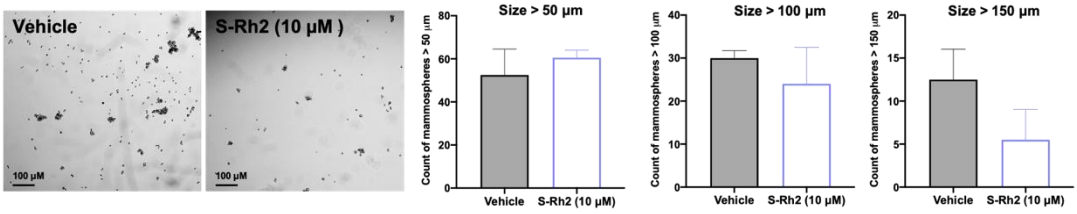

Supplementary Figure 5. Effect of 10 μM S-Rh2 on the formation of MDA-MB-231 mammospheres. MDA-MB-231 cells, at 4000 cell/cm2 of 24-well ultra-low attachment plates, were grown as mammospheres using MammoCult™ Human Medium Kit (Stem Cell Technologies, Vancouver, Canada), exposed to vehicle or 10 μM S-Rh2. After 4 days, the number of mammospheres larger than 50, 100 and 150 μm was counted. The experiment was performed in duplicate and the results are shown as mean ± SD.

References

1. Nakhjavani M, Hardingham JE, Palethorpe HM, Tomita Y, Smith E, Price TJ, Townsend AR. Ginsenoside Rg3: Potential molecular targets and therapeutic indication in metastatic breast cancer. Medicines 2019;6(1):17.
2. Nakhjavani M, Smith E, Townsend AR, Price TJ, Hardingham JE. Anti-Angiogenic Properties of Ginsenoside Rg3. Molecules 2020;25(21):4905.
3. Pan L, Zhang T, Sun H, Liu G. Ginsenoside Rg3 (Shenyi Capsule) Combined with Chemotherapy for Digestive System Cancer in China: A Meta-Analysis and Systematic Review. Evid Based Complement Alternat Med 2019;2019:2417418.
4. Lu P, Su W, Miao ZH, Niu HR, Liu J, Hua QL. Effect and mechanism of ginsenoside Rg3 on postoperative life span of patients with non-small cell lung cancer. Chin J Integr Med 2008;14(1):33-6.
5. Zhou B, Yan Z, Liu R, Shi P, Qian S, Qu X, Zhu L, Zhang W, Wang J. Prospective Study of Transcatheter Arterial Chemoembolization (TACE) with Ginsenoside Rg3 versus TACE Alone for the Treatment of Patients with Advanced Hepatocellular Carcinoma. Radiology 2016;280(2):630-9.
6. Li Y, Wang Y, Niu K, Chen X, Xia L, Lu D, Kong R, Chen Z, Duan Y, Sun J. Clinical benefit from EGFR-TKI plus ginsenoside Rg3 in patients with advanced non-small cell lung cancer harboring EGFR active mutation. Oncotarget 2016;7(43):70535-45.
7. Xie HT, Wang GJ, Sun JG, Tucker I, Zhao XC, Xie YY, Li H, Jiang XL, Wang R, Xu MJ, et al. High performance liquid chromatographic-mass spectrometric determination of ginsenoside Rg3 and its metabolites in rat plasma using solid-phase extraction for pharmacokinetic studies. J Chromatogr B Analyt Technol Biomed Life Sci 2005;818(2):167-73.
8. Wang H, Zou H, Kong L, Zhang Y, Pang H, Su C, Liu G, Hui M, Fu L. Determination of ginsenoside Rg3 in plasma by solid-phase extraction and high-performance liquid chromatography for pharmacokinetic study. Journal of Chromatography B: Biomedical Sciences and Applications 1999;731(2):403-9.
9. Huan P, Hailin W, Li F, Chengye S. Pharmacokinetics of 20 (R)-ginsenoside Rg3 in human volunteers. JOURNAL OF CHINESE PHARMACEUTICAL SCIENCES 2001;10(3):140-3.
10. Peng M, Li X, Zhang T, Ding Y, Yi Y, Le J, Yang Y, Chen X. Stereoselective pharmacokinetic and metabolism studies of 20(S)- and 20(R)-ginsenoside Rg3 epimers in rat plasma by liquid chromatography-electrospray ionization mass spectrometry. Journal of Pharmaceutical and Biomedical Analysis 2016;121:215-24.
11. Nakhjavani M, Palethorpe HM, Tomita Y, Smith E, Price TJ, Yool AJ, Pei JV, Townsend AR, Hardingham JE. Stereoselective anti-cancer activities of ginsenoside Rg3 on triple negative breast cancer cell models. Pharmaceuticals 2019;12(3):117.
12. De Ieso ML, Yool AJ. Mechanisms of aquaporin-facilitated cancer invasion and metastasis. Front Chem 2018;6:135.
13. Smith E, Palethorpe HM, Tomita Y, Pei JV, Townsend AR, Price TJ, Young JP, Yool AJ, Hardingham JE. The Purified Extract from the Medicinal Plant Bacopa monnieri, Bacopaside II, Inhibits Growth of Colon Cancer Cells In Vitro by Inducing Cell Cycle Arrest and Apoptosis. Cells 2018;7(7).

14. Paltoglou S, Das R, Townley SL, Hickey TE, Tarulli GA, Coutinho I, Fernandes R, Hanson AR, Denis I, Carroll JS, et al. Novel Androgen Receptor Coregulator GRHL2 Exerts Both Oncogenic and Antimetastatic Functions in Prostate Cancer. Cancer Res 2017;77(13):3417-30.
15. Tomita Y, Palethorpe HM, Smith E, Nakhjavani M, Townsend AR, Price TJ, Yool AJ, Hardingham JE. Bumetanide-derived aquaporin 1 inhibitors, AqB013 and AqB050 inhibit tube formation of endothelial cells through induction of apoptosis and impaired migration in vitro. Int J Mol Sci 2019;20(8):1818.
16. Palethorpe HM, Smith E, Tomita Y, Nakhjavani M, Yool AJ, Price TJ, Young JP, Townsend AR, Hardingham JE. Bacopasides I and II act in synergy to inhibit the growth, migration and invasion of breast cancer cell lines. Molecules 2019;24(19):3539.
17. Mosnier LO, Griffin JH. Inhibition of staurosporine-induced apoptosis of endothelial cells by activated protein C requires protease-activated receptor-1 and endothelial cell protein C receptor. Biochemical Journal 2003;373(1):65-70.
18. Zinonos I, Labrinidis A, Liapis V, Hay S, Panagopoulos V, Denichilo M, Ponomarev V, Ingman W, Atkins GJ, Findlay DM, et al. Doxorubicin overcomes resistance to drozitumab by antagonizing Inhibitor of Apoptosis Proteins (IAPs). Anticancer Res 2014;34(12):7007-20.
19. Information NCfB. PubChem Compound Summary for CID 119307, Ginsenoside Rh2. 2020 [Available from: https://pubchem.ncbi.nlm.nih.gov/compound/Ginsenoside-Rh2.
20. Information NCfB. PubChem Compound Summary for CID 11213350, (20S)-Protopanaxadiol 2020 [Available from: https://pubchem.ncbi.nlm.nih.gov/compound/20S_-Protopanaxadiol.
21. Pei JV, Kourghi M, De Ieso ML, Campbell EM, Dorward HS, Hardingham JE, Yool AJ. Differential inhibition of water and ion channel activities of mammalian aquaporin-1 by two structurally related bacopaside compounds derived from the medicinal plant bacopa monnieri. Molecular pharmacology 2016;90(4):496-507.
22. Snyder AG, Hubbard NW, Messmer MN, Kofman SB, Hagan CE, Orozco SL, Chiang K, Daniels BP, Baker D, Oberst A. Intratumoral activation of the necroptotic pathway components RIPK1 and RIPK3 potentiates antitumor immunity. Sci Immunol 2019;4(36).
23. Shlomovitz I, Speir M, Gerlic M. Flipping the dogma–phosphatidylserine in non-apoptotic cell death. Cell Communication and Signaling 2019;17(1):1-12.
24. Pietkiewicz S, Schmidt JH, Lavrik IN. Quantification of apoptosis and necroptosis at the single cell level by a combination of Imaging Flow Cytometry with classical Annexin V/propidium iodide staining. J Immunol Methods 2015;423:99-103.
25. Yool AJ, Brown EA, Flynn GA. Roles for novel pharmacological blockers of aquaporins in the treatment of brain oedema and cancer. Clin Exp Pharmacol Physiol 2010;37(4):403-9.
26. Park E-H, Kim Y-J, Yamabe N, Park S-H, Kim H-k, Jang H-J, Kim JH, Cheon GJ, Ham J, Kang KS. Stereospecific anticancer effects of ginsenoside Rg3 epimers isolated from heat-processed American ginseng on human gastric cancer cell. J Ginseng Res 2014;38(1):22-7.

27. Kim Y-J, Choi W-I, Jeon B-N, Choi K-C, Kim K, Kim T-J, Ham J, Jang HJ, Kang KS, Ko H. Stereospecific effects of ginsenoside 20-Rg3 inhibits TGF-β1-induced epithelial–mesenchymal transition and suppresses lung cancer migration, invasion and anoikis resistance. Toxicology 2014;322:23-33.
28. Oh J, Yoon H-J, Jang J-H, Kim D-H, Surh Y-J. The standardized Korean Red Ginseng extract and its ingredient ginsenoside Rg3 inhibit manifestation of breast cancer stem cell–like properties through modulation of self-renewal signaling. J Ginseng Res 2019;43(3):421-30.
29. Kim S-J, Kim AK. Anti-breast cancer activity of Fine Black ginseng (Panax ginseng Meyer) and ginsenoside Rg5. J Ginseng Res 2015;39(2):125-34.
30. Peng M, Li X, Zhang T, Ding Y, Yi Y, Le J, Yang Y, Chen X. Stereoselective pharmacokinetic and metabolism studies of 20 (S)-and 20 (R)-ginsenoside Rg3 epimers in rat plasma by liquid chromatography-electrospray ionization mass spectrometry. J Pharm Biomed Anal 2016;121:215-24.
31. Zhu S, Liu X, Xue M, Li Y, Cai D, Wang S, Zhang L. 20(S)-ginsenoside Rh2 induces caspase-dependent promyelocytic leukemia-retinoic acid receptor A degradation in NB4 cells via Akt/Bax/caspase9 and TNF-α/caspase8 signaling cascades. J Ginseng Res 2020.
32. Xia T, Zhang J, Zhou C, Li Y, Duan W, Zhang B, Wang M, Fang J. 20(S)-Ginsenoside Rh2 displays efficacy against T-cell acute lymphoblastic leukemia through the PI3K/Akt/mTOR signal pathway. J Ginseng Res 2020;44(5):725-37.
33. Yang J, Yuan D, Xing T, Su H, Zhang S, Wen J, Bai Q, Dang D. Ginsenoside Rh2 inhibiting HCT116 colon cancer cell proliferation through blocking PDZ-binding kinase/T-LAK cell-originated protein kinase. J Ginseng Res 2016;40(4):400-8.
34. Kang S, Im K, Kim G, Min H. Antiviral activity of 20(R)-ginsenoside Rh2 against murine gammaherpesvirus. J Ginseng Res 2017;41(4):496-502.
35. Liu J, Shimizu K, Yu H, Zhang C, Jin F, Kondo R. Stereospecificity of hydroxyl group at C-20 in antiproliferative action of ginsenoside Rh2 on prostate cancer cells. Fitoterapia 2010;81(7):902-5.
36. Jo H, Jang D, Park SK, Lee M-G, Cha B, Park C, Shin YS, Park H, Baek J-m, Heo H, et al. Ginsenoside 20(S)-protopanaxadiol induces cell death in human endometrial cancer cells via apoptosis. J Ginseng Res 2020.
37. Li G, Wang Z, Sun Y, Liu K, Wang Z. Ginsenoside 20 (S)-protopanaxadiol inhibits the proliferation and invasion of human fibrosarcoma HT1080 cells. Basic Clin Pharmacol Toxicol 2006;98(6):588-92.
38. Popovich DG, Kitts DD. Ginsenosides 20 (S)-protopanaxadiol and Rh2 reduce cell proliferation and increase sub-G1 cells in two cultured intestinal cell lines, Int-407 and Caco-2. Can J Physiol Pharmacol 2004;82(3):183-90.
39. Gao J-L, Lv G-Y, He B-C, Zhang B-Q, Zhang H, Wang N, Wang C-Z, Du W, Yuan C-S, He T-C. Ginseng saponin metabolite 20 (S)-protopanaxadiol inhibits tumor growth by targeting multiple cancer signaling pathways. Oncol Rep 2013;30(1):292-8.
40. Choi S, Kim TW, Singh SV. Ginsenoside Rh2-mediated G1 phase cell cycle arrest in human breast cancer cells is caused by p15 Ink4B and p27 Kip1-dependent inhibition of cyclin-dependent kinases. Pharm Res 2009;26(10):2280-8.

41. Kwak JH, Park JY, Lee D, Kwak JY, Park EH, Kim KH, Park H-J, Kim HY, Jang HJ, Ham J. Inhibitory effects of ginseng sapogenins on the proliferation of triple negative breast cancer MDA-MB-231 cells. Bioorganic Med Chem Lett 2014;24(23):5409-12.
42. Gong Y, Fan Z, Luo G, Yang C, Huang Q, Fan K, Cheng H, Jin K, Ni Q, Yu X. The role of necroptosis in cancer biology and therapy. Molecular cancer 2019;18(1):1-17.
43. Han W, Li L, Qiu S, Lu Q, Pan Q, Gu Y, Luo J, Hu X. Shikonin circumvents cancer drug resistance by induction of a necroptotic death. Mol Cancer Ther 2007;6(5):1641-9.
44. Shlomovitz I, Speir M, Gerlic M. Flipping the dogma–phosphatidylserine in non-apoptotic cell death. Cell Commun Signal 2019;17(1):1-12.
45. Su Z, Yang Z, Xu Y, Chen Y, Yu Q. Apoptosis, autophagy, necroptosis, and cancer metastasis. Mol Cancer 2015;14(1):48.
46. Xuan Y, Hu X. Naturally-occurring shikonin analogues–a class of necroptotic inducers that circumvent cancer drug resistance. Cancer Lett 2009;274(2):233-42.
47. Fu Z, Deng B, Liao Y, Shan L, Yin F, Wang Z, Zeng H, Zuo D, Hua Y, Cai Z. The anti-tumor effect of shikonin on osteosarcoma by inducing RIP1 and RIP3 dependent necroptosis. BMC cancer 2013;13(1):1-10.
48. Usami Y, Liu Y-N, Lin A-S, Shibano M, Akiyama T, Itokawa H, Morris-Natschke SL, Bastow K, Kasai R, Lee K-H. Antitumor agents. 261. 20 (S)-protopanaxadiol and 20 (S)-protopanaxatriol as antiangiogenic agents and total assignment of 1H NMR spectra. J Nat Prod 2008;71(3):478-81.
49. Wang X, Xia HY, Qin HY, Kang XP, Hu HY, Zheng J, Jiang JY, Yao LA, Xu YW, Zhang T. 20 (S)-protopanaxadiol induces apoptosis in human umbilical vein endothelial cells by activating the PERK-eIF2alpha-ATF4 signaling pathway. J Cell Biochem 2019;120(4):5085-96.
50. Zhang XP, Li KR, Yu Q, Yao MD, Ge HM, Li XM, Jiang Q, Yao J, Cao C. Ginsenoside Rh2 inhibits vascular endothelial growth factor-induced corneal neovascularization. FASEB J 2018;32(7):3782-91.
51. Brozzo MS, Bjelić S, Kisko K, Schleier T, Leppänen V-M, Alitalo K, Winkler FK, Ballmer-Hofer K. Thermodynamic and structural description of allosterically regulated VEGFR-2 dimerization. Blood, The Journal of the American Society of Hematology 2012;119(7):1781-8.
52. Christensen J. A preclinical review of sunitinib, a multitargeted receptor tyrosine kinase inhibitor with anti-angiogenic and antitumour activities. Ann Oncol 2007;18:x3-x10.
53. De Smet F, Christopoulos A, Carmeliet P. Allosteric targeting of receptor tyrosine kinases. Nat Biotechnol 2014;32(11):1113-20.
54. Pei JV, Kourghi M, De Ieso ML, Campbell EM, Dorward HS, Hardingham JE, Yool AJ. Differential inhibition of water and ion channel activities of mammalian aquaporin-1 by two structurally related bacopaside compounds derived from the medicinal plant bacopa monnieri. Mol Pharmacol 2016;90(4):496-507.

Chapter 6 Conclusion

In the research conducted for this thesis, an evaluation of combined Rg3 epimers was performed as a treatment option for TNBC. A series of experiments were conducted not only to produce novel experimental data on the optimisation of a combination of SRg3 and RRg3, but also to test the efficacy of this combination using *in silico*, *in vitro* and *in vivo* models. The following sections demonstrate the significance of this study and make some recommendations for future studies.

6.1. Significance of the presented study

In this project, a thorough and deep literature review was performed considering pharmacokinetic, pharmacodynamic and toxicity aspects of administering this drug. Furthermore, a comprehensive review was performed on TNBC, the currently available treatment options, the success rates of the current treatments and the potential targets for the treatment of this disease. Based on this background and preliminary *in silico* molecular docking studies between ginsenoside molecules and AQP1, lab-based experiments were performed and a novel candidate for the treatment of TNBC was introduced. The first important contribution of this project was to show the stereoselectivity of Rg3 epimers and their blocking effect on AQP1. This led to the second significance of this project, optimising the combination of the drugs for their anti-cancer actions. The following conclusions were drawn:

1. It is known that AQP1 plays several roles in cancer progression. It is involved in cell proliferation, migration, invasion and angiogenesis. Specifically, overexpression of AQP1 is correlated with worse prognosis of TNBC, higher tumour grade and lower overall survival. In this research, for the first time, using *in silico* molecular docking, the interaction between Rg3 and AQP1 water channel was shown. This indicated that Rg3 had potential as a treatment option for TNBC. Further studies using *in vitro* oocyte swelling assay showed that only SRg3 blocked AQP1-mediated water transport function of AQP1. Rg3 epimers were not potent inhibitors of cell proliferation in TNBC *in vitro* models and only SRg3 inhibited the proliferation of MDA-MB-231, a mesenchymal basal-like cell line. SRg3 and RRg3, differently inhibited cell migration in 2D and 3D models and only RRg3 inhibited invasion of these TNBC cells. The overall conclusion of these studies was that Rg3 epimers have stereoselective efficacies in these models and could be considered as separate drugs.
2. In several published studies, Rg3 was extracted in experimental settings, without sufficient information on the purity and the type of specific epimer used. Extraction procedures might lead to different ratios of SRg3 and RRg3, and considering the stereospecific functions of Rg3, it is critical to identify the purity of specific epimers and the ratio between them. In the current study, the effects of purified (> 98%) epimers were investigated. Following demonstrating the stereoselectivity of the epimers in TNBC models, for the first time, an RSM

model was developed to optimise the combination of SRg3 and RRg3. The optimised combination showed efficacy on endothelial and TNBC cells. Furthermore, it was shown that in HUVEC, these epimers as a single agent, did not induce apoptosis, but potentiate each other in combination and induced apoptosis in a dose-dependent pattern.

3. A critical aspect of the action of any investigational drug candidate in preclinical studies is to show time- and dose-dependency in its actions. In this research, combinations of SRg3 and RRg3 were studied at two time-points on loop formation and migration of endothelial cells. It was shown that Rg3 combinations followed these basic principles of pharmacokinetics.
4. The key driver of angiogenesis is the interaction of VEGF and VEGFR2. Previously, some studies suggested that Rg3 had inhibitory effects on the expression of VEGF and hence affected angiogenesis. For the first time, in this research, the interaction of Rg3 epimers with VEGFR2 was studied. It was shown that Rg3 epimers had allosteric modulatory action on the dose-response curve of VEGF. Allosteric modulators, due to higher target-specificity and lower toxicity profile, are of special interest to pharmaceutical industries.
5. The optimised combination of Rg3 epimers showed the best efficacy on AKT signalling in endothelial cells grown in normoxia. For endothelial cells grown in hypoxia, the treatment affected AKT signalling and also decreased VEGF expression, which has a great impact on angiogenesis.
6. The optimised combination also affected AKT signalling in TNBC cell lines. These cells were grown as mammospheres, which are enriched with cancer stem cells and compared to 2D models of cell culture, are a better representation of a human breast tumour. For the first time, the effect of the combination of Rg3 epimers was studied on mammospheres. This study showed that the optimised combination of Rg3 epimers also decreased the 'stemness' of TNBC cells via decreased expression of CD44 and decreased ratio of CD44/CD24. Cancer stem cells play several roles in cancer progression and resistance to treatment. The proposed treatment could decrease the expression of stem cell markers and reduce the invasiveness of the disease.
7. Based on the results achieved from the effects of Rg3 on AKT signalling, the common proteins that were affected were those that were related to mTOR signalling. Further *in silico* molecular docking studies showed that Rg3 epimers could be potential mTOR inhibitors, as they have good binding with the rapamycin binding site of mTOR and block the interaction site of Rheb, the mTOR activator protein. Considering the importance of PI3K/AKT signalling inhibitors in general and specifically mTOR inhibitors in the treatment of TNBC patients, inhibition of this signalling by Rg3 could be considered an important mechanism with potential clinical efficacy in these patients.
8. The *in vivo* model of metastatic TNBC used in this study was a highly aggressive model and metastasised tumour cells were detectable in mice as early as two to

three weeks after tumour cell injection. Secondary tumours were detectable with IVIS before the treatment started. Despite this, the treatment could significantly inhibit the growth of the primary tumour and secondary tumours, which is a significant finding in such an aggressive tumour model. In future research, the study could be modified by reducing the number of cells injected into the mammary fat pad and commencing treatment sooner.

9. Several studies showed that Rg3 epimers are prone to extensive metabolism, which is more evident with the orally administered drug. The major active metabolites of Rg3 are deglycosylated forms of Rg3; epimers of Rh2 and epimers of PPD. To find out if these molecules have any contribution to the anti-cancer effects of Rg3, some preliminary testing was performed on a TNBC and an endothelial cell type. For the first time, the results of this study compared the anti-proliferative effects of Rg3 epimers and its deglycosylated metabolites and showed that unlike Rg3, its metabolites are potent anti-proliferative agents. While only SRg3 at 100 μM showed anti-proliferation effects on MDA-MB-231, its metabolites, except R-Rh2, had a dose-dependent anti-proliferative action at 6.2-100 μM range. The other difference between these molecules and their metabolites are their anti-proliferative mechanism. With SRg3, the main anti-proliferative mechanism was cell cycle arrest at G0/G1 and with the metabolites, the major cell death mechanism was a necroptotic cell death. In addition, S-Rh2 could also contribute to the effects of Rg3 on mammosphere formation and stemness of the cells. The different mechanisms involved suggests that a combination of all of these molecules could contribute to the observed anti-cancer effects of Rg3.
10. The anti-angiogenic effects of these deglycosylated molecules were also studied in HUVEC. Except for R-Rh2, these molecules potently (IC_{50} < 10 μM) inhibited the proliferation of HUVEC. These deglycosylated molecules or the parent drug, all activated caspase 3/7 and induced apoptosis in these cells. The most potent anti-loop formation agent was S-Rh2. The anti-loop formation mechanisms of this molecule at different concentrations were different. At high μM concentrations, such as 50 and 100 μM, apoptotic cell death prevailed, but at 1 and 10 μM, other anti-migration mechanisms could be involved in inhibiting loop formation.
11. To investigate the anti-migration effects of these molecules, the interaction of Rh2 and PPD with VEGFR2 and AQPs was studied. For the first time, in this project, it was shown that S-Rh2, similar to its parent drug, had allosteric modulatory action on VEGFR2, which suggests that S-Rh2 also contributed to the anti-angiogenic effects of Rg3. Furthermore, molecular docking results suggested that these molecules are a better blocker for AQP1 rather than AQP5. Both AQP1 and AQP5 localise at the leading edge of migrating cells and facilitate cell migration.

12. One outcome of this research was that, either with Rg3 epimers or its metabolites, endothelial cells were more sensitive to the anti-proliferative effects of either Rg3 epimers or its metabolites. This might suggest that the principal function of these molecules might be anti-angiogenic action, with other mechanisms acting on TNBC cells such as inhibition of AKT signalling.

6.2. Recommended future work

In this thesis, a novel treatment for TNBC patients was proposed. This treatment included a combination of SRg3 and RRg3, which was optimised in RSM models. The efficacy of this treatment on *in vitro* angiogenesis and TNBC models and in an *in vivo* metastatic model of TNBC was demonstrated and some of the mechanisms of action of this drug were proposed. Furthermore, this project investigated the efficacy of deglycosylated metabolites of Rg3 and suggested a possible contribution of these molecules to the observed anti-cancer effects of Rg3. However, despite the significant knowledge developed in this field, some gaps exist that could be considered for further investigation and pave the way for the commercialisation of these findings. Some recommendations are as follows:

1. **Contribution of AQP1 to the anti-angiogenic effects of the drugs**

   Preliminary *in silico* molecular docking studies on the interaction of Rh2 and PPD with AQP1 showed promising results and oocyte swelling assay could be performed to confirm the blocking effect of these molecules. Using this assay, it was shown that SRg3 was a blocker of AQP1 water transport. A growing body of evidence shows the role of AQP1 in angiogenesis and cancer progression. In this thesis, it was shown that the expression of AQP1 in endothelial cells was decreased in long-term exposure to Rg3. However, the drugs showed immediate anti-loop formation effects on non-pretreated cells, too. It could be hypothesised that blocking AQP1 was responsible for that immediate effect. Further studies on endothelial cells could test whether blocking AQP1 plays a major role in anti-angiogenic action of Rg3. In addition, further studies could study the mechanisms of anti-loop formation effects of S-Rh2.

2. **Further *in vivo* animal studies**

   i. In the current study, an immunocompromised mouse model was used to study the efficacy of the proposed drug. This model had some advantages including growing human tumour cells and developing metastasis. However, being an immunocompromised model, the interactions of the immune system with the tumour and the treatment is lacking. Considering the fact that Rg3 epimers have been shown to improve immune function in animal models and the important role of the immune system in preventing cancer progression, it would be recommended to study the efficacy of the optimised combination in an immunocompetent BALB/c mouse model. This

requires further *in vitro* studies on murine breast tumour cell line, 4T1, and injecting those cells into the mammary fat pads of those mice.

ii. Currently, the published literature has suggested the short half-life of Rg3 and in clinical trials, Rg3 is administered two times a day to overcome this issue. In the current study, the dosing schedule of the drug was limited to three doses per week. It is, therefore, recommended to use a more frequent dosing schedule of the drug to have a better estimation of the anti-cancer effects of this drug.

iii. Further animal studies are suggested to evaluate the pharmacokinetic parameters of this drug. Using plasma of animals receiving this drug, not only the pharmacokinetics of the injectable form of the drug will be evaluated, but also the presence of metabolites will be measured. Based on the outcome of that study, it would be easier to predict and conduct more studies on the role of each of the Rg3 epimers, their metabolites, and the combination of those in the observed anti-cancer effects.

iv. Administration of these drugs to mice, at the described dose and dosing schedule, caused no toxicity as recorded by weight score, posture, fur condition, movement, behaviour, breathing and hydration level. Rg3 has also been administered to humans with no serious reported toxicities. To further improve the preclinical studies on these drugs, animal toxicity assays will need to be performed. Several parameters such as type of drug formulation, dose, duration of exposure and route of administration affect the adverse effects. Subacute (14-28 days) and subchronic (90 days) animal toxicity testing including full biochemical and haematological screens and histology of the major organs should be performed to confirm the safety of the drugs prior to administration to humans.

3. Designing novel formulations to improve the solubility and bioavailability of the drug:

Ginsenosides have relatively large triterpenoid structures, with low water solubility and bioavailability. Therefore, the following are recommended:

i. Structure-activity relationship (SAR) and quantitative SAR (QSAR) studies to be performed and evaluate the relationship between the chemical structure of these molecules and their biological activity. Therefore, potentially by modifying the structure, smaller molecules with better solubility and bioavailability could be designed and tested.

ii. Novel pharmaceutical formulation modifications could be used to improve the solubility and bioavailability of these molecules. These modifications could include using nanosuspension and nanocrystal technologies or application of liposomes and cyclodextrins.

Overall, the findings of this thesis show the potential of the SRg3 and RRg3 optimised combination as an anti-cancer treatment for application in TNBC patients.